Physics Reports 485 (2010) 195–259

Contents lists available at ScienceDirect

Physics Reports

journal homepage: www.elsevier.com/locate/physrep

Nuclear astrophysics with radioactive beams

C.A. Bertulani [a,*], A. Gade [b,c]

[a] Department of Physics, Texas A & M University, Commerce, TX 75429, USA

[b] National Superconducting Cyclotron Laboratory, Michigan State University, East Lansing, MI 48824, USA

[c] Department of Physics & Astronomy, Michigan State University, East Lansing, MI 48824, USA

ARTICLE INFO

Article history:
Accepted 26 September 2009
Available online 6 November 2009
editor: G.E. Brown

Keywords:
Nuclear astrophysics
Rare isotopes
Reactions

ABSTRACT

The quest to comprehend how nuclear processes influence astrophysical phenomena is driving experimental and theoretical research programs worldwide. One of the main goals in nuclear astrophysics is to understand how energy is generated in stars, how elements are synthesized in stellar events and what the nature of neutron stars is. New experimental capabilities, the availability of radioactive beams and increased computational power paired with new astronomical observations have advanced the present knowledge. This review summarizes the progress in the field of nuclear astrophysics with a focus on the role of indirect methods and reactions involving beams of rare isotopes.

Contents

* Corresponding author.
E-mail addresses: Carlos_Bertulani@tamu-commerce.edu (C.A. Bertulani), gade@nscl.msu.edu (A. Gade).

0370-1573/$ – see front matter © 2009 Elsevier B.V. All rights reserved.
doi:10.1016/j.physrep.2009.09.002

1. Introduction

Nuclear reactions in stars and stellar explosions are responsible for the ongoing synthesis of the elements [1–9]. Nuclear physics plays an important role as it determines the signatures of isotopic and elemental abundances found in the spectra of stars, novae, supernovae, and X-ray bursts as well as in characteristic γ-ray radiation from nuclear decays, or in the composition of meteorites and presolar grains (see [10] for a review on the nuclear structure input to nuclear astrophysics).

The rapid neutron capture process (r process) is responsible for the existence of about half of the stable nuclei heavier than iron; yet a site that can produce the observed elements self-consistently has not been identified [11,12]. Capture cross-sections for most of the nuclei involved are hard if not impossible to measure in the laboratory and indirect experimental approaches have to be employed to gather the relevant nuclear structure information. Nuclear masses and β-decay half-lives are among the few direct observables that are input for calculations that model nucleosynthesis in the r process. X-ray bursts provide a unique window into the physics of neutron stars. They are the most frequent thermonuclear explosions known. The brightness, frequency and opportunity to be observed with different telescopes makes them unique laboratories for explosive nuclear burning at extreme temperatures and densities [13–15]. The reaction sequence during an X-ray burst proceeds through nuclei at or close to the proton drip line mainly by (p, γ) and (p, α) reactions and β decays (αp and rp process) [16]. Most rp-process reaction rates are still based exclusively on theory. Energy in explosive hydrogen burning events such as X-ray bursts is initially generated in the CNO cycle and as the temperature increases, α-capture on unstable oxygen and neon (^{15}O and ^{18}Ne) leads to a break-out and an ensuing chain of proton captures that can go as far as tin. Supernovae play a crucial role in the understanding of the universe as they are the major source of nucleosynthesis and possibly of cosmic rays. Core-collapse supernovae [17] are one of the proposed sites of the r process. Thermonuclear supernovae (type Ia) are powered by explosive carbon and oxygen burning of a white dwarf that has reached the Chandrasekhar mass limit. For both types of supernovae, the driving processes are not well understood and weak interaction rates play a key role [18]. Temperatures and densities are so high that electron captures on unstable nuclei become crucial.

Most aspects in the study of nuclear physics demand beams of energetic particles to induce nuclear reactions on the nuclei of target atoms. It was from this need that accelerators were developed. Over the years, many ways of accelerating charged particles to ever increasing energies have been devised. Today we have ion beams of all elements from protons to uranium

available at energies well beyond those needed for the study of atomic nuclei. The quantities used in nucleosynthesis calculations are reaction rates. A thermonuclear reaction rate is a function of the density of the interacting nuclei, their relative velocity and the reaction cross-section. Extrapolation procedures are often needed to derive cross-sections in the energy or temperature region of astrophysical relevance. While non-resonant cross-sections can be extrapolated rather well to the low-energy region, the presence of continuum, or sub-threshold resonances, can complicate these extrapolations. We will mention some of the important examples.

In the Sun, the reaction ^{7}Be (p,γ) ^{8}B plays a major role for the production of high energy neutrinos from the β-decay of ^{8}B. These neutrinos come directly from the center of the Sun and are ideal probes of the Sun's structure. *John Bahcall* frequently said that this was the most important reaction in nuclear astrophysics [19]. Our understanding of this reaction has improved considerably with the advent of rare-isotope beam facilities. The reaction ^{12}C (α,γ) ^{16}O is extremely relevant for the fate of massive stars. It determines if the remnant of a supernova explosion becomes a black hole or a neutron star [20]. These two reactions are only two examples of a large number of reactions, which are not yet known with the accuracy needed in astrophysics.

In this review, we summarize recent developments and achievements in nuclear astrophysics with a focus on theoretical approaches and experimental techniques that are applicable to or utilize rare-isotope beams, respectively. Section 2 will cover reactions within stars, Section 3 is devoted to nuclear reaction models, Section 4 reviews the effect of environment electrons, Section 5 outlines approaches with indirect methods and Section 6 summarizes recent nuclear astrophysics experiments with rare-isotope beams. Finally, in Section 7 we present our outlook for the present and future of this field.

2. Reactions within stars

2.1. Thermonuclear cross-sections and reaction rates

The nuclear cross-section for a reaction between a nuclear target j and a nuclear projectile k is defined by

$$\sigma = \frac{\text{number of reactions target}^{-1}\text{s}^{-1}}{\text{flux of incoming projectiles}} = \frac{r/n_j}{n_k v}, \tag{1}$$

where the target number density is given by n_j, the projectile number density is given by n_k, and v is the relative velocity between target and projectile nuclei. The number of reactions per unit volume and time can be expressed as $r = \sigma v n_j n_k$, or, more generally, by

$$r_{j,k} = \int \sigma |v_j - v_k| \mathrm{d}^3 n_j \mathrm{d}^3 n_k. \tag{2}$$

The evaluation of this integral depends on the type of particle and their distributions. For nuclei j and k in an astrophysical plasma, obeying a Maxwell–Boltzmann distribution (MB),

$$\mathrm{d}^3 n_j = n_j \left(\frac{m_j}{2\pi kT}\right)^{3/2} \exp\left(-\frac{m_j^2 v_j}{2kT}\right) \mathrm{d}^3 v_j. \tag{3}$$

Eq. (2) simplifies to $r_{j,k} = \langle \sigma v \rangle\, n_j n_k$, where the reaction rate $\langle \sigma v \rangle$ is the average of σv over the temperature distribution in (3). More specifically,

$$r_{j,k} = \langle \sigma \mathrm{v} \rangle_{j,k}\, n_j n_k \tag{4}$$

$$\langle \sigma \mathrm{v} \rangle_{j,k} = \left(\frac{8}{m_{jk}\pi}\right)^{1/2} (kT)^{-3/2} \int_0^\infty E\sigma(E) \exp\left(-\frac{E}{kT}\right) \mathrm{d}E. \tag{5}$$

Here m_{jk} denotes the reduced mass of the target-projectile system.

2.1.1. Photons

When in Eq. (2) particle k is a photon, the relative velocity is always c and there is no need to integrate quantities over $\mathrm{d}^3 n_j$. Thus, one obtains $r_j = \lambda_{j,\gamma} n_j$ where $\lambda_{j,\gamma}$ results from an integration of the photodisintegration cross-section over a Planck distribution for photons of temperature T

$$\mathrm{d}^3 n_\gamma = \frac{E_\gamma^2}{\pi^2 (c\hbar)^3} \frac{1}{\exp(E_\gamma/kT) - 1} \mathrm{d}E_\gamma, \tag{6}$$

which leads to

$$r_j = \lambda_{j,\gamma}(T) n_j = \frac{1}{\pi^2 (c\hbar)^3} \int \mathrm{d}^3 n_j \int_0^\infty \frac{c\sigma(E_\gamma) E_\gamma^2}{\exp(E_\gamma/kT) - 1} \mathrm{d}E_\gamma. \tag{7}$$

There is, however, no direct need to evaluate photodisintegration cross-sections, because, due to detailed balance, they can be expressed by the capture cross-sections for the inverse reaction $l + m \to j + \gamma$ [21]

$$\lambda_{j,\gamma}(T) = \left(\frac{\xi_l \xi_m}{\xi_j}\right)\left(\frac{A_l A_m}{A_j}\right)^{3/2}\left(\frac{m_u kT}{2\pi\hbar^2}\right)^{3/2}\langle\sigma \mathrm{v}\rangle_{l,m}\exp\left(-\frac{Q_{lm}}{kT}\right), \tag{8}$$

where $m_u = m_{^{12}C}/12$ is the mass unit, Q_{lm} is the reaction Q-value, T is the temperature, $\langle\sigma \mathrm{v}\rangle_{j,k}$ is the inverse reaction rate, $\xi(T) = \sum_i (2J_i + 1)\exp(-E_i/kT)$ are partition functions, and A are the mass numbers of the participating nuclei in a thermal bath of temperature T.

2.1.2. Electron, positron and neutrino capture

The electron is about 2000 times less massive than a nucleon. Thus, the velocity of the nucleus j is negligible in the center of mass system in comparison to the electron velocity ($|v_j - v_e| \approx |v_e|$), and there is no need to integrate quantities over $\mathrm{d}^3 n_j$. The electron capture cross-section has to be integrated either over a Boltzmann or a Fermi distribution of electrons, depending on the astrophysical scenario. The electron capture rates are a function of T and the electron number density, $n_e = Y_e \rho N_A$ [22]. In a completely ionized plasma, $Y_e = \sum_i Z_i Y_i$, i.e., the electron abundance is equal to the total proton abundance in nuclei. Here Y_i denotes the abundance of nucleus i defined by $Y_i = n_i/(\rho N_A)$, where n_i is the number density of nuclei per unit volume and N_A is Avogadro's number. Therefore,

$$r_j = \lambda_{j,e}(T, \rho Y_e) n_j. \tag{9}$$

This treatment can be generalized for the capture of positrons, which are in a thermal equilibrium with photons, electrons, and nuclei. At high densities ($\rho > 10^{12}$ g/cm^3) the neutrino scattering cross-sections on nuclei and electrons are large enough to thermalize the neutrino distribution. Inverse electron (neutrino) capture can also occur and the neutrino capture rate can be expressed similarly to Eqs. (7) or (9), integrating over the neutrino distribution.

2.1.3. Beta-decay

For normal decays, like β or α decays with half-life $\tau_{1/2}$, we obtain an equation similar to Eqs. (7) or (9) with a decay constant $\lambda_j = \ln 2/\tau_{1/2}$ and

$$r_j = \lambda_j n_j. \tag{10}$$

2.1.4. Charged particles

Nuclear cross-sections for charged particles are suppressed at low energies due to the Coulomb barrier. The product of the penetration factor and the Maxwell–Boltzmann (MB) distribution at a given temperature yields an energy window in which most of the reactions occur, known as the Gamow window.

Experimentally, it is more convenient to work with the astrophysical S factor

$$S(E) = E\sigma(E)\exp(2\pi\eta), \tag{11}$$

with η being the Sommerfeld parameter, describing the s-wave barrier penetration, $\eta = Z_j Z_k e^2/\hbar v$, and energy E and v the relative velocity of the ions. In this case, the steep increase of the cross-section is transformed into a rather flat, energy dependent function. One can easily see the two contributions of the velocity distribution and the penetrability in the integral

$$\langle\sigma \mathrm{v}\rangle_{jk} = \left(\frac{8}{\pi m_{jk}}\right)^{1/2}\frac{1}{(kT)^{3/2}}\int_0^\infty S(E)\exp\left[-\frac{E}{kT} - \frac{b}{E^{1/2}}\right] \tag{12}$$

where $b = 2\pi\eta E^{1/2} = (2m_{jk})^{1/2}\pi e^2 Z_j Z_k/\hbar$ and m_{jk} is the reduced mass in units of m_u (unit atomic mass). Experimentally it is very difficult to perform direct measurements of fusion reactions involving charged particles at very small energies. The experimental data at higher energies can be guided by a theoretical model for the cross-section, which can then be extrapolated down to the Gamow energy. However, the extrapolation can be inadequate due to the presence of resonances and subthreshold resonances, for example.

A simple result can be obtained by assuming a constant S-factor, i.e., $S(E) = SE_0$. In this case, the first derivative of the integrand in Eq. (12) yields the location E_0 of the Gamow peak, and the effective width Δ of the energy window, i.e.

$$\begin{aligned} E_0 &= \left(\frac{bkT}{2}\right)^{2/3} = 1.22(Z_j^2 Z_k^2 m_{jk} T_6^2)^{1/3}\ \mathrm{keV}, \\ \Delta &= \left(\frac{16 E_0 kT}{3}\right)^{1/2} = 0.749(Z_j^2 Z_k^2 m_{jk} T_6^5)^{1/6}\ \mathrm{keV}, \end{aligned} \tag{13}$$

carrying the dependence on the charges Z_j, Z_k, the reduced mass m_{jk} of the involved nuclei in units of m_u, and the temperature T_6 given in 10^6 K.

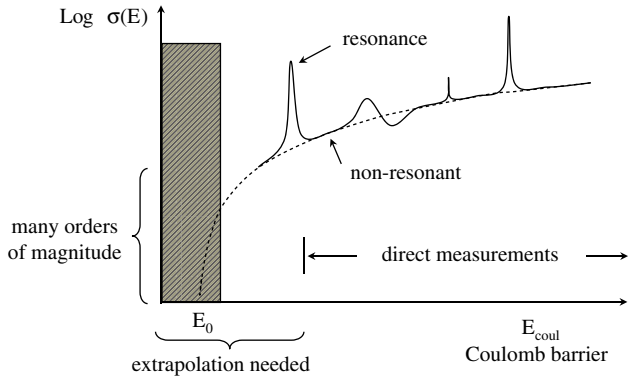

Fig. 1. Schematic representation of the energy dependence of a fusion reaction involving charged particles (Courtesy of C. Spitaleri).

Fig. 1 outlines one of the main challenges in astrophysical reactions with charged particles. The experimental data can be guided by a theoretical model for the cross-section, which can then be extrapolated to the Gamow energy. The solid curve is a theoretical prediction, which supposedly describes the data at high energies. Its extrapolation to lower energies yields the desired value of the S-factor, or cross-section, at the Gamow energy E_0. The extrapolation can be complicated by the presence of unknown resonances.

2.1.5. Neutron-induced reactions

For neutron-induced reactions, the effective energy window for s-wave neutrons ($l = 0$) is given by the location and width of the peak of the MB distribution function. For $l > 0$, the penetrability of the centrifugal barrier shifts the effective energy E_0 to higher values. For neutrons with energies less than the height of the centrifugal barrier one gets [23]

$$E_0 \approx 0.172 T_9 \left(l + \frac{1}{2}\right) \text{ MeV}, \qquad \Delta \approx 0.194 T_9 \left(l + \frac{1}{2}\right)^{1/2} \text{ MeV} \tag{14}$$

Usually, E_0 is not much different (in magnitude) from the neutron separation energy.

2.2. Reaction networks

The time evolution of the number densities, n_i, of each of the species i in an astrophysical plasma (at constant density) is obtained by solving equations of the type

$$\left(\frac{\partial n_i}{\partial t}\right)_{\rho=const} = \sum_j N_j^i r_j + \sum_{j,k} N_{j,k}^i r_{j,k} + \sum_{j,k,l} N_{j,k,l}^i r_{j,k,l}, \tag{15}$$

where the N_x^i can be positive or negative numbers that specify how many particles of species i are created or destroyed in a reaction x. The reactions x fall in three categories:

(1) decays, photodisintegrations, electron and positron captures and neutrino-induced reactions, $r_j = \lambda_j n_j$,
(2) two-particle reactions, $r_{j,k} = \langle \sigma \mathrm{v} \rangle_{j,k} n_j n_k$, and
(3) three-particle reactions, $r_{j,k,l} = \langle \sigma \mathrm{v} \rangle_{j,l,k} n_j n_k n_l$, like the triple-$\alpha$ process $\left(\alpha + \alpha + \alpha \longrightarrow {}^{12}\mathrm{C} + \gamma\right)$.

The N^i's are given by:

$$N_j^i = N_i, \qquad N_{j,k}^i = \frac{N_i}{\prod_{m=1}^{n_m} |N_{j_m}|!}, \quad \text{and} \quad N_{j,k,l}^i = \frac{N_i}{\prod_{m=1}^{n_m} |N_{j_m}|!},$$

where the products in the denominators run over the n_m different species destroyed in the reaction and avoid double counting when identical particles react with each other.

In terms of the nuclear abundances, $Y_i = n_i/(\rho N_A)$ such that for a nucleus with atomic weight A_i, $A_i Y_i$ represents the mass fraction of this nucleus, $\sum A_i Y_i = 1$ and the reaction network equations can be rewritten as

$$\frac{\mathrm{d}Y_i}{\mathrm{d}t} = \sum_j N_j^i \lambda_j Y_j + \sum_{j,k} N_{j,k}^i \rho N_A \langle \sigma \mathrm{v} \rangle_{j,k} Y_j Y_k + \sum_{j,k,l} N_{j,k,l}^i \rho^2 N_A^2 \langle \sigma \mathrm{v} \rangle_{j,l,k} Y_j Y_k Y_l. \tag{16}$$

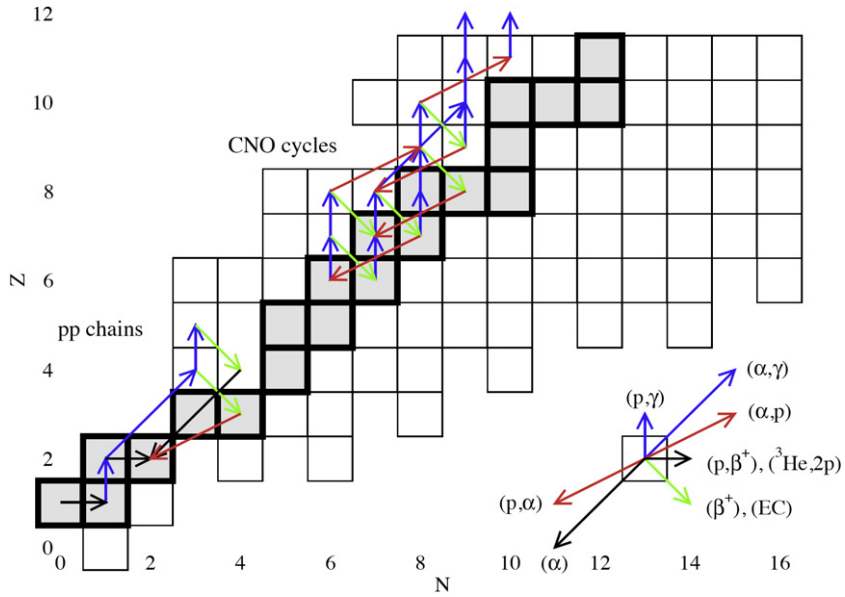

Fig. 2. Example of reaction networks (pp-chains and CNO-cycles). A particular nucleus on the Segrè chart can take different paths along the reaction network, as shown in the inset at the lower right side. (Courtesy of S. Typel).

The energy generation per unit volume in a time interval Δt is expressed in terms of the mass excess $\Delta M_i c^2$ of the participating nuclei

$$\Delta\epsilon = -\sum_i \Delta Y_i N_A \Delta M_i c^2, \qquad \frac{d\epsilon}{dt} = -\sum_i \frac{dY_i}{dt} N_A \Delta M_i c^2. \tag{17}$$

The solution of the above group of equations allows one to deduce the path for the r process until the heavier elements are reached. The relative abundances of elements are also obtained theoretically by means of these equations by using stellar models for the initial conditions, as the neutron density and the temperature. Nuclear physics has to contribute with β-decay half-lives, electron and positron capture rates, photo-nuclear and neutrino cross-sections.

Simple examples of reaction networks are shown in Fig. 2 for typical pp-chains and CNO-cycles. On the right we show a particular nucleus on the Segrè chart from where different paths can start along the reaction network.

3. Nuclear reaction models

Explosive nuclear burning in astrophysical environments produces short-lived, exotic nuclei, which again can be targets for subsequent reactions. In addition, it involves a very large number of stable nuclei, which are still not fully explored by experiments. Thus, it is necessary to be able to predict reaction cross-sections and thermonuclear rates with the aid of theoretical models. Especially during the hydrostatic burning stages of stars, charged-particle induced reactions proceed at such low energies that a direct cross-section measurement is often not possible with existing experimental techniques. Hence extrapolations down to the stellar energies of the cross sections measured at the lowest possible energies in the laboratory are usually applied. To be trustworthy, such extrapolations should have as strong a theoretical foundation as possible. Theory is even more mandatory when excited nuclei are involved in the entrance channel, or when unstable, very neutron-rich or neutron-deficient nuclides (many of them being even impossible to produce with present-day experimental techniques) have to be considered. Such situations are often encountered in the modeling of explosive astrophysical scenarios.

3.1. Potential and DWBA models

Potential models assume that the physically important degrees of freedom are the relative motion between structureless nuclei in the entrance and exit channels. The only microscopic information is introduced in terms of spectroscopic factors and parameters of the optical potential. The weakness of the models is that the nucleus-nucleus potentials adopted for calculating the initial and final wavefunctions from the Schrödinger equation cannot be unambiguously defined. Single-particle wavefunctions are calculated using nuclear potentials of the form

$$V(\mathbf{r}) = V_0(r) + V_S(r)\,(\mathbf{l}.\mathbf{s}) + V_C(r) \tag{18}$$

where $V_0(r)$ and $V_S(r)$ are the central and spin–orbit interactions, respectively, and $V_C(r)$ is the Coulomb potential of a uniform distribution of charges. The potentials $V_0(r)$ and $V_S(r)$, are usually given in terms of a Woods–Saxon (WS) parameterization. The parameters of the potentials — their depth, range and diffuseness, are chosen to reproduce the ground state energy E_B (or the energy of an excited state). For knockout reactions, they are also adjusted to reproduce the orbital radius of the nucleon. Most often, the same parameters do not reproduce the proper continuum wavefunctions, and do not yield location and widths of resonances, etc. These can be obtained by readjusting the strengths of the potentials, effectively increasing the number of parameters at hand.

The WS parameterization is well suited to describe any reaction of interest, except perhaps for those cases in which one of the partners is a neutron-rich halo nucleus. Then, the extended radial dependence leads to unusual forms for the potentials. Also, for capture reactions in which the light partner is either a deuteron, triton, α-particle or a heavier nucleus, folding models are more appropriate. The central part of the potential is obtained by a folding of an effective interaction with the ground state densities, ρ_A and ρ_B, of the nuclei A and B:

$$V(\mathbf{r}) = \lambda_0 \int \mathrm{d}^3 r_1 \mathrm{d}^3 r_2 \rho_A(\mathbf{r}_1)\rho_B(\mathbf{r}_2) v_{eff}(\mathbf{s}), \tag{19}$$

with $\mathbf{s} = |\mathbf{r} + \mathbf{r}_2 - \mathbf{r}_1|$. λ_0 is a normalization factor which is close to unity.

Folding models are based on an effective nucleon–nucleon interaction, v_{eff}, and nuclear densities, ρ_i, which are either obtained experimentally (not really, because only charge densities can be accurately determined from electron scattering), or calculated from some microscopic model (typically Hartree–Fock or relativistic mean field models). The effective interactions as well as the nuclear densities are subject of intensive theoretical studies.

Potential models have been applied to all kinds of calculations for nuclear astrophysics. For simplicity, let us consider radiative capture reactions involving a target nucleus and a nucleon. The wavefunctions for the nucleon (n) + nucleus (x) system are calculated by solving the radial Schrödinger equation

$$-\frac{\hbar^2}{2m_{nx}}\left[\frac{\mathrm{d}^2}{\mathrm{d}r^2} - \frac{l(l+1)}{r^2}\right] u_\alpha(r) + V(r) u_\alpha(r) = E_\alpha u_\alpha(r)\,. \tag{20}$$

The nucleon n, the nucleus x, and the $n + x = a$—system have intrinsic spins labeled by $s = 1/2$, I_x and J, respectively. The orbital angular momentum for the relative motion of $n + x$ is described by l. Angular momenta are usually coupled as $\mathbf{l} + \mathbf{s} = \mathbf{j}$ and $\mathbf{j} + \mathbf{I}_x = \mathbf{J}$, where $\mathbf{J}$ is called the channel spin. In Eq. (18), for V one uses $\mathbf{s}\cdot\mathbf{l} = [j(j+1) - l(l+1) - 3/4]/2$ and α in Eq. (20) denotes the set of quantum numbers, $\alpha_b = \{E_b, l_b, j_b, J_b\}$ for the bound state, and $\alpha_c = \{E_c, l_c, j_c, J_c\}$ for the continuum states.

The bound-state wavefunctions are normalized to unity, $\int \mathrm{d}r \left|u_{\alpha_b}(r)\right|^2 = 1$, whereas the continuum wavefunctions have boundary conditions at large distances given by

$$u_{\alpha_c}(r \to \infty) = \mathrm{i}\sqrt{\frac{m_{nx}}{2\pi k \hbar^2}}\left[H_l^{(-)}(r) - S_{\alpha_c} H_l^{(+)}(r)\right] \mathrm{e}^{\mathrm{i}\sigma_l(E)} \tag{21}$$

where $S_{\alpha_c} = \exp\left[2\mathrm{i}\delta_{\alpha_c}(E)\right]$, with $\delta_{\alpha_c}(E)$ and $\sigma_l(E)$ being the nuclear and the Coulomb phase shifts, respectively. In Eq. (21), $H_l^{(\pm)}(r) = G_l(r) \pm \mathrm{i}F_l(r)$, where F_l and G_l are the regular and irregular Coulomb wavefunctions. For neutrons, the Coulomb functions reduce to the usual spherical Bessel functions, $j_l(r)$ and $n_l(r)$. With these definitions, the continuum wavefunctions are normalized as $\left\langle u_{E_c'} | u_{E_c}\right\rangle = \delta\left(E_c' - E_c\right)\delta_{\alpha\alpha'}$.

For $n + x \to a + \gamma$ and $\pi L(\pi = E, (M) =$ electric (magnetic) L-pole) transitions, the cross-sections are obtained from

$$\sigma^{\text{rad.cap.}}_{\pi L, J_b} = \frac{(2\pi)^3}{k^2}\left(\frac{E_{nx} + E_b}{\hbar c}\right)^{2L+1} \frac{2(2I_a+1)}{(2I_n+1)(2I_x+1)} \frac{L+1}{L[(2L+1)!!]^2} \sum_{J_c j_c l_c} (2J_c+1)$$
$$\times \begin{Bmatrix} j_c & J_c & I_x \\ J_b & j_b & L \end{Bmatrix}^2 \left|\langle l_c j_c \| \mathcal{O}_{\pi L} \| l_b j_b\rangle\right|^2, \tag{22}$$

where E_b is the binding energy and $\langle l_c j_c \| \mathcal{O}_{\pi L} \| l_b j_b\rangle$ is the multipole matrix element. For electric multipole transitions,

$$\langle l_c j_c \| \mathcal{O}_{EL} \| l_b j_b\rangle = (-1)^{l_b + l_c - j_c + L - 1/2} \frac{e_L}{\sqrt{4\pi}} \sqrt{(2L+1)(2j_b+1)} \begin{pmatrix} j_b & L & j_c \\ 1/2 & 0 & -1/2 \end{pmatrix} \int_0^\infty \mathrm{d}r\, r^L u_b(r) u_c(r), \tag{23}$$

where e_L is the effective charge, which takes into account the displacement of the center-of-mass, $e_L = Z_n e\,(-m_n/m_a)^L + Z_x e\,(m_x/m_a)^L$. In comparison with electric dipole transitions, the cross-sections for magnetic dipole transitions are reduced by a factor of v^2/c^2, where v is the relative velocity of the $n + x$ system. At very low energies, $v \ll c$, $M1$ transitions will be much smaller than the electric transitions. Only in the case of sharp resonances, do the $M1$ transitions play a significant role.

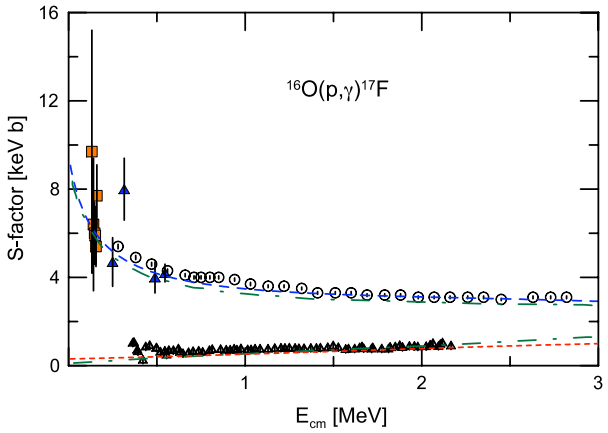

Fig. 3. Potential model calculation [24] for the reaction $^{16}O(p,\gamma)^{17}F$. The dotted line and the dashed line are for the capture to the ground state and to the first excited state respectively. The experimental data are from Refs. [25–27]. The dotted-dashed lines are the result of shell model calculations published in Ref. [28].

The total radiative capture cross-section is obtained by adding all multipolarities and final spins of the bound state ($E \equiv E_{nx}$),

$$\sigma^{\text{rad.cap.}}(E) = \sum_{L,J_b} (SF)_{J_b}\, \sigma^{\text{d.c.}}_{L,J_b}(E), \tag{24}$$

where $(SF)_{J_b}$ are spectroscopic factors.

As an example, Fig. 3 shows a potential model calculation [24] for the S-factor of the $^{16}O(p,\gamma)^{17}F$ reaction. The rate of this reaction influences sensitively the $^{17}O/^{16}O$ isotopic ratio predicted by models of massive ($\geq 4M_\odot$) AGB stars, where proton capture occurs at the base of the convective envelope (hot bottom burning). A fine-tuning of the $^{16}O(p,\gamma)^{17}F$ reaction rate may account for the measured anomalous $^{17}O/^{16}O$ abundance ratio in small grains which are formed by the condensation of the material ejected from the surface of AGB stars via strong stellar winds [29]. The agreement of the potential model calculation with the experimental data seen in Fig. 3 is very good and comparable with more elaborate calculations [28].

3.2. Microscopic models

In microscopic models, nucleons are grouped into clusters and the completely antisymmetrized relative wavefunctions between the various clusters are determined by solving the Schrödinger equation for a many-body Hamiltonian with an effective nucleon–nucleon interaction. Typical cluster models are based on the Resonating Group Method (RGM) or the Generator Coordinate Method (GCM). They are based on a set of coupled integro-differential equations of the form

$$\sum_{\alpha'} \int \mathrm{d}^3 r' \left[\mathcal{H}^{AB}_{\alpha\alpha'}(\mathbf{r},\mathbf{r}') - E\mathcal{N}^{AB}_{\alpha\alpha'}(\mathbf{r},\mathbf{r}')\right] g_{\alpha'}(\mathbf{r}') = 0, \tag{25}$$

where

$$\mathcal{H}^{AB}_{\alpha\alpha'}(\mathbf{r},\mathbf{r}') = \langle \Psi_A(\alpha,\mathbf{r})|H|\Psi_B(\alpha',\mathbf{r}')\rangle \quad \text{and} \quad \mathcal{N}^{AB}_{\alpha\alpha'}(\mathbf{r},\mathbf{r}') = \langle \Psi_A(\alpha,\mathbf{r})|\Psi_B(\alpha',\mathbf{r}')\rangle.$$

In these equations H is the Hamiltonian for the system of two nuclei (A and B) with the energy E, $\Psi_{A,B}$ is the wavefunction of nucleus A (and B), and $g_\alpha(\mathbf{r})$ is a function to be found by numerical solution of Eq. (25), which describes the relative motion of A and B in channel α. Full antisymmetrization between nucleons of A and B are implicit.

Modern nuclear shell-model calculations, such as the Monte-Carlo shell model, or the no-core shell model, are able to provide the wavefunctions $\Psi_{A,B}$ for light nuclei. But so far they cannot describe scattering wavefunctions with a full account of anti-symmetrization. Moreover, the road to an effective NN interaction which can simultaneously describe bound and continuum states has not been an easy one. Thus, methods based on Eq. (25) seem to be the best way to obtain scattering wavefunctions needed for astrophysical purposes. Old interactions, such as Volkov interactions, are still used for practical purposes. It is also worth mentioning that this approach has provided the best description of bound, resonant, and scattering states of nuclear systems [40].

As an example of applications of this method, we again give a radiative capture reaction. The creation and destruction of ^{7}Be in astrophysical environments is essential for the description of several stellar and cosmological processes and is not well understood. ^{8}B also plays an essential role in understanding our Sun. High energy ν_e neutrinos produced by ^{8}B decay in the Sun oscillate into other active species on their way to earth [41]. Precise predictions of the production rate of ^{8}B solar neutrinos are important for testing solar models, and for limiting the allowed neutrino mixing parameters. The most uncertain reaction leading to ^{8}B formation in the Sun is the $^7Be(p,\gamma)^8B$ radiative capture reaction [35]. Additionally, the Coulomb dissociation method, discussed later in this review, has given some new insights about the electromagnetic

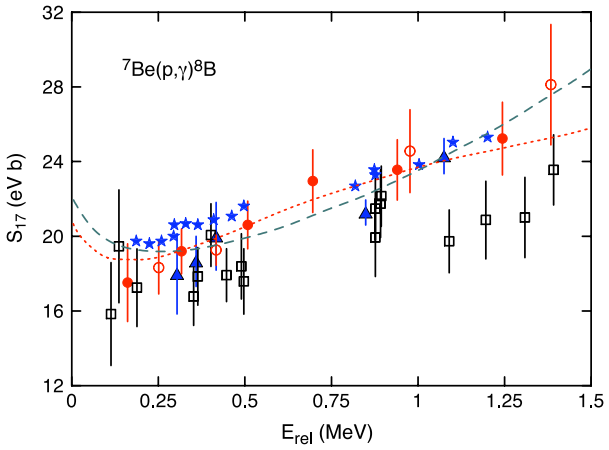

Fig. 4. Microscopic calculations for the reaction ^{7}Be $(p,\gamma)^8$B. The dashed line is the no-core shell-model calculation of Ref. [30] and the dotted line is from the resonant group method calculation of Ref. [31]. Experimental data are from Refs. [32–39].

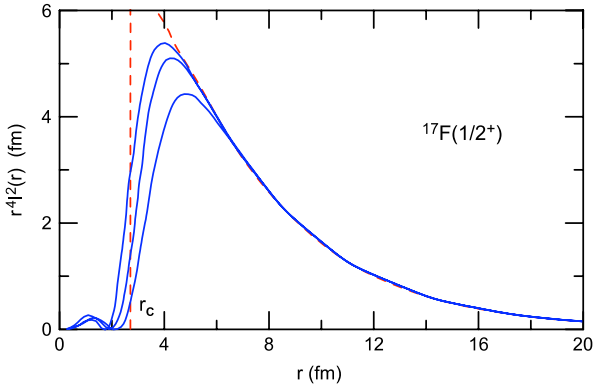

Fig. 5. Comparison of various radial overlap integrals $r^4I^2(r)$ for $^{17}F^*(1/2^+)$ with the normalized Whittaker function (dashed curve). Most of the contribution to the rms radius comes from the region outside the core, with radius r_c.

matrix elements for this reaction. Fig. 4 shows a comparison of microscopic calculations for the reaction ^{7}Be $(p,\gamma)^8$B with experimental data. The dashed–dotted line is the no-core shell-model calculation of Ref. [30] and the dotted line is for the resonant group method calculation of Ref. [31]. Experimental data are from Refs. [32–39]. It is evident that both theory and experiment, need improvement for this important reaction.

3.2.1. Asymptotic normalization coefficients

Although the potential model works well for many nuclear reactions of interest in astrophysics, it is often necessary to pursue a more microscopic approach to reproduce experimental data. Instead of the single-particle wavefunctions one often makes use of overlap integrals, $I_b(\mathbf{r})$, and a many-body wavefunction for the relative motion, $\Psi_c(\mathbf{r})$. Both $I_b(\mathbf{r})$ and $\Psi_c(\mathbf{r})$ might be very complicated to calculate, depending on how elaborate the microscopic model is. The variable $\mathbf{r}$ is the relative coordinate between the nucleon and the nucleus x, with all the intrinsic coordinates of the nucleons in x being integrated out. The radiative capture cross-sections are obtained from the calculation of $\sigma^{\text{rad.cap.}}_{L,J_b} \propto |\langle I_b(r)\|r^L Y_L\|\Psi_c(r)\rangle|^2$.

The imprints of many-body effects will eventually disappear at large distances between the nucleon and the nucleus. One thus expects that the overlap function asymptotically matches the solution of the Schrödinger equation (20), with $V = V_C$ for protons and $V = 0$ for neutrons. That is, when $r \to \infty$,

$$\begin{aligned} I_b(r) &= C_1 \frac{W_{-\eta,l_b+1/2}(2\kappa r)}{r}, \quad \text{for protons} \\ &= C_2\sqrt{\frac{2\kappa}{r}} K_{l_b+1/2}(\kappa r), \quad \text{for neutrons} \end{aligned} \tag{26}$$

where the binding energy of the $n + x$ system is related to κ by means of $E_b = \hbar^2\kappa^2/2m_{nx}$, $W_{p,q}$ is the Whittaker function and K_μ is the modified Bessel function. In Eq. (26), C_i is the asymptotic normalization coefficient (ANC). In Fig. 5 we show the

comparison of the ANC for $^{17}\mathrm{F}(1/2^+)$ as a function of the distance r, with the Whittaker function, Eq. (26). As can be seen, most of the contribution to the rms radius comes from the region outside the core.

In the calculation of $\sigma^{\mathrm{rad.cap.}}_{L,J_b}$ above, one often meets the situation in which only the asymptotic part of $I_b(r)$ and $\Psi_c(r)$ contributes significantly to the integral over r. In these situations, $\Psi_c(r)$ is also described well by a simple two-body scattering wave (e.g. Coulomb waves). Therefore, the radial integration in $\sigma^{\mathrm{rad.cap.}}_{L,J_b}$ can be done accurately and the only remaining information from the many-body physics at short distances is contained in the asymptotic normalization coefficient C_i, i.e. $\sigma^{\mathrm{rad.cap.}}_{L,J_b} \propto C_i^2$. We thus run into an effective theory for radiative capture cross-sections, in which the constants C_i carry all information about the short-distance physics, where the many-body aspects are relevant. It is worthwhile mentioning that these arguments are reasonable for proton capture at very low energies because of the Coulomb barrier.

The asymptotic normalization coefficients, C_α, can also be obtained from the analysis of peripheral transfer and breakup reactions. As the overlap integral, Eq. (26), asymptotically becomes a Whittaker function, so does the single-particle bound-state wavefunction u_α, calculated with Eq. (20). If we label the single-particle ANC by b_i, then the relation between the ANC obtained from experiment, or a microscopic model, with the single-particle ANC given by $(SF)_i b_i^2 = C_i^2$ (this becomes clear from Eq. (24)). The values of $(SF)_i$ and b_i obtained with the simple potential model are useful telltales of the complex short-range many-body physics of radiative capture reactions. One can also invert this argumentation and obtain spectroscopic factors if the C_i are deduced from a many-body model, or from experiment, and the b_i are calculated from a single-particle potential model [42].

Microscopic calculations of ANCs rely on obtaining the projection, or overlap, of the many-body wave functions of nuclei A and $A-1$. The overlap integral $\langle (A-1)|A\rangle \equiv I_b(r)$ must have the correct asymptotic behavior with respect to the variable r which is the distance between the nucleon N and the c.m. of the nucleus $A-1$. The most common methods are: (a) the resonating group method (RGM), as described above, (b) the Fadeev method for three-body systems, (c) a combination of the microscopic cluster method and $\mathcal{R}$-matrix approaches, to be discussed later, (d) Green's function Monte-Carlo method, (e) the no-core shell model, or (f) hyperspherical functions method. As an example, early applications of the ANC method have obtained $S_{17}(0) = 15.5$ eV b for the $^7\mathrm{Be}(p,\gamma)^8\mathrm{B}$ reaction using ANCs calculated with $0\hbar\omega$ oscillator wave functions and M3Y(E) effective NN potential as a model for $|A\rangle$ and $\langle (A-1)\bigotimes N|$ [43]. The M3Y NN interaction is an effective interaction constructed as in Eq. (19), with v_{eff} given in terms of sums of (3) Yukawa functions.

3.2.2. Threshold behavior and the r-process

The threshold behavior of radiative capture cross-sections is fundamental in nuclear astrophysics because of the small projectile energies in the thermonuclear region. For example, for neutron capture near the threshold, the cross-section can be written as [44]

$$\sigma_{if} = \frac{\pi}{k^2}\left(-4kR\frac{\mathrm{Im}\mathcal{L}_0}{|\mathcal{L}_0|^2}\right),$$

where $\mathcal{L}_0$ is the logarithmic derivative for the s wave at a channel radius. Since $\mathcal{L}_0$ is only weakly dependent on the projectile energy, one obtains for low energies the well-known $1/v$-behavior.

With increasing neutron energy, higher partial waves with $l > 0$ contribute more significantly to the radiative capture cross-section. Thus the product σv becomes a slowly varying function of the neutron velocity and one can expand this quantity in terms of v or $\sqrt{E}$ around zero energy,

$$\sigma v = S^{(n)}(0) + \dot{S}^{(n)}(0)\sqrt{E} + \ddot{S}^{(n)}(0)\frac{E}{2} + \cdots.$$

The quantity $S^{(n)}(E) = \sigma v$ is the astrophysical S-factor for neutron-induced reactions and the dotted quantities represent derivatives with respect to $E^{1/2}$, i.e.,

$$\dot{S}^{(n)} = 2\sqrt{E}\frac{\mathrm{d}S^{(n)}}{\mathrm{d}E} \quad \text{and} \quad \ddot{S}^{(n)} = 4E\frac{\mathrm{d}^2S^{(n)}}{\mathrm{d}E^2} + 2\frac{\mathrm{d}S^{(n)}}{\mathrm{d}E}.$$

The astrophysical S-factor for neutron-induced reactions is different from that for charged-particle induced reactions. In the astrophysical S-factor for charged-particle induced reactions the penetration factor through the Coulomb barrier also has to be considered (Eq. (11)). Inserting this into Eq. (5), one obtains for the reaction rate of neutron-induced reactions

$$\langle \sigma v\rangle = S(0) + \left(\frac{4}{\pi}\right)^{\frac{1}{2}}\dot{S}(0)(k_{\mathrm{B}}T)^{\frac{1}{2}} + \frac{3}{4}\ddot{S}(0)k_{\mathrm{B}}T + \cdots. \tag{27}$$

In most astrophysical neutron-induced reactions, neutron s-waves will dominate, resulting in a cross-section showing a $1/v$-behavior (i.e., $\sigma(E) \propto 1/\sqrt{E}$). In this case, the reaction rate will become independent of temperature, $R = \text{const.}$ Therefore it will suffice to measure the cross-section at one temperature in order to calculate the rates for a wider range of temperatures. The rate can then be computed very easily by using

$$R = \langle \sigma v\rangle = \langle \sigma\rangle_T v_T = \text{const.}, \tag{28}$$

with $v_T = (2kT/m)^{1/2}$.

The mean lifetime $\tau_{\rm n}$ of a nucleus against neutron capture, i.e., the mean time between subsequent neutron captures, is inversely proportional to the available number of neutrons $n_{\rm n}$ and the reaction rate $R_{{\rm n}\gamma}$, $\tau_{\rm n} = (n_{\rm n} R_{{\rm n}\gamma})^{-1}$. If this time is shorter than the β-decay half-life of the nucleus, it will be likely to capture a neutron before decaying (r process). In this manner, more and more neutrons can be captured to build up nuclei along an isotopic chain until the β-decay half-life of an isotope finally becomes shorter than $\tau_{\rm n}$. With the very high neutron densities encountered in several astrophysical scenarios, isotopes very far off stability can be synthesized.

3.2.3. Halo nuclei

For low values of the binding energy $|E_B|$, e.g. for *halo-nuclei*, the simple $1/v$-law does not apply any longer. A significant deviation can be observed if the neutron energy is of the order of the $|E_B|$-value. For radiative capture to weakly-bound final states, the bound-state wave function $u_{lj}(r)$ in Eq. (23) decreases very slowly in the nuclear exterior, so that the contributions come predominantly from far outside the nuclear region, i.e., from the nuclear halo. For this asymptotic region, the scattering and bound wave functions in Eq. (23) can be approximated by their asymptotic expressions neglecting the nuclear potential, $u_l(kr) \propto j_l(kr)$, and $u_{l_0}(r) \propto h^{(+)}_{l_0}(i\xi r)$, where j_l and $h^{(+)}_{l_0}$ are the spherical Bessel, and the Hankel function of the first kind, respectively. The separation energy $|E_B|$ in the exit channel is related to the parameter ξ by $|E_B| = \hbar^2 \xi^2/(2m_{nx})$.

Performing calculations of the radial integrals in Eq. (23), one readily obtains the energy dependence of the radiative capture cross-section for halo nuclei [45]. For example, for a transition $s \to p$ becomes

$$\sigma^{({\rm rc})}_{(E1)}(s \to p) \propto \frac{1}{\sqrt{E}} \frac{(E + 3|E_B|)^2}{E + |E_B|}, \tag{29}$$

while a transition $p \to s$ has the energy dependence

$$\sigma^{({\rm rc})}_{(E1)}(p \to s) \propto \frac{\sqrt{E}}{E + |E_B|}. \tag{30}$$

If $E \ll |E_B|$, the conventional energy dependence is recovered. From the above equations one obtains that the reaction rate is not constant (for s-wave capture) or proportional to T (for p-wave capture) in the case of small $|E_B|$-values.

In the case of charged particles, $S(E)$ is expected to be a slowly varying function in energy for non-resonant nuclear reactions. In this case, $S(E)$ can be expanded in a McLaurin series, as was done to obtain Eq. (27). Using the expansion in Eq. (12) and approximating the product of the exponentials $\exp(-E/k_{\rm B}T)$ and $\exp[2\pi\eta(E)]$ by a Gaussian centered at the energy E_0, Eq. (12) can be evaluated as [46]

$$\langle \sigma v \rangle = \left(\frac{2}{m_{ab}}\right)^{1/2} \frac{\Delta}{(kT)^{3/2}} S_{\rm eff}(E_0) \exp\left(-\frac{3E_0}{kT}\right) \tag{31}$$

with

$$S_{\rm eff}(E_0) = S(0)\left[1 + \frac{5}{12\tau} + \frac{\dot{S}(0)}{S(0)}\left(E_0 + \frac{35E_0}{12\tau}\right) + \frac{\ddot{S}(0)}{2S(0)}\left(E_0^2 + \frac{89E_0^2}{12\tau}\right)\right]. \tag{32}$$

The quantity E_0 defines the effective mean energy for thermonuclear fusion and is given by Eq. (13). The quantity τ is given by $\tau = 3E_0/kT$, and Δ is given by Eq. (13).

3.2.4. Resonances

For the case of resonances, where E_r is the resonance energy, we can approximate $\sigma(E)$ by a Breit–Wigner resonance formula,

$$\sigma_{\rm r}(E) = \frac{\pi\hbar^2}{2\mu E} \frac{(2J_R + 1)}{(2J_a + 1)(2J_b + 1)} \frac{\Gamma_p \Gamma_\gamma}{(E_{\rm r} - E)^2 + (\Gamma_{\rm tot}/2)^2}, \tag{33}$$

where J_R, J_a, and J_b are the spins of the resonance and the nuclei a and b, respectively, and the total width $\Gamma_{\rm tot}$ is the sum of the particle decay partial width Γ_p and the γ-ray partial width Γ_γ. The particle partial width, or entrance channel width, Γ_p, can be expressed in terms of the single-particle spectroscopic factor SF_i and the single-particle width $\Gamma_{\rm s.p.}$ of the resonance state, $\Gamma_p = SF_i \times \Gamma_{\rm s.p.}$. The single-particle width $\Gamma_{\rm s.p.}$ can be calculated from the scattering phase shifts of a scattering potential with the potential parameters being determined by matching the resonance energy. The γ partial widths Γ_γ are calculated from the reduced electromagnetic transition probabilities $B(J_i \to J_f; L)$ which carry the nuclear structure information of the resonance states and the final bound states. The reduced transition rates are usually computed within the framework of the nuclear shell model.

Most of the typical transitions are $M1$ or $E2$ transitions. For these, the relations are

$$\Gamma_{\rm E2}[{\rm eV}] = 8.13 \times 10^{-7}\, E_\gamma^5\, [{\rm MeV}] B(E2)\, [e^2{\rm fm}^4] \tag{34}$$

and

$$\Gamma_{\rm M1}[\text{eV}] = 1.16 \times 10^{-2}\, E_\gamma^3\ [\text{MeV}] B(M1)\ [\mu_N^2]. \tag{35}$$

For the case of narrow resonances, with width $\Gamma \ll E_r$, the Maxwellian exponent $\exp(-E/kT)$ can be taken out of the integral, and one finds

$$\langle \sigma v \rangle = \left(\frac{2\pi}{m_{ab}kT}\right)^{3/2} \hbar^2\, (\omega\gamma)_R \exp\left(-\frac{E_r}{kT}\right), \tag{36}$$

where the resonance strength is defined by

$$(\omega\gamma)_R = \frac{2J_R+1}{(2J_a+1)(2J_b+1)}\ (1+\delta_{ab})\ \frac{\Gamma_p\,\Gamma_\gamma}{\Gamma_{\rm tot}}. \tag{37}$$

For broad resonances, Eq. (12) is usually calculated numerically. An interference term has to be added. The total capture cross-section is then given by [47]

$$\sigma(E) = \sigma_{\rm nr}(E) + \sigma_{\rm r}(E) + 2\,[\sigma_{\rm nr}(E)\sigma_{\rm r}(E)]^{1/2} \cos[\delta_{\rm R}(E)]. \tag{38}$$

In this equation $\delta_{\rm R}(E)$ is the resonance phase shift. Only the contributions with the same angular momentum of the incoming wave interfere in Eq. (38).

3.3. $\mathcal{R}$-matrix theory

Reaction rates dominated by the contributions from a few resonant or bound states are often extrapolated to energies of astrophysical interest in terms of $\mathcal{R}$- *or K-matrix* fits. The appeal of these methods rests on the fact that analytical expressions can be derived from underlying formal reaction theories that allow for a rather simple parameterization of the data. However, the relation between the parameters of the $\mathcal{R}$-matrix model and the experimental data (resonance energies and widths) is only quite indirect. The K-matrix formalism solves this problem, but suffers from other drawbacks [48].

3.4. Elastic and inelastic scattering reactions

In the $\mathcal{R}$-matrix formalism, the eigenstates of the nuclear Hamiltonian in the interior region of a nucleus are denoted by X_λ, with energy E_λ, and are required to satisfy the boundary condition

$$r\frac{{\rm d}X_\lambda}{{\rm d}r} + bX_\lambda = 0$$

at the channel radius $r = R$, where the constant b is a real number. The true nuclear wavefunction Ψ for the compound system is not stationary, but since the X_λ form a complete set, it is possible to expand Ψ in terms of X_λ, i.e.

$$\Psi = \sum_\lambda A_\lambda X_\lambda, \quad \text{where } A_\lambda = \int_0^R X_\lambda\ \Psi\, {\rm d}r.$$

The differential equations for Ψ and X_λ are (for s-wave neutrons)

$$-\frac{\hbar^2}{2m}\frac{{\rm d}^2\Psi}{{\rm d}r^2} + V\Psi = E\Psi \tag{39}$$

$$-\frac{\hbar^2}{2m}\frac{{\rm d}^2X_\lambda}{{\rm d}r^2} + VX_\lambda = E_\lambda X_\lambda, \quad r \le R. \tag{40}$$

Multiplying Eq. (39) by Ψ and Eq. (40) by X_λ, subtracting and integrating, we have

$$A_\lambda = \frac{1}{E-E_\lambda}\frac{\hbar^2}{2mR} X_\lambda(R)\left[R\Psi'(R) + b\Psi(R)\right],$$

where the prime indicates the differentiation with respect to r. This result, together with the definition of Ψ, gives

$$\Psi(R) = \mathcal{R}\left[R\Psi'(R) + b\Psi(R)\right] \tag{41}$$

where the function $\mathcal{R}$ relates the value of $\Psi(R)$ at the surface to its derivative at the surface:

$$\mathcal{R} = \frac{\hbar^2}{2mR}\sum_\lambda \frac{X_\lambda(R)\, X_\lambda(R)}{E_\lambda - E}. \tag{42}$$

Rearranging Eq. (41) we have $R\Psi'(R)/\Psi(R) = (1-b\mathcal{R})/\mathcal{R}$, which is just the logarithmic derivative $\mathcal{L}^I$ which can be used to determine the S-matrix element S_0 in terms of the $\mathcal{R}$ function. This gives

$$S_0 = \left[1 + \frac{2ikR\mathcal{R}}{1-(b+ikR)\mathcal{R}}\right] {\rm e}^{-2ikR}.$$

Finally, we assume that E is near to a particular E_λ, say E_α, neglect all terms $\lambda \neq \alpha$ in Eq. (42), and define

$$\Gamma_\alpha = \frac{\hbar^2 k}{m} X_\alpha^2(R), \quad \text{and} \quad \Delta_\alpha = -\frac{b}{2kR}\Gamma_\alpha,$$

so that the S-matrix element becomes

$$S_0 = \left[1 + \frac{i\Gamma_\alpha}{(E_\alpha + \Delta_\alpha - E) - i\Gamma_\alpha/2}\right] e^{-2ikR} \tag{43}$$

and the scattering cross-section is

$$\sigma_{sc} = \frac{\pi}{k^2}\left|e^{2ikR} - 1 + \frac{i\Gamma_\alpha}{(E_\alpha + \Delta_\alpha - E) - i\Gamma_\alpha/2}\right|^2. \tag{44}$$

We see that the procedure of imposing the boundary conditions at the channel radius leads to isolated s-wave resonances of Breit–Wigner form. If the constant b is non-zero, the position of the maximum in the cross-section is shifted. The level shift does not appear in the simple form of the Breit–Wigner formula because $E_\alpha + \Delta_\alpha$ is defined as the resonance energy. In general, a nucleus can decay through many channels and when the formalism is extended to take this into account, the $\mathcal{R}$-function becomes a matrix. In this $\mathcal{R}$-matrix theory the constant b is real and $X_\lambda(R)$ and E_λ can be chosen to be real so that the eigenvalue problem is Hermitian [54].

The $\mathcal{R}$-matrix theory can be easily generalized to account for higher partial waves and spin-channels. If we define the reduced width by $\gamma_\lambda^2 = \hbar^2 X_\lambda^2(R)/2mR$, which is a property of a particular state and not dependent of the scattering energy E of the scattering system, we can write

$$\mathcal{R}_{\alpha\alpha'} = \sum_\lambda \frac{\gamma_{\lambda\alpha'}\gamma_{\lambda\alpha}}{E_\lambda - E},$$

where α is the channel label. $\gamma_{\lambda\alpha}$, E_λ, and b are treated as parameters in fitting the experimental data. If we write the wavefunction for any channel as $\Psi \sim I + S_\alpha O$, where I and O are incoming and outgoing waves, Eq. (41) means

$$R\frac{I'(R) + S_\alpha O'(R)}{I(R) + S_\alpha O(R)} = \frac{1 - b\mathcal{R}}{\mathcal{R}}.$$

Thus, as in Eq. (43), the S-matrix is related to the $\mathcal{R}$-matrix and from the above relation we obtain that,

$$S_\alpha = \frac{I(R)}{O(R)}\left[\frac{1 - (\mathcal{L}^I)^*\mathcal{R}}{1 - \mathcal{L}^I\mathcal{R}}\right]. \tag{45}$$

The total cross-sections for states with angular momenta and spins given by l, s and J is

$$\sigma_{\alpha\alpha'} = \frac{\pi}{k_\alpha^2}\sum_{JJ'll'ss'} g_J\left|S_{\alpha Jls,\alpha' J'l's'}\right|^2, \quad \alpha \neq \alpha', \tag{46}$$

where g_J are spin geometric factors.

In the statistical model, it can be argued that because the S-matrix elements vary rapidly with energy, the statistical assumption implies that there is a random phase relation between the different components of the S-matrix. The process of energy averaging then eliminates the cross terms and gives

$$\sigma_{abs} = \sum_{\alpha'\neq\alpha, J'l's'}\sigma_{\alpha\alpha'} = \frac{\pi}{k_\alpha^2}\sum_{Jls} g_J\left[1 - \left|S_{\alpha Jls}\right|^2\right] = \frac{\pi}{k_\alpha^2}\sum_{Jls} g_J T_{ls}^J(\alpha), \tag{47}$$

where the symmetry properties of the S-matrix in the form $\sum_{\alpha'\neq\alpha,\mathcal{J}'} S_{\alpha\mathcal{J},\alpha'\mathcal{J}'} S^*_{\alpha\mathcal{J},\alpha'\mathcal{J}'} = 1$ with $\mathcal{J} = Jls$, $\mathcal{J}' = J'l's'$ have been used, and we have introduced the general definition of the transmission coefficient

$$T_{ls}^J(\alpha) = 1 - \left|S_{\alpha Jls}\right|^2. \tag{48}$$

3.5. Radiative capture reactions

Consider an $\mathcal{R}$-matrix calculation of the radiative capture reaction $n + x \to a + \gamma$ to a state of nucleus a with a given spin J_f. The cross-section can be written as [55] $\sigma_{J_f} = \sum_{J_i}\sigma_{J_i J_f}$, with

$$\sigma_{J_i J_f} = \frac{\pi}{k^2}\frac{2J_i + 1}{(2J_n + 1)(2J_x + 1)}\sum_{Il_i}|T_{Il_i J_f J_i}|^2. \tag{49}$$

Here, J_i is the total angular momentum of the colliding nuclei n and x in the initial state, J_n and J_x are their spins, and I, k, and l_i are their channel spin, wave number and orbital angular momentum in the initial state. $T_{Il_i J_f J_i}$ is the transition amplitude from the initial continuum state (J_i, I, l_i) to the final bound state (J_f, I). In the one-level, one-channel approximation, the resonant amplitude for the capture into the resonance with energy E_{R_n} and spin J_i, and subsequent decay into the bound

state with the spin J_f can be expressed as

$$T^R_{Il_iJ_fJ_i} = -\mathrm{i}e^{\mathrm{i}(\sigma_{l_i}-\phi_{l_i})}\frac{[\Gamma^{J_i}_{bll_i}(E)\Gamma^{J_i}_{\gamma J_f}(E)]^{1/2}}{E-E_{R_n}+\mathrm{i}\frac{\Gamma_{J_i}}{2}}. \tag{50}$$

Here we assume that the boundary parameter is equal to the shift function at the resonance energy and ϕ_{l_i} is the hard-sphere phase shift in the l_ith partial wave,

$$\phi_{l_i} = \arctan\Big[\frac{F_{l_i}(k,r_c)}{G_{l_i}(k,r_c)}\Big], \tag{51}$$

where F_{l_i} and G_{l_i} are the regular and irregular Coulomb functions, r_c is the channel radius, and σ_{l_i} is the Coulomb phase factor, $\sigma_{l_i} = \sum_{k=1}^{l_i}\arctan(\eta_i/k)$, where η_i is the Sommerfeld parameter. $\Gamma^{J_i}_{nll_i}(E)$ is the observable partial width of the resonance in the channel $n+x$, $\Gamma^{J_i}_{\gamma J_f}(E)$ is the observable radiative width for the decay of the given resonance into the bound state with the spin J_f, and $\Gamma_{J_i} \approx \sum_l \Gamma^{J_i}_{nll_i}$ is the observable total width of the resonance level. The energy dependence of the partial widths is determined by

$$\Gamma^{J_i}_{nll_i}(E) = \frac{P_{l_i}(E)}{P_{l_i}(E_{R_n})}\Gamma^{J_i}_{nll_i}(E_{R_n}) \tag{52}$$

and

$$\Gamma^{J_i}_{\gamma J_f}(E) = \left(\frac{E+\varepsilon_f}{E_{R_n}+\varepsilon_f}\right)^{2L+1}\Gamma^{J_i}_{\gamma J_f}(E_{R_n}), \tag{53}$$

where $\Gamma^{J_i}_{nll_i}(E_{R_n})$ and $\Gamma^{J_i}_{\gamma J_f}(E_{R_n})$ are the experimental partial and radiative widths, ε_f is the binding energy of the bound state in nucleus a, and L is the multipolarity of the γ-ray transition. The penetrability $P_{l_i}(E)$ is expressed as

$$P_{l_i}(E) = \frac{kr_c}{F^2_{l_i}(k,r_c)+G^2_{l_i}(k,r_c)}. \tag{54}$$

The non-resonant amplitude can be calculated by

$$\begin{aligned} T^{NR}_{Il_iJ_fJ_i} &= -(2)^{3/2}\mathrm{i}^{l_i+L-l_f+1}e^{\mathrm{i}(\sigma_{l_i}-\phi_{l_i})}\frac{(\mu_{nx}k_\gamma r_c)^{L+1/2}}{\hbar k}e_L\sqrt{\frac{(L+1)(2L+1)}{L[(2L+1)!!]^2}}C_{J_fll_f}F_{l_i}(k,r_c) \\ &\quad\times G_{l_i}(k,r_c)W_{l_f}(2\kappa r_c)\sqrt{P_{l_i}}(l_i0L0|l_f0)U(Ll_fJ_iI;\,l_iJ_f)J'_L(l_il_f), \end{aligned} \tag{55}$$

where, e_L is the effective charge, U is a geometric coefficient, and

$$J'_L(l_il_f) = \frac{1}{r_c^{L+1}}\int_{r_c}^{\infty}\mathrm{d}r\,r\frac{W_{l_f}(2\kappa r)}{W_{l_f}(2\kappa r_c)}\left[\frac{F_{l_i}(k,r)}{F_{l_i}(k,r_c)}-\frac{G_{l_i}(k,r)}{G_{l_i}(k,r_c)}\right]. \tag{56}$$

$W_l(2\kappa r)$ is the Whittaker hypergeometric function, $\kappa = \sqrt{2\mu_{nx}\varepsilon_f}$ and l_f are the wave number and relative orbital angular momentum of the bound state, and $k_\gamma = (E+\varepsilon_f)/\hbar c$ is the wave number of the emitted photon.

The non-resonant amplitude contains the radial integral ranging only from the channel radius r_c to infinity since the internal contribution is contained within the resonant part. Furthermore, the $\mathcal{R}$-matrix boundary condition at the channel radius r_c implies that the scattering of particles in the initial state is given by the hard sphere phase. Hence, the problems related to the interior contribution and the choice of incident channel optical parameters do not occur. Therefore, the direct capture cross-section only depends on the ANC and the channel radius r_c.

The $\mathcal{R}$-matrix method described above can be extended to the analysis of other types of reactions, e.g. transfer reactions [56]. The goal of the $\mathcal{R}$-matrix method is to parameterize some experimentally known quantities, such as cross-sections or phase shifts, with a small number of parameters, which are then used to extrapolate the cross-section down to astrophysical energies. One example is given in Fig. 6 which shows the experimental data and $\mathcal{R}$-matrix fits for the cross-section of the reaction $^{12}\mathrm{C}(\alpha,\gamma)^{16}\mathrm{O}$ cross-section, of relevance to helium burning [53].

3.6. Statistical models

A large fraction of the reactions of interest proceed through compound systems that exhibit high enough level densities for statistical methods to provide a reliable description of the reaction mechanism. The theoretical treatment of nuclear reactions leading to formation and decay of compound nuclei was developed by Ewing and Weisskopf [57], based on two ideas: (a) the compound nucleus formation independence hypothesis as proposed by Niels Bohr [58], and (b) the reciprocity

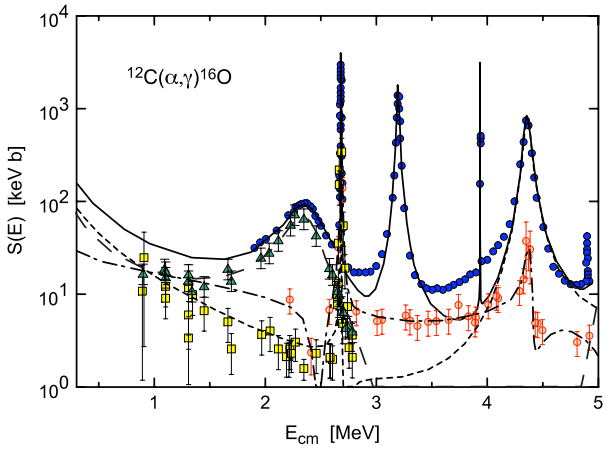

Fig. 6. Total S factor data (filled-in circles) [49] for $^{12}C(\alpha,\gamma)^{16}O$ compared with E1 (open triangles) and E2 (open squares) contributions [50,51]. The solid line represents the sum of the single amplitudes of an $\mathcal{R}$-matrix fit [26] (the dotted and dashed lines are the $E1$ and $E2$ amplitudes, respectively). In addition, the $\mathcal{R}$ matrix fit of [52] to their data (dotted-dashed line) is shown. (Adapted from Ref. [53]).

theorem, or time-reversal properties of the underlying Hamiltonian. This allows one to relate capture and decay cross-sections, usually expressed in terms of transmission probabilities, defined in Eq. (48).

Later, the Ewing–Weisskopf theory was extended to include angular momentum dependence by Hauser and Feshbach [59]. The Hauser–Feshbach (HF) model has been widely used with considerable success in nuclear astrophysics. Explosive burning in supernovae involves in general intermediate mass and heavy nuclei. Due to a large nucleon number, they have intrinsically a high density of excited states. A high level density in the compound nucleus at the appropriate excitation energy allows for the use of the statistical-model approach for compound nuclear reactions [59] which averages over resonances.

A high level density in the compound nucleus also allows for the use of averaged transmission coefficients T, which do not reflect resonance behavior, but rather describe absorption via an imaginary part of the (optical) nucleon–nucleus potential as described in Ref. [60]. This leads to the expression derived

$$\sigma_i^{\mu\nu}(j,o;E_{ij}) = \frac{\pi\,\hbar^2/(2\mu_{ij}E_{ij})}{(2J_i^\mu+1)(2J_j+1)}\sum_{J,\pi}(2J+1)\frac{T_j^\mu(E,J,\pi,E_i^\mu,J_i^\mu,\pi_i^\mu)T_o^\nu(E,J,\pi,E_m^\nu,J_m^\nu,\pi_m^\nu)}{T_{tot}(E,J,\pi)} \tag{57}$$

for the reaction $i^\mu(j,o)m^\nu$ from the target state i^μ to the excited state m^ν of the final nucleus, with a center of mass energy E_{ij} and reduced mass μ_{ij}. J denotes the spin, E the corresponding excitation energy in the compound nucleus, and π the parity of excited states. When these properties are used without subscripts they describe the compound nucleus, subscripts refer to states of the participating nuclei in the reaction $i^\mu(j,o)m^\nu$ and superscripts indicate the specific excited states. Experiments measure $\sum_\nu \sigma_i^{0\nu}(j,o;E_{ij})$, summed over all excited states of the final nucleus, with the target in the ground state. Target states μ in an astrophysical plasma are thermally populated and the astrophysical cross section $\sigma_i^*(j,o)$ is given by

$$\sigma_i^*(j,o;E_{ij}) = \frac{\sum_\mu(2J_i^\mu+1)\exp(-E_i^\mu/kT)\sum_\nu\sigma_i^{\mu\nu}(j,o;E_{ij})}{\sum_\mu(2J_i^\mu+1)\exp(-E_i^\mu/kT)}. \tag{58}$$

The summation over ν replaces $T_o^\nu(E,J,\pi)$ in Eq. (57) by the total transmission coefficient

$$T_o(E,J,\pi) = \sum_{\nu=0}^{\nu_m} T_o^\nu(E,J,\pi,E_m^\nu,J_m^\nu,\pi_m^\nu) + \int_{E_m^{\nu_m}}^{E-S_{m,o}}\sum_{J_m,\pi_m} T_o(E,J,\pi,E_m,J_m,\pi_m)\rho(E_m,J_m,\pi_m)\mathrm{d}E_m. \tag{59}$$

Here $S_{m,o}$ is the channel separation energy, and the summation over excited states above the highest experimentally known state ν_m is changed to an integration over the level density ρ. The summation over target states μ in Eq. (58) has to be generalized accordingly.

The important ingredients of statistical-model calculations, as indicated in the above equations, are the particle and γ-transmission coefficients T and the level density of excited states ρ. Therefore, the reliability of such calculations is determined by the accuracy with which these components can be evaluated (often for unstable nuclei).

Fig. 7 – adapted from Ref. [65] – shows the cross-section data for two sets of $^{75}As(p,n)$ measurements (squares: [61]; circles: [62]) in comparison with Hauser–Feshbach predictions (solid line: [63]). Also shown is the experimental cross-section of $^{85}Rb(p,n)$ (crosses with error bars: [64]) in comparison with HF predictions (dashed line: [63]). The experimental results are on average lower than the HF predictions.

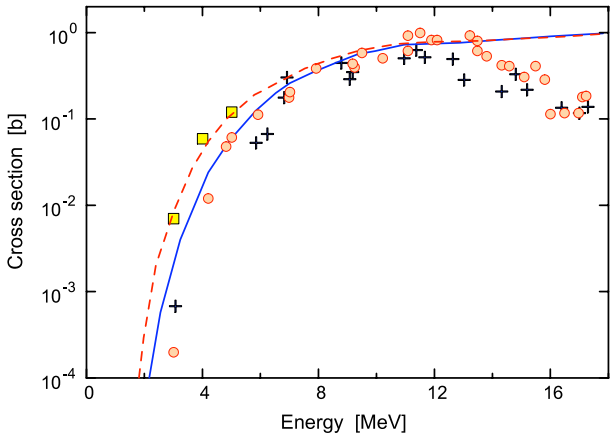

Fig. 7. Cross-section data for two sets of ^{75}As(p, n) measurements (squares: [61]; circles: [62]) in comparison with Hauser–Feshbach predictions (solid line: [63]). Also shown is the experimental cross-section of ^{85}Rb(p, n) (crosses with error bars: [64]) in comparison with HF predictions (dashed line: [63]). (Adapted from Ref. [65]).

3.7. Spin–isospin response

Beta-decay, electron capture and neutrino scattering involve similar operators and nuclear matrix elements. We thus consider only the case of neutrino scattering. In the following, $p_\ell \equiv \{\mathbf{p}_\ell, E_\ell\}$ and $q_\nu \equiv \{\mathbf{q}, E_\nu\}$ are the lepton and the neutrino momenta, $k = P_i - P_f \equiv \{\mathbf{k}, k_\emptyset\}$, is the momentum transfer, P_i and P_f are momenta of the initial and final nucleus, M is the nucleon mass, m_ℓ is the mass of the charged lepton, and g_V, g_A, g_M and g_P are, respectively, the vector, axial-vector, weak-magnetism and pseudoscalar effective dimensionless coupling constants. Their numerical values are typically given by $g_V = 1, g_A = 1.26, g_M = \kappa_p - \kappa_n = 3.70$, and $g_P = g_A(2\mathrm{M}m_\ell)/(k^2 + \mathrm{m}_\pi^2)$.

For the neutrino–nucleus reaction the momentum transfer is $k = p_\ell - q_\nu$, and the corresponding cross-section reads

$$\sigma(E_\ell, J_f) = \frac{|\mathbf{p}_\ell| E_\ell}{2\pi} F(Z \pm 1, E_\ell) \int_{-1}^{1} \mathrm{d}(\cos\theta) \mathcal{T}_\sigma(\mathrm{q}, J_f),$$

where

$$F(Z \pm 1, E_\ell) = \frac{2\pi\eta}{\exp(2\pi\eta) - 1}, \quad \text{with } \eta = \frac{Z_\pm Z_e \alpha}{v_\ell},$$

is the Fermi function ($Z_\pm = Z + 1$, for neutrino, and $Z - 1$, for antineutrino), $\theta \equiv \hat{\mathbf{q}} \cdot \hat{\mathbf{p}}$ is the angle between the incident neutrino and ejected lepton, and the transition amplitude for initial (final) angular momentum $J_i(J_f)$ is

$$\mathcal{T}_\sigma(\kappa, J_f) = \frac{1}{2J_i + 1} \sum_{s_\ell, s_\nu} \sum_{M_i, M_f} \left| \langle J_f M_f | H_W | J_i M_i \rangle \right|^2.$$

One can cast the transition amplitude in the compact form [66][1]

$$\mathcal{T}_\sigma(\kappa, J_f) = \frac{4\pi G^2}{2J_i + 1} \sum_{\mathsf{J}} \left[\left| \langle J_f \| \mathsf{O}_{\emptyset \mathsf{J}} \| J_i \rangle \right|^2 \mathcal{L}_\emptyset + \sum_{\mathsf{M}=0\pm1} \left| \langle J_f \| \mathsf{O}_{\mathsf{M}\mathsf{J}} \| J_i \rangle \right|^2 \mathcal{L}_{\mathsf{M}} - 2\Re \left(| \langle J_f \| \mathsf{O}_{\emptyset \mathsf{J}} \| J_i \rangle \langle J_f \| \mathsf{O}_{0\mathsf{J}} \| J_i \rangle \right) \mathcal{L}_{\emptyset z} \right], \tag{60}$$

where $G = (3.04545 \pm 0.00006) \times 10^{-12}$ is the Fermi coupling constant (in natural units), and

$$\mathcal{L}_\emptyset = 1 + \frac{|\mathbf{p}| \cos\theta}{E_\ell}, \qquad \mathcal{L}_{\emptyset z} = \left(\frac{q_z}{E_\nu} + \frac{p_z}{E_\ell} \right),$$

$$\mathcal{L}_0 \equiv \mathcal{L}_z = 1 + \frac{2 q_z p_z}{E_\ell E_\nu} - \frac{|\mathbf{p}| \cos\theta}{E_\ell}, \qquad \mathcal{L}_{\pm1} = 1 - \frac{q_z p_z}{E_\ell E_\nu} \pm \left(\frac{q_z}{E_\nu} - \frac{p_z}{E_\ell} \right) S_1, \tag{61}$$

with

$$q_z = \hat{k} \cdot \mathbf{q} = \frac{E_\nu(|\mathbf{p}| \cos\theta - E_\nu)}{\kappa}, \qquad p_z = \hat{k} \cdot \mathbf{p} = \frac{|\mathbf{p}|(|\mathbf{p}| - E_\nu \cos\theta)}{\kappa}, \tag{62}$$

[1] The indices $\emptyset$ and z denote the time-component and the third-component of four-vectors, respectively.

being the z-components of the neutrino and lepton momenta, and $S_1 = \pm 1$ for neutrino scattering and antineutrino scattering, respectively.

Explicitly, the operators in (60) are

$$\begin{aligned} \mathsf{O}_{\emptyset \mathsf{J}} &= g_{\mathsf{V}} \mathcal{M}^{V}_{\mathsf{J}} + 2i\overline{g}_{\mathsf{A}} \mathcal{M}^{A}_{\mathsf{J}} + i(\overline{g}_{\mathsf{A}} + \overline{g}_{\mathsf{P1}}) \mathcal{M}^{A}_{z\mathsf{J}}, \\ \mathsf{O}_{\mathsf{MJ}} &= i(\delta_{\mathsf{Mz}} \overline{g}_{\mathsf{P2}} - g_{\mathsf{A}} + \mathsf{M}\overline{g}_{\mathsf{W}}) \mathcal{M}^{A}_{\mathsf{MJ}} + 2\overline{g}_{\mathsf{V}} \mathcal{M}^{V}_{\mathsf{MJ}} - \delta_{\mathsf{Mz}} \overline{g}_{\mathsf{V}} \mathcal{M}^{V}_{\mathsf{J}}, \end{aligned} \tag{63}$$

where $\hat{\mathbf{k}} = \mathbf{k}/\kappa$, $\kappa \equiv |\mathbf{k}|$, and the following short notation

$$\overline{g}_{\mathsf{V}} = g_{\mathsf{V}} \frac{\kappa}{2\mathsf{M}}; \qquad \overline{g}_{\mathsf{A}} = g_{\mathsf{A}} \frac{\kappa}{2\mathsf{M}}; \qquad \overline{g}_{\mathsf{W}} = (g_{\mathsf{V}} + g_{\mathsf{M}}) \frac{\kappa}{2\mathsf{M}}; \qquad \overline{g}_{\mathsf{P1}} = g_{\mathsf{P}} \frac{\kappa}{2\mathsf{M}} \frac{q_{\emptyset}}{\mathsf{m}_{\ell}}; \qquad \overline{g}_{\mathsf{P2}} = g_{\mathsf{P}} \frac{\kappa}{2\mathsf{M}} \frac{\kappa}{\mathsf{m}_{\ell}}, \tag{64}$$

has also been introduced. The elementary operators are given by

$$\begin{aligned} &\mathcal{M}^{V}_{\mathsf{J}} = j_{\mathsf{J}}(\rho) Y_{\mathsf{J}}(\hat{\mathbf{r}}); \qquad \mathcal{M}^{A}_{\mathsf{J}} = \kappa^{-1} j_{\mathsf{J}}(\rho) Y_{\mathsf{J}}(\hat{\mathbf{r}}) (\boldsymbol{\sigma} \cdot \boldsymbol{\nabla}); \\ &\mathcal{M}^{A}_{\mathsf{MJ}} = \sum_{\mathsf{L}} i^{\mathsf{J}-\mathsf{L}-1} F_{\mathsf{MLJ}} j_{\mathsf{L}}(\rho) \left[Y_{\mathsf{L}}(\hat{\mathbf{r}}) \otimes \boldsymbol{\sigma} \right]_{\mathsf{J}}; \qquad \mathcal{M}^{V}_{\mathsf{MJ}} = \kappa^{-1} \sum_{\mathsf{L}} i^{\mathsf{J}-\mathsf{L}-1} F_{\mathsf{MLJ}} j_{\mathsf{L}}(\rho) [Y_{\mathsf{L}}(\hat{\mathbf{r}}) \otimes \boldsymbol{\nabla}]_{\mathsf{J}}, \end{aligned} \tag{65}$$

where $\rho = \kappa r$. Notice that the initial and final states of the matrix elements in Eq. (60) involve an isospin unit change, and implicitly contain isospin operators $\tau_{\pm}$.

3.7.1. Fermi and Gamow–Teller matrix elements

Most reactions in typical stellar scenarios involve small momentum transfer such that $\rho \ll 1$. In this case, the angular dependence of the above operators becomes irrelevant. Using $j_m(\rho) \sim \delta_{m0}$ for the spherical Bessel functions in Eqs. (65) and after some algebra one can show that (for charged-current)

$$\mathcal{T}_{\sigma}(\kappa, J_f) \sim \mathcal{C} \left[\left| \left\langle J_f \| \sum_{k=1}^{A} \tau_{\pm}(k) \| J_i \right\rangle \right|^2 + g_A^2 \left| \left\langle J_f \| \sum_{k=1}^{A} \sigma(k) \tau_{\pm}(k) \| J_i \right\rangle \right|^2 \right], \tag{66}$$

where $\mathcal{C}$ is a function depending on the lepton and neutrino energies. The τ_+ operator corresponds to β^- decay and the τ_- to β^+ decay, so that $\tau_+ |n\rangle = |p\rangle$ and $\tau_- |p\rangle = |n\rangle$, changing a neutron into a proton and vice-versa.

The spin-independent and spin-dependent operators appearing on the right-hand side of the above equation are known as the Fermi and Gamow–Teller operators. The Fermi operator is the isospin raising/lowering operator: in the limit of good isospin, which typically is good to 5% or better in the description of low-lying nuclear states, it can only connect states within the same isospin multiplet. That is, it is capable of exciting only one state, the state identical to the initial state in terms of space and spin, but with $(T, M_T) = (T_i, M_{Ti} \pm 1)$ for β^- and β^+ decay, respectively.

Eq. (66) is only appropriate at the lowest-order expansion in ρ, when the nucleus responds like an elementary particle. Then we can characterize its response by its macroscopic quantum numbers, the spin and charge. The next-to-leading-order term of the expansion in powers of ρ probes the nucleus at shorter length scales. The operators in Eq. (65) are obtained by an expansion of the plane-wave lepton wavefunction, which, for not too large $\mathbf{k}$, becomes $\exp(i\mathbf{k} \cdot \mathbf{r}) \sim 1 + i\mathbf{k} \cdot \mathbf{r}$. Thus, the next term in the expansion includes a "first forbidden" term $\sum_{i=1}^{A} \mathbf{r}_i \tau_3(i)$ and similarly for the spin operator $\sum_{i=1}^{A} [\mathbf{r}_i \otimes \boldsymbol{\sigma}(i)]_{J=0,1,2} \tau_3(i)$. These operators generate collective radial excitations, leading to the so-called "giant resonance" excitations, with a typical excitation energy of 10–25 MeV. They tend to exhaust the Thomas–Reiche–Kuhn sum rule,

$$\sum_f \left| \langle f | \sum_{i=1}^{A} r(i) \tau_3(i) \, | \mathrm{i} \rangle \right|^2 \sim \frac{NZ}{A} \sim \frac{A}{4} \tag{67}$$

where the sum extends over a complete set of final nuclear states. The first-forbidden operators tend to dominate the cross-sections for scattering the high energy supernova neutrinos (ν_μ s and ν_τ s), with $E_\nu \sim 25$MeV, off light nuclei. It also follows from Eq. (67) that the cross-sections per target nucleon are roughly constant. This conclusion changes when high energy neutrinos, with high energy transfers, are considered.

The number of events detected for supernova explosions can be calculated as,

$$N_\alpha = N_t \int_0^\infty \mathcal{F}_\alpha(E_\nu) \cdot \sigma(E_\nu) \cdot \epsilon(E_\nu) \mathrm{d}E_\nu,$$

where the index $\alpha = \nu_e, \bar{\nu}_e, \nu_x$ and ($\nu_x = \nu_\tau, \nu_\mu, \bar{\nu}_\mu, \bar{\nu}_\tau$) indicates the neutrino or antineutrino type, N_t is the number of target nuclei, $\mathcal{F}_\alpha(E_\nu)$ is the neutrino flux, $\sigma(E_\nu)$ is the neutrino–nucleus cross section, $\epsilon(E_\nu)$ is the detection efficiency, and E_ν is the neutrino energy.

In Fig. 8 (from Reference [69]), we show calculations for the number of events of detected supernova neutrinos due to $(\nu_e + \bar{\nu}_e)$ interactions on ^{56}Fe, such as those performed in the KARMEN collaboration [71]. The N_e and $\tilde{N}_e$ are calculated as a function of the neutrino temperatures T_{ν_e} and T_{ν_x}, folding $\sigma_e(E_\nu)$ from different nuclear structure models with the neutrino

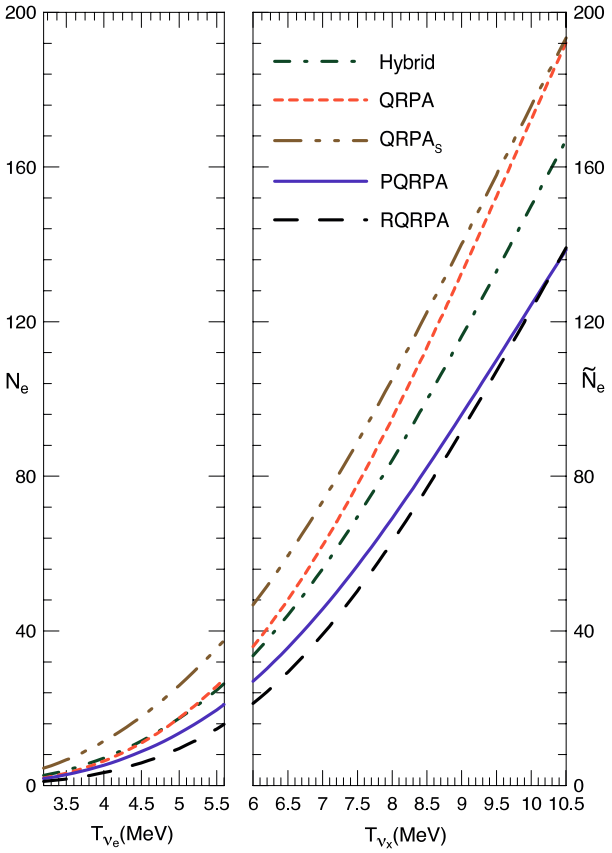

Fig. 8. Number of events obtained from the convolution of the neutrino fluxes with the cross-section obtained with different nuclear structure models: Hybrid (dashed–dot line) [67], quantum phase approximation (QRPA) (dashed line), QRPA$_S$ (dashed–dot dot line) [68], projected QRPA (PQRPA) (solid line) [69], and renormalized QRPA (RQRPA) (dashed line) [70]. (Adapted from Ref. [69]).

fluxes $\mathcal{F}_{\nu_e}(E_\nu, T_{\nu_e})$ and $\mathcal{F}_{\nu_x}(E_\nu, T_{\nu_x})$, respectively [72]. The fluxes depend on the distance to the supernova, the neutrino energy, and the neutrino effective temperature. The number of events is obtained from the convolution of the neutrino fluxes with the cross-section obtained with different nuclear-structure models: Hybrid (dashed–dot line) [67], quantum phase approximation (QRPA) (dashed line), QRPA$_S$ (dashed–dot dot line) [68], projected QRPA (PQRPA) (solid line) [69], and renormalized QRPA (RQRPA) (dashed line) [70]. One clearly sees that the differences between the calculated cross-sections with different nuclear models increase as a function of the neutrino temperatures. This is an example of the limitations of nuclear models in describing weak-interaction processes in stars.

3.8. Field theories

Field theories adopt a completely independent approach for nuclear physics calculations in which the concept of nuclear potentials is not used. The basic method of field theories is to start with a Lagrangian for the fields. From this Lagrangian one can "read" the Feynman diagrams and make practical calculations, not without bypassing well-known complications such as regularization and renormalization. Quantum chromodynamics (QCD) is the proper quantum field theory for nuclear physics. But it is a very hard task to bridge the physics from QCD to the one in low-energy nuclear processes. Effective field theory (EFT) tries to help in this construction by making use of the concept of the separation of scales. One can form small expansion parameters from the ratios of short and long distance scales, defined by

$$\epsilon = \frac{\text{short distance scales}}{\text{long distance scales}} \tag{68}$$

and try to explain physical observables in terms of powers of ϵ.

In low-energy nuclear processes, the characteristic momenta are much smaller than the mass of the pion, which is the lightest hadron that mediates the strong interaction. In this regime, one often uses the pionless effective field theory, in which pions are treated as heavy particles and are integrated out of the theory [73]. In this theory, the dynamical degrees of freedom are nucleons and the pion and the delta resonance degrees of freedom are hidden in the contact interactions between nucleons. The scales of the problem are the nucleon–nucleon scattering length, a, the binding energy, B, and

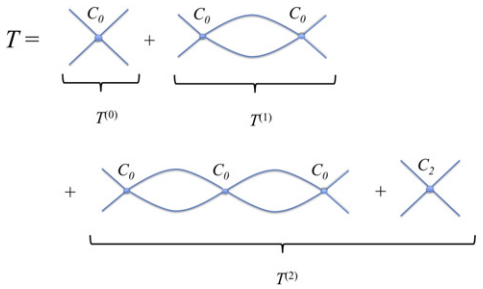

Fig. 9. Feynman diagram series for *NN*-scattering in pionless effective field theory.

the typical nucleon momentum k in the center-of-mass frame. Then, the nucleon–nucleon interactions are calculated perturbatively with the small expansion parameter

$$p = \frac{(1/a, B, k)}{\Lambda} \tag{69}$$

which is the ratio of the light to the heavy scale. The heavy scale Λ is set by the pion mass ($m_\pi \sim 140$ MeV).

The pionless effective Lagrangian will only involve the nucleon field $\Psi^T = (p, n)$ and its derivatives. It must obey the symmetries observed in strong interactions at low energies, such as parity, time-reversal, and Galilean invariance. The Lagrangian can then be written as a series of local operators with increasing dimensions. In the limit where the energy goes to zero, the interactions of lowest dimension dominate. To leading order (*LO*), the relevant Lagrangian ($\hbar = c = 1$) is given by

$$\mathcal{L} = \Psi^\dagger \left(\mathrm{i}\partial_t + \frac{\nabla^2}{2m} \right) \Psi - C_0 (\Psi^T \mathcal{P} \Psi)(\Psi^T \mathcal{P} \Psi)^\dagger, \tag{70}$$

where m is the nucleon mass [74]. The projection operators $\mathcal{P}$ enforce the correct spin and isospin quantum numbers in the channels under investigation. For spin-singlet interactions $\mathcal{P}_i = \sigma_2 \tau_2 \tau_i / \sqrt{8}$, while for spin-triplet interactions $\mathcal{P}_i = \sigma_2 \sigma_i \tau_2 / \sqrt{8}$.

The Feynman-diagram rules can be directly "read" from the Lagrangian at hand. In the case that the scattering length a is large, i.e., $a \gg 1/\Lambda$, as it is in the nucleon–nucleon system, the full scattering amplitude T is obtained from an infinite sum of such Feynman diagrams (see Fig. 9), leading to a geometric series that can be written analytically as

$$T(p) = \frac{C_0}{1 - C_0 J(p)}, \qquad J(p) = \int \frac{\mathrm{d}^3 q}{(2\pi)^3} \frac{1}{E - \mathbf{q}^2/m + \mathrm{i}\epsilon}, \tag{71}$$

where $E = p^2/m$ is the total center-of-mass energy (see, e.g., Ref. [75]). The integral is linearly divergent but is finite using *dimensional regularization*. One gets

$$J = -(\mu + \mathrm{i}p) \frac{m}{4\pi},$$

where μ is the regularization parameter. The scattering amplitude $T(p)$ has then the same structure as the s-wave partial-wave amplitude,

$$T = -\frac{4\pi}{p \cot \delta - \mathrm{i}p},$$

and one obtains the effective range expansion for the phase shift δ,

$$p \cot \delta = -\frac{1}{a} + r_0 \frac{p^2}{2} + \cdots$$

in the zero-momentum limit when the coupling constant takes the renormalized value

$$C_0(\mu) = \frac{4\pi}{m} \frac{1}{(1/a - \mu)}. \tag{72}$$

In leading order, we see that the effective range vanishes, or $r_0 = 0$. The small inverse $1/a$ scattering length is given by the difference between two large quantities. For example, in proton–neutron scattering we have $a_{pn} = -23.7$ fm in the pn spin-singlet channel. Choosing the value $\mu = m_\pi$ for the regularization parameter, one obtains $C_0 = 3.54$ fm^2. Physical results should be independent of the exact value of the renormalization mass μ as long as $1/a < \mu \ll m_\pi$.

The theory is now ready for practical applications. For example, this procedure has been applied to obtain the electromagnetic form factor of the deuteron, the electromagnetic polarizability and the Compton scattering cross-section

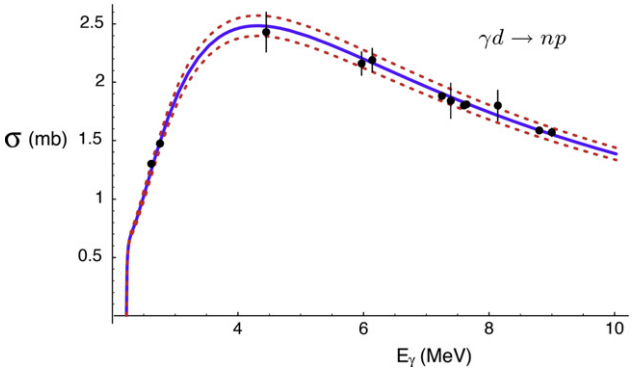

Fig. 10. The cross-section for $d \rightarrow np$. The curves correspond to EFT calculations for cold $np \rightarrow d$ and the dashed lines denote the a 3% theoretical uncertainty. Ref. [76] has further reduced this uncertainty to below 1%. (Adapted from Ref. [76]).

for the deuteron, the radiative neutron capture on protons, and the continuum structure of halo nuclei. Based on the same effective field theory, the three-nucleon system and neutron–deuteron scattering have been investigated [75]. Better agreement with data can be obtained in higher orders (next-to-leading order [*NLO*], next-to-next-to leading order [N^2LO], etc.). For nuclear processes involving momenta p comparable to m_π, the starting effective, pionfull, Lagrangian is more complicated. But the basic field theoretic method remains the same. The EFT unifies single-particle approaches in a model-independent framework, with the added power counting that allows for an a priori estimate of errors. Concepts of quantum field theory, such as regularization and renormalization, are key ingredients of the theory.

In nuclear astrophysics, this theory has been applied to $np \rightarrow d\gamma$ for big-bang nucleosynthesis [77,76]; νd reactions for supernovae physics [78] and the solar pp fusion process [79]. EFT has also been used to deduce observables in reactions with halo nuclei and loosely bound states, with promising applications to astrophysics [80–82]. So far, perhaps the most enlightening application of EFT for nuclear physics is the $np \rightarrow d\gamma$ cross-section, specially because there is no data at the energies of relevance for the big bang nucleosynthesis (BBN). EFT has provided a calculation with 1% error [76] in the energy range relevant to BBN. The EFT predictions also agree with a very recent measurement of the inverse process in the same energy region (see Fig. 10).

4. Effects of environment electrons

The form of the astrophysical S factor given in Eq. (11) assumes that the electric charges of nuclei are "bare" charges. However, neither at very low laboratory energies, nor in stellar environments is this the case. In stars, the bare Coulomb interaction between the nuclei is screened by the electrons in the plasma surrounding them. If one measures reaction rates in the laboratory, using atomic targets (always), then atomic electrons screen as well. But the screening is different from the screening in the stellar plasma. Therefore we discuss these two problems separately in the following subsections.

4.1. Stellar electron screening problem

In astrophysical plasmas with high densities and/or low temperatures, effects of electron screening are very important, as will be discussed later. This means that the reacting nuclei, due to the background of electrons and nuclei, feel a different Coulomb repulsion than in the case of bare nuclei. Under most conditions (with non-vanishing temperatures), the generalized reaction-rate integral can be separated into the traditional expression without screening (4) and a screening factor

$$\langle \sigma \mathrm{v} \rangle^*_{j,k} = f_{scr}(Z_j, Z_k, \rho, T, Y_i)\, \langle \sigma \mathrm{v} \rangle_{j,k}\,, \tag{73}$$

in terms of the nuclear abundances, defined in Section 2.2.

This screening factor is dependent on the charge of the involved particles, the density, temperature, and the composition of the plasma. At high densities and low temperatures, screening factors can enhance reactions by many orders of magnitude and lead to pycnonuclear ignition.

Consider a concentration of negative and positive charges with neutral total charge, that is, $\sum_i Z_i e c_{i0} = 0$, where c_{i0} is the spatially uniform concentration of positive ($i = +$) or negative ($i = -$) charges. Because of the interaction between the charges, these concentrations are no more spatially uniform, with smaller charges tending to concentrate around larger charges.

The concentrations around the charges are populated according to the statistical distribution of the individual charge energies in the presence of a Coulomb field $V(r)$, yet to be found. Assuming Boltzmann statistics, this argumentation implies

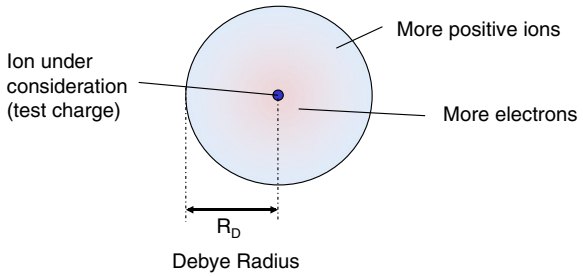

Fig. 11. Schematic view of the Debye–Hückel sphere. An ion at the center of the sphere is surrounded by a cloud of ions, with the ions of opposite charge (electrons) agglomerating closer to it.

that

$$c_+(r) = c_{+0}\exp\left[-\frac{Z_+eV(r)}{kT}\right] \quad \text{and} \quad c_-(r) = c_{-0}\exp\left[-\frac{Z_-eV(r)}{kT}\right]. \tag{74}$$

If the ion close to which we are considering the screening is positive, then $V(r) > 0$ and $c_+(r) < c_{+0}$, or $c_-(r) > c_{-0}$, and the reverse is true if $V(r) < 0$.

The charge density at position r is given by

$$\rho(r) = \sum_i Z_i e c_i = \sum_i Z_i e c_{i0}\exp\left[-\frac{Z_i eV(r)}{kT}\right]. \tag{75}$$

If $Z_i eV(r)/kT \ll 1$ (*weak screening*), then $\rho(r) = -(e^2V(r)/kT)\sum_i Z_i^2 c_{i0}$.

To obtain the potential $V(r)$ one has to solve the Poisson equation for the potential $V(r)$ which, for the above charge distribution, becomes

$$-\frac{1}{r^2}\frac{\mathrm{d}}{\mathrm{d}r}\left[r^2\frac{\mathrm{d}V}{\mathrm{d}r}\right] = 4\pi\rho(r) = \left(\frac{1}{R_D}\right)^2 V,$$

where the *Debye radius* R_D is defined by

$$R_D^2 = \frac{kT}{4\pi e^2\sum_i Z_i^2 c_{i0}}. \tag{76}$$

Since $V(r) \to 0$ as $r \to \infty$, the solution of this equation is $V(r) = (A/r)\exp(-r/R_D)$. The normalization constant is fixed by the condition $V(r) \to Z_i e/r$ as $r \to 0$. Thus,

$$V(r) = \frac{Z_i e}{r}\exp\left(-\frac{r}{R_D}\right). \tag{77}$$

Screening modifies the Coulomb potential between the nuclear radius R and the classical turning point R_0, and consequently modifies the barrier penetration. For weak screening $R_D \gg R, R_0$. In other words, we can expand $V(r)$ around $r = 0$. To first order, the barrier energy for an incoming projectile with charge Z_2e is $V(r) = Z_1Z_2e^2/r + U(r)$, where the Debye-Hueckel *screening potential*, $U(r) = U(0) = const.$, is given by $U_0 = -Z_1Z_2e^2/R_D$.

The impact of the screening potential on the barrier penetrability and therefore on the astrophysical reaction rates can be approximated through a screening factor $f = \exp(U_0/kT)$, which, in the weak screening limit, becomes $f \simeq 1 - U_0/kT$.

In summary, for the weak screening limit, the reaction rates are modified according to

$$\langle\sigma v\rangle_{screened} = f\langle\sigma v\rangle_{bare} \tag{78}$$

where

$$f = 1 + 0.188\frac{Z_1Z_2\rho^{1/2}\xi^{1/2}}{T_6^{3/2}}, \quad \text{where } \xi = \sum_i (Z_i^2 + Z_i)^2 Y_i. \tag{79}$$

The Debye–Hückel model (Fig. 11) is an ideal plasma since the average interaction energy between particles is smaller than the average kinetic energy of a particle [83,84]. In the case of *strong screening*, in low density plasmas, the potential energy cannot not be described by the Debye–Hückel model since the probability of finding other charged particles in a Debye sphere almost vanishes. For a strongly coupled plasma, the ion-sphere model [85,86] is more suitable. The ion-sphere model is equivalent to the *Wigner–Seitz sphere* used in condensed-matter theory. It assumes an ion having Z_b bound electrons, positioned at $r = 0$, and Z_f free electrons ($Z_b + Z_f = Z$) occupying the rest of the ion sphere volume. The plasma effects

are taken into account by confining the ion and the Z_f electrons inside the ion sphere. To obtain the potential $V(r)$ one adds to the bare ion potential, $V = Ze^2/r$, the potential due to bound electrons, V_b, and that due to free electrons, V_f. A Slater type, or Kohn–Sham type, exchange-potential is also added. To obtain the bound and free electron densities one solves the Schrödinger equation, or Dirac equation, with $V(r)$. From this, one builds the bound and free electron densities which are then used to calculate the new potentials V_b and V_f. This process is done iteratively until convergence is reached.

The plasma density enters the ion-sphere model through the boundary conditions imposed on the potential, that is, through the neutrality conditions of the ion-sphere. Approximate schemes to obtain the ion-sphere potential have been developed. A widely used approximation for the potential energy of a single free electron electron inside the ion-sphere is given by

$$V(\mathbf{r},\mathbf{r}') = \left(-\frac{Ze^2}{r} + \frac{e^2}{|\,\mathbf{r}-\mathbf{r}'\,|}\right)\left[1 - \frac{r}{2R_i}\left(3 - \frac{r^2}{R_i^2}\right)\right]\theta(R_i - r), \tag{80}$$

where $\mathbf{r}$ and $\mathbf{r}'$ are the positions of the bound electron and the projectile ion, respectively, $\theta(R_i - r)$ is the step function, the ion-sphere radius $R_i(= [3(Z-1)/4\pi n_e]^{1/3})$ is given by the plasma electron density n_e since the total charge within the ion-sphere is neutral. This hydrogenic ion-sphere potential (80) can be generalized to Z_f free electrons inside the ion-sphere. The ion-sphere model also has its limitations. For instance, charge transfer processes in collisions between positive ions in strongly coupled plasmas has not been fully explored and could modify the range of validity of the model [87].

For screening in plasmas with intermediate densities, i.e., when $n_eR \approx 1$, where $R = R_i$ or $R = R_D$, more complicated models are necessary and are still under theoretical scrutiny. This is based on the simple observation that in the stars along the main sequence, there are only about 1–3 ions within the Debye sphere. Thus, in principle, the Debye screening model should not be applicable to screening in these environments. Also, static models as the Debye–Hückel and ion-sphere models do not contain dynamical effects due to the fast motion of free electrons. Dynamical fluctuations, due to the fast motion of the electrons, and non-spherical effects could modify the screening in non-static models. The possibility of dynamic effects was first mentioned in Ref. [88] and studied in Ref. [89]. But, the existence of dynamic effects was criticized since the reacting particles are in thermodynamic equilibrium and hence such an effect is not expected [90]. According to Ref. [91], higher order effects, beyond the Debye–Hückel approximation, modify the screening enhancement in solar fusion reactions by only a very small amount of about 1%. This conclusion is not in accord with results obtained by other authors [92,87].

More recently, there have been additional claims that mean field models cease to be valid under the conditions prevailing in stellar cores in general and in the Sun, because particle fluctuations within the Debye–Hückel sphere are percent-wise large. These claims have been substantiated with molecular dynamics calculations [92]. However, it has not been pursued further and has not been verified independently. This certainly deserves further theoretical studies.

4.2. Laboratory atomic screening problem

Laboratory screening has been studied in more detail experimentally, as one can control different charge states of the projectile + target system in the laboratory [93–95]. Experimental techniques improve steadily and one can measure fusion cross-sections at increasingly lower energies where the screened Coulomb potential can be significantly smaller than the bare Coulomb potential. The deviation from the bare Coulomb potential is seen as an increase in the astrophysical S-factor extracted at the lowest energies (see Fig. 12). This enhancement has been experimentally observed for a large number of systems [96–100]. The screening effects of the atomic electrons can be calculated [93] in the adiabatic approximation at the lowest energies and in the sudden approximation at higher energies with a smooth transition in between [101].

In the adiabatic approximation one assumes that the velocities of the electrons in the target are much larger than the relative motion between the projectile and the target nucleus. In this case, the electronic cloud adjusts to the ground-state of a "molecule" consisting of two nuclei separated by a time-dependent distance $R(t)$, at each time instant t. Since the closest-approach distance between the nuclei is much smaller than typical atomic cloud sizes, the binding energy of the electrons will be given by the ground-state energy of the $Z_P + Z_T$ atom, $B(Z_P + Z_T)$. Energy conservation implies that the relative energy between the nuclei increases by $U_e = B(Z_P + Z_T) - B(Z_T)$. This energy increment enhances the fusion probability because the tunneling probability through the Coulomb barrier between the nuclei increases accordingly. In other words, the fusion cross-section measured at laboratory energy E represents in fact a fusion cross-section at energy $E + U_e$, with U_e being known as the *screening potential*. Using Eq. (11), one gets for non-resonant reactions

$$\sigma(E + U_e) = \exp\left[\pi\eta(E)\frac{U_e}{E}\right]\sigma(E), \tag{81}$$

where we assumed that the factor $S(E)/E$ varies much slower with E, as compared to the energy dependence of $\exp[-2\pi\eta(E)]$.

The exponential factor on the right-hand side of Eq. (81) is the enhancement factor due to screening by the atomic electrons in the target. For light systems, the velocity of the atomic electrons is comparable to the relative motion between the nuclei. Thus, a dynamical calculation is more appropriate to study the effect of atomic screening [101]. However, the screening potential U_e obtained from a dynamical calculation cannot exceed that obtained in the adiabatic approximation because the dynamical calculation includes atomic excitations, which reduce the energy transferred from the electronic binding to the relative motion. The adiabatic approximation is thus the *upper limit* of the enhancement due to laboratory screening.

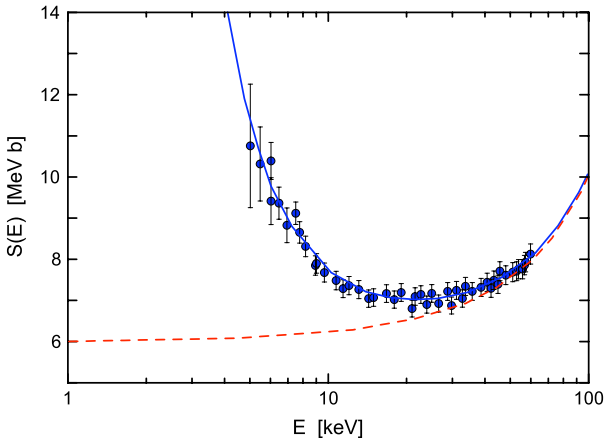

Fig. 12. S-factor data for the ^{3}He$(d, p)^4$He reaction from Ref. [102]. The dashed curve represents the S-factor for bare nuclei and the solid curve that for screened nuclei with $U_e = 219$ eV.

The experimental value of U_e needed to reproduce the experimental data by using Eq. (81) are systematically larger than the adiabatic model by a factor of 2 [93–95]. For example, the cross-section of the ^{3}He$(d, p)^4$He reaction was studied over a wide range of energies [102]: the results led to $U_e = 219 \pm 15$ eV, significantly larger than the adiabatic limit from atomic physics, $U_{ad} = 119$ eV. Many theoretical attempts to explain this puzzle have been carried out (see, e.g., Refs. [101,103–106]). The fusion cross-sections change exponentially with a small variation of the relative energy between the nuclei. Many small effects have been considered theoretically and, as shown in Ref. [103], they are not able to explain the differences between the experimental and theoretical values of U_e. The calculated fractional change in the cross-sections involving light nuclei at astrophysical energies are: (a) vacuum polarization (10^{-2}), (b) relativity (10^{-3}), (c) Bremsstrahlung (10^{-3}), (d) atomic polarization (10^{-5}) and nuclear polarization (10^{-10}) [103]. In Ref. [95] effects due to thermal motion, vibrations inside atomic, molecular or crystal systems, and due to a finite beam energy width were considered. All these effects are marginal at the energies, which are presently measurable (at the level of 10^{-3}, or below).

A possible solution of the laboratory screening problem was proposed in Refs. [107,108]. Experimentalists often use the extrapolation of the *Andersen–Ziegler* tables [109] to obtain the average value of the projectile energy due to stopping in the target material. The stopping is due to ionization, electron-exchange, and other atomic mechanisms. However, the extrapolation is challenged by theoretical calculations, which predict a lower stopping. Smaller stopping was indeed verified experimentally [95]. At very low energies, it is thought that the stopping mechanism is mainly due to electron exchange between projectile and target. This has been studied in Ref. [110] in the simplest situation; proton + hydrogen collisions. The calculated stopping power was added to the nuclear stopping power mechanism, i.e. to the energy loss by the Coulomb repulsion between the nuclei (Rutherford scattering). The obtained stopping power is shown to be smaller than the extrapolations from the Andersen–Ziegler, as verified experimentally by [111].

The stopping power in atomic $He^+ + He$ collisions using the two-center molecular orbital basis was calculated in Ref. [112], and a good agreement with the data of Ref. [111] at low energies was obtained. In particular, it was found that a threshold effect exists, sharply decreasing the stopping power at lower energies due to the disappearance of resonant tunneling in the electron-exchange mechanism. The agreement with the data disappears when the nuclear recoil is included. In fact, an unexpected "quenching" of the nuclear recoil was observed experimentally in Ref. [113], for stopping of deuteron projectiles on deuteron targets. But this cannot be explained in terms of a threshold cutoff effect and it seems to violate a basic principle of nature, as the nuclear recoil is due to Coulomb repulsion (Rutherford scattering) between projectile and target atoms. Energy loss due to Rutherford straggling is though to be well described theoretically [109]. The fusion reaction $d(d, p)t$ was recently studied in deuterated metals and insulators, i.e. for 58 samples across the periodic table, where a dramatic increase was observed for all the metals [114]. The experimentally determined values of the screening energy are about one order of magnitude larger than the value achieved in a gas-target experiment and significantly larger than the theoretical predictions [115]. This result has not been proven independently.

The present status of the laboratory screening of nuclear fusion reactions is rather confusing, and more research is obviously needed. However, for the solar fusion reaction chains, the effects of laboratory and stellar screening by electrons seem to be under control.

5. Solutions with indirect methods

5.1. Elastic scattering

Elastic scattering of nuclei is sensitive to their matter distribution. This is due to the dependence of the optical potential on the matter distribution of nuclei. Folding optical potentials, often used in the analysis of experiments, depend on the

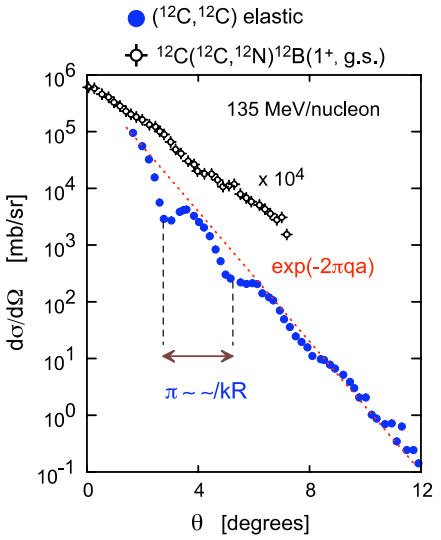

Fig. 13. Elastic scattering data for (^{12}C, ^{12}C) is shown [116,117], together with data for the inelastic scattering for the excitation of Gamow–Teller states in the ^{12}C(^{12}C, ^{12}N)^{12}B reaction at $E = 135$ MeV/nucleon.

nuclear projectile, P, and target, T, densities as

$$U_{opt} = (1 + \mathrm{i}\alpha) \int \rho_P(\mathbf{r}_1)\rho_T(\mathbf{r}_2)v_{eff}(\mathbf{r}_1, \mathbf{r}_2)\mathrm{d}^3r_1\mathrm{d}^3r_2, \tag{82}$$

where v_{eff} is the effective nucleon–nucleon interaction and α is a parameter to fit the imaginary normalization of the optical potential. Nuclear densities are a basic input in theoretical calculations of astrophysical reactions at low energies.

Elastic scattering in high-energy collisions essentially measures the Fourier transform of the matter distribution. Considering for simplicity the one-dimensional case, for light nuclei one has

$$\int \mathrm{e}^{\mathrm{i}qx}\rho(x)\mathrm{d}x \sim \int \mathrm{d}x \frac{\mathrm{e}^{\mathrm{i}qx}}{a^2 + x^2} = \frac{\pi}{a}\,\mathrm{e}^{-qa}, \tag{83}$$

where $q = 2k \sin\theta/2$, for a c.m. momentum k, and a scattering angle θ. For heavy nuclei, the density ρ is better described by a Fermi function, and

$$\int \mathrm{d}x \frac{\mathrm{e}^{\mathrm{i}qx}}{1 + \mathrm{e}^{(x-R)/a}} \sim (4\pi)\,\sin(qR)\,\mathrm{e}^{-\pi qa}, \tag{84}$$

for $R \gg a$, and $qa \gg 1$. A similar result emerges from the elastic scattering amplitude, $F(q)$, for the momentum transfer q, calculated in the eikonal approximation (see below), i.e.,

$$f_{\mathrm{el}}(q) \sim \int \mathrm{d}bbJ_0(qb)[1 - \mathrm{e}^{\mathrm{i}\chi(b)}] \sim \int \mathrm{d}bb \frac{J_0(qb)}{1 + \exp\left[\left(\frac{b-R}{a}\right)\right]} \sim \frac{R}{q}J_1(qR)\exp(-\pi qa),$$

where J_n are Bessel functions of order n. Thus, the distance between minima in elastic scattering cross-sections measures the nuclear size, while its exponential decay dependence reflects the surface diffuseness.

During recent years, elastic proton scattering has been one of the major sources of information on the matter distribution of unstable nuclei at radioactive beam facilities. Information on the matter distribution of many nuclei important for the nucleosynthesis in inhomogeneous Big Bang and in r-processes scenarios could also be obtained from elastic scattering experiments. Due to the loosely-bound character and small excitation energies of many of these nuclei, high energy resolution is often necessary. But the data deviate from this simple behavior as soon as the energy transfer, or Q-value, differs from zero, as manifest in the inelastic scattering data.

For low-energy nucleus–nucleus scattering, the distorted wave Born approximation (DWBA) amplitude is given by

$$f_{\mathrm{DWBA}}(\theta) = -\frac{\mu}{2\pi\,\hbar^2} \int \chi_\beta^{(-)^*}(\mathbf{k}', \mathbf{r})U_{opt}^{\alpha\beta}(\mathbf{r})\chi_\alpha^{(+)}(\mathbf{k}, \mathbf{r})\mathrm{d}^3r, \tag{85}$$

where μ is the reduced mass, $\chi_\beta^{(-)}$ ($\chi_\alpha^{(+)}$) are incoming (outgoing) distorted waves in channel α (β), and $U_{opt}^{\alpha\beta}$ is the optical potential.

Reactions with secondary beams have been studied at relatively high energies, $E_{\rm lab} \gtrsim 30$ MeV/nucleon. The distorted waves can be approximated by eikonal waves. This is valid for small-angle scattering and the scattering amplitude in the eikonal approximation is

$$f_{\rm el}(\theta) = {\rm i}k \int b{\rm d}bJ_0(qb)\left[1 - {\rm e}^{{\rm i}\phi(b)}\right] \tag{86}$$

where $k = \sqrt{2\mu E}/\hbar$ is the relative momentum, and

$$\phi(b) = \phi_C(b) + \phi_N(b), \qquad \phi_N(b) = -\frac{1}{\hbar {\rm v}} \int_{-\infty}^{\infty} {\rm d}zU\left[\sqrt{b^2 + z^2}\right], \tag{87}$$

is the nuclear eikonal phase and $\chi_C(b)$ is the Coulomb eikonal phase

$$\phi_C(b) = \frac{2Z_1Z_2e^2}{\hbar v} \ln(kb).$$

Optical potentials are usually parameterized in the form

$$U_N(r) = -V_R f_V(r) - {\rm i}W_R f_W(r) + 4{\rm i}a_I V_I \frac{\rm d}{{\rm d}r} f_W(r) + 2\left(\frac{\hbar}{m_\pi c}\right)^2 \frac{1}{r}\frac{\rm d}{{\rm d}r}\left[V_S f_S(r)\right](\boldsymbol{l}\cdot\boldsymbol{s}) + V_{\rm coul.} \tag{88}$$

where

$$f_i(r) = \frac{1}{1 + \exp[(r - R_i)/a_i]} \tag{89}$$

for $i = V, W$ and S; with $R_i = r_i A^{1/3}$. The first (second) term is the usual real (imaginary) part of the optical potential. The third term is peaked at the surface of the nucleus and is used to simulate a stronger absorption of the incoming nucleon at the surface of the nucleus. It is a correction due to the Pauli blocking effect. The last term in Eq. (88) is a spin–orbit correction. It causes interference between the scattering from opposite sides of the nucleus.

Sometimes one has to go beyond the optical model description of inelastic scattering and introduce the effects of polarization potentials. Under the action of a small interaction, a wavefunction is modified in lowest order to

$$|\psi_n'\rangle = |\psi_n\rangle + \sum_{m\neq n} \frac{\langle\psi_m|U|\psi_n\rangle}{E_n - E_m}|\psi_m\rangle. \tag{90}$$

If we assume that $|\psi_n\rangle$ is the ground state, this equation says that during the action of the potential U, the wavefunction acquires small components from excited states. At the end of this process, the wavefunction can return to its initial state again. The modification of the wavefunction during the action of the potential is called "polarization".

While elastic scattering data is considered a simpler way to access the sizes, density profile, and other geometric features of nuclei, inelastic scattering requires many more pieces of information about the intrinsic properties of nuclei. This is shown in Fig. 13, where the elastic scattering data for (^{12}C, ^{12}C) is shown [116,117] together with data for the inelastic scattering for the excitation of spin-dipole states in the ^{12}C(^{12}C, ^{12}N)^{12}B reaction at $E = 135$ MeV/nucleon. The beautiful exponential decrease of the cross-section with the nuclear diffuseness is clearly seen for the elastic scattering data. The inelastic data is much more sensitive to the models used to describe the nuclear excitation. Sometimes, further complications, such as polarization effects, must be taken into account. The coupling to other inelastic channels also has to be considered. This is often necessary and complicates the nice feature of elastic scattering as a probe of the nuclear geometry and density profiles.

5.2. Coulomb excitation and dissociation

In low-energy collisions, the theory of Coulomb excitation is very well understood [118] and has been used to analyze experiments on multiple excitations and reorientation effects [119]. At the other end of the beam energy scale – Coulomb excitation of intermediate-energy or relativistic heavy ions – the kinematics is characterized by straight-line trajectories [120]. In the experiment, the selection of impact parameters b exceeding the sum of the radii of the two colliding nuclei by several fm (via restrictions on scattering angles) keeps the colliding systems at "safe" distances, minimizing the nuclear contribution to the excitation also in reactions above the Coulomb barrier. Most Coulomb-excitation experiments at rare-isotope beam facilities to date have been performed at intermediate bombarding energies of 50–100 MeV/nucleon. It has been a very successful tool to extract precious information on electromagnetic properties of nuclear transitions with relevance to nuclear structure as well as nuclear astrophysics [121].

5.2.1. Coulomb excitation

Following multipole expansion of the electromagnetic field of a nucleus with charge Z_2 as it evolves along a classical Rutherford trajectory, and with first order time-dependent perturbation theory, the Coulomb excitation cross-section is

given by [118]

$$\frac{d\sigma_{i\to f}}{d\Omega} = \left(\frac{d\sigma}{d\Omega}\right)_{el} \frac{16\pi^2 Z_2^2 e^2}{\hbar^2} \sum_{\pi\lambda\mu} \frac{B(\pi\lambda, I_i \to I_f)}{(2\lambda+1)^3} |S(\pi\lambda,\mu)|^2, \tag{91}$$

where $B(\pi\lambda, I_i \to I_f)$ is the reduced transition probability of the projectile nucleus, $\pi\lambda = E1, E2, M1, \ldots$ is the multipolarity of the excitation, and $\mu = -\lambda, -\lambda+1, \ldots, \lambda$. The orbital integrals $S(\pi\lambda,\mu)$ contain the information on the dynamics of the reaction [122]. Inclusion of absorption effects in $S(\pi\lambda,\mu)$ due to the imaginary part of an optical nucleus–nucleus potential were worked out in Ref. [123]. These orbital integrals depend on the Lorentz factor $\gamma = (1 - v^2/c^2)^{-1/2}$, with c being the speed of light, on the multipolarity $\pi\lambda\mu$, and on the adiabacity parameter $\xi(b) = \omega_{fi} b/\gamma v < 1$, where $\omega_{fi} = \left(E_f - E_i\right)/\hbar = E_x/\hbar$ is the excitation energy (in units of $\hbar$) and b is the impact parameter.

Because, the Coulomb excitation process is an external process, i.e., it occurs when the nucleons from one nucleus are outside the nuclear matter distribution from the other nucleus, the matrix elements for Coulomb excitation are the same as those for excitation by real photons (except for $E0$ Coulomb excitations, which are extremely small). Therefore, Coulomb excitation cross-sections are directly related to the photonuclear cross-sections by means of the equation [122]

$$\frac{d\sigma_C(E_x)}{dE_x} = \sum_{E\lambda} \frac{n_{E\lambda}(E_x)}{E_x} \sigma^{\gamma}_{E\lambda}(E_x) + \sum_{M\lambda} \frac{n_{M\lambda}(E_x)}{E_x} \sigma^{\gamma}_{M\lambda}(E_x), \tag{92}$$

where $\sigma^{\gamma}_{\pi\lambda}(E_x)$ are the photonuclear cross sections for the multipolarity $\pi\lambda$ and E_x is the excitation energy.

The photonuclear cross-sections are related to the reduced matrix elements, for the excitation energy E_x, through the relation [122]

$$\sigma^{\pi\lambda}_{\gamma}(E_x) = \frac{(2\pi)^3(\lambda+1)}{\lambda\left[(2\lambda+1)!!\right]^2} \left(\frac{E_x}{\hbar c}\right)^{2\lambda-1} \frac{dB(\pi\lambda, E_x)}{dE_x} \tag{93}$$

where dB/dE_x are the electromagnetic response functions, such that

$$B(\pi\lambda, I_i \to I_f) = \int dE_x \frac{dB(\pi\lambda, E_x)}{dE_x}.$$

For differential cross-sections one obtains

$$\frac{d\sigma_C(E_x)}{d\Omega} = \frac{1}{E_x} \sum_{\pi\lambda} \frac{dn_{\pi\lambda}}{d\Omega}(E_x,\theta) \sigma^{\pi\lambda}_{\gamma}(E_x), \tag{94}$$

where Ω denotes the solid scattering angle.

Due to the use of high-energy projectiles in radioactive beam facilities, it is important to account for the strong absorption properly, as it occurs at small impact parameters. The eikonal formalism developed in Ref. [123] is appropriate for this purpose. The virtual photon numbers in Eq. (92) become

$$n_{\pi\lambda}(E_x) = Z_1^2 \alpha \frac{\lambda\left[(2\lambda+1)!!\right]^2}{(2\pi)^3(\lambda+1)} \sum_m |G_{\pi\lambda m}|^2 g_m(E_x), \tag{95}$$

and

$$g_m(E_x) = 2\pi \left(\frac{E_x}{\gamma\hbar v}\right)^2 \int dbbK_m^2\left(\frac{E_x b}{\gamma\hbar v}\right) \exp\left\{-2\phi_I(b)\right\}, \tag{96}$$

where $\phi_I(b)$ is the imaginary part of the eikonal phase $\phi(b)$, Eq. (87). The functions $G_{\pi\lambda m}(c/v)$ are given in Ref. [120].

In Fig. 14 we show a calculation (with $E_\gamma \equiv E_x$) of the virtual photons for the $E1$ multipolarity, "as seen" by a projectile passing by a lead target at impact parameters equal to and exceeding $b = 12.3$ fm, for three typical bombarding energies. As the projectile energy increases, more virtual photons of large energy are available for the reaction. This increases the number of states accessed in the excitation process.

5.2.2. Coulomb dissociation

Coulomb dissociation is a process analogous to what happened to the comet Shoemaker–Levy as it disintegrated during its approximation to Jupiter in 1994 (see Fig. 15). Approximately 1.5 to 2.2 h after closest approach, the comet (which was presumably a single body at the time) was broken apart by tidal forces into at least 21 pieces. The pieces continued to orbit Jupiter with a period of approximately 2 years. Due to gravitational forces from the Sun, which changed the orbits slightly on the next approach to Jupiter, the pieces impacted the planet. Much stronger tidal forces occur when nuclei come close to each other due to their mutual electromagnetic field. This leads to their dissociation, especially for weakly-bound nuclei (see insert to Fig. 15).

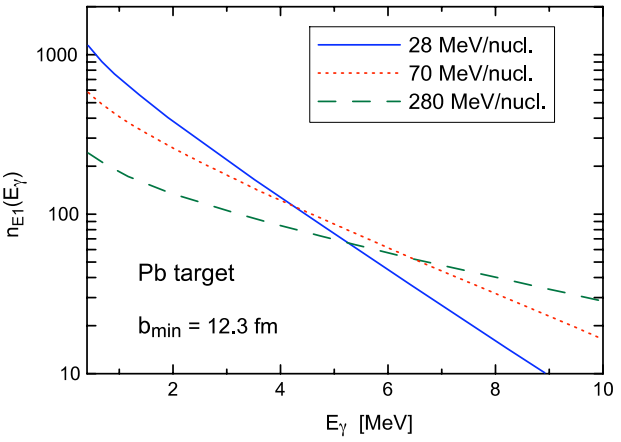

Fig. 14. Total number of virtual photons for the $E1$ multipolarity, "as seen" by a projectile passing by a lead target at impact parameters $b_{\min} = 12.3$ fm and larger, for three typical bombarding energies. (Adapted from T. Glasmacher [121]).

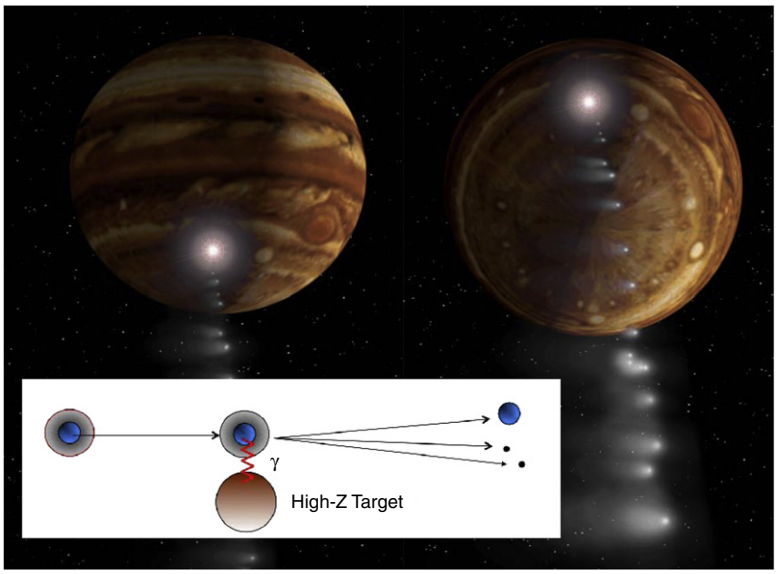

Fig. 15. Jupiter and comet Shoemaker–Levy 9, as imaged by the Hubble Space Telescope (HST), on May 18, 1994, when the giant planet was at a distance of 420 million miles (670 million km) from Earth. The gravitational interaction of Jupiter with the comet has broken it up into many pieces (picture from NASA). Much stronger tidal forces occur when nuclei come close to each other due to their mutual electromagnetic fields. The insert shows the dissociation of a fast nuclear projectile passing by the Coulomb field of a high-Z projectile.

The idea behind the Coulomb dissociation method is relatively simple. The (differential, or angle-integrated) Coulomb breakup cross-section for $a + A \to b + c + A$ follows from Eq. (91). It can be rewritten as

$$\frac{\mathrm{d}\sigma_C^{\pi\lambda}(E_\gamma)}{\mathrm{d}\Omega} = F^{\pi\lambda}(E_\gamma;\theta;\phi)\cdot\sigma^{\pi\lambda}_{\gamma+a\to b+c}(E_\gamma), \tag{97}$$

where E_γ is the energy transferred from the relative motion to the breakup, and $\sigma^{\pi\lambda}_{\gamma+a\to b+c}(E_\gamma)$ is the photo-dissociation cross-section for the multipolarity $\pi\lambda$ and photon energy E_γ. Time reversal allows one to deduce the radiative capture cross-section $b + c \to a + \gamma$ from $\sigma^{\pi\lambda}_{\gamma+a\to b+c}(E_\gamma)$,

$$\sigma^{\pi\lambda}_{b+c\to a+\gamma}(E_\gamma) = \frac{2(2j_a+1)}{(2j_b+1)(2j_c+1)}\frac{k^2}{k_\gamma^2}\sigma^{\pi\lambda}_{\gamma+a\to b+c}(E_\gamma), \tag{98}$$

where $k^2 = 2m_{bc}(E_\gamma - S)$ with S equal to the separation energy, and $k_\gamma = E_\gamma/\hbar c$.

This method was proposed in Ref. [127] and has been tested successfully in a number of reactions of interest to astrophysics. The most celebrated case is the reaction $^7\mathrm{Be}(p,\gamma)^8\mathrm{B}$, first studied in Ref. [128], followed by numerous experiments in the last decade (see Section 6.2.3 for the details of Coulomb dissociation experiments).

The two-neutron capture on ^{4}He could perhaps play a role in the post-collapse phase in type-II supernovae. The bottleneck in this nucleosynthesis scenario is the formation of nuclei with $A \geq 9$ from nucleons and α-particles. In principle, the reaction $^4\mathrm{He}(2n, \gamma)^6\mathrm{He}$ could be relevant in bridging the instability gap at $A = 5$, although it is believed that this reaction cannot compete with the $(\alpha n, \gamma)$ process in a type-II supernova scenario. Experiments with Coulomb dissociation have been used to study this question, as shown in the example presented in Fig. 16. The upper part of the figure displays the electric dipole response function for ^{6}He. The shaded areas represent the experimental results from a Coulomb dissociation experiment [124]. The dashed and dotted lines correspond to results from three-body decay models from Refs. [125,126]. In the lower figure we show the measurement of two-body correlations in the three-body decay of ^{6}He. The lower panels display the ratio between the measured α–n and n–n relative-energy spectra (upper panels) and the spectra simulated (histograms) according to standard phasespace distributions [124]. From the analysis of this experiment it was found that 10% of the dissociation cross-section proceeds via the formation of ^{5}He. A rough estimate yields 1.6 mb MeV for the photoabsorption cross section for $^6\mathrm{He}(\gamma, n)^5\mathrm{He}$, which agrees with theoretical calculations [129]. From this experiment one concludes that the cross-sections for formation of ^{5}He and ^{6}He via one (two) neutron capture by ^{4}He are not large enough to compete with the $(\alpha n, \gamma)$ capture process (for more details, see Ref. [130]). Nonetheless, this and the previously mentioned examples, show the relevance of the Coulomb dissociation method to assess some of the basic questions of relevance for nuclear astrophysics.

5.2.3. Higher-order effects and nuclear dissociation

Eq. (97) is based on first-order perturbation theory. It further assumes that the nuclear contribution to the breakup is small, or that it can be separated under certain experimental conditions. The contribution of the nuclear breakup has been examined by several authors (see, e.g. [123]). For example, ^{8}B has a small proton separation energy ($\approx$140 keV). For such loosely-bound systems it was shown that multiple-step, or higher-order effects, are important [131,132]. These effects occur by means of continuum–continuum transitions. The role of higher multipolarities (e.g., $E2$ contributions [133] in the breakup reactions and the coupling to high-lying states) also has to be investigated carefully. Investigations related to the effects of relativity have attracted much theoretical interest as well [134–137].

5.3. Transfer reactions

Transfer reactions, $A(a, b)B$, are effective when a momentum matching exists between the transferred particle and the internal particles in the nucleus. Therefore, beam energies should be in the range of a few 10 MeV/nucleon [138]. One of the many advantages of using transfer reaction techniques as surrogates for direct measurements in nuclear astrophysics is to avoid the treatment of the screening problem [139].

5.3.1. Trojan horse method

Low-energy reaction cross-sections of astrophysical interest can be extracted directly from breakup reactions $A + a \to b + c + C$ by means of the *Trojan horse* method, as proposed in Ref. [140] (see Fig. 17). If the Fermi momentum of the particle x inside $a = (b + x)$ compensates for the initial projectile velocity v_a, the low-energy reaction $A + x = C + c$ is induced at very low (even vanishing) relative energy between A and x (for more details, see Refs. [141,142]).

Without loss of generality, we neglect the effects of spin, and write the cross-section for $A + x \to c + C$ at an energy E_x close to the threshold as

$$\sigma_{A+x\to B+c} = \frac{\pi}{k_x^2}\sum_l (2l+1)|S_{lx}|^2, \tag{99}$$

where k_x is the wave number in the incident channel, and S_{lx} is the matrix element for the l-th partial wave.

In DWBA, the cross-section for the breakup reaction $A + a \to b + c + C$ is[2]

$$\frac{\mathrm{d}^3}{\mathrm{d}\Omega_b \mathrm{d}\Omega_c \mathrm{d}E_b} = \frac{m_a m_b m_c}{(2\pi)^5\,\hbar^6}\,\frac{k_b k_c}{q_a}\left|\sum_{lm} T_{lm}(\mathbf{k}_a, \mathbf{k}_b, \mathbf{k}_x) S_{lc} Y_{lm}(\mathbf{k_c})\right|^2, \tag{100}$$

with

$$T_{lm} = \left\langle \chi_b^{(-)} Y_{lm} f_l \left| V_{bx} \right| \chi_a^+ \phi_{bx} \right\rangle, \tag{101}$$

where the χ's denote the scattering waves and the interaction between b and x is denoted by V_{bx}. The internal projectile wavefunction corresponding to this potential is ϕ_{bx}.

The radial motion of particles $x + A$ is governed by the function f_l which asymptotically is given by

$$f_l \sim \frac{1}{k_x r}\left[G_l(\eta, k_x r) + \mathrm{i}F_l(\eta, k_x r)\right],$$

where F_l and G_l are the regular and irregular Coulomb wavefunctions, respectively.

[2] In a simple two-body reaction, T is related to the scattering amplitude, Eq. (85), by $f = -\mu T/(2\pi\,\hbar^2)$.

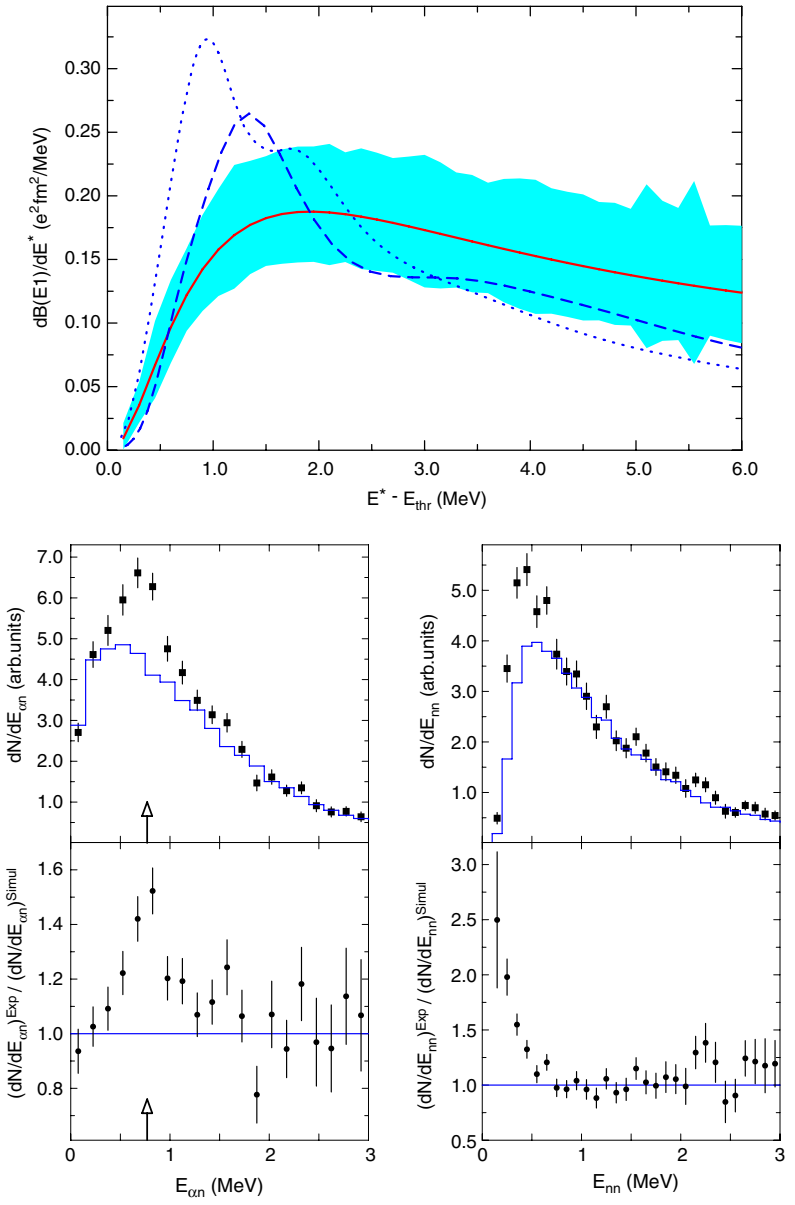

Fig. 16. Upper figure: Electric dipole response function for ^{6}He. The shaded area represents the experimental results from a Coulomb dissociation experiment [124]. The dashed and dotted lines correspond to results from three-body decay models from Refs. [125,126]. Lower figure: Measurement of two-body correlations in the three-body decay of ^{6}He. The lower panels show the ratio between the measured α–n and n–n relative-energy spectra (upper panels) and the spectra simulated (histograms) according to standard phasespace distributions [124]. (Courtesy of T. Aumann).

The threshold behavior of E_x for the reaction $A + x = C + c$ is well known: since $|S_{lx}| \sim \exp(-2\pi\eta)$. Thus,

$$\sigma_{A+x\to C+c} \sim \frac{1}{k_x^2}\sum_l (2l+1)\exp(-2\pi\eta), \tag{102}$$

independent of the partial wave l. Thus, it follows that $\sigma_{A+x\to B+c} \sim (1/k_x^2)\ \exp(-2\pi\eta)$. In addition to the threshold behavior of S_{lx}, the three-body cross-section given by Eq. (100) is also governed by the threshold behavior of $f_l(r)$. This is determined from the behavior of the irregular Coulomb function $G_l(\eta, k_x r)$ for $k_x \to 0$ ($\eta \to \infty$). The combined threshold behavior of $f_l(r)$, which for $r \to \infty$ is given by

$$f_{l_x} \sim (k_x r)^{1/2}\ \exp(\pi\eta)\ K_{2l+1}(\xi),$$

where K_l denotes the modified Bessel function of the second kind. The quantity ξ is independent of k_x and is given by $\xi = (8r/a_B)^{1/2}$, where $a_B = \hbar^2/mZ_AZ_xe^2$ is the Bohr length.

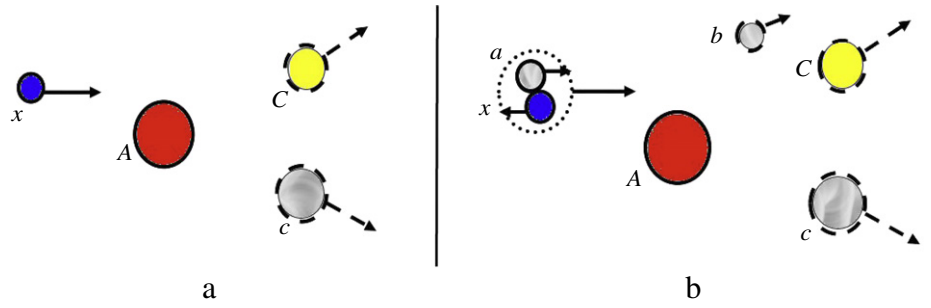

Fig. 17. (a) Charged-particle reactions at low energies, $A+x \to c+C$, are strongly hindered by Coulomb repulsion. (b) But, if particle x is brought into the reaction zone of nucleus A inside a projectile $a = (b+x)$ with velocity v_a, it can induce a reactions at low energies, corresponding to $v_x \sim v_a - v_{Fermi} \ll v_a$.

Based on the arguments given above, the cross-section for the reaction $A+a \to b+c+C$ close to the threshold of $A+x$, with x "hidden" in a, is given by [140]

$$\frac{\mathrm{d}^3\sigma}{\mathrm{d}\Omega_b \mathrm{d}\Omega_c \mathrm{d}E_b}(E_x \to 0) \approx \text{const.} \tag{103}$$

That is, the coincidence cross-section tends to be a constant which, in general, will be different from zero. This is in striking contrast to the threshold behavior of the two particle reaction $A + x = c + C$. The strong barrier penetration effect on the charged particle reaction cross-section is canceled completely by the behavior of the factor T_{lm} for $\eta \to \infty$. Thus, from a measurement of reaction $A+a \to b+c+C$ and a theoretical calculation of the factors T_{lm} in Eq. (100), one extracts the matrix elements S_{lc} needed for $A+x = c+C$. Basically, this technique extends the method of transfer reactions to continuum states. Very successful results using this technique have been reported by many authors, e.g. Refs. [143,144,139]. The problem with the method is that the $x + A$ scattering is off-the-energy shell. The initial- and final-state interactions should be taken into account to get a correct absolute value of the extracted astrophysical factor.

The main characteristic of the Trojan horse method is the suppression of both Coulomb barrier and screening effects in the off-shell two-body cross-section [141,142]. However, the quasifree $A + x$ process can occur at very low, sub-Coulomb energies, even lower than the simple composition of projectile velocity + Fermi velocity, thanks to the role of the (A, x)-binding energy in compensating for the $A + a$ relative motion. This is a different approach to the Trojan horse method compared to the original idea of Ref. [140]. In particular, in plane-wave impulse approximation (PWIA) the cross-section of the $A + a \to c + C + b$ three-body reaction can be factorized as given by

$$\frac{\mathrm{d}^3}{\mathrm{d}\Omega_c \mathrm{d}\Omega_C \mathrm{d}E_c} = KF \left(\frac{\mathrm{d}\sigma}{\mathrm{d}\Omega}\right)_{off} |\Phi(\mathbf{k}_{xb})|^2 , \tag{104}$$

where $(\mathrm{d}\sigma/\mathrm{d}\Omega)_{off}$ is the off-energy-shell differential cross section for the two-body reaction $A + x \to c + C$ and KF is a kinematical factor given by

$$KF = \frac{\mu_{Aa} m_c}{(2\pi)^5 \hbar^7} \frac{k_C k_c^3}{k_{Aa}} \left[\left(\frac{\mathbf{k}_{Bx}}{\mu_{Bx}} - \frac{\mathbf{k}_{Cc}}{m_c}\right) \cdot \frac{\mathbf{k}_c}{k_c}\right]^{-1} , \tag{105}$$

where $B = A + x$. In Eq. (104), $\Phi(\mathbf{k}_{xb})$ is the Fourier transform of the bound-state wavefunction of $a = b + x$. Of course, the plane-wave impulse approximation is an idealistic approximation and corrections to this method are certainly necessary. For example: (a) the plane wave might be replaced by a Coulomb, or distorted, wave in the final channel; (b) the initial and final channels might be treated differently; (c) higher-order processes might be relevant and so on. These corrections have been discussed, e.g. in Refs. [141,142].

Fig. 18 shows the S-factor obtained with the Trojan horse method (full red dots) for the reaction $^{15}\mathrm{N}(p,\alpha)^{12}\mathrm{C}$ (from Ref. [139]) using the $^2\mathrm{H}(^{15}\mathrm{N}, \alpha\,^{12}\mathrm{C})\mathrm{n}$ reaction at $E_{lab} = 60$ MeV. This reaction is important for nucleosynthesis in AGB stars. The direct data from Refs. [145–147] are also shown as open symbols (circles, squares, and triangles, respectively). The red line represents a fit to the data. For comparison, a Breit–Wigner parameterization is also shown as the black line [145].

Fig. 19 shows in the left panel the bare $S_b(E)$ factor data (filled circles) for the reaction $^6\mathrm{Li}(d,\alpha)\alpha$ obtained with the trojan horse method [148]. It also shows the screened $S(E)$ factor data (open diamonds) from direct experiments [97]. The dashed curve is a polynomial fit to $S(E)$ and the solid curve includes the effects of electron screening with $U_e = 340$ eV. On the right panel one sees $S(E)$ for $^6\mathrm{Li}(p,\alpha)^3\mathrm{He}$ obtained with the trojan horse reaction $^6\mathrm{Li}(d,n)^3\mathrm{He}$ (solid circles) [149] compared to direct data (open triangles [150] and open circles [97]). The line shows the result of a second-order polynomial fit to the trojan horse reaction data [149]. It is apparent that an independent measurement of the screening potential can be obtained in experiments with the trojan horse method [151]. The results agree with the direct measurements for U_e [151]. The method also shows that bare S-factors can be obtained directly with this method.

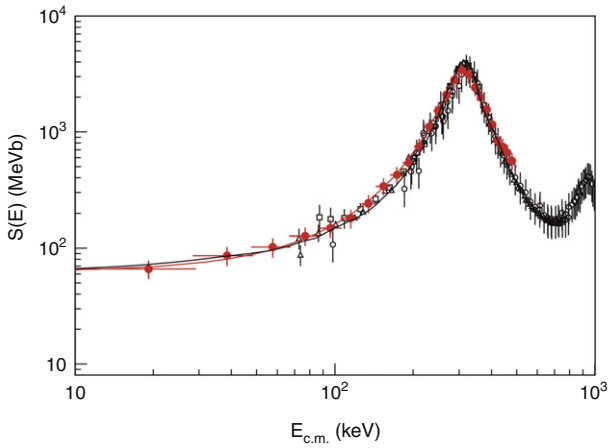

Fig. 18. S-factor obtained with the Trojan horse method (full red dots) for the reaction ^{15}N$(p,\alpha)^{12}$C (from Ref. [139]) using the ^{2}H(^{15}N, α^{12}C)n reaction at $E_{lab} = 60$ MeV. The direct data from Refs. [145–147] are also shown as open symbols (circles, squares, and triangles, respectively). The red line represents a fit to the data. For comparison, a Breit–Wigner parameterization is also displayed as the black line [145].(For interpretation of the references to colour in this figure legend, the reader is referred to the web version of this article.)

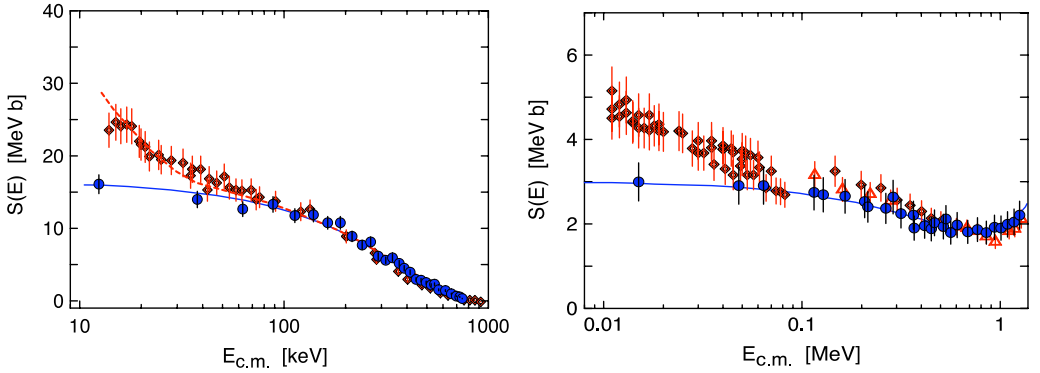

Fig. 19. Left: Bare $S_b(E)$ factor data (filled circles) for the reaction ^{6}Li$(d,\alpha)\alpha$ from the trojan horse method [148] and screened $S(E)$ factor data (open diamonds) from direct experiments [97]. The dashed curve is a polynomial fit to $S(E)$ and the solid curve includes the effects of electron screening with $U_e = 340$ eV. Right: $S(E)$ for ^{6}Li$(p,\alpha)^{3}$He obtained with the trojan reaction ^{6}Li$(d,n)^{3}$He (solid circles) [149] compared to direct data (open triangles [150] and open circles [97]). The line shows the result of a second-order polynomial fit to the trojan horse reaction data [149].

5.3.2. Asymptotic normalization coefficients

The asymptotic normalization coefficient (ANC) method relies on the fact that the amplitude for the radiative capture cross-section $b + x \to a + \gamma$ is given by

$$\mathcal{M}_{\pi\lambda} = \left\langle I^{a}_{bx}(\mathbf{r_{bx}})\, |\mathcal{O}_{\pi\lambda}(\mathbf{r_{bx}})|\, \psi^{(+)}_{i}(\mathbf{r_{bx}}) \right\rangle, \tag{106}$$

as was described in previous sections. The overlap integral

$$I^{a}_{bx}(\mathbf{r_{bx}}) = \langle \phi_a(\boldsymbol{\xi}_b,\ \boldsymbol{\xi}_x,\ \mathbf{r_{bx}}) | \phi_x(\boldsymbol{\xi}_x)\phi_b(\boldsymbol{\xi}_b) \rangle \tag{107}$$

corresponds to the integration over the internal coordinates $\boldsymbol{\xi}_b$, and $\boldsymbol{\xi}_x$, of b and x, respectively. For low energies, the overlap integral I^{a}_{bx} is dominated by contributions from large r_{bx}. Thus, what matters for the calculation of the matrix element $\mathcal{M}_{\pi\lambda}$ is the asymptotic value which, for charged particles is according to Eq. (26), $I^{a}_{bx} \sim C^{a}_{bx}\, W_{-\eta_{bx},1/2}(2\kappa_{bx} r_{bx})/r_{bx}$, where C^{a}_{bx} is the ANC and W is the Whittaker function. This coefficient is the product of the spectroscopic factor and a normalization constant, which depends on the details of the wavefunction in the interior part of the potential. Thus, C^{a}_{bx} is the only unknown factor needed to calculate the direct capture cross-section.

The normalization coefficients can be found from: (1) analysis of classical nuclear reactions such as elastic scattering by extrapolation of the experimental scattering phase shifts to the bound-state pole in the energy plane, or (2) peripheral transfer reactions whose amplitudes contain the same overlap function as the amplitude of the corresponding astrophysical radiative capture cross-section. This is shown schematically in Fig. 20, where the left panel shows a schematic diagram for a radiative capture reaction. The upper half of the diagram on the right contains part of the information of the diagram on the left. If the collision is peripheral, only the tail of the bound-state wavefunction of p + B is involved, allowing the extraction

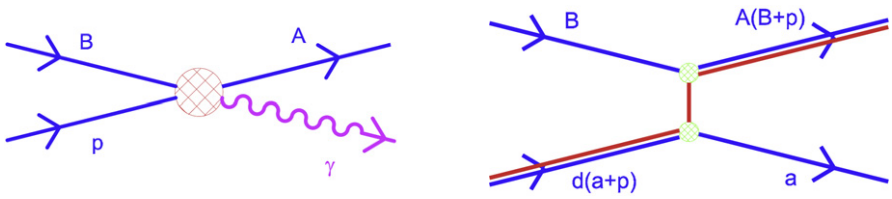

Fig. 20. Left: Schematic diagram for a radiative capture reaction. Right: The upper half of this diagram contains part of the information of the diagram on the left. If the collision is peripheral, only the tail of the bound-state wavefunction of p + B is involved, allowing the extraction of its ANC by a DWBA analysis of the experimental data.

of its ANC by an DWBA analysis of the experimental data. This method was proposed in Ref. [43] and has been used with success for many reactions of astrophysical interest, as discussed, e.g. in Ref. [144] and mentioned in Section 6.2.6.

To illustrate this technique, let us consider the proton transfer reaction $A(d, a)B$, where $d = a + p$, $B = A + p$. Using the asymptotic form of the overlap integral, the DWBA cross-section is given by

$$\frac{\mathrm{d}\sigma}{\mathrm{d}\Omega} = \sum_{J_B j_d} \left[\frac{\left(C^d_{Ap}\right)^2}{\beta^2_{Ap}}\right]\left[\frac{\left(C^d_{ap}\right)^2}{\beta^2_{ap}}\right]\tilde{\sigma} \tag{108}$$

where $\tilde{\sigma}$ is the reduced cross-section, not depending on the nuclear structure, β_{ap} (β_{Ap}) are the asymptotic normalization of the shell-model bound-state proton wave functions in nucleus $d(B)$, which are related to the corresponding ANC's of the overlap function as $(C^d_{ap})^2 = S^d_{ap}\beta^2_{ap}$. Here S^d_{ap} is the spectroscopic factor. Suppose the reaction $A(d, a)B$ is peripheral. Then each of the bound-state wavefunctions entering $\tilde{\sigma}$ can be approximated by its asymptotic form and $\tilde{\sigma} \propto \beta^2_{Ap}\beta^2_{ap}$. Hence

$$\frac{\mathrm{d}\sigma}{\mathrm{d}\Omega} = \sum_{j_i} \left(C^d_{Ap}\right)^2 \left(C^d_{ap}\right)^2 R_{Bd}, \quad \text{where } R_{Bd} = \frac{\tilde{\sigma}}{\beta^2_{Ap}\beta^2_{ap}} \tag{109}$$

is independent of β^2_{Ap} and β^2_{ap}. Thus for surface-dominated reactions, the DWBA cross-section is actually parameterized in terms of the product of the square of the ANC's of the initial and the final nuclei $(C^d_{Ap})^2(C^d_{ap})^2$ rather than spectroscopic factors. This effectively removes the sensitivity in the extracted parameters to the internal structure of the nucleus.

Now consider the elastic $a + p$ scattering amplitude. It has a pole in the momentum plane [152]

$$f_{l_d j_d}(k) = \frac{S_{l_d j_d} - 1}{2\mathrm{i}k} \xrightarrow{k\to k_0} \frac{1}{2\mathrm{i}k_0}\frac{W_{l_d j_d}}{k - k_0}, \tag{110}$$

where, for the bound state of d for $k_0 = \mathrm{i}\kappa$ and for a resonance for $k_0 = k_R$, with $k_R = k_r - \mathrm{i}k_i$, and where $S_{l_d j_d}$ is the elastic S-matrix. The residue in the pole $W_{l_d j_d}$ is

$$W_{l_d j_d} = -(-1)^{l_d}\mathrm{i}\mathrm{e}^{\mathrm{i}\pi\eta_d}\left(C^d_{apl_d j_d}\right)^2, \quad k_0 = \mathrm{i}\kappa, \tag{111}$$

$$W_{l_d j_d} = -(-1)^{l_d}\mathrm{i}\left(C^d_{apl_d j_d(R)}\right)^2, \quad k_0 = k_R. \tag{112}$$

For narrow resonances, $k_I \ll k_r$,

$$\left(C^d_{apl_d j_d(R)}\right)^2 = (-1)^{l_d}\frac{\mu_{ap}}{k_i}\mathrm{e}^{\pi\eta_r}\mathrm{e}^{2\mathrm{i}\delta_{l_d j_d}(k_r)}\Gamma_{l_d j_d}. \tag{113}$$

Here, η_r is the Sommerfeld parameter for the resonance at momentum k_r, $\delta_{l_d j_d}(k_r)$ is the potential (non-resonant) scattering phase shift taken at the momentum k_r [152].

For elastic scattering close to the threshold, the bound-state pole behaves (see Section 3.3) as

$$f_{l_d j_d}(k) \xrightarrow{k\to 0} = -\frac{1}{2k}\mathrm{e}^{-2\mathrm{i}\left(\phi_{l_d} - \sigma_{l_d}\right)}\frac{\Gamma_d}{E + \varepsilon_d + \mathrm{i}\Gamma_d/2}, \tag{114}$$

where $\Gamma_d = 2P_{l_d}(E)\gamma^2_d$, and $P_{l_d}(E)$ is the Coulomb barrier penetrability. In this equation, ϕ_{l_d} is the hard-sphere phase shift in the partial wave l_d and $\sigma_{l_d} = \sum_{n=1}^{l_d}\tan^{-1}(\eta_s d/n)$,$\gamma^2_d$ is the reduced width:

$$\gamma^2_d = \frac{1}{2\mu_{ap}}\frac{W_{-\eta_d, l_d+1/2}(2\kappa r_c)}{r_c}\left(C^d_{apl_d j_d(r_c)}\right)^2, \tag{115}$$

where r_c is the channel radius.

Thus, close to threshold and in the presence of a bound state, the scattering amplitude behaves as the high-energy tail of the resonance located at energy $E = -\varepsilon_c$, also called a "subthreshold" resonance. It is not a resonance because the

real resonance is located at complex energies on the second energy sheet, while the subthreshold resonance is a bound state located on the first energy sheet at negative energy. At negative energies (positive imaginary momenta), Eq. (114) reduces to Eq. (110). Thus, the elastic scattering amplitude (phase shift) offers another possibility to determine the ANC by extrapolating Eq. (110) to the bound-state pole [153].

5.4. Nucleon knockout reactions

Modern shell-model calculations are now able to include the effects of residual interactions between pairs of nucleons, using forces that reproduce the measured masses, charge radii and low-lying excited states of a large number of nuclei. For very exotic nuclei, the small additional stability that comes with the filling of a particular orbital can have profound effects upon their existence as bound systems, their lifetime and structure. Thus, the verification of the ordering, spacing and the occupancy of orbitals is essential in assessing how exotic nuclei evolve in the presence of large neutron or proton excess and to what extent theories have predictive power. Such spectroscopy of the single-particle structure in short-lived nuclei typically uses direct nuclear reactions.

Heavy-ion induced single-nucleon knockout reactions – performed at intermediate energies and in inverse kinematics – have become a specific and quantitative tool for studying the location and occupancy of single-particle states and correlation effects in the nuclear many-body system, as discussed in Refs. [154–157]. In a peripheral, sudden collision of the fast-moving projectile with mass A with a light target (typically Be or C), a single nucleon is removed from the projectile, producing projectile-like residues with mass $A-1$ in the exit channel [156]. Typically, the final state of the target and that of the struck nucleon are not observed, but instead the energy of the final state of the residue can be identified by measuring the decay γ-rays emitted in flight by the excited projectile-like residues (see Section 6.2.6).

The momentum distributions of the projectile-like residues in one-nucleon knockout are a measure of the spatial extent of the wavefunction of the struck nucleon, while the cross-section for the nucleon removal scales with the occupation amplitude, or probability (spectroscopic factor), for the given single-particle configuration in the projectile ground state. The longitudinal momentum distributions are given by (see, e.g., Refs. [158,159])

$$\frac{\mathrm{d}\sigma_{\mathrm{str}}}{\mathrm{d}k_z} = (C^2S)\frac{1}{(2\pi)^2}\frac{1}{2l+1}\sum_m \int_0^\infty \mathrm{d}^2b_n \left[1-|S_n(b_n)|^2\right]\int_0^\infty \mathrm{d}^2\rho \ |S_c(b_c)|^2 \left|\int_{-\infty}^{\infty}\mathrm{d}z \ \exp\left[-\mathrm{i}k_z z\right]\psi_{lm}(\mathbf{r})\right|^2, \quad (116)$$

where k_z represents the longitudinal component of $\mathbf{k}_c$ (final momentum of the core of the projectile nucleus) and (C^2S) is the spectroscopic factor, and $\psi_{lm}(\mathbf{r})$ is the wavefunction of the core plus (valence) nucleon system $(c+n)$ in a state with single-particle angular momentum l, m. In this equation, $\mathbf{r}\equiv(\boldsymbol{\rho}, z, \phi) = \mathbf{r}_n - \mathbf{r}_c$, so that

$$b_c = |\boldsymbol{\rho} - \mathbf{b}_n| = \sqrt{\rho^2 + b_n^2 - 2\rho\, b_n\cos\phi} = \sqrt{r^2\sin^2\theta + b_n^2 - 2r\sin\theta\, b_n\cos\phi}. \quad (117)$$

$S(b)$ are the S-matrices for core-target and nucleon-target scattering obtained from the nuclear ground-state densities and the nucleon–nucleon cross-sections by the relation [44]

$$S(b) = \exp\left[\mathrm{i}\phi(b)\right], \quad \text{with} \quad \phi_N(b) = \frac{1}{k_{NN}}\int_0^\infty \mathrm{d}q\, q\, \rho_p(q)\,\rho_t(q)\, f_{NN}(q) J_0(qb), \quad (118)$$

where $\rho_{p,t}(q)$ is the Fourier transform of the nuclear density of the projectile (nucleon or core) and the target nucleus, and $f_{NN}(q)$ is the high-energy nucleon–nucleon scattering amplitude at forward angles, which can be parameterized by [160]

$$f_{NN}(q) = \frac{k_{NN}}{4\pi}\sigma_{NN}(\mathrm{i}+\alpha_{NN})\exp\left(-\beta_{NN}q^2\right), \quad (119)$$

where k_{NN} is the nucleon–nucleon relative momentum, σ_{NN} is the nucleon–nucleon total cross-section, and α_{NN} and β_{NN} are parameters fitted to (free) nucleon–nucleon scattering data.

The first term in the integral in Eq. (116), $1-|S_n|^2$, represents the probability for the knockout of the nucleon from its location at b_n, whereas the second integral carries the term $|S_c|^2$ which is the probability of core survival at impact parameter b_c. At high energies, the S-matrices do not depend on the longitudinal direction. That is why the bound-state wavefunction is probed by the longitudinal Fourier transform in the last integral of Eq. (116). These results arise naturally by using eikonal scattering waves. For the transverse momentum distributions, the same formalism yields

$$\frac{\mathrm{d}\sigma_{\mathrm{str}}}{\mathrm{d}^2k_\perp} = (C^2S)\frac{1}{2\pi}\frac{1}{2l+1}\int_0^\infty \mathrm{d}^2b_n\left[1-|S_n(b_n)|^2\right]\sum_{m,\,p}\int_{-\infty}^{\infty}\mathrm{d}z\left|\int \mathrm{d}^2\rho\ \exp\left(-\mathrm{i}\mathbf{k}_c^{\perp}\cdot\boldsymbol{\rho}\right)S_c(b_c)\,\psi_{lm}(\mathbf{r})\right|^2. \quad (120)$$

Extensions of the nucleon knockout formalism include the treatment of final-state interactions were discussed in Ref. [158] where one has shown that the inclusion of the Coulomb final-state interactions are of relevance. They can be done by just adding the Coulomb phase $\phi = \phi_N + \phi_C$ in the eikonal phase described above [158]. Other higher-order effects have been included [161] and a theory for two-nucleon knockout [162–165] has been developed. Knockout reactions represent a

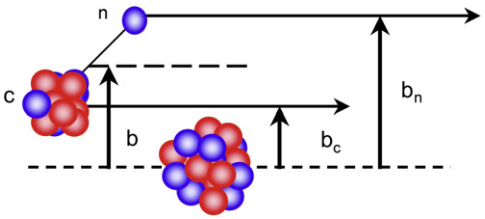

Fig. 21. Coordinates used to describe knockout reactions in the text. (Adapted from J.A. Tostevin).

particular case for which higher projectiles energies allow a simpler theoretical treatment of the reaction mechanism, due to the simplicity of the eikonal scattering waves and the assumption of a single-step process (Fig. 21).

Many new experimental approaches based on nucleon knockout reactions have been developed and shown to reduce the uncertainties in astrophysical (rapid proton capture) rp-process calculations by the provision of nuclear structure data. One utilizes neutron removal from a rare-isotope beam to populate nuclear states of interest in the knockout residue. In the first case studied with astrophysical background, e.g., in Refs. [166,167], excited states in ^{33}Ar were measured with uncertainties of several keV. The 2-orders-of-magnitude improvement in the uncertainty of the level energies resulted in a 3-orders-of-magnitude improvement in the uncertainty of the calculated ^{32}Cl$(p,\gamma)^{33}$Ar rate that is critical to the modeling of the rp process (see Section 6.2.6 for experimental details). This approach has the potential to measure key properties of almost all interesting nuclei on the rp-process path.

5.5. *Quasifree* (p, pN) *reactions*

Quasifree (p, pN) reactions (N = proton or neutron) represent one of the most direct ways to measure single-particle properties in nuclei. They have been used and extensively studied for over 4 decades (see [168,169] for reviews). In quasifree (p, pN) scattering, an incident proton of intermediate energy (200–1000 MeV) knocks out a bound nucleon. The only violent interaction of this process occurs between the incident particle and the ejected nucleon. The wavefunctions of incoming and outgoing nucleons are distorted while traversing the nucleus. From the measured energies and momenta of the emerging nucleons, direct information on single-particle separation energy spectra and nucleon momentum distributions can be obtained. Over the last four decades, quasifree scattering experiments have been performed with this basic purpose.

A popular framework used in the analysis of quasi-free scattering is the so-called "impulse approximation", which yields for the quasifree cross-section

$$\frac{\mathrm{d}^3\sigma}{\mathrm{d}T_N \mathrm{d}\Omega_p \mathrm{d}\Omega_N} = K \frac{\mathrm{d}\sigma_{pN}}{\mathrm{d}\Omega} |F(\mathbf{Q})|^2, \tag{121}$$

where K is a kinematic factor, $|F(\mathbf{Q})|^2$ is the momentum distribution of the knocked-out nucleon N in the nucleus and $\mathrm{d}\sigma_{pN}/\mathrm{d}\Omega$ the free p–N cross section. In the knockout formalism, the off-shell p–N t-matrix is required, and the factorized form that appears in Eq. (121) is valid only if off-shell effects are not very important. In proton-induced knockout reactions, this is probably adequate since the energy variation of the free nucleon–nucleon cross-section is small. As expected, there is an evident similarity between this equation and Eq. (104) used in the analysis of transfer reactions.

Improvements of the above formulation can be easily made, assuming that (on-shell or off-shell) multiple-scattering effects are small. In the distorted-wave impulse approximation (DWIA), the scattering matrix for the $A(p, pN)B$ reaction is given by

$$T_{p,pN} = \left\langle \chi^{(-)}_{\mathbf{K}'_p} \chi^{(-)}_{\mathbf{K}'_N} \left| \tau_{pN} \right| \chi^{(+)}_{\mathbf{K}_p} \psi_0 \right\rangle \tag{122}$$

where $\chi^{(-)}_{\mathbf{K}'_p}$ ($\chi^{(-)}_{\mathbf{K}'_N}$) is the distorted wave for an outgoing proton (knocked-out nucleon) in the presence of the residual nucleus B, $\chi^{(+)}_{\mathbf{K}_p}$ is the distorted wave for an incoming proton in the presence of the target nucleus A, and ϕ_0 is the bound-state wavefunction of the knocked-out nucleon; ϕ_0 includes the spectroscopic amplitude. The p–N scattering matrix is denoted by τ_{pN}. The matrix element given by Eq. (122) can be written as

$$\begin{aligned} T_{p,pN} = \frac{1}{2\pi} \int & \mathrm{d}^3 r'_{pB} \mathrm{d}^3 r'_{NB} \mathrm{d}^3 r_{pA} \mathrm{d}^3 r_{NB} \mathrm{d}^3 P_p \mathrm{d}^3 P_N \mathrm{d}^3 P'_p \mathrm{d}^3 P'_N \tau \left(\mathbf{P}_p, \mathbf{P}_N; \mathbf{P}'_p, \mathbf{P}'_N\right) \\ & \times \tilde{\chi}^{(-)*}_{\mathbf{K}'_p}(\mathbf{P}'_p) \tilde{\chi}^{(-)*}_{\mathbf{K}'_N}(\mathbf{P}'_N) \tilde{\chi}^{(+)}_{\mathbf{K}_p}(\mathbf{P}_p) \psi_0(\mathbf{r}_{NB}) \delta\left(\mathbf{P}'_p + \mathbf{P}'_N - \mathbf{P}_{pA} - \mathbf{P}_N\right), \end{aligned} \tag{123}$$

where $\tilde{\chi}_{\mathbf{K}}(\mathbf{P})$ are the Fourier transforms of $\chi_{\mathbf{K}}(\mathbf{r})$, which are normalized so that $\int \mathrm{d}^3 r \chi_{\mathbf{k}}(\mathbf{r}) \chi_{\mathbf{k}'}(\mathbf{r}) = (2\pi)^3 \delta(\mathbf{k} - \mathbf{k}')$.

The in-medium effects due to the propagation of the incoming proton and the outgoing particles in the nuclear interior can be included in the distorted waves $\chi_i(\mathbf{r})$. The effective interaction τ_{pN} must also include medium and energy dependence

effects. Spin dependence of the p–N t-matrix and of the scattering and bound states also needs to be included. Thus, a deviation from the simple formulation based on Eq. (122) is expected. By using inverse kinematics, quasifree scattering will become a major tool for the investigation of the properties of rare isotopes with relevance for nuclear astrophysics [170].

5.6. Charge-exchange reactions

Charge exchange induced in (p, n) reactions is often used to obtain values of Gamow–Teller matrix elements, $B(GT)$, which cannot be extracted from β-decay experiments. This approach relies on the similarity in spin–isospin space of charge-exchange reactions and β-decay operators. As a result of this similarity, the cross-section $\sigma(p, n)$ at small momentum transfer q is closely proportional to $B(GT)$ for strong transitions [171], i.e.,

$$\frac{\mathrm{d}\sigma}{\mathrm{d}q}(q=0) = KN_D|J_{\sigma\tau}|^2 B(\alpha), \tag{124}$$

where K is a kinematical factor, N_D is a distortion factor (accounting for initial and final state interactions), $J_{\sigma\tau}$ is the the modulus of the $\sigma\tau$ component of the nucleon–nucleon t-matrix, and $B(\alpha = F, GT)$ is the reduced transition probability for non-spin-flip,

$$B(F) = \frac{1}{2J_i+1}\,|\langle f||\sum_k \tau_k^{(\pm)}||\mathrm{i}\rangle|^2\,,$$

and spin-flip,

$$B(GT) = \frac{1}{2J_i+1}\,|\langle f||\sum_k \sigma_k\tau_k^{(\pm)}||\mathrm{i}\rangle|^2\,,$$

transitions. The Fourier transform of the effective interaction yields the largest values for the $|J_{\sigma\tau}|^2$ component at energies around 100–300 MeV. This indicates that the energy range of 100–300 MeV/nucleon will be appropriate to extract GT (F) matrix elements from studies charge-exchange experiments in inverse kinematics involving rare-isotope beams. The condition $q \sim 0$ is met for very small scattering angles, such that $\theta \ll 1/kR$, where R is the nuclear radius and k is the projectile wavenumber.

Eq. (124) is easily understood in the plane-wave Born-approximation (although this assumption is not necessary). Then the charge-exchange matrix element is given by [172]

$$\mathcal{M}_{exch}(\mathbf{q}) = \left\langle \Psi_a^{(f)}(\mathbf{r}_a)\Psi_b^{(f)}(\mathbf{r}_b)\left|\mathrm{e}^{-\mathrm{i}\mathbf{q}\cdot\mathbf{r}_a} v_{exch}(\mathbf{q})\mathrm{e}^{\mathrm{i}\mathbf{q}\cdot\mathbf{r}_b}\right|\Psi_a^{(i)}(\mathbf{r}_a)\Psi_b^{(i)}(\mathbf{r}_b)\right\rangle, \tag{125}$$

where $\mathbf{q}$ is the momentum transfer, $\Psi_{a,b}^{(i,f)}$ are the intrinsic wavefunctions of nuclei a and b for the initial and final states, $\mathbf{r}_{a,b}$ are the nucleon coordinates within a and b, and v_{exch} is the part of the nucleon–nucleon interaction responsible for charge exchange, which contains spin and isospin operators. For forward scattering, low-momentum transfers, $\mathbf{q} \sim 0$, and small reaction Q-values, the matrix element (125) becomes

$$\mathcal{M}_{exch}(\mathbf{q}\sim 0) \sim v_{exch}^{(0)}(\mathbf{q}\sim 0)\mathcal{M}_a(F, GT)\mathcal{M}_b(F, GT), \tag{126}$$

where $v_{exch}^{(0)}$ is the spinless part of the interaction, and $\mathcal{M}_{exch}(F, GT) = \left\langle \Psi_{a,b}^{(f)}\|(1\mathrm{or}\sigma)\tau\|\Psi_{a,b}^{(i)}\right\rangle$ are Fermi or Gamow–Teller (GT) matrix elements for the nuclear transition. The result above is also valid if, instead of plane waves, one uses the eikonal scattering waves for the nuclei. One can thus conclude that the ability to extract information on Fermi or Gamow–Teller transition densities in charge-exchange reactions in a simple way depends on the validity of the low-momentum transfer assumption in high-energy collisions. Recently, also for the (^{3}He,t) reaction at 420 MeV, the proportionality between the cross-section and the Gamow–Teller strength was shown to follow simple trends as function of the mass number [173].

Another assumption in Eq. (124), the validity of one-step processes, was proven to work rather well for (p, n) reactions (with a few exceptions). For heavy-ion induced charge-exchange reactions the formula might not work so well as has been investigated in Refs. [174,172]. In Ref. [174] it was shown that multi-step processes involving the physical exchange of a proton and a neutron can still play an important role up to bombarding energies of 100 MeV/nucleon. Refs. [172] use the isospin terms of the effective interaction to show that deviations from the Taddeucci formula are common under many circumstances. As shown in Ref. [175], for important GT transitions whose strengths are a small fraction of the sum rule, the direct relationship between $\sigma(p,\ n)$ and $B(GT)$ values also can fail. Similar discrepancies have been observed [176] for reactions on some odd-A nuclei including ^{13}C, ^{15}N, ^{35}Cl, and ^{39}K and for charge exchange induced by heavy ions [177]. It is still an open question as to whether Taddeucci's formula is valid in general [178,179].

Electron capture by nuclei in pf-shell plays a pivotal role in the deleptonization of a massive star prior to core-collapse [180]. During the period of silicon burning, supernova collapse occurs due to a competition of gravity and the weak interaction, with electron captures on nuclei and protons and β-decay playing crucial roles. Weak-interaction processes become important when nuclei with masses $A \sim 45$–120 are most abundant in the supernova core. Weak interactions

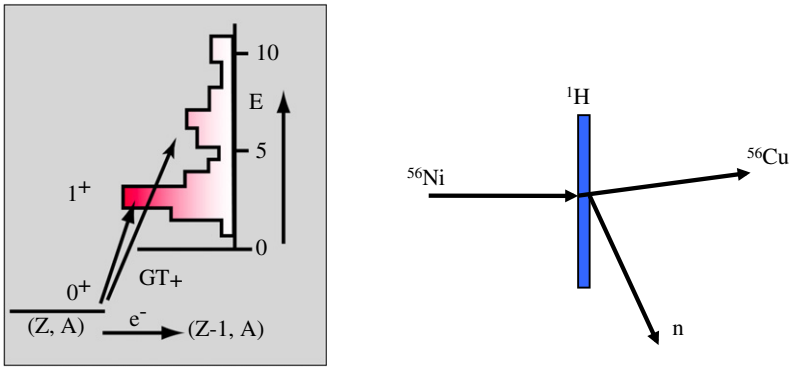

Fig. 22. *Left:* Electron captures by nuclei are dominated by Gamow–Teller (GT+) transitions. *Right:* The matrix elements for such transitions can be probed by using rare-isotope beams interaction with protons in inverse kinematics, as shown schematically for the reaction ^{56}Ni$(p, n)^{56}$Cu. (Adapted from work of D. Frekers and R. Zegers).

change Y_e and electron capture dominates, the Y_e value is successively reduced from its initial value ∼0.5. Electron capture (EC) yields more neutron-rich and heavier nuclei, as nuclei with decreasing Z/A ratios are more bound for heavier nuclei. For densities $\rho \leq 10^{11}$ g/cm^3, weak-interaction processes are dominated by Gamow–Teller and sometimes by Fermi transitions. This is shown schematically on the left panel of Fig. 22. Fuller, Fowler and Newman [181,182,22] made systematic estimates of EC-rates in stellar environments. But their calculations obtain only the centroid of the Gamow–Teller response function. More recently, $B(GT)$-distributions have been obtained with modern shell-model calculations [183–186]. Some marked deviations from the previous rates [181,182,22] have emerged, e.g. Y_e increases to about 0.445 instead of the value of 0.43 found previously [181,182,22].

Most such theoretical developments need support and validation from experiments. A satisfactory understanding of how weak interaction rates influence stellar evolution will rely on experiments using charge-exchange reactions such as the traditional (^{3}He,t) reaction and novel inverse-kinematics (p, n) reactions on rare-isotope projectile beams (right panel of Fig. 22). Reactions with unstable nuclei will provide crucial information on hitherto unknown $B(F)$ and $B(GT)$ values needed for astrophysical purposes and the validation of the handling of weak interactions by large-scale shell-model calculations.

5.7. Central collisions

At intermediate energies of $E_{lab} \sim$ 100–1000 MeV/nucleon, the nucleons and the products of their collisions can be described individually and their propagation can be calculated by semiclassical equations. Hadronic transport theories have been quite successful in describing a multitude of measured particle spectra.

The nuclear equation of state (EOS), $e(\rho, \delta)$, expresses the energy per nucleon of nuclear matter as a function of the nucleon density ρ and the relative neutron excess δ. It is a fundamental quantity in theories of neutron stars and supernova explosions. The main measured quantities, which can provide information about the EOS are, for example, binding energies and other data of finite nuclei. As the finite nuclei are in states near the standard nuclear matter state with normal nucleon density ρ_0 and zero neutron excess, $\delta = 0$, our knowledge about the EOS can be confirmed experimentally only in a small region around $\rho \sim \rho_0$ and $\delta \sim 0$. With very neutron-rich nuclei and energetic heavy-ion collisions, the nuclear EOS can be tested well beyond this region.

If one assumes that the system of nucleons forms a dilute system (or gas) of particles, such that the total volume of the gas particles is small compared to the volume available to the gas, then $na^2 \ll 1$, where n is the number density of particles and a is the (interaction) radius of a particle. Since the particles in a neutral gas do not have long-range forces like the particles in a plasma, they are assumed to interact only when they collide, i.e., when the separation between two particles is not much larger than $2a$. The term "collision" normally means the interaction between two such nearby particles. A particle moves in a straight line between collisions. The average distance traveled by a particle between two collisions is known as the mean free path. The mean free path depends on the cross-section $\sigma \sim a^2$, and is given by $\lambda = 1/n\sigma$. One consequence of the requirement that the gas be dilute is that $\lambda \gg a$. If the gas is dilute, the probability of three-body collisions is much lower than that for two-body collisions and they can be neglected.

Assuming that these conditions are valid, a practical equation describing nucleus–nucleus collisions in terms of nucleon–nucleon collisions can be deduced. A popular transport equation is the Boltzmann–Uehling–Uhlenbeck (BUU) equation,

$$\frac{\partial f}{\partial t} + \left(\frac{\mathbf{p}}{m} + \nabla_{\mathbf{p}} U\right) \cdot \nabla_{\mathbf{r}} f - \nabla_{\mathbf{r}} U \cdot \nabla_{\mathbf{r}} f = \int \mathrm{d}^3 p_2 \int \mathrm{d}\Omega \; \sigma_{NN}(\Omega) \, |\mathbf{v}_1 - \mathbf{v}_2| \times \left\{ f_1' f_2' \left[1 - f_1\right]\left[1 - f_2\right] - f_1 f_2 \left[1 - f_1'\right]\left[1 - f_2'\right] \right\}, \tag{127}$$

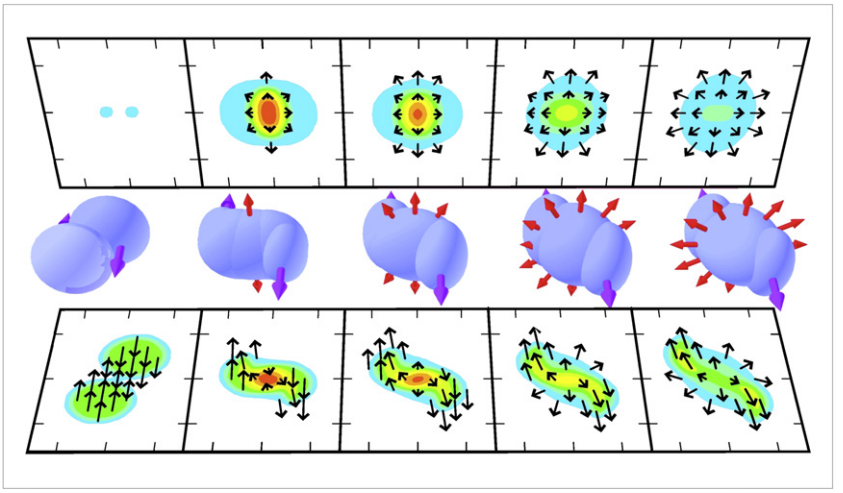

Fig. 23. Matter distribution at several time stages of a nearly central nucleus–nucleus collision. (Courtesy of P. Danielewicz).

where f is defined so that, if dN is the number of particles in the volume element d^3r whose momenta fall in the momentum element d^3p at time t, then the distribution function f ($\mathbf{r}$, $\mathbf{p}$, t) is given by d$N = f$ ($\mathbf{r}$, $\mathbf{p}$, t) d^3rd^3p. The left-hand side of the above equation is due to the variations of f by means of a mean field U. When the right-hand side is taken as zero, the resulting equation is known as the Vlasov equation. The right-hand side of Eq. (127) is the collisional term, which accounts for binary collisions between nucleons by using the nucleon–nucleon cross-section σ_{NN}. This equation incorporates the Pauli principle through the $(1-f)$-terms to avoid scattering into occupied states.

Eq. (127) needs as basic ingredients the mean field U and the cross-section σ_{NN}. Because these two quantities are related to each other, one should in principle derive them in a self-consistent microscopic approach, as the Brueckner theory, for example. However, in practice the simulations are often done with a phenomenological mean field and free nuclear cross-sections. The most commonly used mean field is of Skyrme-type, eventually with a momentum dependent part [187]. Another important ingredient in the transport theory calculations is the compressibility K of nuclear matter, which refers to the second derivative of the compressional energy E with respect to the density:

$$K = 9\rho^2 \frac{\partial^2}{\partial \rho^2}\left(\frac{E}{A}\right). \tag{128}$$

This is an important quantity, e.g., for nuclear astrophysics. In fact, the mechanism of supernova explosions is strongly dependent on the value K. Supernova models might or might not lead to explosions depending on the value of K. The central collisions of heavy nuclei are one of the few probes of this quantity in the laboratory. The dependence of the calculations on K follow from the dependence of the mean field potential U ($U \sim E/A +$ kinetic energy terms) on the particle density ρ.

Following an initial interpenetration of projectile and target densities, the NN collisions begin to thermalize matter in the overlap region making the momentum distribution there centered at zero momentum in the c.m. system. The density in the overlap region rises above normal and a disk of excited and compressed matter forms at the center of the system. More and more matter dives into the region with compressed matter that begins to expand in transverse directions. At late stages, when the whole matter is excited, transverse expansion dominates. A further view of the situation is illustrated in Fig. 23. The measurement of the matter distribution in these collisions and the comparison with transport theories allows one to deduce the incompressibility of nuclear matter. With neutron-rich nuclei, one will also able to extract the EOS dependence on the asymmetry properties of nuclear matter. Measuring other observables, such as particle production and their kinematic properties, also have a valuable contribution from the use of neutron-rich projectiles.

Using a transport theory based on the BUU equation together with available experimental data, Ref. [188] determined that maximum pressures achieve in central collisions in the range of $P = 80$ to 130 MeV/fm^3 in collisions as 2 GeV/nucleon. This corresponds to 1.3×10^{34} to 2.1×10^{34} Pa). A similar analysis for collisions at 6 GeV/nucleon yields the respective values of $P = 210$ to 350 MeV/fm^3 (3.4×10^{34} to 5.6×10^{34} Pa, respectively). These correspond to pressures 23 orders of magnitude larger than the maximum pressure ever observed in the laboratory, being 19 orders of magnitude larger than pressures within the core of the Sun. They are, in fact, only comparable to pressures within neutron stars. The analysis seems to be consistent with bounds for K of Eq. (128) within the range $K = 170$–380 MeV [188]. Fig. 24 shows the pressure for neutron matter as a function of the density. The different curves are based on theoretical models. The shadow bands display the range of possibilities for the EOS based on the analysis of experiments using a soft (lower shadow region) and stiff (upper shadow region) EOS (adapted from Ref. [188]). Rare-isotope beams have not yet been used for experimental work along these lines.

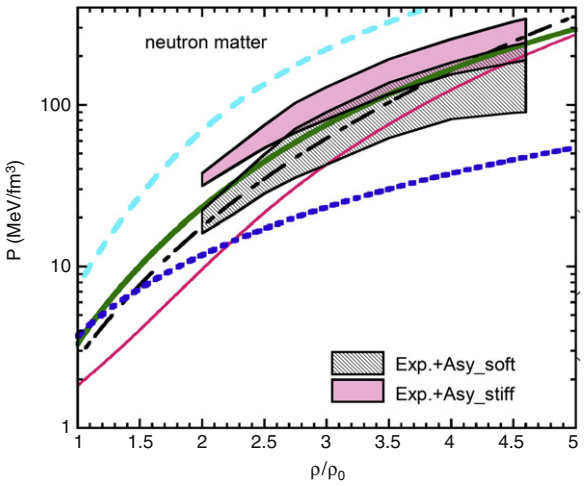

Fig. 24. Pressure for neutron matter as a function of density. The different curves are based on theoretical models. The shadow bands display the range of possibilities for the EOS based on the analysis of experiments using a soft (lower shadow region) and stiff (upper shadow region) EOS. (Adapted from Ref. [188]).

5.8. Electron scattering on radioactive beams

Electron vs. radioactive-beam colliders have been proposed in the framework of the physics programs of few rare-isotope beam facilities [189,190]. Since the reaction mechanism for electron scattering is very well-known, the extraction of valuable physical quantities such as charge distributions, transition densities, and nuclear response functions can be obtained with good accuracy.

In the plane-wave Born approximation (PWBA), the relation between the charge density and the cross-section is given by

$$\left(\frac{\mathrm{d}\sigma}{\mathrm{d}\Omega}\right)_{\mathrm{PWBA}} = \frac{\sigma_M}{1+(2E/M_A)\sin^2(\theta/2)}|F_{ch}(q)|^2, \tag{129}$$

where $\sigma_M = (e^4/4E^2)\cos^2(\theta/2)\sin^{-4}(\theta/2)$ is the Mott cross-section, the term in the denominator is a recoil correction, E is the electron total energy, M_A is the mass of the nucleus and θ is the scattering angle.

The charge form factor $F_{ch}(q)$ for a spherical mass distribution is given by

$$F_{ch}(q) = 4\pi\int_0^\infty \mathrm{d}r\, r^2 j_0(qr)\,\rho_{ch}(r)\,, \tag{130}$$

where $q = 2k\sin(\theta/2)$ is the momentum transfer, $\hbar k$ is the electron momentum, and $E = \sqrt{\hbar^2 k^2 c^2 + m_e^2 c^4}$. The low-momentum expansion of Eq. (130) yields the leading terms

$$F_{ch}(q)/Z = 1 - \frac{q^2}{6}\langle r_{ch}^2\rangle + \cdots. \tag{131}$$

Thus, a measurement at low-momentum transfer yields a direct assessment of the root mean squared radius of the charge distribution, $\langle r_{ch}^2\rangle^{1/2}$. As more details of the charge distribution are probed, more terms of this series are needed and, for a precise description of it, the form factor dependence for large momenta q is needed as well.

The systematics of the charge-density distributions, with the inclusion of nuclei having extreme proton–neutron asymmetry, forms a basis for investigations addressing both the structure of nuclei and the properties of bulk nuclear matter. Information about the nuclear matter incompressibility [191,192], the nuclear symmetry energy [193], and the slope of the neutron matter equation of state in its dependence on density [194] can be extracted. Despite the importance of the nuclear equation of state (EOS), some of its features remain fairly obscure. Electron-scattering studies will allow new constraints on the EOS.

Inelastic electron scattering is a powerful tool for studying the properties of excited states of nuclei, in particular their spins, parities, and the strengths and structure of the transition operators connecting ground and excited states (e.g. Refs. [195,196]). Electron scattering is the only method which can be used to determine the detailed spatial distributions of the transition densities for a variety of single-particle and collective transitions. These investigations provide a stringent test of nuclear many-body wavefunctions.

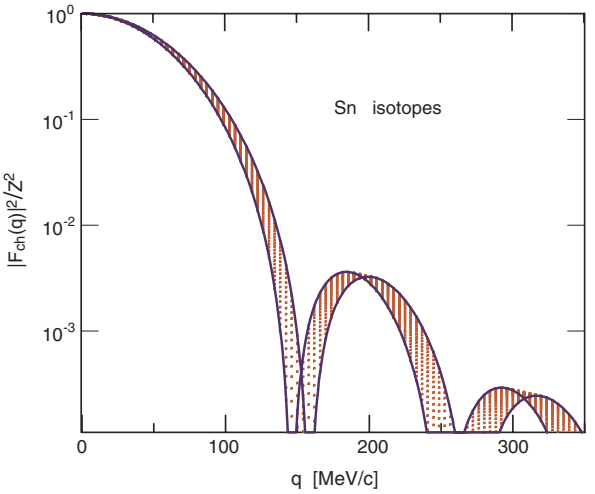

Fig. 25. Calculated charge form factor squared for elastic electron scattering off tin isotopes as a function of the momentum transfer. The two curves are for the extreme values of the asymmetry parameter $\delta = (N - Z)/A$, that is $\delta = 0$ ($N = Z = 50$), and $\delta = 4/9$ ($N = 90$). The curves form an envelope around other curves with intermediate values of δ. (From Ref. [199]).

In the plane-wave Born approximation (PWBA), the cross-section for inelastic electron scattering is given by [195,196]

$$\frac{\mathrm{d}\sigma}{\mathrm{d}\Omega} = \frac{8\pi e^2}{(\hbar c)^4}\left(\frac{p'}{p}\right)\sum_L \left\{ \frac{EE' + c^2\mathbf{p}\cdot\mathbf{p}' + m^2c^4}{q^4} |\mathcal{M}(\mathbf{q}; CL)|^2 + \frac{EE' - c^2(\mathbf{p}\cdot\mathbf{q})(\mathbf{p}'\cdot\mathbf{q}) - m^2c^4}{c^2\left(q^2 - q_0^2\right)^2}\left[|\mathcal{M}(\mathbf{q}; ML)|^2 + |\mathcal{M}(\mathbf{q}; EL)|^2\right]\right\} \tag{132}$$

where J_i (J_f) is the initial (final) angular momentum of the nucleus, $(E, \mathbf{p})$ and $(E', \mathbf{p}')$ are the initial and final energy and momentum of the electron, and $(q_0, \mathbf{q}) = (\Delta E/\hbar c, \Delta\mathbf{p}/\hbar)$ is the energy and momentum transfer in the reaction. $F_{ij}(q; \Pi L)$ are form factors for momentum transfer q and for Coulomb (C), electric (E) and magnetic (M) multipolarities, $\Pi = C, E, M$, respectively. Only for small momentum transfers and forward scattering, the matrix elements in electron scattering are the same as those for real photons and Coulomb excitation. The latter are fixed by the energy and momentum transfer relation $|\Delta\mathbf{p}| = \Delta E/c$. Electron scattering allows probing the momentum and energy transfer response independently.

Due to its strong selectivity, collective and strong single-particle excitations can be studied particularly well in electron scattering. Electric and magnetic giant multipole resonances are of special interest. Several of them have been discovered and studied using electron scattering (see Ref. [197] and references therein). Some of these giant resonances are related, e.g., to the different charge and matter radii of nuclei, quantities that are expected to vary strongly in dripline nuclei. Thus, the difference in radii of the neutron and proton density distributions is accessible via studies of the excitation of giant dipole resonances (GDR) or spin-dipole resonances. The cross-section of these processes depends strongly on the relative neutron-skin thickness [198].

The reaction theory of electron scattering is very well understood. Even in situations for which higher order processes, such as radiative effects, are of importance, the theory can be handled with precision. That is why electron scattering has the potential to become a precious tool for studies with rare-isotope beams in the future.

An example of calculated elastic electron-scattering properties for the scattering off exotic nuclei is given in Fig. 25, where the charge form factor squared for elastic electron scattering off tin isotopes is displayed as a function of the momentum transfer [199]. The two curves are for the extreme values of the asymmetry parameter $\delta = (N - Z)/A$, that is $\delta = 0$ ($N = Z = 50$), and $\delta = 4/9$ ($N = 90$). The curves form an envelope around other curves with intermediate values of δ. The sensitiveness of the form factor obtained in electron scattering on the nuclear charge distribution properties is evident and depends essentially on the neutron skin. The size of the neutron skin will provide data on the volume symmetry energy which was used as input to get the estimates presented in Fig. 24. Recent studies of electron scattering off exotic nuclei have been published in Refs. [200–204].

The electromagnetic response of light nuclei, leading to their dissociation, has a direct connection with the nuclear physics needed in several astrophysical sites. In fact, it has been shown [203] that the existence of pygmy resonances might have important implications for theoretical predictions of radiative neutron capture rates in the r-process nucleosynthesis, and consequently to the calculated elemental abundance distribution in the universe. Recently, the implications of inelastic electron scattering for studying the properties of light, neutron-rich nuclei have been discussed in Ref. [204].

6. Nuclear-astrophysics experiments with rare-isotope beams

6.1. Production of exotic ion beams

The first challenge of any experiment with short-lived "exotic" nuclei is their production. Today, a broad range of rare isotopes is available for experiments in form of ion beams. Two main production and separation mechanisms have emerged as the workhorse techniques in rare-isotope beam production and are employed in nuclear physics laboratories around the world:

- Beams of short-lived nuclei are produced, separated "in-flight" via fragment separators and are directly used for experiments (in-flight separation).
- Exotic nuclei are produced, stopped, ionized, and reaccelerated (isotope separation on-line — ISOL).

A third approach for the production of rare-isotope beams is the batch mode, where a "batch" of radioactive material is made into a beam directly in an ion source. This technique is limited to nuclei that have a sufficiently long half-life and that can be produced in a chemically suitable form. This method was successfully used to produce exotic beams of ^{7}Be [205,206], ^{11}C [207], ^{14}C [208], ^{18}F [209,210], ^{44}Ti [211], ^{56}Co [212], ^{56}Ni [212] and ^{76}Kr [213].

In the following subsections we will summarize in-flight separation and ISOL techniques and the underlying production and reaction mechanisms.

6.1.1. Production of exotic nuclei — In-flight separation

A variety of reaction mechanisms employing various projectile-target combinations over a broad range of collision energies is used to produce short-lived neutron-rich or proton-rich nuclei in-flight. Peripheral collisions at and above the Coulomb barrier create isotopes in the proximity of the target and projectile nuclei via nucleon transfer and nucleon exchange. The highest yield for direct one-nucleon transfer or exchange reactions is achieved when the momenta of the transferred or exchanged nucleons are matched in the initial and final state (5–30 MeV/nucleon energy range) [214]. Using stable beams and stable targets, one-nucleon transfers cannot lead very far from stability. Typical production reactions are $d(^{16}\mathrm{O}, ^{17}\mathrm{F})n$, $p(^{7}\mathrm{Li}, ^{7}\mathrm{Be})n$, and $^{3}\mathrm{He}(^{6}\mathrm{Li}, ^{8}\mathrm{B})n$ induced by intense, low-energy beams of ^{16}O or ^{6,7}Li impinging on light targets. The choice of inverse kinematics yields a forward focussing of the projectile-like reaction residues, which can then be guided to a secondary reaction target or detector setup via ion-optical transport systems like superconducting solenoids [215,216] or bending magnets [217]. This low-energy in-flight technique is presently being used at the TwinSol facility at the University of Notre Dame (ND) [218], at Argonne National Laboratory (ANL) [217], at Texas A&M University (TAMU) [219], at CRIB [220] at CNS/Tokyo (Japan) and at the RESOLUT facility at Florida State University (FSU).

In the high-energy collision of a heavy-ion beam with a thin target (typically at energies exceeding 50 MeV/nucleon), exotic nuclei are produced via projectile fragmentation. At high energy, nucleons are removed from the projectile and the non-interacting part of the projectile nucleus proceeds as "spectator" at essentially the initial beam velocity and close to 0° with narrow angular and linear momentum distributions [221,222]. This spectator or prefragment subsequently undergoes statistical deexcitation leading to the observed products [223]. The mass, charge and momentum distributions of the prefragments have been described with macroscopic as well as microscopic models [224]. The macroscopic abrasion-ablation model [225,226] uses the geometric abrasion, with the size of the prefragment calculated from the geometry of the overlap zone in the projectile-target collision. Statistical models can provide the proton-to-neutron ratio, assuming that both nucleon species are abraded independently of each other. Microscopic approaches employ intranuclear cascade models [227,228], where the interaction of target and projectile is formulated in terms of elastic and inelastic nucleon–nucleon scattering. The deexcitation is incorporated with evaporation or transport models. All elements up to uranium can be produced in projectile fragmentation.

A fragment separator behind the production target separates the wanted exotic nuclei from the primary beam and other reaction residues by a combination of magnetic elements (see [229,230] for reviews). A selection according to the ion's magnetic rigidity separates particles with the same momentum-to-charge ratio. A wedge-shaped degrader can remove the degeneracy as the momentum of each species is systematically shifted by the energy loss encountered in the degrader material [231,232]. This in-flight separation is chemistry-independent and a limitation on the lifetime of the exotic nuclei that can be produced for experiments is solely given by the ion's time-of-flight through the separator and to the experimental setup (typically less than 1 μs). The available exotic beams typically have energies exceeding 30 MeV/nucleon and event-by-event particle identification allows for sensitive and efficient experiments also with cocktail beams. The drawbacks of secondary beams produced by projectile fragmentation are the beam energies that are much higher than those required by certain experiments, a poor transversal and longitudinal beam emittance originating from the fragmentation process and, in some cases, limited beam purity. Projectile fragmentation as a production mechanism was pioneered at the BEVALAC in Berkeley [233,234] and has been the main technique for the production of fast rare-isotope beams at GANIL (France) [235], GSI (Germany) [236], NSCL/MSU (US) [237], and RIBF/RIKEN (Japan) [238].

Although projectile fragmentation is extensively used to produce neutron-rich nuclei, the maximum production yield is realized for neutron-deficient species. Nuclear fission is a process known to be a source of very neutron-rich nuclei [239]. When a fissioning nucleus is moving at energies large compared to the fission recoil, the fission products can be collected and separated using in-flight techniques similar to those described for projectile fragmentation [230]. In a pioneering

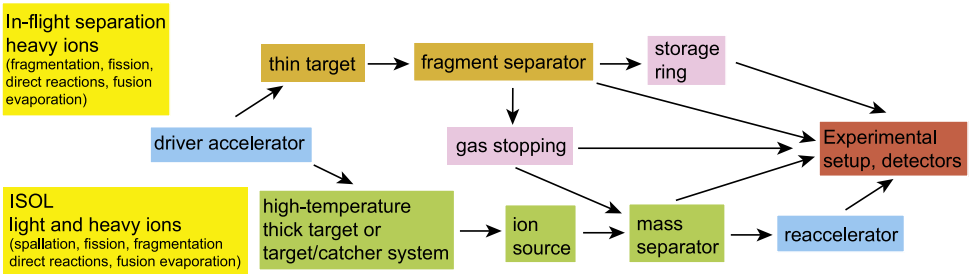

Fig. 26. Schematic view of the production of radioactive nuclear beams with in-flight separation and the ISOL technique. Also shown is the hybrid approach envisioned for the facility for rare isotope beams (FRIB) in the US, employing radioactive beams produced by projectile fragmentation or fission, thermalized in a gas stopper, for example, and reaccelerated.

experiment at GSI, it was shown that the fission fragments produced by a ^{238}U projectile beam impinging upon a lead target at 750 MeV/nucleon can be separated and identified [240].

6.1.2. Isotope Separation On-Line (ISOL) techniques

In the ISOL method, radioactive nuclei are produced in a target, thermalized in a catcher (often target and catcher are one and the same system), ionized in an ion source – if extracted from the target/catcher in atomic form – separated and reaccelerated [241]. In the traditional ISOL approach, a beam of accelerated stable nuclei bombards a target to produce short-lived nuclei via target fragmentation, spallation, direct reactions, fusion or fission. The so produced atoms are extracted from the target/catcher system — typically with heat applied to accelerate the diffusion process. The nuclei are transported from the target/catcher to the ion source. After extraction from the ion source, the low-energy ion beam is mass-separated and reaccelerated to projectile energies required by the experiment. Coolers and charge breeders are used to improve the ion optical properties of the extracted beam and to increase the reacceleration efficiency, respectively [241–243]. When gas catchers are used, a fraction of the thermalizing nuclei will still be in ionic form so that ionization in an ion source can be avoided. This scheme is referred to as Ion Guide Isotope Separation Online (IGISOL) [244,245].

Various projectiles over a broad range of energies impinging upon a variety of targets are used to produce the rare isotopes of interest. Light-ion induced fusion evaporation or direct reactions produce a limited number of neutron-deficient species and rare isotopes close to stability at high conversion rates. For example, at Louvain-la-Neuve, a 30 MeV proton beam on a thick ^{13}C target (>1 g/cm^2) is used to produce a high-intensity beam of ^{13}N with the ^{13}C$(p, n)^{13}$N reaction [246]. Heavy-ion fusion evaporation reactions allow one to access very neutron-deficient nuclei. However, energy loss considerations require comparably thin targets (about 1 mg/cm^2) and thus result in much lower conversion rates for these reactions.

Projectile fragmentation reactions (e.g. heavy-ion beam on a thick carbon target [247]) and target fragmentation (e.g. high-energy protons on heavy targets [242,243]) produce a variety of nuclei in the regions close the initial projectile and target nucleus, respectively, as well as very light nuclei. For example, ^{11}Li is produced with this technique.

The fission of ^{235,238}U, ^{232}Th and long-lived actinides is used to produce neutron-rich nuclei over a wide mass range. Low- and high-energy protons, fast heavy ions, fast or thermal neutrons and electrons (photo fission) are employed to induce fission. Most fission products have a large range in the target material and thus, unlike in heavy-ion induced fusion evaporation reactions, thick targets can be used to increase the yield of the wanted rare isotopes. In the collision of the high-energy proton beam with a target, spallation, fragmentation and fission can occur [248–251]. In spallation reactions, a large numbers of protons, neutrons and α particles are ablated from the target nucleus, for example ^{238}U. Spallation products are typically neutron deficient while fission gives access to neutron-rich nuclei.

Due to the available high flux of protons or light ions, ISOL can provide very intense low-energy beams of rare isotopes with very high beam quality. However, the effectiveness of the thick-target ISOL technique strongly depends upon the chemistry of the wanted element, with large differences observed for different elements [252]. Refractory elements (e.g., vanadium, zirconium and molybdenum), that have a very high melting point and low vapor pressure, cannot be released from an ISOL target in atomic form. Chemical evaporation techniques and the formation of molecular sidebands are being discussed to overcome this limitation for some refractory elements [253,254]. As the thick-target ISOL technique relies on the diffusion of the wanted atoms out of the target and their effusion into the ion source, decay losses significantly limit the intensity for species with short lifetimes [255–257]. For nuclei with lifetimes of milliseconds or less, decay losses are often the most limiting factor. The gas-catcher based IGISOL scheme is characterized by shorter release times and is applicable to refractory elements and other species difficult to ionize.

ISOL techniques are for example used at HRIBF/ORNL (US) [258], ISAC/TRIUMF (Canada) [259], ISOLDE/CERN (Switzerland) [260], SPIRAL/GANIL (France) [261], and Louvain-la-Neuve (Belgium) [262]. The IGISOL scheme is used at Jyväskylä (Finland) [245], Louvain-la-Neuve (Belgium) [263], ANL (US) [264] and was recently developed for rare isotopes produced by projectile fragmentation at NSCL/MSU (US) [265].

6.1.3. Outlook

The Facility for Rare-Isotope Beams (FRIB) [266] planned in the US will provide both, fast exotic beams produced *in-flight* via projectile fragmentation or fission and reaccelerated rare-isotope beams at various energies. In an IGISOL-based scheme, short-lived isotopes produced in a chemistry-independent way by projectile fragmentation or projectile fission will be separated in a fragment separator, thermalized in a gas catcher and quickly extracted (order of milliseconds) with the possibility of reacceleration to the beam energies required for experiments. The gas-catcher based thermalization of fast exotic beams produced by projectile fragmentation is presently operational at NSCL/MSU and a reacceleration capability is presently being implemented [267]. At ANL, the CAlifornium Rare Isotope Breeder Upgrade (CARIBU) project [268] will produce neutron-rich isotopes from a ^{252}Cf source for reacceleration through the ATLAS facility and provide new opportunities for experiments with reaccelerated Cf fission fragments (Fig. 26).

In Europe, design studies for the next-generation European ISOL facility EURISOL are ongoing [269]. The aim is to increase the variety of exotic nuclei produced and to increase the production yields by orders of magnitude compared to present-generation ISOL facilities. EURISOL would complement the Facility of Antiproton and Ion Research (FAIR) [270] in Germany, where high-energy rare-isotope beams (GeV/nucleon) will be produced by fragmentation and fission, separated in-flight with the possibility of passive deceleration or cooling in storage ring structures. The SPIRAL2 and ISAC-II(I) upgrades are underway at GANIL [271] and TRIUMF [272], respectively. A major upgrade of the RIKEN facility (RI Beam Factory - RIBF) in Japan became operational recently [273].

6.2. Experimental techniques and applications

This section describes experimental approaches and detection systems developed or adapted to probe properties of exotic nuclei that are important for nuclear astrophysics. Many observables ranging from nuclear masses and ground-state half-lives to specific reaction cross-sections are nuclear physics inputs crucial for the understanding of a large variety of astrophysical processes and scenarios. We tried to focus here on the measurements and developments that were not covered in the review by Smith and Rehm from 2001 [274].

6.2.1. Targets

Hydrogen- and helium-induced reactions are of great importance in many astrophysical scenarios. A variety of hydrogen and helium (enriched) target schemes exists. Thin plastic targets, for example, polyethylene–$(CH_2)_n$– foils with thicknesses between tens of μg/cm^2 and several mg/cm^2, have been used for proton-induced reactions. As helium does not form compounds, solid targets containing helium must be prepared by implantation. Helium-implanted aluminum targets have been developed at Louvain-la-Neuve [275]. The carbon in plastic targets and the heavier elements serving as carriers in implanted targets increase the energy loss of the beam passing through the target and induce intense background reactions, typically dominated by elastic scattering. Aside from physical radiation damage at high beam intensities, hydrogen depletion in plastic targets poses problems as well.

Gas cells have been developed to mitigate some of these problems. While gas cells with windows are easy to handle, even thin windows can degrade the beam energy and produce unwanted background reactions. A He-gas filled chamber is used at Louvain-la-Neuve [276], while cryogenic helium and hydrogen gas cells have been built for experiments at ANL [211] and GANIL [277], for example. When excitation functions are of interest, the so-called thick-target inverse kinematics (TTIK) technique [278] can be employed. For this approach, the beam is slowed down and stopped in a thick target with the light reaction residues escaping and being detected. With this, a reaction can be probed over a wide energy range with one incoming beam energy. The TTIK technique for He-induced reactions on low-energy ^{14}O beams has been used at CRIB in Tokyo [279] and at Texas A&M University [280] with thick He gas targets; a thick polyethylene target was used at HRIBF at Oak Ridge National Laboratory to study resonant reactions with ^{17}F and ^{18}F beams [281,282].

Window-less, differentially-pumped gas targets eliminate background reactions and increased energy loss arising from the presence of windows but require several stages of pumping at high pumping speeds to drop the pressure by orders of magnitude over short distances. At present, window-less gas targets are used in conjunction with the DRAGON setup [283] and at HRIBF/ORNL [284,285].

6.2.2. Direct measurement of (p,γ) and (α,γ) radiative capture reactions

Charged-particle induced radiative capture reactions such as (p,γ) and (α,γ) occur in many stellar environments, for example, in novae and X-ray bursts. In explosive environments – due to the high temperatures and short reaction times – capture reactions involving short-lived nuclei play an important role for energy generation and nucleosynthesis.

Resonant capture reactions on stable and long-lived radioactive targets have been investigated with intense proton and α beams [286,287]. The most recent examples for direct measurements of radiative capture reactions are ^{23}Na$(p,\gamma)^{24}$Mg and ^{17}O$(p,\gamma)^{18}$F studied at the Laboratory for Experimental Nuclear Astrophysics (LENA) at TUNL [288–290] and the ^{3}He$(\alpha,\gamma)^7$Be [291–293] and ^{14}N$(p,\gamma)^{15}$O reactions [294–297] at the Laboratory Underground Nuclear Astrophysics (LUNA) facility [298,299] located in the Gran Sasso Laboratory.

For the resonant capture on short-lived nuclei, the experiments have to be performed in inverse kinematics. Recoil separators are typically used to detect and identify the recoiling reaction products and to reject the direct beam. The

separators that are presently used for inverse-kinematics capture reactions with stable and rare-isotope beams include DRAGON [283] at TRIUMF (Canada), ARES [300] at Louvain-la-Neuve (Belgium), the Daresbury Recoil Separator (DRS) [284] at HRIBF/ORNL (US), the FMA [301] at ANL (US) and, for stable beams only, ERNA [302] at Bochum (Germany). The STrong Gradient Electro-magnetic Online Recoil separator for capture Gamma ray Experiments (St. George) is under construction at the University of Notre Dame and will be used for inverse-kinematics (α, γ) capture reactions induced by a He-jet target [303].

The pioneering measurement with a rare-isotope beam was the first direct determination of the $^{13}N(p, \gamma)^{14}O$ reaction cross section using a radioactive ^{13}N beam produced at Louvain-la-Neuve [304,305]. A ^{13}N beam with an intensity of 3×10^8 particles per second and an energy of 8.2 MeV impinged upon a 180 $\mu g/cm^2$ polyethylene target. A surface-barrier diode located at 17° with respect to the beam axis detected the scattered ^{13}N and the carbon and hydrogen target recoils. Assuming pure Rutherford scattering on the ^{12}C in the target, the number of incident ^{13}N was determined. The resonant radiative proton capture was tagged via the 5.173 MeV capture γ-ray originating from the ground-state decay of the first excited 1^- state of ^{14}O measured with a large volume Ge diode. The peak-to-total in the γ-ray spectrum was improved by vetoing cosmic rays with Cherenkov detectors positioned above the γ-ray detector setup. The Γ_γ width of the dominant ^{14}O 1^- level was determined for the first time from a direct measurement. Compared to the previously adopted $^{13}N(p, \gamma)^{14}O$ reaction rate, the results of the measurement by Delbar et al. suggested that the reaction actually proceeds twice as fast [306,305]. After studies of the non-resonant capture cross-section [307], the γ width of the 5.173 MeV state in ^{14}O now poses the largest uncertainty of this reaction rate [308].

The later study of the $^{19}Ne(p, \gamma)^{20}Na$ reaction at Louvain-la-Neuve used the resolving power of the recoil separator ARES to identify ^{20}Na events from capture through the 2.643 MeV level [309]. An upper limit of the resonance strength of the 2.643 MeV level was determined with this approach that bypasses low-efficiency γ-ray detection. It was concluded that an increased transmission and efficiency of ARES would be required to be able to determine more than an upper limit [309].

Some of the most recent resonant capture reactions induced by radioactive and stable beams in inverse kinematics have been measured at the DRAGON facility at TRIUMF. DRAGON is a recoil mass separator at ISAC dedicated for the measurement of low-energy reactions of astrophysical interest. Radioactive and stable beams with energies between 0.15 and 1.5 MeV are delivered by ISAC. The DRAGON facility consists of a recirculating, differentially-pumped window-less gas target surrounded by a 30-crystal BGO γ-ray detection array, an electromagnetic separator and a heavy-ion recoil detection system [283]. At the DRAGON facility, seven resonances in ^{22}Mg have been characterized in the reaction $^{21}Na(p, \gamma)^{22}Mg$ at center-of-mass energies between $E_{cm} = 200 - 1103$ keV [310,311], the strength of the $E_{cm} = 184$ keV resonance in the $^{26g}Al(p, \gamma)^{27}Si$ reaction was determined for the first time from a direct measurement in inverse kinematics [312] and the $^{40}Ca(\alpha, \gamma)^{44}Ti$ reaction was probed with a ^{40}Ca beam of 0.6–1.15 MeV/nucleon covering the relevant temperature range for the α-rich freeze-out during a core-collapse supernova [313].

At HRIBF/ORNL, the cross-section of the $^{17}F(p, \gamma)^{18}Ne$ reactions was measured directly for the first time [314]. A cocktail beam of ^{17}O and ^{17}F was produced at HRIBF and impinged upon ORNL's differentially pumped, windowless hydrogen target. The Daresbury Recoil Separator was tuned to transmit the ^{18}Ne recoils to the focal plane where they were identified in the gas-filled ionization chamber. Two normalization schemes for counting the incoming beam were used, (i) the detection and counting of elastically scattered protons in surface-barrier detectors and (ii) beam-current measurements facilitated by a metal plate and two plastic scintillator paddles; the decays of ^{17}F nuclei implanted into the metal plate that was inserted into the beam from time to time and retracted to sit between the scintillator paddles were measured [314]. The strength of the 3^+ resonance in ^{18}Ne (about 600 keV above the proton separation energy corresponding to a 10.83 MeV ^{17}F beam energy for the resonant-capture measurement) was determined. At an off-resonance ^{17}F beam energy (800 keV above the proton threshold), an upper limit for the direct capture away from the dominating resonances could be determined [314]. Compared to previous nova nucleosynthesis calculations [315], the abundance of the important galactic γ-emitter ^{18}F, the β-decay daughter of ^{18}Ne, increased in the hottest zone of a 1.35 solar mass white dwarf nova by a factor of 1.6 over the previously adopted rate. The uncertainty of the measured rate leads to a spread of a factor of 2.4 in the final abundance of ^{18}F, while varying the previous resonant contribution by a factor of 10 resulted in a spread of as much as 15–16 times in the final abundance of ^{18}F [314]. Further measurements, for example the determination of the $^{17}F(p, \gamma)^{18}Ne$ direct capture cross-section and the $^{18}F(p, \alpha)^{15}O$ reaction cross-section, are needed to further reduce uncertainties in the production of ^{18}F in novae [314]. The impact on X-ray bursts is under investigation; there are indications that the abundances of ^{17}O and ^{17}F in X-ray bursts can be modified by more than an order of magnitude at a reduction in uncertainty by a factor of 20 compared to previous network calculations [314].

The cross-section for radiative capture has been observed to show the characteristic resonances of the reaction on top of a background that slowly varies with beam energy [25,286]. This smooth background is attributed to the direct capture process – a transition for the projectile from an initial continuum state to a final bound state via the electromagnetic interaction – that depends on the properties of the bound states of the compound nucleus [25]. This direct non-resonant capture can become important for stellar reaction rates when the nuclear level density is low in the region of the Gamow window. Also interference effects between resonant and non-resonant capture can occur. For capture reactions involving stable nuclei important in hydrostatic burning, the contributions from direct capture have been estimated from capture cross-sections measured away from resonances [316]. The total cross-section for direct proton capture is of order $\mu\, b$ [286] in the relevant energy range and except for the case of $^7Be(p, \gamma)^8B$ [317,35], direct measurements of direct capture with radioactive beams have not been performed due to the high beam intensity requirements.

6.2.3. Coulomb dissociation — The time-reversed approach to radiative capture

The dissociation of a fast-moving projectile in the Coulomb field of a high-Z nucleus – Coulomb excitation of continuum states – was proposed as alternative method to determine radiative capture cross-sections [127,318]. For the Coulomb dissociation approach, the residual nucleus B of the radiative capture reaction of interest, $A(x,\gamma)B$, is Coulomb excited in the electromagnetic field of a high-Z nucleus to an unbound state that decays into $A+x$. Coulomb dissociation is mediated by the absorption of a virtual photon, $B(\gamma_{virt},x)A$, which is related to photodisintegration via the virtual photon method [319,320]. As photodisintegration is the time reverse process of radiative capture, the cross-sections of the two processes can be related via the detailed balance theorem (see Section 5.2.2 for the theoretical formalism of Coulomb dissociation).

In Coulomb dissociation measurements at intermediate beam energies, the relative energy of the residues A and x is determined from their invariant mass, which is deduced from the measured velocity vectors of A and x. The relative energy corresponds to the center-of-mass energy of the $A(x,\gamma)B$ capture. Experimental advantages of the Coulomb breakup method are threefold, (i) the typically large number of virtual photons leads to a big Coulomb dissociation cross-section, (ii) the photoabsorption cross-section is favored compared to the radiative capture cross-section by two to three orders of magnitude (phase space), and (iii) thick targets can be used in the regime of fast beams (higher luminosity) [321]. A challenging requirement for experiments, however, is the need for the measurement of angular distributions. The multipolarities have to be disentangled since the electromagnetic multipoles contribute with different strengths to Coulomb excitation and capture processes. Particularly important are the non-negligible contributions and interference of electric dipole ($E1$) and electric quadrupole ($E2$) excitations. The applicability of the Coulomb dissociation approach is limited by the fact that preferentially $E1$ modes are excited and that the detailed balance theorem cannot be used for the extraction of the radiative capture cross-section in case the capture feeds bound excited states that decay by γ-ray emission with unknown branching ratio [321]. The main body of experimental work utilizing Coulomb breakup of rare isotopes for nuclear astrophysics has been aimed at exploring radiative proton capture reactions.

An extensive experimental program that utilizes Coulomb breakup reactions for the extraction of radiative capture cross-sections was initiated first at RIKEN/Japan by Motobayashi et al. [322,323]. In the pioneering experiment, the electromagnetic transition strength for the excited 1^- resonance in ^{14}O was determined in the Coulomb dissociation, $^{14}\mathrm{O}\rightarrow{}^{13}\mathrm{N}+p$, induced by 87.5 MeV/nucleon ^{14}O impinging upon a 350 mg/cm^2 Pb target [322]. The Coulomb dissociation cross-section was determined from coincidence spectroscopy of protons and ^{13}N in position-sensitive detection systems consisting of telescopes of 24 position-sensitive Si detectors for ΔE measurements backed by CsI(Tl) scintillators for E measurements [324] and plastic-scintillator hodoscopes with x–y position sensitivity. The complete kinematics – total energy and relative momentum vectors of the $p+{}^{13}$N system – were determined [322]. The radiative width Γ_γ was deduced and found in agreement with the direct measurement performed at Louvain-la-Neuve [304] (see Section 6.2.2 for the direct measurement).

Subsequent experiments at RIKEN were aimed at the Coulomb dissociation of ^{8}B [128,325,326] to extract the reaction rate of the crucial $^7\mathrm{Be}(p,\gamma)^8\mathrm{B}$ reaction, which is of great importance for the neutrino production in the Sun through the β decay of ^{8}B. In the first experiment in 1994, the breakup of a ^{8}B beam of 46.5 MeV/nucleon incident on a 50 mg/cm^2 ^{208}Pb target, used a two-layered, x–y position-sensitive plastic-scintillator hodoscope with an active area of 1×0.96 m^2 for the detection of the coincident $^7\mathrm{Be}+p$ breakup products. The hodoscope with a ΔE layer of 5 mm thick plastic (10 segments) and the E plane of 60 mm thick plastic (16 segments) was positioned 5 m downstream of the Pb target. The energy of the breakup fragments was deduced from the time-of-flight (TOF) over the 5 m flight path, the angle from the location of the hits in the segmented hodoscope. The particle identification was performed with the ΔE–E method and from TOF–E information. A helium-filled bag was inserted between the target and the hodoscope to reduce the background due to breakup in air [128]. In a second experiment [325,326], the hodoscope was modified for higher count-rate capability and moved closer to expand the angular range covered from 6° to 10°. Also, the NaI(Tl) scintillator γ-ray detection array DALI was positioned around the target to tag the fraction of the breakup leading to the 429 keV bound excited state in ^{7}Be. The larger angular range covered by the hodoscope allowed for angular-distribution measurements and an assessment of the $E2$ contribution to the breakup process [325,326]. Similarly, the reactions $^8\mathrm{B}(p,\gamma)^9\mathrm{C}$, $^{11}\mathrm{C}(p,\gamma)^{12}\mathrm{N}$ and $^{12}\mathrm{N}(p,\gamma)^{13}\mathrm{O}$, important for the hot pp mode nuclear burning in hydrogen-rich, very massive objects [327], were studied via Coulomb breakup at RIKEN to extract the reaction rates relevant to explosive hydrogen burning [323]. Subsequent measurements on sd-shell nuclei aimed at the study of the breakup of ^{23}Al [328] and ^{27}P [329] into $^{22}\mathrm{Mg}+p$ and $^{26}\mathrm{Si}+p$, respectively, continued to use γ-ray spectroscopy with DALI and employed a position-sensitive Si detector telescope in front of the plastic hodoscope for the identification of the projectile-like breakup residues. The experimental results in the sd shell are relevant to the reaction path in Ne novae [330], where at high temperature and density many nuclear reactions involving rare isotopes contribute in the hot CNO cycle and the NeNa- and MgAl-cycles [13]. A specific signature is the nucleosynthesis of long-lived galactic γ emitters such as ^{22}Na and ^{26}Al, and nucleosynthesis up to the silicon and calcium range [331]. Assuming temperature and density conditions given by nova models [332], the radiative width obtained in the RIKEN study indicates that the main reaction path favors the β decay rather than the proton capture on ^{22}Mg [328]. For $^{26}\mathrm{Si}+p$, the preliminary result of the γ-decay width of the first excited state in ^{27}P is ten times smaller than the value estimated based on a shell-model calculation in [333]. This indicates that the $^{26}\mathrm{Si}(p,\gamma)^{27}\mathrm{P}$ reaction does not contribute significantly to the amount of ^{26}Al produced in novae [329].

At GANIL, the Coulomb dissociation cross-sections of $^{14}\mathrm{O}\rightarrow{}^{13}\mathrm{N}+p$ [334] and $^{12}\mathrm{N}\rightarrow{}^{11}\mathrm{C}+p$ [335] were measured. Radioactive beams of ^{14}O at 70 MeV/nucleon and ^{12}N at 65.5 MeV/nucleon were provided by the ALPHA spectrometer and guided onto 100 mg/cm^2 and 120 mg/cm^2 ^{208}Pb targets, respectively. In both experiments, the heavy breakup residues

were characterized with the SPEG spectrometer and its focal-plane detection system consisting of two drift chambers and a plastic scintillator. The protons were detected in CsI(Tl) detectors downstream of the Pb target [334,335].

Much higher beam energies are available for Coulomb dissociation experiments at GSI. The breakup of $^8B \rightarrow {}^7Be + p$ was measured in two experiments at 254 MeV/nucleon ^8B beam energy [36,38]. Both experiments utilized the KaoS spectrometer [336]. Beam particles were identified with the TOF–ΔE method using a plastic timing detector upstream of the target and a large-area scintillator wall close to the focal plane of KaoS. Momentum vectors of the reaction residues were analyzed by trajectory reconstruction with KaoS using position sensitive microstrip detectors and two 2d multi-wire proportional counters (MWPC). The first experiment used a 199 mg/cm^2 ^{208}Pb target, the second experiment used a Pb target of 50 mg/cm^2 thickness. Tracking of the angle of the incoming beam with parallel-plate avalanche counters allowed one to measure angular distributions to disentangle contributing multipolarities in the second experiment [38,337].

At MSU, inclusive and exclusive measurements of the $^8B \rightarrow {}^7Be + p$ Coulomb dissociation were performed [37,338]. Inclusive measurements used 44 and 81 MeV/nucleon ^8B beams provided by the A1200 fragment separator at NSCL. The S800 spectrograph [339] was used to detect the ^7Be residues from the Coulomb dissociation of ^8B impinging upon 27 mg/cm^2 Ag and 28 mg/cm^2 Pb targets. The longitudinal momentum distributions of ^7Be were derived from trajectory reconstruction using the position information provided by the position-sensitive cathode readout drift chambers of the spectrograph's focal-plane detection system [340]. Particle identification was achieved with the ΔE–E method employing the S800 ionization chamber for ΔE and the first focal-plane plastic scintillator for E measurements [340]. In comparison to model calculations, a rather high $E2$ contribution to the Coulomb breakup was deduced, which has not been confirmed by any other measurement to date. An exclusive measurement at 83 MeV/nucleon on a 47 mg/cm^2 Pb target in front of a 1.5 T dipole magnet was performed in addition. Two multi-wire drift chambers (MWDCs) each were used to track the flight paths of the ^7Be and the proton after passage through the magnetic field. An array of plastic scintillators was placed behind the MWDCs. Particle identification was performed with the energy loss measured in the plastic scintillator array and the TOF information. The invariant mass method was used to calculate the relative energy of the breakup residues [37,338].

In a recent comprehensive study, M. Gai [341] summarized the results of the various ^8B Coulomb dissociation measurements and the extracted astrophysical $S_{17}(0)$ factor in comparison to the results of direct capture measurements.

Recently, the neutron capture reaction on ^{14}C has been explored using Coulomb dissociation of $^{15}C \rightarrow {}^{14}C + n$ at 69 MeV/nucleon in the field of a 224 mg/cm^2 Pb target at RIKEN [342]. The ^{14}C residues were analyzed with a magnetic spectrometer that used a drift chamber and plastic scintillator hodoscopes. The momentum vector of ^{14}C was determined by combining the tracking data and time-of-flight information. Particle identification was achieved with ΔE–TOF and tracking information. The breakup neutron was detected by two layers of neutron hodoscope arrays with an active area of 2.14×0.92 m^2 positioned almost 5 m downstream of the Pb target. The neutron momentum vector was extracted from the hit position of the neutron and its TOF. The spectral shape and amplitude was found to be consistent with similar data taken at higher beam energies at GSI [342]. The deduced direct capture cross-section agrees with the most recent direct capture measurement and demonstrates that the Coulomb breakup with a neutron in the exit channel is a useful tool to derive the radiative capture cross-section. A program aimed at Coulomb breakup of neutron-rich nuclei, not exclusively with an astrophysical background, is also ongoing at GSI at higher beam energies [343–345,130].

6.2.4. *Direct* (p, α) *and* (α, p) *measurements*

Proton-induced reactions are of great importance in many astrophysical scenarios as the corresponding reaction cross-sections are high due to the small Coulomb barrier. The predominant reactions in nova outbursts, for example, are of type (p, γ) and (p, α). A significant fraction of the energy produced during nova explosions stems from proton-induced reactions on pre-existing carbon, nitrogen, and oxygen seed nuclei. The (p, α) reactions play a crucial role in cycling reaction flow back to lower masses. At sufficiently high temperatures, breakout sequences can occur and heavier nuclei are synthesized through reactions on neutron-deficient nuclei. In X-ray bursts, for example, a sequence of (α, p) and (p, γ) reactions (α p process) leads to nuclei up to mass $A = 40$, eventually followed by rapid proton capture reactions (rp process) and β decays resulting in the formation of nuclei with $A \approx 100$ [6].

The study of reactions with charged particles in the exit channel advanced tremendously with the advent of large-area silicon strip detectors. Si strip detectors can be single-sided – providing segmentation in one dimension – or double-sided for two-dimensional segmentation. Detector thicknesses between 50–1000 μm are typically available. A high degree of segmentation also allows for higher total counting rates (without pileup) than could be achieved with a single detector of the same total area. When operated in transmission geometry, silicon detectors can be stacked to enable Z identification of a broad range of particles by measuring energy loss and total energy ($\Delta E - E$ method).

The Louvain–Edinburgh Detector Array (LEDA) [346] was one of the pioneering charged-particle arrays for the detection of reaction residues in low-energy nuclear astrophysics experiments. For LEDA, the strips are curved in a circular pattern to realize an annular geometry. The CD-like detector consists of eight sectors with 16 strips (5 mm pitch) per sector. For such a configuration, the range of scattering angles and the angular resolution are determined by the target-detector distance. The removal of two sectors from the complete annular LEDA detector allows the remaining six sectors to be arranged as a six-sided cone (referred to as the LAMP configuration) providing very large solid-angle coverage at poorer angular resolution [346]. ORNL's Silicon Detector Array (SIDAR) [347] consists of single-sided silicon strip detectors of the LEDA-type (128 strips each) and a smaller CD-like detector with 64 strips in total for the detection and identification of the heavy

recoil [348,347]. The TRIUMF UK Detector Array (TUDA) facility at ISAC/TRIUMF is a cylindrical scattering chamber, where large-area silicon detectors of the LEDA-type or similar CD-shaped detectors can be mounted [349].

For the TUDA facility at TRIUMF, a large solid angle active target for the detection of low-energy charged particles in measurements of astrophysical reaction rates is being developed. The TRIUMF Annular Chamber for Tracking and Identification of Charged particles (TACTIC) [350] is a cylindrical ionization (time projection) chamber with segmented anode strips for the energy loss and total energy determination of light charged particles emerging from reactions. Measurements of the drift time provide trajectory reconstruction. Gas electron multipliers (GEM) will amplify the signals. Digital readout and pulse shape analysis of the signals is envisioned [350]. The chamber gas will serve as target similar to the active target device MAYA [351].

The $^{18}F(p,\alpha)^{15}O$ reaction has received much attention as it is of importance for nova γ-ray astronomy [352]. The γ-ray spectrum emitted from novae in the first few hours after expansion is dominated by the positron annihilation from the β^+ decay of radioactive nuclei. One of the main contributors is ^{18}F with a β-decay half-life of 110 min. Therefore, its production and destruction – via $^{18}F(p,\alpha)^{15}O$ – is of great importance. Direct measurements with ^{18}F radioactive beams have been performed at LLN [353–356], ANL [357] and ORNL [358–360]. Most of the early measurements [353,355,357,358] where performed at center-of-mass energies exceeding 550 keV, which dominate the reaction rate at temperatures above 0.4 GK. Graulich et al. in 1997 [354] found evidence for a $3/2^-$ resonance at $E_{cm} = 330$ keV but with insufficient statistics to determine the resonance strength. In 2002 Bardayan et al. [359] used a ^{18}F beam provided by the Holifield facility at ORNL with an intensity of 2×10^6 particles/s interacting with a CH_2 target to measure the $^{18}F(p,\alpha)^{15}O$ reaction. The α-^{15}O coincidences were unambiguously identified with the SIDAR setup and the $3/2^-$ resonance strength at $E_{cm} = 330$ keV could be determined for the first time. This resonance dominates the reaction rate over a range of temperatures important for ONeMg novae [359]. The region of lower center-of-mass energies, which is relevant for typical nova temperatures (≈ 0.25 GK), has remained inaccessible to direct measurement. Recent work at LLN [356] and ORNL [360] constrains the interference of $3/2^+$ resonances located just above the proton separation energy from new measurements at $E_{cm} > 400$ keV and $E_{cm} = 663 - 877$ keV, respectively, and from the wealth of previous data in comparison to $\mathcal{R}$-matrix calculations.

In explosive hydrogen burning up to a temperature of 0.2 GK, the burning with carbon takes place through a series of reactions known as the hot CNO cycle. At higher temperatures of about 0.4 GK, the ^{14}O waiting point can be bypassed by a chain of reactions initiated by $^{14}O(\alpha,p)^{17}F$. At still higher temperatures, the breakout from the CNO cycle becomes possible. The reaction that dominates the leak rate is $^{15}O(\alpha,\gamma)^{19}Ne$ [361]. However, in the regime of high temperature, alternative breakout routes have been suggested, in particular the $^{18}Ne(\alpha,p)^{21}Na$ reaction [362]. While a direct measurement of the key rate $^{15}O(\alpha,\gamma)^{19}Ne$ has not been feasible so far, the $^{18}Ne(\alpha,p)^{21}Na$ [363,364] and $^{14}O(\alpha,p)^{17}F$ [279] reactions have been probed directly in experiments induced by ^{18}Ne and ^{14}O radioactive beams at LLN and CRIB-Tokyo, respectively. The experiments at Louvain-la-Neuve covered the energy region of $E_{cm} = 2.04$–3.01 MeV [363] and $E_{cm} = 1.7$–2.9 MeV [364]. The measurements of the $^{18}Ne(\alpha,p)^{21}Na$ reaction rate were performed with a scattering chamber that consisted of a gas target and a vacuum side. The incoming ^{18}Ne beam interacted with the 500 mbar He gas target. Two double-sided silicon strip detector telescopes in the gas volume for $\Delta E - E$ measurements were used to detect the protons and to reconstruct their trajectories. The normalization of the incoming ^{18}Ne beam rate was based on the detection of elastically scattered ^{18}Ne off a gold foil in surface-barrier detectors on the vacuum side of the scattering chamber [276,363,364]. Groombridge et al. [364] identified eight states in the compound nucleus. Calculations of the enhanced stellar reaction rate using the new resonances as input show good agreement with theoretical predictions by [362]. The experimental reaction rate represents a lower limit and causes a breakout from the CNO cycle via $^{18}Ne(\alpha,p)^{21}Na$ to be delayed by several hundred ms when compared to calculations based on previous rates; further measurements are required at lower energies to map the lower-lying resonances above the α threshold [364].

At the CRIB facility, a ^{14}O beam interacted with a He gas target operated at a temperature of 30 K, enhancing the density compared to room temperature by a factor of 10 [279]. The $^{14}O(\alpha,p)^{17}F$ reaction products were identified with the ΔE–E methods in silicon detector telescopes. The reaction cross-section was measured with the thick-target technique over an energy range of $E_{cm} = 0.8$–3.8 MeV. This constituted the first direct measurement of the $^{14}O(\alpha,p)^{17}F$ reaction. The measured cross-section differs from conclusions based on an indirect measurement and from a direct measurement of the time-reversed reactions as the contributions of the ^{17}F excited states could not be taken into account [279]. The result seems to suggest an increase of 50% for the $^{14}O(\alpha,p)^{17}F$ reaction rate which might impact the ignition phase of X-ray bursts [279].

6.2.5. Resonance properties from elastic and inelastic scattering experiments

Some reaction rates of astrophysical interest are totally or partially dominated by the contribution of resonances. Important experimental methods to study the properties of resonance are resonant elastic and inelastic scattering. In particular, proton resonance scattering measurements have provided an extensive amount of data on unbound states in proton-rich nuclear systems relevant to reaction rates in explosive burning scenarios.

In inverse-kinematics resonant scattering, a rare-isotope beam bombards a proton-rich target — typically $(CH_2)_n$, rarely cryogenic H_2 targets. The spectrum of the scattered protons depends sensitively on resonances present in the compound nucleus. When a resonant state is scanned in the appropriate energy range, the scattered-proton spectrum shows a distinct structure that allows one to extract resonance properties – energy, width, spin and parity – in comparison to $\mathcal{R}$-matrix theory. The energy of the scattered proton is related to the resonant energy and the shape of the spectrum allows to

determine the width and the spin of the resonant state [365]. The protons are typically detected in position-sensitive Si ΔE–E telescopes or with annular Si strip detectors of the LEDA type. Important for the extraction of resonance properties from the shape of the proton recoil spectra in comparison to theory is a complete understanding of the experimental resolutions that contribute to the shape of the detected proton spectrum [365].

Two different experimental approaches are used, the thick-target and the thin-target technique. In the thin-target approach, see for example [366,347,367], the energy region of interest is scanned by using beams at different energy. At ORNL, resonances in the compound nucleus ^{19}Ne were studied with a ^{18}F beam at 15 different energies between 10 and 14 MeV [347] irradiating a 35 μg/cm^2 CH_2 target. The scattered protons were detected in SIDAR and ^{18}F passing through the target was identified in an ionization chamber [347]. In the thick-target approach, the beam is slowed down and stopped in the target and the elastic proton scattering can be performed over a range of energies that depends on the choice of target thickness and beam energy. This technique relies on the fact that the protons escape from the target as their energy loss is negligible compared to that of the heavy ion. This technique was used for example by Angulo et al. at Louvain-la-Neuve [368]. A ^{18}Ne beam at 28 MeV impinged upon a 520 μg/cm^2 CH_2 target. The recoil protons were detected at 20 different angles with LEDA and the first excited state of ^{19}Na could be characterized [368].

Inverse-kinematics resonant proton scattering measurements have been performed, for example, with the thick-target technique at the TUDA facility at TRIUMF/ISAC, ^{21}Na + p [369,370] and ^{20}Na + p [371]; with the thin and thick-target approach at HRIBF/ORNL, ^{17}F + p [366,367] and ^{18}F + p [347,372]; at Louvain-la-Neuve with the thick-target technique, ^{13}N, C + p [373], ^{19}Ne + p [374], ^{18}F + p [355],^{18}Ne + p [368], and ^{7}Be + p [375]; at CRIB in Tokyo with the thick-target technique, ^{11}C + p [376], ^{22}Mg + p [377] ^{13}N + p [378,379], and ^{7}Be + p [380]; at the BEARS facility in Berkeley, ^{14}O + p [381], ^{11}C + p [382] and ^{15}O + p [383]; as well as at Texas A&M [384,382], Notre Dame [385,386], ANL [387] and Spiral/GANIL [388].

Inelastic resonance proton scattering has been employed to probe the properties of states in the compound nucleus in the cases where particle decay to excited states is energetically possible. Recently, proton emitting states in ^{19}Ne were studied with the inelastic scattering reaction H(^{19}Ne, p)^{19}Ne*(p)^{18}F at Louvain-la-Neuve. Resonance energies and widths were assigned from the shape of the scattered proton spectrum, while spins were assigned using proton-proton angular correlations between recoil and decay protons [389].

Inelastic scattering gains importance when rates are derived from measurements of the inverse reaction. For example, when the reaction $A(p,\alpha)B$ is measured, A is typically in its ground state and the rate of $B(\alpha,p)A_{gs}$ can be deduced from the detailed balance. However, contributions from $B(\alpha,p)A^*$ leading to an excited state in A are not accessible from the inverse reaction with A in the ground state. Inelastic scattering $A + p \rightarrow A^*$ can then reveal important excitations that may contribute. One example is the ^{14}O$(\alpha,p)^{17}$F reaction, which was studied from measurements of the inverse reaction ^{17}F$(p,\alpha)^{14}$O [390,391]. Proton inelastic scattering ^{17}F + p were measured at ANL [387] and ORNL [367] to characterize resonances of importance for the ^{14}O$(\alpha,p)^{17}$F reaction rate. For the measurement of inelastic scattering, thin targets are typically used to separate elastic and inelastic channels from the spectroscopy of the protons [367] or γ-ray spectroscopy is used to tag bound final states, see for example [380], where NaI detectors were used to measure ^{7}Be$(p,p')^{7}$Be*.

6.2.6. Nucleon transfer reactions, nucleon knockout and population of excited states in fragmentation and projectile fission

For stable nuclei, light-ion induced transfer reactions in normal kinematics have been widely used to explore stellar reaction rates by extracting spectroscopic information on resonances close to the threshold that dominate the reactions of interest. The parameters of a resonance – energy, orbital angular momentum, partial and total width, spectroscopic factors and decay modes, for example – can be determined. In general, the sensitivity of transfer reactions to the single-particle degree of freedom continues to provide important data to benchmark nuclear structure models, in particular the nuclear shell model which provides important input to the modeling of many astrophysical processes (see Section 5.3 for details on the theoretical treatment of transfer reactions).

Neutron capture cross-sections are important in the r process, in which heavier nuclei are formed from seed elements by consecutive neutron capture reactions and β decays. In an environment of high neutron density, tens of neutron captures may occur until the β decay half-lives become shorter than the half-life against neutron capture. Consequently, the process proceeds off the valley of stability towards neutron-rich nuclei. For most neutron capture cross-sections, statistical models can be applied. However, near closed shells – in a regime of low level density – direct capture becomes important [392]. For direct capture calculations, level properties (excitation energies, spins and parities) have to be known accurately unlike for statistical calculations where averages over resonances are considered.

Following pioneering inverse-kinematics (d,p) one-neutron transfer experiments induced by stable Xe beams impinging upon deuterated Ti targets performed at GSI [393], a program of low-energy (d,p) transfer experiments in mass regions relevant to the r process was started at HRIBF at ORNL. The experimental study of d(^{124}Sn, p) in inverse kinematics at energies close to the Coulomb barrier proved that Q-value spectra and angular distributions can be extracted for low-energy inverse-kinematics transfer reactions with heavy beams [394]. This experiment used a deuterated polyethylene target (CD_2) of 100 μg/cm^2 thickness that was angled to achieve an effective thickness of 200 μg/cm^2 and to enable proton detection under $\theta_{lab} = 90°$. Two silicon telescopes were positioned covering angles of $\theta_{lab} = 70°$–$102°$ and $\theta_{lab} = 85°$–$110°$, respectively. The silicon detector array SIDAR was mounted in half-lampshade configuration covering backward angles of $\theta_{lab} = 130°$–$160°$. The states were determined from the Q-value spectrum and the angular distributions were used to determine the orbital angular momentum (ℓ value) of the transferred neutron. An absolute normalization of the cross-sections was performed using the elastically scattered deuterons [394]. The results were found to be in agreement with

normal-kinematics ^{124}Sn(d, p) and demonstrated that this important mass region for the r process can be accessed with low-energy, inverse-kinematics transfer reactions.

The first (d, p) transfer on a neutron-rich r process nucleus, ^{2}H(^{82}Ge, p)^{83}Ge at 330 MeV on a 430 μg/cm^2 $(CD_2)_n$ target, was subsequently performed at HRIBF [395]. Protons were detected with SIDAR, subtending $\theta_{lab} = 105°$–$150°$. A segmented ion chamber was employed to determine the Z of the projectile-like reaction residues. The measured reaction Q-value provided an indirect measurement of the mass of ^{83}Ge. The extracted neutron separation energy $S_n = 3.69$ MeV was found low suggesting that the ^{82}Ge$(n, \gamma)^{83}$Ge reaction rate has a significant direct neutron capture component. The excitation energy of the $1/2^+$ excited state followed the falling trend as semi-magic ^{79}Ni is approached [395]. ^{84}Se was the main contaminant in the beam and the (d, p) neutron transfer to ^{85}Se was studied at the same time [396]. Direct-semidirect contributions to the neutron capture cross-sections were computed [396]. Recently, neutron capture extracted from (d, p) transfer reactions was benchmarked for ^{48}Ca$(d, p)^{49}$Ca at different deuteron energies [397].

One of the key reactions in nova γ-ray astronomy, ^{18}F$(p, \alpha)^{15}$O, has been explored indirectly by exploiting ^{2}H(^{18}F, p)^{19}F neutron transfer reactions and the ^{19}Ne–^{19}F mirror symmetry [398–400]. Spectroscopic information on excited states just above the proton separation energy in the compound nucleus ^{19}Ne is needed for the determination of the ^{18}F$(p, \alpha)^{15}$O reaction rate at nova temperatures. Some of the levels in ^{18}F$+p$ cannot be reached in resonance scattering experiments since the resonances are well below the Coulomb barrier. With the availability of a ^{18}F rare-isotope beam, neutron spectroscopic factors of the analog levels in the mirror nucleus of ^{19}Ne, ^{19}F, can be studied with (d, p) reactions in the corresponding energy region and – invoking mirror symmetry – serve as input to calculate the proton width in ^{19}Ne. At Louvain-la-Neuve, a 14 MeV ^{18}F beam impinging upon a 100 μg/cm^2 CD_2 target was used to induce the (d, p) neutron transfer reaction [398]. The relevant levels are above the α separation energy leading to $^{19}\mathrm{F}^* \rightarrow {}^{15}\mathrm{N} + \alpha$. The measurement employed the LEDA detector for the detection of ^{15}N (downstream) and the LAMP detector (backward) for proton detection. Spectroscopic factors deduced in comparison to DWBA calculations were used to put new limits to the contribution of low-energy resonances to the ^{18}F$(p, \alpha)^{15}$O reaction rate [398]. A similar experiment was performed at HRIBF at ORNL at a much higher energy with a 108.49 MeV beam of ^{18}F on a 160(10) μg/cm^2 CD_2 target [399,400]. The protons emerging from the ^{2}H(^{18}F, p)^{19}F transfer reaction were detected with the silicon strip detector array SIDAR at $\theta_{lab} = 118°$–$157°$. Another silicon strip detector at the focal plane of the Daresbury Recoil Separator was used to tag particle-stable $A = 19$ reaction residues and α-decaying final states in coincidence with the protons detected in SIDAR. Neutron spectroscopic factors for eight [399] and 13 [400] analog levels of astrophysical relevance in the mirror ^{19}Ne were determined. The results implied significantly reduced ^{18}F$(p, \gamma)^{19}$Ne and ^{18}F$(p, \alpha)^{15}$O rates compared to what was reported previously [399].

The (d, n) transfer reaction has been used at the RESOLUT facility at Florida State University as surrogate for proton capture. The reaction $^{25}\mathrm{Al}(d, n)^{26}\mathrm{Si}^* \rightarrow p + {}^{25}\mathrm{Al}$ was induced by a 91.5 MeV beam of ^{25}Al impinging upon a 1.66 mg/cm^2 thick CD_2 target [401]. The decay protons were detected under forward angles with the $\Delta E - E$ method using a hybrid ion chamber and a double-sided silicon strip detector backed by a second, unsegmented silicon detector. The lowest $\ell = 0$ proton resonance in ^{26}Si could be identified. This shifts the main experimental uncertainty in the synthesis of ^{26}Al to the destruction of ^{26m}Al through the (p, γ) reaction, which is planned to be studied at RESOLUT in the future [401].

The use of heavy-ion induced, peripheral, proton-adding transfer reactions of type (^{14}N,^{13}C) [402,403,307], (^{10}B,^{9}Be) [404, 405,402] and (^{13}C,^{12}C) [406] in inverse kinematics as well as (^{3}He, d) in normal kinematics [407–409] has been pioneered at Texas A & M to indirectly assess the non-resonant direct-capture contribution in (p, γ) reactions. Asymptotic normalization coefficients (ANCs) [42,407,402] are deduced from the measured angular distributions in transfer reactions at energies above the Coulomb barrier where the cross-sections are orders of magnitude higher than for direct capture processes at astrophysical energies (see Section 5.3.2). Radioactive beams of ^{7}Be (84 MeV), ^{11}C (10 MeV/u), and ^{13}N (11.8 MeV/u) were produced at Texas A & M and separated with the MARS spectrometer. ^{10}B(^{7}Be,^{8}B)^{9}Be, ^{14}N(^{7}Be,^{8}B)^{13}C, ^{14}N(^{13}N,^{14}O)^{13}C, and ^{14}N(^{11}C,^{12}N)^{13}C transfer reactions induced by ^{10}B and melamine ($C_3N_6H_6$) targets, respectively, were used to determine the ANCs for $^{8}\mathrm{B} \rightarrow {}^{7}\mathrm{Be} + p$, $^{14}\mathrm{O} \rightarrow {}^{13}\mathrm{N} + p$, and $^{12}\mathrm{N} \rightarrow {}^{11}\mathrm{C} + p$ to deduce the non-resonant capture rates for the ^{7}Be$(p, \gamma)^{8}$B, ^{13}N$(p, \gamma)^{14}$O and ^{11}C$(p, \gamma)^{12}$N reactions. In these experiments, the elastically scattered projectile beam and transfer products are observed simultaneously in two detector telescopes consisting of position-sensitive 16-strip Si ΔE detectors backed by Si E detectors. Particle identification is then done via the ΔE–E method. The reaction telescopes were cooled down to -6 °C to reduce thermal noise. A slightly different approach was taken at HRIBF at ORNL to study the ^{17}F$(p, \gamma)^{18}$Ne direct capture cross-section [410]. A beam of 170 MeV ^{17}F impinged upon a melamine target inducing the ^{14}N(^{17}F,^{18}Ne)^{13}C reaction. Recoiling ^{18}Ne nuclei were detected via energy loss in position-sensitive Si strip detectors covering center-of-mass angles from 2° to 9°. To be able to distinguish the transfer to individual excited states, γ rays emitted by ^{18}Ne were detected in CLARION in coincidence and allowed to tag the final state. Preliminary results are reported [410].

The ANC technique was also applied to a sub-Coulomb α-transfer reaction ^{13}C(^{6}Li, d) performed at FSU with a ^{13}C beam at 60 MeV to study the astrophysical reaction rate of ^{13}C$(\alpha, n)^{16}$O which – at low energies – is dominated by a $1/2^+$ sub-threshold resonance in ^{17}O [411]. The application of the ANC method also to one-nucleon removal and breakup reactions induced by weakly-bound projectile nuclei and light as well as heavy target nuclei was proposed [412,413].

A different experimental approach that utilizes the high luminosity of fast-beam experiments at fragmentation facilities was developed at NSCL. The one-neutron removal from a projectile beam of ^{34}Ar upon collision with a CH_2 target at 84 MeV/nucleon was used to populate excited states in ^{33}Ar [166]. In-beam γ-ray spectroscopy using the segmented germanium array SeGA [414] provided precision information on the excitation energy of states in the proximity of the proton separation energy and for states above S_p that have a γ branch. High-resolution γ-ray spectroscopy allowed to determine

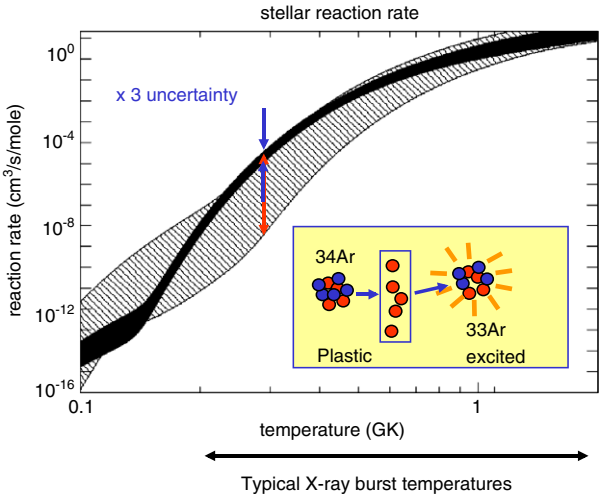

Fig. 27. Total astrophysical ^{32}Cl$(p,\gamma)^{33}$Ar ground-state capture rate as function of T_9 [167]. The black region shows the capture rate restricted by the one-neutron knockout measurement of Clement et al. [166] relative to the previously possible range of rates (gray band). The total estimated uncertainty of the rate ranges from a factor of 3 to a factor of 6. (Figure adapted from Hendrik Schatz and Ref. [167]).

the excitation energy with uncertainties of several keV. The 2-orders of magnitude improvement in the uncertainty of the level energy translated into an 3-orders of magnitude improvement for the rate of ^{32}Cl$(p,\gamma)^{33}$Ar [166] (see Fig. 27). Similar measurements have been performed to precisely determine relevant level energies in ^{30}S [415]. Pioneered at NSCL, ^{9}Be-induced one-nucleon removal reactions from fast exotic beams have proven to be a crucial tool to study the detailed evolution of nuclear shell structure in exotic nuclei [156,416]. Their reach to the most exotic nuclei and the sensitivity to the single-particle degree of freedom continue to probe the predictability achieved by large-scale shell model calculations, which provide crucial input for many astrophysical processes (see also Section 5.4).

A less selective method is the population of isomeric excited states in projectile fragmentation or fission and the spectroscopy of the level structure fed by the long-lived state(s). At GSI, γ-ray decays of excited states in the $N = 82$ r-process waiting-point nucleus ^{130}Cd were observed unambiguously for the first time [417]. An 8^+ isomeric state in ^{130}Cd with a two-quasiparticle structure was populated in the fragmentation of a ^{136}Xe beam and in the fission of ^{238}U. In the two parts of the experiment, heavy, neutron-rich beams were produced by fragmentation of a ^{136}Xe beam at 750 MeV/nucleon impinging upon a 4 g/cm^2 ^{9}Be target and by a 650 MeV/nucleon ^{238}U beam fissioning upon collision with a 1 g/cm^2 thick ^{9}Be target. The produced ^{130}Cd nuclei were separated with the GSI fragment separator (FRS) and identified via the measured energy loss, time of flight, magnetic rigidity, and various position measurements. The nuclei were implanted into a passive stopper surrounded by 15 large-volume Ge cluster detectors [418]. The new 2_1^+ energy of 1395 keV for ^{130}Cd is not consistent with the previous tentative assignment of the 2^+ state at 957 keV [419]. The evidence for the existence of an 8^+ isomer in ^{130}Cd is in line with expectations based on the valence analog ^{98}Cd. These new results on the level scheme of ^{130}Cd provided no evidence for a reduction of the $N = 82$ shell gap in the vicinity of ^{132}Sn contrary to what was implied by the results of a previous experiment [420]. In a similar measurement at GSI, excited states in the magic nucleus ^{204}Pt (neutron number $N = 126$) were populated in the fragmentation of ^{208}Pb at 1 GeV/nucleon beam energy [421]. Medium spin isomers with half-lives between 150 ns and 55 μs and the level structures fed by their decays were identified. The data suggested a revision of the two-body interactions for $N = 126$ and $Z < 82$, which is important for the evolution of nuclear structure toward the waiting points of the r process in this region [421].

6.2.7. *Weak-interaction strength*

Supernovae are a major source of nucleosynthesis. For both types of supernovae – core-collapse and thermonuclear – weak interaction rates play are crucial role [181,182,18]. In particular electron capture rates for many nuclei in the *fp*-shell and beyond are among the important nuclear physics ingredients needed for supernova models [422]. The weak-interaction rates are largely provided by nuclear structure calculations, as for example by large-scale shell-model calculations [183,185]. Important experimental benchmarks necessary for the reliable modeling of weak-interaction rates by nuclear theory are provided by measured Gamow–Teller (GT) strength distributions (see Section 5.6 for details on the theoretical formalism).

GT transition strength ($B(GT)$ values) can be obtained from Gamow–Teller β decays within excitation-energy limitations given by decay Q-value window. Charge-exchange reactions, however, can map the GT strength distributions over a wider range of excitation energies. A variety of charge-changing reactions can be employed, for example, ^{A}Z$(p,n)^{A}$(Z+1) [423,171], ^{A}Z$(n,p)^{A}$(Z − 1) [424], ^{A}Z$(d,{}^{2}\mathrm{He})^{A}$(Z − 1) [425], ^{A}Z$({}^{3}\mathrm{He},t)^{A}$(Z + 1) [426–429], and ^{A}Z$(t,{}^{3}\mathrm{He})^{A}$(Z − 1) [430–433]. In charge-exchange reactions at beam energies exceeding 100 MeV/nucleon, the cross-section at low momentum transfer (small angles) is proportional to the $B(GT)$ transition strength [434–436,171,173]. GT transitions have been probed extensively

with the charge-exchange reactions induced by stable projectiles on stable targets (see references above). Charge-exchange reactions on short-lived exotic nuclei in inverse kinematics are proposed to be developed into spectroscopic tools at FAIR (Germany) [437] and at NSCL (US) [438]. At FAIR, the utilization of charge-exchange reactions is proposed by the EXL [439] and by the R^3B [440] collaborations. At R^3B, (p, n) charge-exchange reactions will be induced by rare-isotope beams at relativistic energies impinging upon a liquid hydrogen target with the emerging slow neutrons measured by plastic scintillators surrounding the target [440]. The EXL collaboration envisions the study of charge exchange via (p, n), $(^3\mathrm{He}, t)$, and $(d, ^2\mathrm{He})$ reactions with unmatched luminosity induced by rare isotopes circulating in a storage ring passing through a gas jet target [439]. Two avenues are taken at NSCL, the first program utilizes the $^{A}\mathrm{Z}(^7\mathrm{Li},^7\mathrm{Be})^{A}(\mathrm{Z\text{-}1})$ induced charge-exchange reaction where the spin transfer is tagged with the 430 keV γ-ray decay $(1/2^- \rightarrow 3/2^-)$ in the target-like reaction residue ^{7}Be [441]. For a second program, the Low-Energy Neutron Detector Array (LENDA) [442] is presently constructed for slow-neutron detection in (p, n) charge-exchange reactions induced by rare-isotope beams bombarding a hydrogen target. In all NSCL experiments, the projectile-like fragments will be tracked and identified with the S800 spectrograph [438].

6.2.8. Beta-decay half-lives and β-delayed neutron emission probabilities

Isotopes of elements beyond iron are almost exclusively produced in neutron-capture processes. The two main neutron-capture processes for astrophysical nucleosynthesis are the slow s process and the rapid r process (see [4] for a review). The attributes slow and rapid refer to the timescale between subsequent neutron captures relative to the competing time scale for β decay. While the s process stays close to the valley of stability, the r process leads to very neutron-rich nuclei. To determine the path of the r process, among others, β-decay properties are crucial. Beta decay competes with the neutron capture and the drives the path toward stable nuclei and fission determines the heaviest nuclei produced. On the proton-rich side of the nuclear chart, β-decay half-lives are an important input for nucleosynthesis models that describe the reaction flow in the rp process and the final abundances. While much data has been available on the proton-rich side of the nuclear chart, some information in key regions, as for example around the nuclei ^{92,94}Mo and ^{96,98}Ru, which are found in the solar system in unexpectedly large abundances, could only be gathered recently with technical improvements crucial for experiments on proton-rich nuclei.

Two approaches have been taken to measure the β-decay half-lives and β-delayed neutron emission probabilities. At the Jyväskylä (IGISOL) and the CERN/ISOLDE facilities, neutron-rich isotopes of interest are produced by fission, mass-separated and implanted into a collection tape, which moves at pre-set times to suppress the β and γ activity from longer-lived isobaric contaminants. Time spectra are recorded for γ-ray, neutron and β events where the half-lives and production rates can be derived from the growth and decay curves of the collected activities during the pulsed beam mode. At fragmentation facilities, tracking and event-by-event particle identification become possible in the regime of fast beams [443]. The fast-moving beam particles are, for example, implanted into a double-sided silicon strip detector (DSSD) with subsequent β decays detected on an event-by-event basis and correlated with the position of a specific implantation. All events are typically time-stamped and the decay curve is constructed from the time difference between implant and correlated decay. This method is applicable at rates of less than 0.1 particles per second.

In early experiments at Jyväskylä, the β-decay half-lives and β-delayed neutron emission branching ratios of neutron-rich Y, Nb, and Tc isotopes produced in the proton-induced fission of ^{238}U were determined [444,445]. The mass-separated nuclei of interest were implanted onto a collection tape and their decays were measured inside the Mainz 4π neutron long counter used for the detection of β-delayed neutrons. The β-particle detection and γ-ray detection were performed with a thin plastic scintillator and a planar germanium detector, respectively, positioned inside the Mainz counter. The neutron long counter consisted of 42 ^{3}He ionization chamber tubes, arranged in two concentric rings embedded in a polyethylene matrix surrounding the implantation point [444,445]. At CERN/ISOLDE, the β-decay properties of ^{130,131,132}Cd were studied [446,420]. In 2000, the heavier ^{131,132}Cd isotopes were produced from proton-induced uranium fission and purified with resonance-ionization laser ion source (RILIS) and subsequent separation of the extracted nuclei with the General Purpose Separator (GPS). Beta-decay half-lives and β-delayed neutron decay branching ratios P_n were determined using the βn spectroscopy with the Mainz neutron long counter and a $\Delta E\beta$ plastic scintillator [446]. Superior separation was achieved for the study of ^{130}Cd and its decay daughter ^{130}In, in the vicinity of the $Z = 50, N = 82$ r-process waiting point. ^{130}Cd was produced by fission induced with fast reaction neutrons – generated from a 1 GeV proton beam impinging upon a Ta or W rod – interacting with the uranium carbide/graphite production target. The highest chemical selectivity was achieved with RILIS and separation using the High-Resolution Separator (HRS). $\beta\gamma$ and $\beta\gamma\gamma$ spectroscopy around the moving-tape-collector was performed with ΔE–$E\beta$ telescope and four large-volume high-purity germanium detectors in close geometry [420].

On the proton-rich side of the nuclear chart and important for ONe novae, ^{23}Al was studied at Texas A&M [447]. ^{23}Al was produced via the $p(^{24}\mathrm{Mg}, ^{23}\mathrm{Al})2n$ reaction, separated by the MARS separator and collected with a moving-tape system to a detector setup for β and $\beta\gamma$ spectroscopy consisting of a thick plastic scintillator for β detection and a high-purity germanium detector for γ-ray detection [447]. Beta branching ratios and log ft values for transitions to levels in ^{23}Mg were extracted. From this, the ground-state spin and parity $5/2^+$ of ^{23}Al were determined unambiguously. This excludes the large increases in the radiative proton capture cross-section for the reaction $^{22}\mathrm{Mg}(p, \gamma)$ at astrophysical energies, which were implied by earlier claims that the spin and parity of the ^{23}Al ground state are $1/2^+$ [447].

Rare-isotope beams produced by projectile fragmentation are used at NSCL to measure the β-decay properties of exotic nuclei of importance to nuclear astrophysics. In-flight tracking and event-by-event particle identification become possible

in the regime of fast beams. The fast-moving beam particles are implanted into a double-sided silicon strip detector (DSSD) with 40 horizontal and vertical strips resulting in a pixelation of 1600, the center piece of NSCL's Beta Counting Station (BCS) [448]. Subsequent β decays are detected on an event-by-event basis and correlated with the position of a specific implantation. Downstream of the DSSD, six single-sided Si strip detectors (SSSDs) and two Si PIN detectors comprise the β calorimeter part of the BCS. All events in the BCS carry an absolute time stamp and the time difference between implant and decay serves to map the β decay curve. Coincident γ-ray spectroscopy and β-delayed neutron spectroscopy can be performed with the Segmented Germanium Array (SeGA) [414] and the Neutron Emission Ratio Observer (NERO) [449] — a neutron long counter with ^{3}He and BF_3 gas counters. As the γ-rays are emitted by nuclei at rest, the segmentation of SeGA is not used. NERO consists of 60 proportional gas-counter tubes – 16 filled with ^{3}He and 44 filled with B_3F – embedded in a polyethylene moderator. The counters are arranged parallel with the beam direction in three concentric rings around the vacuum beam line that accommodates the BCS. A DSSD-based β counting system similar to the BCS is being developed for experiments at GSI with the RISING setup [450]. A challenge in implant and decay setups is the large difference in the energy response to fragments that are stopped and implanted in the DSSD (several GeV) and the energy signals of charged-particle decays (hundreds of keV). The β-decay detection system for RISING will use logarithmic preamplifiers to cover the required dynamic range [450] while NSCL's BCS is using preamplifiers with dual gain capability, low gain for the fragment implantation and high gain for the detection of decays [448].

The half-life of the doubly-magic nucleus ^{78}Ni is important input for r-process model predictions of the nucleosynthesis around $A = 80$ [451]. At NSCL, ^{78}Ni was produced via projectile fragmentation from a beam of ^{86}Kr at 140 MeV/nucleon impinging upon a beryllium target of 376 mg/cm^2 thickness. Each nucleus in the secondary beam was individually identified in flight by measuring energy loss and time of flight (TOF). The ions were continuously implanted into the DSSD. In the regime of very low beam rate for this exotic nucleus, the typical total implantation rate for the entire detector was under 0.1 per second. The DSSD registered the time and position of the decays following the implantation. This allowed the correlation of 7 implanted nuclei with subsequent decay events. The measured half-life indicated a rather short time scale for the buildup of heavy elements beyond $N = 50$ compared to some earlier predictions and thus unraveled an acceleration of the r process in this region [451].

For a similar experiment near the $N = 82$ neutron shell closure, neutron-rich Tc, Ru, Rh, Pd, and Ag isotopes were produced at the NSCL by fragmentation of a 121.8 MeV/nucleon ^{136}Xe primary beam impinging onto a 206 mg/cm^2 Be target [452]. The secondary beam was then transmitted to the experimental vault, where a second plastic scintillator provided the stop signal for the TOF measurement (relative to a timing signal from a scintillator located at the intermediate image of the A1900 fragment separator) before the beam was implanted into the NSCL's BCS for the study of the subsequent β decay. The average implantation rate in the DSSD was 0.4 Hz. Implantation and decay events were time stamped and correlated via their pixel locations. Coincident β-delayed neutrons were detected with NERO. β-delayed neutron emission branchings (or upper limits) for the neutron-rich nuclei $^{116-120}$Rh, $^{120-122}$Pd, and ^{124}Ag were determined as well as β-decay half-lives for neutron rich $^{114-115}$Tc, $^{114-118}$Ru, $^{116-121}$Rh, and $^{119-124}$Pd near the proposed the r-process path [452]. A little lower in Z, the β-decay properties of Y, Zr and Mo nuclei around $A = 110$ were measured [453]. Fast beams of neutron-rich Y, Zr, Nb, Mo, and Tc isotopes were produced at NSCL by fragmentation of a 120 MeV/nucleon ^{136}Xe beam on a thick Be target. The species of interest were separated and identified with the A1900 fragment separator using the $B\rho$–ΔE–$B\rho$ method and implanted in the BCS which was surrounded by NERO. New half-lives for ^{105}Y, ^{106,107}Zr, and ^{111}Mo, along with new P_n values for ^{104}Y and ^{109,110}Mo and P_n upper limits for $^{103-107}$Zr and ^{108,111}Mo were determined. Analysis of the measured $T_{1/2}$ and P_n values in the framework of QRPA calculations brought new insights in terms of deformation and shape coexistence, compatible with the hypothesis of a quenched $N = 82$ shell gap invoked by some to explain the r-process abundances around $A = 110$. An experimental complication at high Z is the presence of charge states in the secondary beam [453]. Measurements of the ion's total kinetic energy with the PIN detectors and the DSSD of the BCS are used to separate the fully stripped ions from charge states; isomer tagging with germanium detectors of the SeGA array is typically performed to confirm the particle identification.

The $N = Z$ nuclei ^{84}Mo and ^{100}Sn and nuclei in the vicinity of $N = Z = 50$, ^{96}Cd and ^{98}In, that lie along the rp-process path became accessible for β-decay measurements at NSCL only after implementation of the Radio-Frequency Fragment Separator (RFFS). With the energies available at NSCL, secondary beams optimized on neutron-deficient species are of low purity due to extended low-momentum tails of higher-rigidity fragments which overlap with the fragment momentum distribution of interest. The RFFS applies a transverse RF electric field which deflects nuclear species in the secondary beam based on their phase difference with the primary beam. Secondary beams containing ^{96}Cd, ^{98}In, ^{100}Sn [454] and ^{84}Mo [455] were produced by projectile fragmentation of ^{112}Sn and ^{124}Xe primary beams, respectively, and purified by the RFFS. The BCS was used in both cases to measure the β-decay half-lives. The new result for ^{84}Mo resolved a previously reported deviation from theoretical predictions [455] and the measurements around ^{96}Cd revealed that the rp process in X-ray bursts is not the main source of the unexpectedly large amount of ^{96}Ru in the solar system [454].

More technical details and applications to nuclear structure research can be found in the recent review articles by Mantica [443] and Rubio and Gelletly [456].

6.2.9. Mass measurements

Atomic masses of rare isotopes across the nuclear chart are among the key input data for large-scale reaction network calculations that quantify the nucleosynthesis, for example, via the rp process, ν p process and the r process (see for

example [457]). Experimental methods for the determination of atomic masses basically fall into two categories. Approaches that measure the Q values in decays or reactions make use of Einstein's mass-energy equivalence; mass measurements that are based on the deflection of ions in electromagnetic fields determine the mass-to-charge ratio. The highest precision in mass spectrometry today is obtained by frequency measurements. The revolution or cyclotron frequencies of ions in a magnetic field are measured to deduce the mass-to-charge ratio in Penning trap experiments, in time-of-flight measurements involving cyclotrons and in storage rings. The different experimental methods are optimized for different beam energy regimes and are thus linked to the production and separation schemes of the rare isotopes.

Penning traps use the three-dimensional confinement of ions with static magnetic and electric fields. Mass measurements in a trap are based on the determination of the cyclotron frequency of the stored ions in a magnetic field. The ion motion in the combined magnetic and electric fields is the superposition of three (ideally) independent harmonic motions with eigenfrequencies ω_z (axial motion), ω_+ (modified cyclotron motion) and ω_- (magneton motion). Their frequencies are:

$$\omega_z = \sqrt{\frac{qV_0}{mr^2}}, \qquad \omega_\pm = \frac{\omega_c}{2} \pm \sqrt{\frac{\omega_c^2}{4} - \frac{\omega_z^2}{2}}, \quad \omega_c = \omega_+ + \omega_- \tag{133}$$

with the cyclotron frequency $\omega_c = qB/m$ and the characteristic trap dimension r. The sum $\omega_- + \omega_+ = qB/m$ is directly proportional to the charge-to-mass ratio. Inside the trap, the ions are excited by an azimuthal quadrupolar RF field with frequencies around ω_c. The ions are released from the trap and their kinetic energy is determined from a time-of-flight measurement. In case of a resonant excitation ω_c, the radial kinetic energy of the released ion will be maximal and its time of flight minimal. Unknown masses are then determined relative to calibration measurements of nuclei with precisely known masses. Relative mass uncertainties of order 10^{-8} are routinely achieved. The Penning trap setups used for mass spectrometry of exotic nuclei are ISOLTRAP [458,459] at CERN/ISOLDE (Switzerland), CPT [460,461] at ANL (US), SHIPTRAP [462–464] at GSI (Germany), JYFLTRAP [465,466] at Jyväskylä (Finland), LEBIT [467–469] at NSCL (US) and TITAN [470] at TRIUMF (Canada).

At GSI, rare-isotopes are produced in-flight, selected in the Fragment Separator (FRS) and subsequently injected into the Experimental Storage Ring (ESR) [471]. For two ion species circulating in the ring the relative difference in the mass-to-charge ratio m/q of the revolving ion species is expressed to first order as:

$$\frac{\Delta f}{f} = -\frac{1}{\gamma_t^2}\frac{\Delta(m/q)}{m/q} + \left(1 - \frac{\gamma^2}{\gamma_t^2}\right)\frac{\Delta v}{v}, \tag{134}$$

where f, m/q, v and γ are the mean values of frequency, mass-to-charge ratio, velocity and Lorentz factor, respectively, and $\Delta f = f_1 - f_2$, $\Delta(m/q) = (m_1/q_1) - (m_2/q_2)$ and $\Delta v = v_1 - v_2$ are the corresponding differences for the two ion species. The transition point γ_t characterizes the point where the revolution frequency becomes independent of the energy for each species with fixed m/q. This quantity can be varied within certain limits by adjustments of the ring's ion optics. The ESR can be operated in two different optics modes to deduce mass-to-charge ratios. For longer-lived nuclei ($T_{1/2}$ of the order of seconds), the velocity spread $\Delta v/v$ of the ions can be reduced by electron cooling (Schottky method). Then the term of Eq. (134) that depends on the velocity spread becomes negligible and the m/q can be directly determined from the frequency of revolution. The frequency is determined via the Schottky noise pickup technique. Many species can be stored in the ring simultaneously, with ions of precisely known mass serving as calibrants. Relative mass uncertainties are typically of order 10^{-7} [472,471]. For short-lived nuclei, the ring can be operated in isochronous mode. Here, the Lorentz factor is chosen to match γ_t, where the revolution time becomes independent of the velocity and the mass-to-charge ratio can be deduced. Typically, thin-foil timing detectors are used to measure the time of flight. Since this approach does not require cooling, short-lived ions ($T_{1/2}$ of order 10 μs) can be studied [473,471]. Future measurements at the ESR will probably also address the masses of neutron-rich nuclei, in particular those involved in the r process of stellar nucleosynthesis, as these can be produced efficiently by uranium projectile fission with subsequent separation in-flight by the FRS at GSI.

Another frequency-based mass measurement concept is implemented at ISOLDE with the radiofrequency transmission mass spectrometer MISTRAL [474,475], where in a homogeneous magnetic field a controlled and coherent manipulation of the ion trajectory is performed to determine the mass via the cyclotron frequency.

Time-of-flight measurements in combination with magnetic spectrometers or cyclotrons are used in various experimental schemes to determine the mass-to-charge ratio of short-lived ions. An ion's motion in a magnetic field can be characterized by the magnetic rigidity $B\rho$ which is connected to the mass-to-charge ratio via the ion's velocity v or cyclotron frequency ω_c:

$$B\rho = \frac{\gamma m v}{q} = \frac{vB}{\omega_c}, \tag{135}$$

where γ is the Lorentz factor. The magnetic rigidity can be measured with high-resolution magnetic spectrometers, the velocity can be determined from the acceleration potential at low energy [476] (ISOLDE) or directly from time-of-flight measurements at higher beam energies [477,478] at GANIL and NSCL, for example. For a given detector time resolution, the resolution of the time-of-flight measurement is limited by the total flight time. An increased flight time can be realized with the use of cyclotrons [479]. For two ions with masses m and $m + \delta m$, accelerated simultaneously in a cyclotron, the time

difference δT, after n_T turns is given to first order by $\delta T/T = \delta m/m$. Relative to a well-known mass m, the mass $m + \delta m$ can be derived from the flight times of the ions.

Q-values of radioactive decays can provide accurate mass differences between parent and daughter nuclei. For a long time, β decay was one of the main sources of mass determinations (β^+ decay and electron capture (EC) for proton-rich nuclei and β^- decay on the neutron-rich side of the nuclear chart). If the decay proceeds to excited states in the daughter nucleus, the mass difference has to be adjusted for the excitation energy, meaning that in addition to the determination of the β end-point energy, spectroscopy of the daughter has to be performed in coincidence (see [480] for a review). Q_α or Q_p measurements are less complicated owing to the fact that the α particle or proton do not share their energy with a neutrino, thus making the energy difference a more direct observable for ground-state to ground-state decays [481]. Mass differences may also be derived from the energy balance in reactions. In a two-body reaction, $A(B, C)D$, the mass excesses Δ are related via the amount of released energy Q:

$$Q = \Delta_A + \Delta_B - \Delta_C - \Delta_D. \tag{136}$$

If three of the masses are well known, the determination of the Q-value from a measurement of the reaction kinematics will allow the mass of the remaining reaction partner to be extracted. This method also works for extracting the mass of unbound systems when the decay particle is detected (invariant mass method) [482]. For both approaches based on decay or reaction Q values, the mass differences that enter the energy balance must be linked to known masses.

Measured masses are evaluated in the 2003 Atomic Mass Evaluation (2003AME) [483,484]. Below, we summarize some of the more recent mass measurements of exotic nuclei with relevance to nuclear astrophysics.

The rapid neutron-capture process (r process) is responsible for the synthesis of roughly half of the elements beyond iron. However, its site and reaction path is not known with certainty. The abundance patterns of various r-process models show a significant dependence on the underlying nuclear physics (see [11,3,485,12,9,486] for reviews). High precision mass measurements of $^{71m,72-81}$Zn were performed with ISOLTRAP at CERN [487]. From ^{81}Zn and ^{80}Zn, the neutron separation energy and neutron-capture Q-value of ^{80}Zn were determined for the first time. Depending on the stellar environment, the r-process path either includes the slow β decay of ^{80}Zn making it a major waiting point or it proceeds rapidly to ^{81}Zn and beyond via neutron capture [487]. The new results improved the mass-related uncertainties for r-process calculations compared to the previously used 2003AME. In the temperature regime below 1.5 GK, where the $(n, \gamma) \rightleftharpoons (\gamma, n)$ equilibrium begins to break down, the previously dominating mass uncertainties to the reaction flow in this region have become negligible with the new results. High-precision Penning trap mass measurements of ^{132,134}Sn carried out with the ISOLTRAP setup revealed a 0.5 MeV deviation of the binding energy of ^{134}Sn compared to the previously accepted value [488]. The new deduced value for the $N = 82$ shell gap in ^{132}Sn was found to be larger than the $N = 28$ shell gap of the stable doubly magic nucleus ^{48}Ca. The $N = 82$ shell gap is thought to influence the fission cycling in the r process [489] since, in the presence of a shell gap, the r process slows down and more neutrons are created by photodisintegration inducing more fission [488].

X-ray bursts are initiated when the temperature and the density in the accreted layer on a neutron star become high enough to allow a breakout from the hot CNO cycle. The nuclei start to capture protons and proceed along a capture chain via the rp process. The capture rate is favorable compared to the β-decay rate of the nuclei involved until a nucleus with a small Q value for the proton-capture reaction is encountered. There, an equilibrium between the (p, γ) proton capture and (γ, p) photodisintegration develops and the rp process is delayed until the subsequent β-decay of this so-called "waiting-point" nucleus [16,6]. The effective lifetime of a waiting-point nucleus depends strongly on its proton separation energy which can be directly determined from mass differences. The effective lifetime of a nucleus in an X-ray burst is exponentially dependent on the proton separation energy and thus accurate mass values – preferably with less than 10 keV uncertainty – are desired for X-ray burst model calculations [490,491]. The selfconjugate nuclei ^{64}Ge, ^{68}Se and ^{72}Kr are believed to be important, long-lived waiting point nuclei [6].

Mass measurements of ^{68}Se, ^{68}As and ^{68}Ge with the Canadian Penning Trap (CPT) confirmed ^{68}Se to be a waiting point nucleus, causing a considerable delay in the rp process [492]. Penning trap mass spectrometry of ^{63,64}Ga, ^{64,65,66}Ge, ^{66,67,68}As and ^{69}Se was performed at the LEBIT facility at NSCL [493]. By using theoretical Coulomb-shift energies and measured masses of ^{65,66}Ge, ^{67}As, and ^{69}Se, mass values for ^{65}As, ^{66,67}Se, and ^{69}Br were predicted with an uncertainty of about 100 keV [493]. The results together with the measured masses were used to calculate improved effective lifetimes of the rp-process waiting-point $N = Z$ nuclei ^{64}Ge and ^{68}Se. It was found that ^{64}Ge is less of a waiting point while ^{68}Se poses a larger delay in the rp process than previously thought [493]. Recently, the masses of ^{68}Se, ^{70}Se, ^{70m}Br and ^{71}Br were measured with experimental uncertainties of 0.15–15 keV with the LEBIT facility at NSCL [494]. The new and improved data were used in conjunction with Coulomb displacement energies as input for rp-process calculations. An increase of the effective lifetime of the waiting point nucleus ^{68}Se was found and more precise information on the luminosity of type I X-ray bursts and final element abundances after the burst were obtained [494]. At ISOLTRAP, the mass of the selfconjugate nucleus ^{72}Kr was measured for the first time with Penning trap mass spectrometry yielding a precision of 8 keV [495]. The masses of ^{73,74}Kr were determined with an order of magnitude improvement in accuracy compared to previous results. ^{72}Kr was found to be an important waiting point in the rp process during X-ray bursts, delaying energy generation with at least 80% of its β^+-decay half-life [495].

Of interest is the possible existence of an endpoint to the rp process. Reaction network calculations suggest that the rp process in X-ray bursts terminates at tellurium and is limited by the SnSbTe cycle [496]. The nuclei $^{104-108}$Sn, $^{106-110}$Sb, ^{108,109}Te, and ^{111}I, in the vicinity of the expected endpoint of the astrophysical rp process, were produced in fusion-evaporation reactions with a ^{58}Ni beam irradiating a natural Ni target at the IGISOL facility in Jyväskylä [497]. Their mass

values were precisely measured at the JYFLTRAP Penning trap facility. For ^{106,108,110}Sb, these were the first direct mass measurements. One-proton separation energies were derived and the low value for ^{106}Sb excludes a strong SnSbTe cycle starting at ^{105}Sn [497]. Masses of 34 neutron-deficient nuclei along the rp-process path were measured with SHIPTRAP at GSI with an uncertainty of 10 keV [464]. The nuclei relevant for the rp-process path above $A = 90$ were produced in fusion-evaporation reactions induced by ^{40}Ca, ^{50}Cr and ^{58}Ni beams impinging upon a ^{58}Ni target. Preliminary results were reported for ^{101,102,103,104}Cd, ^{102,103,104,105}In and ^{105,106}Sn, and ^{99,101,103}Ag, ^{112,111,110,109}Te, ^{113,112,111}I, ^{113}Xe, ^{107,109,111}Sb. Except for ^{105}In and several tellurium isotopes, the measured masses were found to agree well with the 2003AME. The rp process proceeds along the Sn isotopic chain until the proton separation energy of Sb isotopes becomes large enough to delay the competing photodisintegration and hence, causes the rp process to proceed up to tellurium where SnSbTe cycles prevent the production of heavier elements. With the masses measured at SHIPTRAP, more accurate proton separation energies can be deduced in order to clarify which SnSbTe cycle dominates [464]. The Q values for the proton emission from ^{104}Sb and ^{105}Sb were also recently deduced indirectly from α-decay measurements carried out at HRIBF (ORNL) [498].

The ν p process occurs in explosive environments when proton-rich matter is ejected in the presence of strong neutrino fluxes [499]. This includes the inner ejecta of core-collapse supernova [500], for example. Neutron-deficient nuclei from yttrium to palladium of relevance to the ν p process were produced in fusion-evaporation reactions and studied at SHIPTRAP (GSI) and JYFLTRAP (Jyväskylä) [501]. Precise masses of 21 nuclei were determined with Penning trap mass spectrometry, the masses of ^{88}Tc, $^{90-92}$Ru, $^{92-94}$Rh, and ^{94,95}Pd for the first time. The data was used for ν p-process nucleosynthesis calculations to probe their impact on reaction flow and final abundances. In particular the reaction flow around ^{88}Tc was found to be significantly modified as the new measurements give a proton separation energy that differs from the previously used 2003AME by 1 MeV. However, the final abundances were basically unchanged [501].

Direct mass measurements of the short-lived nuclei ^{44}V, ^{48}Mn, ^{41}Ti and ^{45}Cr were performed with the isochronous mass spectrometry at the experimental storage ring (ESR) at GSI [502]. An accuracy of about 100–500 keV was achieved. The results largely confirmed the previously employed theoretical mass predictions and thus lead only to small changes in the rp process in astrophysical X-ray burst models [502].

The mass and electron capture Q value of ^{26}Si was measured with JYFLTRAP Penning trap facility and a ten times improved precision was achieved [503]. This leads to an improvement of the reaction Q value for the ^{25}Al$(p,\gamma)^{26}$Si proton capture. The new result changed the stellar production rate of ^{26}Si at nova ignition temperatures by about 10% and makes the limiting factor for higher precision of the reaction Q value the mass of ^{25}Al [503].

7. Outlook

Tremendous progress has been made over the past years in experimental nuclear astrophysics as well as in the developments of the multi-faceted theoretical framework that is crucial to link the study of nuclear structure and reactions to astrophysical processes in stars and explosive scenarios. The future for nuclear physics and nuclear astrophysics looks bright with next-generation rare-isotope facilities on the horizon like GSI/FAIR in Germany and FRIB in the United States and major upgrades on the way at GANIL in France and TRIUMF in Canada.

Short-term, the RIBF facility in JAPAN, which became operational recently, and significant capability upgrades at NSCL, TRIUMF, ANL, HRIBF/ORNL, and CERN/ISOLDE (see Section 6.1) will continue to provide a multitude of exciting opportunities to advance the experimental research in nuclear astrophysics at all fronts. For example, the nuclear equation of state (EOS) – crucial for an understanding of neutron stars and supernova explosions – can be probed with fast-beam heavy-ion collisions induced by projectiles with extreme N/Z ratios utilizing the present NSCL fast-beam capability as well as the different energies available at GSI and RIBF. Pioneering programs at NSCL aimed at charge-exchange reactions on exotic nuclei will measure electron-capture rates for exotic nuclei and generate crucial input for the nucleosynthesis in supernovae. The CARIBU at the ATLAS facility at ANL will provide low-energy and reaccelerated beams of neutron-rich ^{252}Cf fission products and enable experiments in the proximity of r-process path in several mass regions [268]. The ReA3 reaccelerator addition underway at NSCL will deliver for the first time reaccelerated beams of rare isotopes produced by projectile fragmentation and fission with final energies ranging from 0.3 to 3 MeV/nucleon for ions with a charge-to-mass ratio of 0.25, and 0.3 to 6 MeV/nucleon for ions with a ratio of charge to A of 0.5, which are of great interest for direct and indirect nuclear astrophysics measurements across the chart [267,438].

The important scientific questions to be addressed both experimentally and theoretically in nuclear physics of exotic nuclei with relevance for astrophysics comprise: (a) How do loosely-bound systems survive and what are the general laws of their formation and destruction? (b) Are new types of radioactivity possible? (c) Are new types of nuclear symmetry and spatial arrangement possible? (d) What are the limits of nuclear existence? (e) How do the properties of nuclear matter change as a function of density, temperature and proton-to-neutron ratio? (f) How do thermal and quantum phase transitions occur in small systems? (g) What determines the shape and symmetry properties of an exotic nucleus? (h) How does quantum tunneling of composite particles occur in the process of reactions and decay? (i) What are the manifestations of fundamental forces and symmetries in unusual conditions? (j) How were the elements heavier than iron formed in stellar explosions? (k) How do rare isotopes shape stellar explosions? (l) What is the role of rare isotopes in neutron stars?

These questions provide extreme challenges for experiments and theory. On the experimental side, producing the beams of radioactive nuclei needed to address the scientific questions has been an enormous challenge. Pioneering experiments have established the techniques and present-generation facilities have produced first exciting science results, but the

field is still at the beginning of an era of discovery and exploration that will be fully underway once the range of next-generation facilities becomes operational. The theoretical challenges relate to wide variations in nuclear composition and rearrangements of the bound and continuum structure, sometimes involving near-degeneracy of the bound and continuum states [504]. The extraction of reliable information from experiments requires a solid understanding of the reaction process, in addition to the structure of the nucleus. In astrophysics, new observations, for example the expected onset of data on stellar abundances, will require rare-isotope science for their interpretation.

Acknowledgements

This work was supported in part by the U.S. DOE grants DE-FG02-08ER41533 and DE-FC02-07ER41457 (UNEDF, SciDAC-2), by the Research Corporation, and by the US National Science Foundation under grant PHY-0606007. A.G. acknowledges discussions with Hendrik Schatz.

References

[1] E.M. Burbidge, G.R. Burbidge, W.A. Fowler, F. Hoyle, Rev. Modern Phys. 29 (1957) 547.
[2] W.A. Fowler, Rev. Modern Phys. 56 (1984) 149.
[3] K.-L. Kratz, J.-P. Bitouzet, F.-K. Thielemann, P. Moeller, B. Pfeiffer, Astrophys. J. 403 (1993) 216.
[4] G. Wallerstein, I. Iben, P. Parker, A.M. Boesgaard, G.M. Hale, A.E. Champagne, C.A. Barnes, F. Käppeler, V.V. Smith, R.D. Hoffman, F.X. Timmes, C. Sneden, R.N. Boyd, B.S. Meyer, D.L. Lambert, Rev. Modern Phys. 69 (1997) 995.
[5] F. Käppeler, F.-K. Thielemann, M. Wiescher, Ann. Rev. Nucl. Part. Sci. 48 (1998) 175.
[6] H. Schatz, A. Aprahamian, J. Görres, M. Wiescher, T. Rauscher, J.F. Rembges, F.K. Thielemann, B. Pfeiffer, P. Möller, K.L. Kratz, H. Herndl, B.A. Brown, H. Rebel, Phys. Rev. 294 (1998) 167.
[7] M. Arnould, K. Takahashi, Rep. Prog. Phys. 62 (1999) 395.
[8] K. Langanke, M. Wiescher, Rep. Prog. Phys. 64 (2001) 1657.
[9] M. Arnould, S. Goriely, Phys. Rev. 384 (2003) 1.
[10] H. Grawe, K. Langanke, G. Martinez-Pinedo, Rep. Prog. Phys. 70 (2007) 1525.
[11] J.J. Cowan, F.-K. Thielemann, J.W. Truran, Phys. Rep. 208 (1991) 267.
[12] Y.Z. Qian, Prog. Part. Nuclear Phys. 50 (2003) 153.
[13] A.E. Champagne, M. Wiescher, Ann. Rev. Nucl. Part. Sci. 42 (1992) 39.
[14] H. Schatz, K. Rehm, Nuclear Phys. A 777 (2006) 601.
[15] J.L. Fisker, H. Schatz, F.-K. Thielemann, Astrophys. J. Suppl. Ser. 174 (2008) 261.
[16] R.K. Wallace, S.E. Woosley, Astrophys. J. Suppl. Ser. 45 (1981) 389.
[17] S. Woosley, T. Janka, Nature Phys. 1 (2005) 147.
[18] K. Langanke, G. Martínez-Pinedo, Rev. Modern Phys. 75 (2003) 819.
[19] J.N. Bahcall, Neutrino Astrophysics, Cambridge University Press, Cambridge, 1989.
[20] S.E. Woosley, in: L. Buchmann, J. D'Auria (Eds.) Proceedings of the Accelerated Beam Workshop, TRIUMF, Canada, 1985.
[21] W.A. Fowler, G.E. Caughlan, B.A. Zimmermann, Ann. Rev. Astron. Astrophys. 5 (1967) 525.
[22] G.M. Fuller, W.A. Fowler, M. Newman, Astrophys. J. 293 (1985) 1.
[23] R.V. Wagoner, Astrophys. J. Suppl. 18 (1969) 247.
[24] J. Huang, C.A. Bertulani, V. Guimaraes, arXiv:0810.3867.
[25] C. Rolfs, Nuclear Phys. A 217 (1973) 29.
[26] R.E. Hester, R.E. Pixley, W.A. Lamb, Phys. Rev. 111 (1958) 1604.
[27] N. Tanner, Phys. Rev. 114 (1959) 1060.
[28] R. Morlock, R. Kunz, M. Jaeger, A. Müller, J.W. Hammer, P. Mohr, H. Oberhummer, A. Mayer, G. Staudt, V. Kölle, Phys. Rev. Lett. 79 (1997) 3837.
[29] H.J. Habing, H. Olofsson, Asymptotic Giant Branch Stars, Springer, Heidelberg, 2004.
[30] P. Navrátil, C.A. Bertulani, E. Caurier, Phys. Lett. B 634 (2006) 191; Phys. Rev. C73 (2006) 065801.
[31] P. Descouvemont, D. Baye, Nuclear Phys. A 567 (1994) 341.
[32] F.J. Vaughn, R.A. Chalmers, D. Kohler, L.F. Chase, Phys. Rev. C 2 (1970) 1657.
[33] B.W. Filippone, A.J. Elwyn, C.N. Davids, D.D. Koetke, Phys. Rev. C 28 (1983) 2222.
[34] L.T. Baby, C. Bordeanu, G. Goldring, M. Hass, L. Weissman, V.N. Fedoseyev, U. Köster, Y. Nir-El, G. Haquin, H.W. Gäggeler, Phys. Rev. Lett. 90 (2003) 022501.
[35] A.R. Junghans, E.C. Mohrmann, K.A. Snover, T.D. Steiger, E.G. Adelberger, J.M. Casandjian, H.E. Swanson, L. Buchmann, S.H. Park, A. Zyuzin, A.M. Laird, Phys. Rev. C 68 (2003) 065803.
[36] N. Iwasa, F. Boué, G. Surówka, K. Sümmerer, T. Baumann, B. Blank, S. Czajkowski, A. Förster, M. Gai, H. Geissel, E. Grosse, M. Hellström, P. Koczon, B. Kohlmeyer, R. Kulessa, F. Laue, C. Marchand, T. Motobayashi, H. Oeschler, A. Ozawa, M.S. Pravikoff, E. Schwab, W. Schwab, P. Senger, J. Speer, C. Sturm, A. Surowiec, Phys. Rev. Lett. 83 (1999) 2910.
[37] B. Davids, D.W. Anthony, T. Aumann, S.M. Austin, T. Baumann, D. Bazin, R.R.C. Clement, C.N. Davids, H. Esbensen, P.A. Lofy, T. Nakamura, B.M. Sherrill, J. Yurkon, Phys. Rev. Lett. 86 (2001) 2750.
[38] F. Schümann, F. Hammache, S. Typel, F. Uhlig, K. Sümmerer, I. Böttcher, D. Cortina, A. Förster, M. Gai, H. Geissel, U. Greife, N. Iwasa, P. Koczoń, B. Kohlmeyer, R. Kulessa, H. Kumagai, N. Kurz, M. Menzel, T. Motobayashi, H. Oeschler, A. Ozawa, M. Płoskoń, W. Prokopowicz, E. Schwab, P. Senger, F. Strieder, C. Sturm, Phys. Rev. Lett. 90 (2003) 232501.
[39] R.W. Kavanagh, T.A. Tombrello, J.M. Mosher, D.R. Goosman, Bull. Am. Phys. Soc. 14 (1969) 1209.
[40] P. Descouvemont, Few-Body Syst. 43 (2008) 45; J. Phys. G 35 (2008) 014006.
[41] Q.R. Ahmad, et al., Phys. Rev. Lett. 87 (2001) 071301.
[42] H.M. Xu, C.A. Gagliardi, R.E. Tribble, A.M. Mukhamedzhanov, N.K. Timofeyuk, Phys. Rev. Lett. 73 (1994) 2027.
[43] A.M. Mukhamedzhanov, N.K. Timofeyuk, JETP Lett. 51 (1990) 282.
[44] C.A. Bertulani, P. Danielewicz, Introduction to Nuclear Reactions, IOP, London, 2004.
[45] C.A. Bertulani, A. Sustich, Phys. Rev. C46 (1992) 2340.
[46] C. Rolfs, W.S. Rodney, Cauldrons in the Cosmos, University of Chicago Press, Chicago, 1988.
[47] C. Rolfs C, R.E. Azuma, Nuclear Phys. A227 (1974) 291.
[48] F.C. Barker, Nuclear Phys. A575 (1994) 361.
[49] D. Schürmann, A. Di Leva, L. Gialanella, D. Rogalla, F. Strieder, N. De Cesare, A. D'Onofrio, G. Imbriani, R. Kunz, C. Lubritto, A. Ordine, V. Roca, C. Rolfs, M. Romano, F. Schümann, F. Terrasi, H.-P. Trautvetter, Eur. Phys. J. A 26 (2005) 301.

[50] M. Assunção, M. Fey, A. Lefebvre-Schuhl, J. Kiener, V. Tatischeff, J.W. Hammer, C. Beck, C. Boukari-Pelissie, A. Coc, J.J. Correia, S. Courtin, F. Fleurot, E. Galanopoulos, C. Grama, F. Haas, F. Hammache, F. Hannachi, S. Harissopulos, A. Korichi, R. Kunz, D. LeDu, A. Lopez-Martens, D. Malcherek, R. Meunier, Th. Paradellis, M. Rousseau, N. Rowley, G. Staudt, S. Szilner, J.P. Thibaud, J.L. Weil, Phys. Rev. C 73 (2006) 055801.
[51] C. Matei, L. Buchmann, W.R. Hannes, D.A. Hutcheon, C. Ruiz, C.R. Brune, J. Caggiano, A.A. Chen, J. D'Auria, A. Laird, M. Lamey, Z.H. Li, W.P. Liu, A. Olin, D. Ottewell, J. Pearson, G. Ruprecht, M. Trinczek, C. Vockenhuber, C. Wrede, Phys. Rev. Lett. 97 (2006) 242503.
[52] R. Kunz, M. Fey, M. Jaeger, A. Mayer, J.W. Hammer, G. Staudt, S. Harissopulos, T. Paradellis, Astrophys. J. 567 (2002) 643.
[53] F. Strieder, J. Phys. G 35 (2008) 014009.
[54] E.P. Wigner E P, L. Eisenbud, Phys. Rev. 72 (1947) 29.
[55] F.C. Barker, T. Kajino, Aust. J. Phys. 44 (1991) 693.
[56] P. Descouvement, Abderrahim Adahchour, Carmen Angulo, Alain Coc, Elisabeth Vangioni-Flam, At. Data Nucl. Data Tables 88 (2004) 203.
[57] V.F. Weisskopf, D.H. Ewing, Phys. Rev. 57 (1940) 935.
[58] N. Bohr, Nature 137 (1936) 344.
[59] W. Hauser, H. Feshbach, Phys. Rev. 87 (1952) 366.
[60] C. Mahaux, H.A. Weidenmüller, Ann. Rev. Part. Nucl. Sci. 29 (1979) 1.
[61] S. Kailas, M.K. Mehta, S.K. Gupta, Y.P. Viyogi, N.K. Ganguly, Phys. Rev. C 20 (1979) 1272.
[62] A. Mushtaq, S.M. Qaim, G. Stoecklin, Appl. Radiat. Isotopes 39 (1988) 1085.
[63] T. Rauscher, F.-K. Thielemann, At. Data Nucl. Data Tables 79 (2001) 47.
[64] S. Kastleiner, S.M. Qaim, F.M. Nortier, G. Blessing, T.N. van der Walt, H.H. Coenenet, Appl. Radiat. Isotopes 56 (2002) 685.
[65] W. Rapp, J. Görres, M. Wiescher, H. Schatz, F. Käppeler, Astrophys. J. 653 (2006) 474.
[66] F. Krmpotić, A. Mariano, A. Samana, Phys. Rev. C 71 (2005) 044319.
[67] E. Kolbe, K. Langanke, Phys. Rev. C 63 (2001) 025802.
[68] R. Lazauskas, C. Volpe, Nuclear Phys. A792 (2007) 219.
[69] A. Samana, C.A. Bertulani, Phys. Rev. C C78 (2008) 024312.
[70] N. Paar, D. Vretenar, T. Marketin, P. Ring, Phys. Rev. C 77 (2008) 024608.
[71] KARMEN Collaboration, R. Maschuw, et al., Prog. Part. Phys. 40 (1998) 183. and references therein.
[72] N.Yu. Agafonova, et al., Astron. Phys. 27 (2007) 254.
[73] D.B. Kaplan, M.J. Savage, M.B. Wise, Nuclear Phys. B478 (1996) 629.
[74] J.-W. Chen, G. Rupak, M.J. Savage, Nuclear Phys. A653 (1999) 386.
[75] P. Bedaque, U. van Kolck, Ann. Rev. Nucl. Part. Sci. 52 (2002) 339.
[76] G. Rupak, Nuclear Phys. A678 (2000) 405.
[77] J.W. Chen, M.J. Savage, Phys. Rev. C 60 (1999) 065205.
[78] X. Kong, F. Ravndal, Nuclear Phys. A656 (1999) 421; Nuclear Phys. A665 (2000) 137; Phys. Lett. B 470 (1999) 1; Phys. Rev. C 64 (2001) 044002.
[79] M. Butler, J.W. Chen, Phys. Lett. B 520 (2001) 87.
[80] C.A. Bertulani, H.-W. Hammer, U. van Kolck, Nuclear Phys. A 712 (2002) 37.
[81] P.F. Bedaque, H.-W. Hammer, U. van Kolck, Phys. Lett. B 569 (2003) 159.
[82] R. Higa, H.-W. Hammer, U. van Kolck, Nuclear Phys. A809 (2008) 171.
[83] G.A. Kobzev, I.T. Iakubov, M.M. Popovich, M. M, Transport and Optical Properties of Nonideal Plasma, Plenum, 1995.
[84] B.F. Baimbetov, Kh.T. Nurekenov, T.S. Ramazanov, Phys. Lett. A 202 (1995) 211.
[85] E.E. Salpeter, Aust. J. Phys. 7 (1954) 373.
[86] T. Fujimoto, Plasma Spectroscopy, Oxford University Press, 2004.
[87] Y.-D. Jung, Europhys. Lett. 69 (2005) 753.
[88] H.E. Mitler, Astrophys. J. 212 (1977) 513.
[89] C. Carraro, A. Schaeffer, S.E. Koonin, Astrophys. J. 331 (1988) 565.
[90] L.S. Brown, R.F. Sawyer, Astrophys. J. 489 (1997) 968.
[91] A.V. Gruzinov, John N. Bahcall, Astrophys. J. 504 (1998) 996.
[92] N.J. Shaviv, G. Shaviv, Astrophys. J. 558 (2001) 925; Astrophys. J. 529 (2000) 1054;
G. Shaviv, Proc. Int. Conf. Fusion-03, Matsushima, Miyagi, Japan, November 12–15, 2003.
[93] H.J. Assenbaum, K. Langanke, C. Rolfs, Z. Phys. A327 (1987) 461.
[94] C. Rolfs, E. Somorjai, Nucl. Inst. Meth. B99 (1995) 297.
[95] C. Rolfs, Prog. Part. Nuclear Phys. 46 (2001) 23.
[96] S. Engstler, A. Krauss, K. Neldner, C. Rolfs, U. Schröder, K. Langanke, Phys. Lett. B2 (1988) 179.
[97] S. Engstler, G. Raimann, C. Angulo, U. Greife, C. Rolfs, U. Schröder, E. Somorjai, B. Kirch, Z. Phys. A342 (1992) 471.
[98] C. Angulo, S. Engstler, G. Raimann, C. Rolfs, W.H. Schulte, E. Somorjai, Z. Phys. A345 (1993) 231.
[99] P. Prati, C. Arpesella, F. Bartolucci, H.W. Becker, E. Bellotti, C. Broggini, P. Corvisiero, G. Fiorentini, A. Fubini, G. Gervino, F. Gorris, U. Greife, C. Gustavino, M. Junker, C. Rolfs, W.H. Schulte, H.P. Trautvetter, D. Zahnow, Z. Phys. A350 (1994) 171.
[100] U. Greife, F. Gorris, M. Junker, C. Rolfs, D. Zahnow, Z. Phys. A351 (1995) 107.
[101] T.D. Shoppa, S.E. Koonin, K. Langanke, R. Seki, Phys. Rev. C48 (1993) 837.
[102] M. Aliotta, F. Raiola, G. Gyürky, A. Formicola, R. Bonetti, C. Broggini, L. Campajola, P. Corvisiero, H. Costantini, A. D'Onofrio, Z. Fülöp, G. Gervino, L. Gialanella, A. Guglielmetti, C. Gustavino, G. Imbriani, M. Junker, P.G. Moroni, A. Ordine, P. Prati, V. Roca, D. Rogalla, C. Rolfs, M. Romano, F. Schümann, E. Somorjai, O. Straniero, F. Strieder, F. Terrasi, H.P. Trautvetter, S. Zavatarelli, Nuclear Phys. A690 (2001) 790.
[103] A.B. Balantekin, C.A. Bertulani, M.S. Hussein, Nuclear Phys. A627 (1997) 324.
[104] V.V. Flambaum, V.G. Zelevinsky, Phys. Rev. Lett. 83 (1999) 3108.
[105] K. Hagino, A.B. Balantekin, Phys. Rev. C 66 (2002) 055801.
[106] G. Fiorentini, C. Rolfs, F.L. Villante, B. Ricci, Phys. Rev. C67 (2003) 014603.
[107] K. Langanke, T.D. Shoppa, C.A. Barnes, C. Rolfs, Phys. Lett. B369 (1996) 211.
[108] J.M. Bang, L.S. Ferreira, E. Maglione, J.M. Hansteen, Phys. Rev. C53 (1996) R18.
[109] H. Andersen, J.F. Ziegler, The Stopping and Ranges of Ions in Matter, Pergamon, NY, 1977.
[110] C.A. Bertulani, D.T. de Paula, Phys. Rev. C62 (2000) 045802.
[111] R. Golser, D. Semrad, Phys. Rev. Lett. 14 (1991) 1831.
[112] C.A. Bertulani, Phys. Lett. B 585 (2004) 35.
[113] A. Formicola, M. Aliotta, G. Gyürky, F. Raiola, R. Bonetti, C. Broggini, L. Campajola, P. Corvisiero, H. Costantini, A. D' Onofrio, Z. Fülöp, G. Gervino, L. Gialanella, A. Guglielmetti, C. Gustavino, G. Imbriani, M. Junker, A. Ordine, P. Prati, V. Roca, D. Rogalla, C. Rolfs, M. Romano, F. Schümann, E. Somorjai, O. Straniero, F. Strieder, F. Terrasi, H.P. Trautvetter, S. Zavatarelli, Eur. Phys. J. A8 (2000) 443.
[114] F. Raiola, P. Migliardi, G. Gyŕky, M. Aliotta, A. Formicola, R. Bonetti, C. Broggini, L. Campajola, P. Corvisiero, H. Costantini, J. Cruz, A. D'Onofrio, Z. Fülöp, G. Gervino, L. Gialanella, A. Guglielmetti, G. Imbriani, C. Gustavino, A.P. Jesus, M. Junker, R.W. Kavanagh, P.G.P. Moroni, A. Ordine, J.V. Pinto, P. Prati, V. Roca, J.P. Ribeiro, D. Rogalla, C. Rolfs, M. Romano, F. Schümann, D. Schürmann, E. Somorjai, F. Strieder, F. Terrasi, H.P. Trautvetter, S. Zavatarelli, Eur. Phys. J. A13 (2002) 377;
F. Raiola, L. Gang, C. Bonomo, G. Gyürky, M. Aliotta, H.W. Becker, R. Bonetti, C. Broggini, P. Corvisiero, A. D'Onofrio, Z. Flöp, G. Gervino, L. Gialanella, M. Junker, P. Prati, V. Roca, C. Rolfs, M. Romano, E. Somorjai, F. Strieder, F. Terrasi, G. Fiorentini, K. Langanke, J. Winter, Eur. Phys. J. A19 (2004) 283;
F. Raiola, B. Burchard, Zs. Fülöp, Gy. Gyrky, S. Zeng, J. Cruz, A. Di Leva, B. Limata, M. Fonseca, H. Luis, M. Aliotta, H.W. Becker, C. Broggini, A. D'Onofrio, L. Gialanella, G. Imbriani, A.P. Jesus, M. Junker, J.P. Ribeiro, V. Roca, C. Rolfs, M. Romano, E. Somorjai, F. Strieder, F. Terrasi, Eur. Phys. J. A27 (2006) 79.

[115] K. Czerski, A. Huke, A. Biller, P. Heide, M. Hoeft, G. Ruprecht, Europhys. Lett. 54 (2001) 449.
[116] T. Ichihara, M. Ishihara, H. Ohnuma, T. Niizeki, Y. Tajima, T. Yamamoto, Y. Fuchi, S. Kubono, M.H. Tanaka, H. Okamura, S. Ishida, S. Miyamoto, H. Toyokawa, Phys. Lett. B 323 (1994) 278.
[117] T. Ichihara, Nuclear Phys. A577 (1994) 93c.
[118] K. Alder, A. Winther, Electromagnetic Excitation, North-Holland, Amsterdam, 1975.
[119] D. Cline, Ann. Rev. Part. Sci. 36 (1988) 683.
[120] A. Winther, K. Alder, Nuclear Phys. A 319 (1979) 518.
[121] T. Glasmacher, Ann. Rev. Nucl. Part. Sci. 48 (1998) 1.
[122] C.A. Bertulani, G. Baur, Phys. Rep. 163 (1988) 299.
[123] C.A. Bertulani, A.M. Nathan, Nuclear Phys. A 554 (1993) 158.
[124] T. Aumann, D. Aleksandrov, L. Axelsson, T. Baumann, M.J.G. Borge, L.V. Chulkov, J. Cub, W. Dostal, B. Eberlein, Th.W. Elze, H. Emling, H. Geissel, V.Z. Goldberg, M. Golovkov, A. Grünschloss, M. Hellström, K. Hencken, J. Holeczek, R. Holzmann, B. Jonson, A.A. Korshenninikov, J.V. Kratz, G. Kraus, R. Kulessa, Y. Leifels, A. Leistenschneider, T. Leth, I. Mukha, G. Münzenberg, F. Nickel, T. Nilsson, G. Nyman, B. Petersen, M. Pfäutzner, A. Richter, K. Riisager, C. Scheidenberger, G. Schrieder, W. Schwab, H. Simon, M.H. Smedberg, M. Steiner, J. Stroth, A. Surowiec, T. Suzuki, O. Tengblad, M.V. Zhukov, Phys. Rev. C 59 (1999) 1252.
[125] B.V. Danilin, I.J. Thompson, J.S. Vaagen, M.V. Zhukov, Nuclear Phys. A 632 (1998) 383.
[126] A. Cobis, D. Fedorov, A. Jensen, Phys. Rev. Lett. 79 (1997) 2411.
[127] G. Baur, C. Bertulani, H. Rebel, Nuclear Phys. A459 (1986) 188.
[128] T. Motobayashi, N. Iwasa, Y. Ando, M. Kurokawa, H. Murakami, J. Ruan(Gen), S. Shimoura, S. Shirato, N. Inabe, M. Ishihara, T. Kubo, Y. Watanabe, M. Gai, R.H. France, K.I. Hahn, Z. Zhao, T. Nakamura, T. Teranishi, Y. Futami, K. Furutaka, T. Delbar, Phys. Rev. Lett. 73 (1994) 2680.
[129] V. Efros, W. Balogh, H. Herndl, R. Honger, H. Oberhummer, Z. Phys. A 355 (1996) 101.
[130] T. Aumann, Eur. Phys. J. A 26 (2006) 441.
[131] G.F. Bertsch, C.A. Bertulani, Nuclear Phys. A 556 (1993) 136; Phys. Rev. C 49 (1994) 2834;
H. Esbensen, G.F. Bertsch, C.A. Bertulani, Nuclear Phys. A581 (1995) 107.
[132] C.A. Bertulani, Phys. Rev. Lett. 94 (2005) 072701.
[133] H. Esbensen, G. Bertsch, Phys. Rev. Lett. A 359 (1995) 13; Nuclear Phys. A600 (1996) 37.
[134] C.A. Bertulani, A.E. Stuchbery, T.J. Mertzimekis, A.D. Davies, Phys. Rev. C 68 (2003) 04460;
C.A. Bertulani, G. Cardella, M. De Napoli, G. Raciti, E. Rapisarda, Phys. Lett. B 650 (2007) 233.
[135] H. Scheit, A. Gade, T. Glasmacher, T. Motobayashi, Phys. Lett. B 659 (2008) 515.
[136] H. Esbensen, Phys. Rev. C 78 (2008) 024608.
[137] K. Ogata, C.A. Bertulani, Progr. Theoret. Phys. (Lett.) 121 (2009) 1399.
[138] A. Bonaccorso, G. Picolo, D.M. Brink, Nuclear Phys. A 441 (1985) 555;
G. Blanchon, A. Bonaccorso, N. Vinh Mau, Nuclear Phys. A739 (2004) 259.
[139] M. La Cognata, et al., Phys. Rev. C76 (2007) 065804.
[140] G. Baur, Phys. Lett. B178 (1986) 135.
[141] S. Typel, H.H. Wolter, Few-Body Syst. 29 (2000) 75.
[142] S. Typel, G. Baur, Ann. of Phys. 305 (2003) 228.
[143] C. Spitaleri, S. Cherubini, A. Del Zoppo, A. Di Pietro, P. Figuera, M. Gulino, M. Lattuada, Dj. Miljanic, A. Musumarra, M.G. Pellegriti, R.G. Pizzone, C. Rolfs, S. Romano, S. Tudisco, A. Tumino, Nuclear Phys. A 719 (2003) 99.
[144] R.E. Tribble, T. Abdullah, C. Fu, C. Gagliardi, A. Mukhamedzhanov, G. Tabacaru, X. Tang, L. Trache, P. Bem, V. Burjan, V. Kroha, J. Piskor, E. Simeckova, J. Vincour, F. Carstoiu, S. Spitaleri, S. Cherubini, V. Crucilla, M. La Cognata, L. Lamia, R.G. Pizzone, S. Romano, A. Tumino, Proceedings of Science (online at: http://pos.sissa.it/index.html), 2007.
[145] A. Redder, H.W. Becker, H. Lorenz-Wirzba, C. Rolfs, P. Schmalbrock, H.P. Trautvetter, Z. Phys. A 305 (1982) 325.
[146] A. Schardt, W.A. Fowler, C.C. Lauritsen, Phys. Rev. 86 (1952) 527.
[147] J.L. Zyskind, P.D. Parker, Nuclear Phys. A320 (1979) 404.
[148] M. Lattuada, R.G. Pizzone, S. Typel, P. Figuera Miljani, A. Musumarra, M.G. Pellegriti, C. Rolfs, C. Spitaleri, H.H. Wolter, Astrophys. J. 562 (2001) 1076.
[149] A. Tumino, C. Spitaleri, A. Di Pietro, P. Figuera, M. Lattuada, A. Musumarra, M.G. Pellegriti, R.G. Pizzone, S. Romano, C. Rolfs, S. Tudisco, S. Typel, Phys. Rev. C 67 (2003) 065803.
[150] A.J. Elwyn, R.E. Holland, C.N. Davids, L. Meyer-Schützmeister, F.P. Mooring, W. Ray Jr., Phys. Rev. C 20 (1979) 1984.
[151] M. La Cognata, C. Spitaleri, A. Tumino, S. Typel, S. Cherubini, L. Lamia, A. Musumarra, R.G. Pizzone, A. Rinollo, C. Rolfs, S. Romano, D. Schŕmann, F. Strieder, Phys. Rev. C 72 (2005) 065802; Nuclear Phys. A758 (2005) 98.
[152] A.M. Mukhamedzhanov, R.E. Tribble, Phys. Rev. C 59 (1999) 3418.
[153] L.D. Blokhintsev, V.I. Kukulin, A.A. Sakharuk, D.A. Savin, E.V. Kuznetsova, Phys. Rev. C 48 (1993) 2390.
[154] P.G. Hansen, Nature 334 (1988) 194.
[155] J.A. Tostevin, J. Phys. G 25 (1999) 735.
[156] P.G. Hansen, J.A. Tostevin, Ann. Rev. Nucl. Part. Sci. 53 (2003) 219.
[157] A. Gade, P. Adrich, D. Bazin, M.D. Bowen, B.A. Brown, C.M. Campbell, J.M. Cook, T. Glasmacher, P.G. Hansen, K. Hosier, S. McDaniel, D. McGlinchery, A. Obertelli, K. Siwek, L.A. Riley, J.A. Tostevin, D. Weisshaar, Phys. Rev. C 77 (2008) 044306.
[158] C.A. Bertulani, P.G. Hansen, Phys. Rev. C70 (2004) 034609.
[159] C.A. Bertulani, A. Gade, Comp. Phys. Comm. 17 (2006) 372.
[160] L. Ray, Phys. Rev. C 20 (1979) 1957.
[161] D. Bazin, R.J. Charity, R.T. de Souza, M.A. Famiano, A. Gade, V. Henzl, D. Henzlova, S. Hudan, J. Lee, S. Lukyanov, W.G. Lynch, S. McDaniel, M. Mocko, A. Obertelli, A.M. Rogers, L.G. Sobotka, J.R. Terry, J.A. Tostevin, M.B. Tsang, M.S. Wallace, Phys. Rev. Lett. 102 (2009) 232501.
[162] J.A. Tostevin, B.A. Brown, Phys. Rev. C 74 (2006) 064604.
[163] E.C. Simpson, J.A. Tostevin, D. Bazin, B.A. Brown, A. Gade, Phys. Rev. Lett. 102 (2009) 132502.
[164] E.C. Simpson, J.A. Tostevin, D. Bazin, A. Gade, Phys. Rev. C 79 (2009) 064621.
[165] D. Bazin, B.A. Brown, C.M. Campbell, J.A. Church, D.C. Dinca, J. Enders, A. Gade, T. Glasmacher, P.G. Hansen, W.F. Mueller, H. Olliver, B.C. Perry, B.M. Sherrill, J.R. Terry, J.A. Tostevin, Phys. Rev. Lett. 91 (2003) 012501.
[166] R.R.C. Clement, D. Bazin, W. Benenson, B.A. Brown, A.L. Cole, M.W. Cooper, P.A. DeYoung, A. Estrade, M.A. Famiano, N.H. Frank, A. Gade, T. Glasmacher, P.T. Hosmer, W.G. Lynch, F. Montes, W.F. Mueller, G.F. Peaslee, P. Santi, H. Schatz, B.M. Sherrill, M.-J. van Goethem, M.S. Wallace, Phys. Rev. Lett. 92 (2004) 172502.
[167] H. Schatz, C.A. Bertulani, B.A. Brown, R.R.C. Clement, A.A. Sakharuk, B.M. Sherrill, Phys. Rev. C 72 (2005) 065804.
[168] G. Jacob, Th.A.J. Maris, Rev. Modern Phys. 38 (1966) 121; 45 (1973) 6.
[169] P. Kitching, W.J. McDonald, Th.A.J. Maris, C.A.Z. Vasconcellos, Adv. Nuclear Phys. 15 (1985) 43.
[170] T. Aumann, R. Lemmon, Private communication. 1st International Workshop on Quasi-free Scattering with Radioactive Ion Beams, ECT* Trento, April 7–11, 2008. http://www.nucleartheory.net/QFS/.
[171] T.N. Taddeucci, C.A. Goulding, T.A. Carey, R.C. Byrd, C.D. Goodman, C. Gaarde, J. Larsen, D. Horen, J. Rapaport, E. Sugarbaker, Nuclear Phys. A 469 (1987) 125.

[172] C.A. Bertulani, Nuclear Phys. A 554 (1993) 493;
C.A. Bertulani, P. Lotti, Phys. Lett. B 402 (1997) 237;
C.A. Bertulani, D. Dolci, Nuclear Phys. A674 (2000) 527.
[173] R.G.T. Zegers, T. Adachi, H. Akimune, S.M. Austin, A.M. vanden Berg, B.A. Brown, Y. Fujita, M. Fujiwara, S. Galès, C.J. Guess, M.N. Harakeh, H. Hashimoto, K. Hatanaka, R. Hayami, G.W. Hitt, M.E. Howard, M. Itoh, T. Kawabata, K. Kawase, M. Kinoshita, M. Matsubara, K. Nakanishi, S. Nakayama, S. Okumura, T. Ohta, Y. Sakemi, Y. Shimbara, Y. Shimizu, C. Scholl, C. Simenel, Y. Tameshige, A. Tamii, M. Uchida, T. Yamagata, M. Yosoi, Phys. Rev. Lett. 99 (2007) 202501.
[174] H. Lenske, H.H. Wolter, H.G. Bohlen, Phys. Rev. Lett. 62 (1989) 1457.
[175] S.M. Austin, N. Anantaraman, W.G. Love, Phys. Rev. Lett. 73 (1994) 30.
[176] J.W. Watson, W. Pairsuwan, B.D. Anderson, A.R. Baldwin, B.S. Flanders, R. Madey, R.J. McCarthy, B.A. Brown, B.H. Wildenthal, C.C. Foster, Phys. Rev. Lett. 55 (1985) 1369.
[177] M. Steiner, Sam M. Austin, D. Bazin, W. Benenson, C.A. Bertulani, J.A. Brown, M. Fauerbach, M. Hellström, E. Kashy, J.H. Kelley, R.A. Kryger, T. Kubo, N.A. Orr, R. Pfaff, B.M. Sherrill, M. Thoennessen, S.J. Yennello, B.M. Young, P.D. Zecher, D.J. Morrissey, C.F. Powell, Phys. Rev. Lett. 76 (1996) 26.
[178] A.L. Cole, H. Akimune, Sam M. Austin, D. Bazin, A.M. van den Berg, G.P.A. Berg, J. Brown, I. Daito, Y. Fujita, M. Fujiwara, S. Gupta, K. Hara, M.N. Harakeh, J. Jänecke, T. Kawabata, T. Nakamura, D.A. Roberts, B.M. Sherrill, M. Steiner, H. Ueno, R.G.T. Zegers, Phys. Rev. C 74 (2006) 034333.
[179] K. Amos, Amand Faessler, V. Rodin, Phys. Rev. C 76 (2007) 014604.
[180] H.A. Bethe, G.E. Brown, J. Applegate, J.M. Lattimer, Nuclear Phys. A 324 (1979) 487.
[181] G.M. Fuller, W.A. Fowler, M.J. Newman, Astrophys. J. Suppl. 42 (1980) 447.
[182] G.M. Fuller, W.A. Fowler, M.J. Newman, Astrophys. J. 48 (1982) 279.
[183] E. Caurier, K. Langanke, G. Martínez-Pinedo, F. Nowacki, Nuclear Phys. A 653 (1999) 439.
[184] C. Bäumer, A.M. van den Berg, B. Davids, D. Frekers, D. De Frenne, E.-W. Grewe, P. Haefner, M.N. Harakeh, F. Hofmann, M. Hunyadi, E. Jacobs, B.C. Junk, A. Korff, K. Langanke, G. Martinez-Pinedo, A. Negret, P. von Neumann-Cosel, L. Popescu, S. Rakers, A. Richter, H.J. Wörtche, Phys. Rev. C 68 (2003) 031303.
[185] K. Langanke, G. Martinez-Pinedo, Nuclear Phys. A 673 (2000) 481.
[186] K. Langanke, G. Martinez-Pinedo, At. Data Nucl. Data Tables 79 (2001) 1.
[187] C. Gale, G. Bertsch, S. Das Gupta, Phys. Rev. C35 (1987) 1666.
[188] P. Danielewicz, R. Lacey, W.G. Lynch, Science 298 (2002) 1592.
[189] Technical Proposal for the Design, Construction, Commissioning, and Operation of the ELISe setup, spokesperson Haik Simon, GSI Internal Report, Dec. 2005.
[190] T. Suda, K. Maruayama, Proposal for the RIKEN Beam Factory, RIKEN,2001;
M. Wakasugia, T. Suda, Y. Yano, Nucl. Inst. Meth. Phys. A 532 (2004) 216.
[191] Y.K. Gambhir, S.H. Patil, Z. Phys. A 324 (1986) 9.
[192] C.S. Wang, K.C. Chung, A.J. Santiago, Phys. Rev. C 60 (1999) 034310.
[193] D. Vretenar, T. Nikscaronicacute, P. Ring, N. Paar, G.A. Lalazissis, P. Finelli, Eur. Phys. J. A 20 (2004) 75.
[194] B.A. Brown, Phys. Rev. Lett. 85 (2000) 5296.
[195] W.C. Barber, Ann. Rev. Nucl. Sci. 12 (1962) 1.
[196] J.M. Eisenberg, W. Greiner, Excitation Mechanisms of the Nucleus, North-Holland, Amsterdam, 1988.
[197] F.E. Bertrand, Ann. Rev. Nucl. Sci. 26 (1976) 457.
[198] G.R. Satchler, Nuclear Phys. A 472 (1987) 215.
[199] C.A. Bertulani, J. Phys. G34 (2007) 315.
[200] X. Roca-Maza, M. Centelles, F. Salvat, X. Vinas, Phys. Rev. C 78 (2008) 044332.
[201] Tiekuang Dong, Zhongzhou Ren, Zaijun Wang, Phys. Rev. C 77 (2008) 064302.
[202] S. Karataglidis, K. Amos, AIP Conf. Proc. 1012 (2008) 328.
[203] S. Goriely, Phys. Lett. B 436 (1998) 10.
[204] C.A. Bertulani, Phys. Rev. C 75 (2007) 024606.
[205] L. Gialanella, F. Strieder, K. Brand, L. Campajola, A. D'Onofrio, U. Greife, E. Huttel, F. Petrazzuolo, V. Roca, C. Rolfs, M. Romano, M. Romoli, S. Schmidt, W.H. Schulte, F. Terrasi, H.P. Trautvetter, D. Zahnow, Nucl. Instrum. Methods A 376 (1996) 174.
[206] L. Gialanella, F. Strieder, L. Campajola, A. D'Onofrio, U. Greife, G. Gyurky, G. Imbriani, G. Oliviero, A. Ordine, V. Roca, C. Rolfs, M. Romano, D. Rogalla, C. Sabbarese, E. Somorjai, F. Terrasi, H.P. Trautvetter, Eur. Phys. J. A 7 (2000) 303.
[207] R. Joosten, J. Powell, F.Q. Guo, P.E. Haustein, R.M. Larimer, M.A. McMahan, E.B. Norman, J.P. O'Neil, M.W. Rowe, H.F. VanBrocklin, D. Wutte, X.J. Xu, J. Cerny, Phys. Rev. Lett. 84 (2000) 5066.
[208] R. Maier, G. Korschinek, P. Spolaore, W. Kutschera, H. Maier, W. Goldstein, Nucl. Instrum. Methods 155 (1978) 55.
[209] A.D. Roberts, R.J. Nickles, M. Paul, K.E. Rehm, C.L. Jiang, D.J. Blumenthal, J. Gehring, D. Henderson, J. Nolen, R.C. Pardo, J.P. Schiffer, R.E. Segel, Nucl. Instrum. Methods B 103 (1995) 523.
[210] M. Cogneau, P. Decrock, M. Gaelens, D. Labar, P. Leleux, M. Loiselet, G. Ryckewaert, Nucl. Instrum. Methods A 420 (1999) 489.
[211] A.A. Sonzogni, K.E. Rehm, I. Ahmad, F. Borasi, D.L. Bowers, F. Brumwell, J. Caggiano, C.N. Davids, J.P. Greene, B. Harss, A. Heinz, D. Henderson, R.V.F. Janssens, C.L. Jiang, G. McMichael, J. Nolen, R.C. Pardo, M. Paul, J.P. Schiffer, R.E. Segel, D. Seweryniak, R.H. Siemssen, J.W. Truran, J. Uusitalo, I. Wiedenhöver, B. Zabransky, Phys. Rev. Lett. 84 (2000) 1651.
[212] K.E. Rehm, F. Borasi, C.L. Jiang, D. Ackermann, I. Ahmad, F. Brumwell, C.N. Davids, P. Decrock, S.M. Fischer, J. Gorres, J.P. Greene, G. Hackmann, B. Harss, D. Henderson, W. Henning, R.V.F. Janssens, G. McMichael, V. Nanal, D. Nisius, J. Nolen, R.C. Pardo, M. Paul, P. Reiter, J.P. Schiffer, D. Seweryniak, R.E. Segel, I. Wiedenhover, M. Wiescher, A.H. Wuosmaa, Nucl. Instrum. Methods A 449 (2000) 208.
[213] J. Cooper, L. Bernstein, M. McMahan, J. Powell, D. Wutte, L. Ahle, N. Benczer-Koller, D. Dashdorj, G. Kumbartzki, T. Mertzimekis, A. Schiller, C. Silver, M. Taylor, Nucl. Instrum. Methods A 533 (2004) 287.
[214] N. Anyas-Weiss, J.C. Cornell, P.S. Fisher, P.N. Hudson, A. Menchaca-Rocha, D.J. Millener, A.D. Panagiotou, D.K. Scott, D. Strottman, D.M. Brink, B. Buck, P.J. Ellis, T. Engeland, Phys. Rep. 12 (1974) 201.
[215] J.J. Kolata, A. Morsad, X.J. Kong, R.E. Warner, F.D. Becchetti, W.Z. Liu, D.A. Roberts, J.W. Janecke, Nucl. Instrum. Methods B 40 (1989) 503.
[216] F.D. Becchetti, J.A. Brown, K. Ashktorab, J.W. Janecke, W.Z. Liu, D.A. Roberts, R.J. Smith, J.J. Kolata, K. Lamkin, A. Morsad, R.E. Warner, Nucl. Instrum. Methods B 56 (1991) 554.
[217] B. Harss, R.C. Pardo, K.E. Rehm, F. Borasi, J.P. Greene, R.V.F. Janssens, C.L. Jiang, J. Nolen, M. Paul, J.P. Schiffer, R.E. Segel, J. Specht, T.F. Wang, P. Wilt, B. Zabransky, Rev. Sci. Instrum. 71 (2000) 380.
[218] F.D. Becchetti, M.Y. Lee, T.W. O'Donnell, D.A. Roberts, J.J. Kolata, L.O. Lamm, G. Rogachev, V.G. aes, P.A. DeYoung, S. Vincent, Nucl. Instrum. Methods A 505 (2003) 377.
[219] R.E. Tribble, A. Azhari, C.A. Gagliardi, J.C. Hardy, A. Mukhamedzhanov, X. Tang, L. Trache, S.J. Yennello, Nuclear Phys. A 701 (2002) 278.
[220] Y. Yanagisawa, S. Kubono, T. Teranishi, K. Ue, S. Michimasa, M. Notani, J. He, Y. Ohshiro, S. Shimoura, S. Watanabe, N. Yamazaki, H. Iwasaki, S. Kato, T. Kishida, T. Morikawa, Y. Mizoi, Nucl. Instrum. Methods A 539 (2005) 74.
[221] D.E. Greiner, P.J. Lindstrom, H.H. Heckman, B. Cork, F.S. Bieser, Phys. Rev. Lett. 35 (1975) 152.
[222] D.J. Morrissey, Phys. Rev. C 39 (1989) 460.
[223] D.J. Morrissey, W.R. Marsh, R.J. Otto, W. Loveland, G.T. Seaborg, Phys. Rev. C 18 (1978) 1267.
[224] G.F. Bertsch, S.D. Gupta, Phys. Rep. 160 (1988) 189.
[225] J. Bowmann, W. Swiatecki, C.-F. Tsang, LBL Report No. LBL-2908, 1973.

[226] J. Gosset, H.H. Gutbrod, W.G. Meyer, A.M. Poskanzer, A. Sandoval, R. Stock, G.D. Westfall, Phys. Rev. C 16 (1977) 629.
[227] Y. Yariv, Z. Fraenkel, Phys. Rev. C 20 (1979) 2227.
[228] Y. Yariv, Z. Fraenkel, Phys. Rev. C 21 (1980) 2139.
[229] H. Geissel, G. Münzenberg, K. Riisager, Ann. Rev. Nucl. Part. Sci. 45 (1995) 163.
[230] D.J. Morrissey, B.M. Sherrill, Philos. Trans. R. Soc. Lond. Ser. A. Math. Phys. Eng. Sci. 356 (1998) 1985.
[231] K.-H. Schmidt, E. Hanelt, H. Geissel, G. Münzenberg, J. Dufour, Nucl. Instrum. Methods A 260 (1987) 287.
[232] H. Geissel, T. Schwab, P. Armbruster, J. Dufour, E. Hanelt, K.-H. Schmidt, B. Sherrill, G. Münzenberg, Nucl. Instrum. Methods A 282 (1989) 247.
[233] H.H. Heckman, D.E. Greiner, P.J. Lindstrom, F.S. Bieser, Phys. Rev. Lett. 28 (1972) 926.
[234] T.J.M. Symons, Y.P. Viyogi, G.D. Westfall, P. Doll, D.E. Greiner, H. Faraggi, P.J. Lindstrom, D.K. Scott, H.J. Crawford, C. McParland, Phys. Rev. Lett. 42 (1979) 40.
[235] http://www.ganil.fr/research/index.html.
[236] http://www.gsi.de/.
[237] http://www.nscl.msu.edu.
[238] http://www.nishina.riken.jp/Eng/index.html.
[239] G. Rudstam, P. Aagaard, B. Ekstrom, E. Lund, H. Gokturk, H. Zwicky, Radiochim. Acta 49 (1990) 155.
[240] M. Bernas, S. Czajkowski, P. Armbruster, H. Geissel, P. Dessagne, C. Donzaud, H.-R. Faust, E. Hanelt, A. Heinz, M. Hesse, C. Kozhuharov, C. Miehe, G. Münzenberg, M. Pfützner, C. Röhl, K.H. Schmidt, W. Schwab, C. Stèphan, K. Sümmerer, L. Tassan-Got, B. Voss, Phys. Lett. B 331 (1994) 19.
[241] H.L. Ravn, Phys. Rep. 54 (1979) 201.
[242] E. Kugler, D. Fiander, B. Johnson, H. Haas, A. Przewloka, H.L. Ravn, D.J. Simon, K. Zimmer, Nucl. Instrum. Methods B 70 (1992) 41.
[243] P. Bricault, M. Dombsky, P. Schmor, G. Stanford, Nucl. Instrum. Methods B 126 (1997) 231.
[244] P. Dendooven, Nucl. Instrum. Methods B 126 (1997) 182.
[245] J. Äystö, Nuclear Phys. A 693 (2001) 477.
[246] D. Darquennes, P. Decrock, T. Delbar, W. Galster, M. Huyse, Y. Jongen, M. Lacroix, P. Leleux, I. Licot, E. Lienard, P. Lipnik, M. Loiselet, G. Ryckewaert, S.W. Kitwanga, P. Vanduppen, J. Vanhorenbeeck, J. Vervier, S. Zaremba, Phys. Rev. C 42 (1990) R804.
[247] A.C.C. Villari, Nucl. Instrum. Methods B 204 (2003) 31.
[248] G. Friedlander, L. Friedman, B. Gordon, L. Yaffe, Phys. Rev. 129 (1963) 1809.
[249] B.N. Belyaev, V.D. Domkin, Y.G. Korobulin, L.N. Androneko, G.E. Solyakin, Nuclear Phys. A 348 (1980) 479.
[250] W.G. Lynch, Ann. Rev. Nucl. Part. Sci. 37 (1987) 493.
[251] P. Armbruster, J. Benlliure, M. Bernas, A. Boudard, E. Casarejos, S. Czajkowski, T. Enqvist, S. Leray, P. Napolitani, J. Pereira, F. Rejmund, M.-V. Ricciardi, K.-H. Schmidt, C. Stéphan, J. Taieb, L. Tassan-Got, C. Volant, Phys. Rev. Lett. 93 (2004) 212701.
[252] U. Koester, Radiochem. Acta 89 (2001) 749.
[253] U. Köster, P. Carbonez, A. Dorsival, J. Dvorak, R. Eichler, S. Fernandes, H. Franberg, J. Neuhausen, Z. Novackova, R. Wilfinger, A. Yakushev, Eur. Phys. J. A 150 (2007) 285.
[254] A. Kronenberg, E. Spejewski, H. Carter, B. Mervin, C. Jost, D. Stracener, S. Lapi, T. Bray, Nucl. Instrum. Methods B 266 (2008) 4252.
[255] R. Kirchner, Nucl. Instrum. Methods B 70 (1992) 186.
[256] J.R.J. Bennett, Nuclear Phys. A 701 (2002) 296.
[257] J.R.J. Bennett, U.C. Bergmann, P.V. Drumm, H. Ravn, Nucl. Instrum. Methods B 204 (2003) 215.
[258] http://www.phy.ornl.gov/hribf/.
[259] http://www.triumf.ca/isac/isac_home.html.
[260] http://isolde.web.cern.ch/isolde/.
[261] http://www.ganil.fr/spiral/index.html.
[262] http://fys.kuleuven.be/iks/lisol/exp/lisol.php.
[263] P.V. Duppen, B. Bruyneel, M. Huyse, Y. Kudryavtsev, P.V.D. Bergh, L. Vermeeren, Hyperfine Interact. 127 (2000) 401.
[264] G. Savard, J. Clark, C. Boudreau, F. Buchinger, J.E. Crawford, H. Geissel, J.P. Greene, S. Gulick, A. Heinz, J.K.P. Lee, A. Levand, M. Maier, G. Münzenberg, C. Scheidenberger, D. Seweryniak, K.S. Sharma, G. Sprouse, J. Vaz, J.C. Wang, B.J. Zabransky, Z. Zhou, Nucl. Instrum. Methods B 204 (2003) 582.
[265] L. Weissman, D. Morrissey, G. Bollen, D. Davies, E. Kwan, P. Lofy, P. Schury, S. Schwarz, C. Sumithrarachchi, T. Sun, R. Ringle, Nucl. Instrum. Methods A 540 (2005) 245.
[266] http://www.frib.msu.edu/.
[267] http://www.nscl.msu.edu/exp/sr.
[268] G. Savard, S. Baker, C. Davids, A. Levand, E. Moore, R. Pardo, R. Vondrasek, B. Zabransky, G. Zinkann, Nucl. Instrum. Methods B 266 (2008) 4086.
[269] http://www.eurisol.org/site02/index.php.
[270] http://www.gsi.de/fair/index_e.html.
[271] http://www.ganil.fr/research/developments/spiral2/index.html.
[272] http://www.triumf.info/facility/.
[273] http://www.nishina.riken.jp/Eng/facilities/RIBF.html.
[274] M.S. Smith, K.E. Rehm, Ann. Rev. Nucl. Part. Sci. 51 (2001) 91.
[275] F. Vanderbist, C. Angulo, M. Couder, Y.E. Masri, P. Leleux, M. Loiselet, G. Tabacaru, Nucl. Instrum. Methods B 197 (2002) 165.
[276] W. Bradfield-Smith, T. Davinson, A. DiPietro, A.M. Laird, A.N. Ostrowski, A.C. Shotter, P.J. Woods, S. Cherubini, W. Galster, J.S. Graulich, P. Leleux, L. Michel, A. Ninane, J. Vervier, J. Görres, M. Wiescher, J. Rahighi, J. Hinnefeld, Nucl. Instrum. Methods A 425 (1999) 1.
[277] W. Mittig, P. Roussel-Chomaz, Nuclear Phys. A 693 (2001) 495.
[278] K.P. Artemov, M.S. Golovkov, V.Z. Goldberg, et al., Sov. J. Nuclear Phys. 52 (1990) 406.
[279] M. Notani, S. Kubono, T. Teranishi, Y. Yanagisawa, S. Michimasa, K. Ue, J. He, H. Iwasaki, H. Baba, M. Tamaki, T. Minemura, S. Shimoura, N. Hokoiwa, Y. Wakabayashi, T. Sasaki, T. Fukuchi, A. Odahara, Y. Gono, Z. Fülöp, E. Lee, K. Hahn, J. Moon, C. Yun, J. Lee, C. Lee, S. Kato, Nuclear Phys. A 738 (2004) 411.
[280] C. Fu, V.Z. Goldberg, A.M. Mukhamedzhanov, G.G. Chubarian, G.V. Rogachev, B. Skorodumov, M. McCleskey, Y. Zhai, T. Al-Abdullah, G. Tabacaru, L. Trache, R.E. Tribble, Phys. Rev. C 76 (2007) 021603.
[281] A. Galindo-Uribarri, J.G. del Campo, J.R. Beene, C.J. Gross, J.F. Liang, S.D. Paul, D. Shapira, D.W. Stracener, R.L. Varner, E. Chavez, A. Huerta, M.E. Ortiz, E. Padilla, S. Pascual, Nucl. Instrum. Methods B 172 (2000) 647.
[282] D. Bardayan, J. Blackmon, J.G. del Campo, R. Kozub, J. Liang, Z. Ma, L. Sahin, D. Shapira, M. Smith, Nuclear Phys. A 758 (2005) 737.
[283] D.A. Hutcheon, S. Bishop, L. Buchmann, M.L. Chatterjee, A.A. Chen, J.M. D'Auria, S. Engel, D. Gigliotti, U. Greife, D. Hunter, A. Hussein, C.C. Jewett, N. Khan, M. Lamey, A.M. Laird, W. Liu, A. Olin, D. Ottewell, J.G. Rogers, G. Roy, H. Sprenger, C. Wrede, Nucl. Instrum. Methods A 498 (2003) 190.
[284] R. Fitzgerald, E. Abbotoy, D. Bardayan, J. Blackmon, A. Champagne, A. Chen, U. Greife, D. Hill, A. James, R. Kozub, T. Lewis, R. Livesay, Z. Ma, S. Mahan, J. McConnell, W. Milner, B. Moazen, P. Parker, D. Pierce, M. Roettger, L. Sahin, D. Shapira, M. Smith, F. Strieder, K. Swartz, J. Thomas, D. Visser, Nuclear Phys. A 748 (2005) 351.
[285] http://www.phy.ornl.gov/astrophysics/nuc/rib/gas_tgt.jpg.
[286] C. Rolfs, C.A. Barnes, Ann. Rev. Nucl. Part. Sci. 40 (1990) 45.
[287] C. Rowland, C. Iliadis, A.E. Champagne, A.K. Dummer, R. Fitzgerald, E.C.T. Harley, J. Mosher, R. Runkle, Nucl. Instrum. Methods A 480 (2002) 610.
[288] C. Rowland, C. Iliadis, A.E. Champagne, C. Fox, J. José, R. Runkle, Astrophys. J. Lett. 615 (2004) L37.
[289] C. Fox, C. Iliadis, A.E. Champagne, A. Coc, J. José, R. Longland, J. Newton, J. Pollanen, R. Runkle, Phys. Rev. Lett. 93 (2004) 081102.
[290] C. Fox, C. Iliadis, A.E. Champagne, R.P. Fitzgerald, R. Longland, J. Newton, J. Pollanen, R. Runkle, Phys. Rev. C 71 (2005) 055801.

[291] G. Gyürky, F. Confortola, H. Costantini, A. Formicola, D. Bemmerer, R. Bonetti, C. Broggini, P. Corvisiero, Z. Elekes, Z. Fülöp, G. Gervino, A. Guglielmetti, C. Gustavino, G. Imbriani, M. Junker, M. Laubenstein, A. Lemut, B. Limata, V. Lozza, M. Marta, R. Menegazzo, P. Prati, V. Roca, C. Rolfs, C.R. Alvarez, E. Somorjai, O. Straniero, F. Strieder, F. Terrasi, H.P.T.L. Collaboration, Phys. Rev. C 75 (2007) 035805.
[292] D. Bemmerer, F. Confortola, H. Costantini, A. Formicola, G. Gyürky, R. Bonetti, C. Broggini, P. Corvisiero, Z. Elekes, Z. Fülöp, G. Gervino, A. Guglielmetti, C. Gustavino, G. Imbriani, M. Junker, M. Laubenstein, A. Lemut, B. Limata, V. Lozza, M. Marta, R. Menegazzo, P. Prati, V. Roca, C. Rolfs, C.R. Alvarez, E. Somorjai, O. Straniero, F. Strieder, F. Terrasi, H.P. Trautvetter, Phys. Rev. Lett. 97 (2006) 122502.
[293] F. Confortola, D. Bemmerer, H. Costantini, A. Formicola, G. Gyürky, P. Bezzon, R. Bonetti, C. Broggini, P. Corvisiero, Z. Elekes, Z. Fülöp, G. Gervino, A. Guglielmetti, C. Gustavino, G. Imbriani, M. Junker, M. Laubenstein, A. Lemut, B. Limata, V. Lozza, M. Marta, R. Menegazzo, P. Prati, V. Roca, C. Rolfs, C.R. Alvarez, E. Somorjai, O. Straniero, F. Strieder, F. Terrasi, H.P. Trautvetter, Phys. Rev. C 75 (2007) 065803.
[294] A. Formicola, G. Imbriani, H. Costantini, C. Angulo, D. Bemmerer, R. Bonetti, C. Broggini, P. Corvisiero, J. Cruz, P. Descouvemont, Z. Fülöp, G. Gervino, A. Guglielmetti, C. Gustavino, G. Gyürky, A.P. Jesus, M. Junker, A. Lemut, R. Menegazzo, P. Prati, V. Roca, C. Rolfs, M. Romano, C.R. Alvarez, F. Schümann, E. Somorjai, O. Straniero, F. Strieder, F. Terrasi, H.P. Trautvetter, A. Vomiero, S. Zavatarelli, Phys. Lett. B 591 (2004) 61.
[295] D. Bemmerer, F. Confortola, A. Lemut, R. Bonetti, C. Broggini, P. Corvisiero, H. Costantini, J. Cruz, A. Formicola, Z. Fülöp, G. Gervino, A. Guglielmetti, C. Gustavino, G. Gyürky, G. Imbriani, A. Jesus, M. Junker, B. Limata, R. Menegazzo, P. Prati, V. Roca, C. Rolfs, D. Rogalla, M. Romano, C. Rossi-Alvarez, F. Schümann, E. Somorjai, O. Straniero, F. Strieder, F. Terrasi, H. Trautvetter, Nuclear Phys. A 779 (2006) 297.
[296] A. Lemut, D. Bemmerer, F. Confortola, R. Bonetti, C. Broggini, P. Corvisiero, H. Costantini, J. Cruz, A. Formicola, Z. Fülöp, G. Gervino, A. Guglielmetti, C. Gustavino, G. Gyürky, G. Imbriani, A. Jesus, M. Junker, B. Limata, R. Menegazzo, P. Prati, V. Roca, D. Rogalla, C. Rolfs, M. Romano, C.R. Alvarez, F. Schümann, E. Somorjai, O. Straniero, F. Strieder, F. Terrasi, H. Trautvetter, Phys. Lett. B 634 (2006) 483.
[297] M. Marta, A. Formicola, G. Gyürky, D. Bemmerer, C. Broggini, A. Caciolli, P. Corvisiero, H. Costantini, Z. Elekes, Z. Fülöp, G. Gervino, A. Guglielmetti, C. Gustavino, G. Imbriani, M. Junker, R. Kunz, A. Lemut, B. Limata, C. Mazzocchi, R. Menegazzo, P. Prati, V. Roca, C. Rolfs, M. Romano, C.R. Alvarez, E. Somorjai, O. Straniero, F. Strieder, F. Terrasi, H.P. Trautvetter, A. Vomiero, Phys. Rev. C 78 (2008) 022802.
[298] U. Greife, C. Arpesella, C. Barnes, F. Bartolucci, E. Bellotti, C. Broggini, P. Corvisiero, G. Fiorentini, A. Fubini, G. Gervino, F. Gorris, C. Gustavino, M. Junker, R. Kavanagh, A. Lanza, G. Mezzorani, P. Prati, P. Quarati, W. Rodney, C. Rolfs, W. Schulte, H. Trautvetter, D. Zahnow, Nucl. Instrum. Methods A 350 (1994) 327.
[299] A. Formicola, G. Imbriani, M. Junker, D. Bemmerer, R. Bonetti, C. Broggini, C. Casella, P. Corvisiero, H. Costantini, G. Gervino, C. Gustavino, A. Lemut, P. Prati, V. Roca, C. Rolfs, M. Romano, D. Schürmann, F. Strieder, F. Terrasi, H.P. Trautvetter, S. Zavatarelli, Nucl. Instrum. Methods A 507 (2003) 609.
[300] M. Couder, C. Angulo, W. Galster, J.S. Graulich, P. Leleux, P. Lipnik, G. Tabacaru, F. Vanderbist, Nucl. Instrum. Methods A 506 (2003) 26.
[301] K.E. Rehm, C.L. Jiang, M. Paul, D. Blumenthal, L.A. Daniel, C.N. Davids, P. Decrock, S.M. Fischer, D. Henderson, C. Lister, J. Nickles, J. Nolen, R.C. Pardo, J.P. Schiffer, D. Seweryniak, R.E. Segel, Nucl. Instrum. Methods A 418 (1998) 355.
[302] D. Schürmann, F. Strieder, A.D. Leva, L. Gialanella, N.D. Cesare, A. D'Onofrio, G. Imbriani, J. Klug, C. Lubritto, A. Ordine, V. Roca, H. Röcken, C. Rolfs, D. Rogalla, M. Romano, F. Schümann, F. Terrasi, H. Trautvetter, Nucl. Instrum. Methods A 531 (2004) 428.
[303] M. Couder, G. Berg, J. Görres, P. LeBlanc, L. Lamm, E. Stech, M. Wiescher, J. Hinnefeld, Nucl. Instrum. Methods A 587 (2008) 35.
[304] P. Decrock, T. Delbar, P. Duhamel, W. Galster, M. Huyse, P. Leleux, I. Licot, E. Liénard, P. Lipnik, M. Loiselet, C. Michotte, G. Ryckewaert, P. Van Duppen, J. Vanhorenbeeck, J. Vervier, Phys. Rev. Lett. 67 (1991) 808.
[305] T. Delbar, W. Galster, P. Leleux, I. Licot, E. Liénard, P. Lipnik, M. Loiselet, C. Michotte, G. Ryckewaert, J. Vervier, P. Decrock, M. Huyse, P. Van Duppen, J. Vanhorenbeeck, Phys. Rev. C 48 (1993) 3088.
[306] M. Arnould, G. Paulus, A. Jorissen, Astron. Astrophys 254 (1992) L9.
[307] X. Tang, A. Azhari, C. Fu, C.A. Gagliardi, A.M. Mukhamedzhanov, F. Pirlepesov, L. Trache, R.E. Tribble, V. Burjan, V. Kroha, F. Carstoiu, B.F. Irgaziev, Phys. Rev. C 69 (2004) 055807.
[308] J. Blackmon, C. Angulo, A. Shotter, Nuclear Phys. A 777 (2006) 531.
[309] M. Couder, C. Angulo, E. Casarejos, P. Demaret, P. Leleux, F. Vanderbist, Phys. Rev. C 69 (2004) 022801.
[310] S. Bishop, R.E. Azuma, L. Buchmann, A.A. Chen, M.L. Chatterjee, J.M. D'Auria, S. Engel, D. Gigliotti, U. Greife, M. Hernanz, D. Hunter, A. Hussein, D. Hutcheon, C. Jewett, J. José, J. King, S. Kubono, A.M. Laird, M. Lamey, R. Lewis, W. Liu, S. Michimasa, A. Olin, D. Ottewell, P.D. Parker, J.G. Rogers, F. Strieder, Phys. Rev. Lett. 90 (2003) 162501.
[311] J.M. D'Auria, R.E. Azuma, S. Bishop, L. Buchmann, M.L. Chatterjee, A.A. Chen, S. Engel, D. Gigliotti, U. Greife, D. Hunter, A. Hussein, D. Hutcheon, C.C. Jewett, J. José, J.D. King, A.M. Laird, M. Lamey, R. Lewis, W. Liu, A. Olin, D. Ottewell, P. Parker, J. Rogers, C. Ruiz, M. Trinczek, C. Wrede, Phys. Rev. C 69 (2004) 065803.
[312] C. Ruiz, A. Parikh, J. José, L. Buchmann, J.A. Caggiano, A.A. Chen, J.A. Clark, H. Crawford, B. Davids, J.M. D'Auria, C. Davis, C. Deibel, L. Erikson, L. Fogarty, D. Frekers, U. Greife, A. Hussein, D.A. Hutcheon, M. Huyse, C. Jewett, A.M. Laird, R. Lewis, P. Mumby-Croft, A. Olin, D.F. Ottewell, C.V. Ouellet, P. Parker, J. Pearson, G. Ruprecht, M. Trinczek, C. Vockenhuber, C. Wrede, Phys. Rev. Lett. 96 (2006) 252501.
[313] C. Vockenhuber, C.O. Ouellet, L.-S. The, L. Buchmann, J. Caggiano, A.A. Chen, H. Crawford, J.M. D'Auria, B. Davids, L. Fogarty, D. Frekers, A. Hussein, D.A. Hutcheon, W. Kutschera, A.M. Laird, R. Lewis, E. O'Connor, D. Ottewell, M. Paul, M.M. Pavan, J. Pearson, C. Ruiz, G. Ruprecht, M. Trinczek, B. Wales, A. Wallner, Phys. Rev. C 76 (2007) 035801.
[314] K.A. Chipps, D.W. Bardayan, J.C. Blackmon, K.Y. Chae, U. Greife, R. Hatarik, R.L. Kozub, C. Matei, B.H. Moazen, C.D. Nesaraja, S.D. Pain, W.A. Peters, S.T. Pittman, J.J.F. Shriner, M.S. Smith, Phys. Rev. Lett. 102 (2009) 152502.
[315] S. Parete-Koon, W.R. Hix, M.S. Smith, S. Starrfield, D.W. Bardayan, M.W. Guidry, A. Mezzacappa, Astrophys. J. 598 (2003) 1239.
[316] E.G. Adelberger, S.M. Austin, J.N. Bahcall, A.B. Balantekin, G. Bogaert, L.S. Brown, L. Buchmann, F.E. Cecil, A.E. Champagne, L. de Braeckeleer, C.A. Duba, S.R. Elliott, S.J. Freedman, M. Gai, G. Goldring, C.R. Gould, A. Gruzinov, W.C. Haxton, K.M. Heeger, E. Henley, C.W. Johnson, M. Kamionkowski, R.W. Kavanagh, S.E. Koonin, K. Kubodera, K. Langanke, T. Motobayashi, Rev. Modern Phys. 70 (1998) 1265.
[317] A.R. Junghans, E.C. Mohrmann, K.A. Snover, T.D. Steiger, E.G. Adelberger, J.M. Casandjian, H.E. Swanson, L. Buchmann, S.H. Park, A. Zyuzin, Phys. Rev. Lett. 88 (2002) 041101.
[318] G. Baur, H. Rebel, Ann. Rev. Nucl. Part. Sci. 46 (1996) 321.
[319] E.J. Williams, Phys. Rev. 45 (1934) 729.
[320] C.F.V. Weizsäcker, Z. Phys. A 88 (1934) 612.
[321] T. Motobayashi, Nuclear Phys. A 630 (1998) 328.
[322] T. Motobayashi, T. Takei, S. Kox, C. Perrin, F. Merchez, D. Rebreyend, K. Ieki, H. Murakami, Y. Ando, N. Iwasa, M. Kurokawa, S. Shirato, J. Ruan, T. Ichihara, T. Kubo, N. Inabe, A. Goto, S. Kubono, S. Shimoura, M. Ishihara, Phys. Lett. B 264 (1991) 259.
[323] T. Motobayashi, Nuclear Phys. A 719 (2003) C65.
[324] F. Merchez, S. Kox, C. Perrin, J. Mistretta, J. Gondrand, L. Imouk, P. Gretillat, E. Schwarz, Nucl. Instrum. Methods A 275 (1989) 133.
[325] T. Kikuchi, T. Motobayashi, N. Iwasa, Y. Ando, M. Kurokawa, S. Moriya, H. Murakami, T. Nishio, J. Ruan (Gen), S. Shirato, S. Shimoura, T. Uchibori, Y. Yanagisawa, T. Kubo, H. Sakurai, T. Teranishi, Y. Watanabe, M. Ishihara, M. Hirai, T. Nakamura, S. Kubono, M. Gai, R. France, K.I. Hahn, T. Delbar, P. Lipnik, C. Michotte, Phys. Lett. B 391 (1997) 261.
[326] T. Kikuchi, T. Motobayashi, N. Iwasa, Y. Ando, M. Kurokawa, S. Moriya, H. Murakami, T. Nishio, J. Ruan (Gen), S. Shirato, S. Shimoura, T. Uchibori, Y. Yanagisawa, T. Kubo, H. Sakurai, T. Teranishi, Y. Watanabe, M. Ishihara, M. Hirai, T. Nakamura, S. Kubono, M. Gai, R.H. France III, K. Hahn, T. Delbar, P. Lipnik, C. Michotte, Eur. Phys. J. A 3 (1998) 213.
[327] M. Wiescher, J. Gorres, S. Graff, L. Buchmann, F.-K. Thielemann, Astrophys. J. 343 (1989) 352.
[328] T. Gomi, T. Motobayashi, Y. Ando, N. Aoi, H. Baba, K. Demichi, Z. Elekes, N. Fukuda, Z. Fülöp, U. Futakami, H. Hasegawa, Y. Higurashi, K. Ieki, N. Imai, M. Ishihara, K. Ishikawa, N. Iwasa, H. Iwasaki, S. Kanno, Y. Kondo, T. Kubo, S Kubono, M. Kunibu, K. Kurita, Y.U. Matsuyama, S. Michimasa, T. Minemura, M. Miura, H. Murakami, T. Nakamura, M. Notani, S. Ota, A. Saito, H. Sakurai, M. Serata, S. Shimoura, T. Sugimoto, E. Takeshita, S. Takeuchi, Y. Togano, K. Ue, K. Yamada, Y. Yanagisawa, K. Yoneda, A. Yoshida, J. Phys. G 31 (2005) S1517.

[329] Y. Togano, T. Gomi, T. Motobayashi, Y. Ando, N. Aoi, H. Baba, K. Demichi, Z. Elekes, N. Fukuda, Z. Fülöp, U. Futakami, H. Hasegawa, Y. Higurashi, K. Ieki, N. Imai, M. Ishihara, K. Ishikawa, N. Iwasa, H. Iwasaki, S. Kanno, Y. Kondo, T. Kubo, S. Kubono, M. Kunibu, K. Kurita, Y. Matsuyama, S. Michimasa, T. Minemura, M. Miura, H. Murakami, T. Nakamura, M. Notani, S. Ota, A. Saito, H. Sakurai, M. Serata, S. Shimoura, T. Sugimoto, E. Takeshita, S. Takeuchi, K. Ue, K. Yamada, Y. Yanagisawa, K. Yoneda, A. Yoshida, Nuclear Phys. A 758 (2005) 182.
[330] R.D. Gehrz, G.L. Grasdalen, J.A. Hackwell, Astrophys. J. Lett. 298 (1985) L47.
[331] S. Starrfield, W.M. Sparks, J.W. Truran, M.C. Wiescher, Astrophys. J. Suppl. 127 (2000) 485.
[332] C. Iliadis, A. Champagne, J. Jose, S. Starrfield, P. Tupper, Astrophys. J. Suppl. 142 (2002) 105.
[333] J.A. Caggiano, D. Bazin, W. Benenson, B. Davids, R. Ibbotson, H. Scheit, B.M. Sherrill, M. Steiner, J. Yurkon, A.F. Zeller, B. Blank, M. Chartier, J. Greene, J.A. Nolen, A.H. Wuosmaa, M. Bhattacharya, A. Garcia, M. Wiescher, Phys. Rev. C 64 (2001) 025802.
[334] J. Kiener, A. Lefebvre, P. Aguer, C.O. Bacri, R. Bimbot, G. Bogaert, B. Borderie, F. Clapier, A. Coc, D. Disdier, S. Fortier, C. Grunberg, L. Kraus, I. Linck, G. Pasquier, M.F. Rivet, F.S. Laurent, C. Stephan, L. Tassan-Got, J.P. Thibaud, Nuclear Phys. A 552 (1993) 66.
[335] A. Lefebvre, P. Aguer, J. Kiener, G. Bogaert, A. Coc, F. de Oliveira, J.P. Thibaud, D. Disdier, L. Kraus, I. Linck, S. Fortier, J.A. Scarpaci, C. Stephan, L. Tassan-Got, P. Eudes, F. Guilbault, T. Reposeur, C. Grunberg, P. Roussel-Chomaz, F. Attallah, Nuclear Phys. A 592 (1995) 69.
[336] P. Senger, W. Ahner, P. Beckerle, C. Bormann, D. Brill, M. Cieslak, E. Grosse, W. Henning, P. Koczon, B. Kohlmeyer, W. Konrad, D. Miskowiec, C. Müntz, H. Oeschler, H. Pöppl, W. Prokopowicz, F. Pühlhofer, S. Sartorius, R. Schicker, B. Schlei, E. Schwab, Y. Shin, J. Speer, J. Stein, K. Stiebing, R. Stock, H. Ströbele, C. Sturm, K. Völkel, A. Wagner, W. Walus, Nucl. Instrum. Methods A 327 (1993) 393.
[337] F. Schümann, S. Typel, F. Hammache, K. Sümmerer, F. Uhlig, I. Böttcher, D. Cortina, A. Förster, M. Gai, H. Geissel, U. Greife, E. Grosse, N. Iwasa, P. Koczoń, B. Kohlmeyer, R. Kulessa, H. Kumagai, N. Kurz, M. Menzel, T. Motobayashi, H. Oeschler, A. Ozawa, M.P. Oskoń, W. Prokopowicz, E. Schwab, P. Senger, F. Strieder, C. Sturm, Z.-Y. Sun, G. Surówka, A. Wagner, W. Waluś, Phys. Rev. C 73 (2006) 015806.
[338] B. Davids, S.M. Austin, D. Bazin, H. Esbensen, B.M. Sherrill, I.J. Thompson, J.A. Tostevin, Phys. Rev. C 63 (2001) 065806.
[339] D. Bazin, J.A. Caggiano, B.M. Sherrill, J. Yurkon, A. Zeller, Nucl. Instrum. Methods B 204 (2003) 629.
[340] J. Yurkon, D. Bazin, W. Benenson, D.J. Morrissey, B.M. Sherrill, D. Swan, R. Swanson, Nucl. Instrum. Methods A 422 (1999) 291.
[341] M. Gai, Phys. Rev. C 74 (2006) 025810.
[342] T. Nakamura, N. Fukuda, N. Aoi, N. Imai, M. Ishihara, H. Iwasaki, T. Kobayashi, T. Kubo, A. Mengoni, T. Motobayashi, M. Notani, H. Otsu, H. Sakurai, S. Shimoura, T. Teranishi, Y.X. Watanabe, K. Yoneda, Phys. Rev. C 79 (2009) 035805.
[343] U.D. Pramanik, T. Aumann, K. Boretzky, B.V. Carlson, D. Cortina, T.W. Elze, H. Emling, H. Geissel, A. Grünschloss, M. Hellström, S. Ilievski, J.V. Kratz, R. Kulessa, Y. Leifels, A. Leistenschneider, E. Lubkiewicz, G. Münzenberg, P. Reiter, H. Simon, K. Sümmerer, E. Wajda, W. Walus, Phys. Lett. B 551 (2003) 63.
[344] P. Adrich, A. Klimkiewicz, M. Fallot, K. Boretzky, T. Aumann, D. Cortina-Gil, U.D. Pramanik, T.W. Elze, H. Emling, H. Geissel, M. Hellström, K.L. Jones, J.V. Kratz, R. Kulessa, Y. Leifels, C. Nociforo, R. Palit, H. Simon, G. Surówka, K. Sümmerer, W. Waluś, Phys. Rev. Lett. 95 (2005) 132501.
[345] C. Nociforo, K. Jones, L. Khiem, P. Adrich, T. Aumann, B. Carlson, D. Cortina-Gil, U.D. Pramanik, T. Elze, H. Emling, H. Geissel, M. Hellstrm, J. Kratz, R. Kulessa, T. Lange, Y. Leifels, H. Lenske, E. Lubkiewicz, G. Mnzenberg, R. Palit, H. Scheit, H. Simon, K. Smmerer, S. Typel, E. Wajda, W. Walus, H. Weick, Phys. Lett. B 605 (2005) 79.
[346] T. Davinson, W. Bradfield-Smith, S. Cherubini, A. DiPietro, W. Galster, A.M. Laird, P. Leleux, A. Ninane, A.N. Ostrowski, A.C. Shotter, J. Vervier, P.J. Woods, Nucl. Instrum. Methods A 454 (2000) 350.
[347] D.W. Bardayan, J.C. Blackmon, C.R. Brune, A.E. Champagne, A.A. Chen, J.M. Cox, T. Davinson, V.Y. Hansper, M.A. Hofstee, B.A. Johnson, R.L. Kozub, Z. Ma, P.D. Parker, D.E. Pierce, M.T. Rabban, A.C. Shotter, M.S. Smith, K.B. Swartz, D.W. Visser, P.J. Woods, Phys. Rev. C 62 (2000) 055804.
[348] http://www.phy.ornl.gov/astrophysics/nuc/rib/sidar_overview.jpg.
[349] L. Buchmann, P. Amaudruz, J. D'Auria, D. Hutcheon, C. Matei, J. Pearson, C. Ruiz, G. Ruprecht, M. Trinczek, C. Vockenhuber, P. Walden, Nuclear Phys. A 805 (2008) 462c.
[350] A. Laird, P. Amaudruz, L. Buchmann, S. Fox, B. Fulton, D. Gigliotti, T. Kirchner, P. Mumby-Croft, R. Openshaw, M. Pavan, J. Pearson, G. Ruprecht, G. Sheffer, P. Walden, Nucl. Instrum. Methods A 573 (2007) 306.
[351] C. Demonchy, M.C. No, H. Wang, W. Mittig, P. Roussel-Chomaz, H. Savajols, M. Chartier, D. Cortina-Gil, A. Fomichev, G. Frémont, P. Gangnant, A. Gillibert, L. Giot, M. Golovkov, B. Jurado, J. Libin, A. Obertelli, E. Pollaco, A. Rodin, C. Spitaels, S. Stepantsov, G. Ter-Akopian, R. Wolski, Nucl. Instrum. Methods A 583 (2007) 341.
[352] J. Gómez-Gomar, J. Hernanz, J. José, J. Isern, Mon. Astron. Soc. 296 (1998) 913.
[353] R. Coszach, M. Cogneau, C.R. Bain, F. Binon, T. Davinson, P. Decrock, T. Delbar, M. Gaelens, W. Galster, J. Goerres, J.S. Graulich, R. Irvine, D. Labar, P. Leleux, M. Loiselet, C. Michotte, R. Neal, G. Ryckewaert, A.S. Shotter, J. Vanhorenbeeck, J. Vervier, M. Wiescher, P. Woods, Phys. Lett. B 353 (1995) 184.
[354] J.S. Graulich, F. Binon, W. Bradfield-Smith, M. Cogneau, R. Coszach, T. Davinson, T. Delbar, M. Gaelens, W. Galster, J. Görres, D. Labar, P. Leleux, M. Loiselet, J. McKenzie, R. Neal, G. Ryckewaert, A.C. Shotter, J. Vanhorenbeeck, J. Vervier, M. Wiescher, P. Woods, Nuclear Phys. A 626 (1997) 751.
[355] J.-S. Graulich, S. Cherubini, R. Coszach, S. El Hajjami, W. Galster, P. Leleux, W. Bradfield-Smith, T. Davinson, A. Di Pietro, A.C. Shotter, J. Görres, M. Wiescher, F. Binon, J. Vanhorenbeeck, Phys. Rev. C 63 (2000) 011302.
[356] N.D. Séréville, C. Angulo, A. Coc, N.L. Achouri, E. Casarejos, T. Davinson, P. Descouvemont, P. Figuera, S. Fox, F. Hammache, J. Kiener, A. Laird, A. Lefebvre-Schuhl, P. Leleux, P. Mumby-Croft, N.A. Orr, I. Stefan, K. Vaughan, V. Tatischeff, Phys. Rev. C 79 (2009) 015801.
[357] K.E. Rehm, M. Paul, A.D. Roberts, C.L. Jiang, D.J. Blumenthal, S.M. Fischer, J. Gehring, D. Henderson, J. Nickles, J. Nolen, R.C. Pardo, J.P. Schiffer, R.E. Segel, Phys. Rev. C 53 (1996) 1950.
[358] D.W. Bardayan, J.C. Blackmon, W. Bradfield-Smith, C.R. Brune, A.E. Champagne, T. Davinson, B.A. Johnson, R.L. Kozub, C.S. Lee, R. Lewis, P.D. Parker, A.C. Shotter, M.S. Smith, D.W. Visser, P.J. Woods, Phys. Rev. C 63 (2001) 065802.
[359] D.W. Bardayan, J.C. Batchelder, J.C. Blackmon, A.E. Champagne, T. Davinson, R. Fitzgerald, W.R. Hix, C. Iliadis, R.L. Kozub, Z. Ma, S. Parete-Koon, P.D. Parker, N. Shu, M.S. Smith, P.J. Woods, Phys. Rev. Lett. 89 (2002) 262501.
[360] K.Y. Chae, D.W. Bardayan, J.C. Blackmon, D. Gregory, M.W. Guidry, M.S. Johnson, R.L. Kozub, R.J. Livesay, Z. Ma, C.D. Nesaraja, S.D. Pain, S. Paulauskas, M. Porter-Peden, J.F. S. Jr., N. Smith, M.S. Smith, J.S. Thomas, Phys. Rev. C 74 (2006) 012801.
[361] J.L. Fisker, J. Görres, M. Wiescher, B. Davids, Astrophys. J. 650 (2006) 332.
[362] J. Görres, M. Wiescher, F.-K. Thielemann, Phys. Rev. C 51 (1995) 392.
[363] W. Bradfield-Smith, T. Davinson, A. Di Pietro, A.M. Laird, A.N. Ostrowski, A.C. Shotter, P.J. Woods, S. Cherubini, W. Galster, J.S. Graulich, P. Leleux, L. Michel, A. Ninane, J. Vervier, J. Görres, M. Wiescher, J. Rahighi, J. Hinnefeld, Phys. Rev. C 59 (1999) 3402.
[364] D. Groombridge, A.C. Shotter, W. Bradfield-Smith, S. Cherubini, T. Davinson, A. Di Pietro, J. Görres, J.S. Graulich, A.M. Laird, P. Leleux, A. Musumarra, A. Ninane, A.N. Ostrowski, J. Rahighi, H. Schatz, M. Wiescher, P.J. Woods, Phys. Rev. C 66 (2002) 055802.
[365] C. Angulo, Nuclear Phys. A 746 (2004) 222c.
[366] D.W. Bardayan, J.C. Blackmon, C.R. Brune, A.E. Champagne, A.A. Chen, J.M. Cox, T. Davinson, V.Y. Hansper, M.A. Hofstee, B.A. Johnson, R.L. Kozub, Z. Ma, P.D. Parker, D.E. Pierce, M.T. Rabban, A.C. Shotter, M.S. Smith, K.B. Swartz, D.W. Visser, P.J. Woods, Phys. Rev. Lett. 83 (1999) 45.
[367] J.C. Blackmon, D.W. Bardayan, W. Bradfield-Smith, R. Brummitt, A.E. Champagne, A.A. Chen, T. Davinson, L. Dessieux, M.W. Guidry, K.I. Hahn, G.M. Hale, W.R. Hix, R.L. Kozub, Z. Ma, P.D. Parker, G. Rajbaidya, R.C. Runkle, C.M. Rowland, A.C. Shotter, M.S. Smith, L.A.V. Wormer, D.W. Visser, P.J. Woods, Nuclear Phys. A 718 (2003) 127.
[368] C. Angulo, G. Tabacaru, M. Couder, M. Gaelens, P. Leleux, A. Ninane, F. Vanderbist, T. Davinson, P.J. Woods, J.S. Schweitzer, N.L. Achouri, J.C. Angélique, E. Berthoumieux, F. de Oliveira Santos, P. Himpe, P. Descouvemont, Phys. Rev. C 67 (2003) 014308.
[369] C. Ruiz, F. Sarazin, L. Buchmann, T. Davinson, R.E. Azuma, A.A. Chen, B.R. Fulton, D. Groombridge, L. Ling, A. Murphy, J. Pearson, I. Roberts, A. Robinson, A.C. Shotter, P. Walden, P.J. Woods, Phys. Rev. C 65 (2002) 042801.

[370] C. Ruiz, T. Davinson, F. Sarazin, I. Roberts, A. Robinson, P.J. Woods, L. Buchmann, A.C. Shotter, P. Walden, N.M. Clarke, A.A. Chen, B.R. Fulton, D. Groombridge, J. Pearson, A.S. Murphy, Phys. Rev. C 71 (2005) 025802.
[371] A.S.J. Murphy, M. Aliotta, T. Davinson, C. Ruiz, P.J. Woods, J.M. D'Auria, L. Buchmann, A.A. Chen, A.M. Laird, F. Sarazin, P. Walden, B.R. Fulton, J.E. Pearson, B.A. Brown, Phys. Rev. C 73 (2006) 034320.
[372] D.W. Bardayan, J.C. Blackmon, J. Gómez del Campo, R.L. Kozub, J.F. Liang, Z. Ma, L. Sahin, D. Shapira, M.S. Smith, Phys. Rev. C 70 (2004) 015804.
[373] T. Delbar, W. Galster, P. Leleux, E. Liǹard, P. Lipnik, C. Michotte, J. Vervier, P. Duhamel, J. Vanhorenbeeck, P. Decrock, M. Huyse, P.V. Duppen, D. Baye, P. Descouvemont, Nuclear Phys. A 542 (1992) 263.
[374] R. Coszach, T. Delbar, W. Galster, P. Leleux, I. Licot, E. Liénard, P. Lipnik, C. Michotte, A. Ninane, J. Vervier, C.R. Bain, T. Davinson, R.D. Page, A.C. Shotter, P.J. Woods, D. Baye, F. Binon, P. Descouvemont, P. Duhamel, J. Vanhorenbeeck, M. Vincke, P. Decrock, M. Huyse, P. Van Duppen, G. Vancraeynest, F.C. Barker, Phys. Rev. C 50 (1994) 1695.
[375] C. Angulo, M. Azzouz, P. Descouvemont, G. Tabacaru, D. Baye, M. Cogneau, M. Couder, T. Davinson, A.D. Pietro, P. Figuera, M. Gaelens, P. Leleux, M. Loiselet, A. Ninane, F. de Oliveira Santos, R.G. Pizzone, G. Ryckewaert, N. de Séréville, F. Vanderbist, Nuclear Phys. A 716 (2003) 211.
[376] T. Teranishi, S. Kubono, S. Shimoura, M. Notani, Y. Yanagisawa, S. Michimasa, K. Ue, H. Iwasaki, M. Kurokawa, Y. Satou, T. Morikawa, A. Saito, H. Baba, J.H. Lee, C.S. Lee, Z. Fülöp, S. Kato, Phys. Lett. B 556 (2003) 27.
[377] J.J. He, S. Kubono, T. Teranishi, M. Notani, H. Baba, S. Nishimura, J.Y. Moon, M. Nishimura, H. Iwasaki, Y. Yanagisawa, N. Hokoiwa, M. Kibe, J.H. Lee, S. Kato, Y. Gono, C.S. Lee, Phys. Rev. C 76 (2007) 055802.
[378] T. Teranishi, S. Kubono, H. Yamaguchi, J. He, A. Saito, H. Fujikawa, G. Amadio, M. Niikura, S. Shimoura, Y. Wakabayashi, S. Nishimura, M. Nishimura, J. Moon, C. Lee, A. Odahara, D. Sohler, L. Khiem, Z. Li, G. Lian, W. Liu, Phys. Lett. B 650 (2007) 129.
[379] Y.B. Wang, B.X. Wang, X. Qin, X.X. Bai, B. Guo, C. Jiang, Y.J. Li, Z.H. Li, G. Lian, J. Su, S. Zeng, W.P. Liu, Phys. Rev. C 77 (2008) 044304.
[380] H. Yamaguchi, Y. Wakabayashi, S. Kubono, G. Amadio, H. Fujikawa, T. Teranishi, A. Saito, J. He, S. Nishimura, Y. Togano, Y. Kwon, M. Niikura, N. Iwasa, K. Inafuku, L. Khiem, Phys. Lett. B 672 (2009) 230.
[381] F.Q. Guo, J. Powell, D.W. Lee, D. Leitner, M.A. McMahan, D.M. Moltz, J.P. O'Neil, K. Perajarvi, L. Phair, C.A. Ramsey, X.J. Xu, J. Cerny, Phys. Rev. C 72 (2005) 034312.
[382] K. Peräjärvi, C. Fu, G.V. Rogachev, G. Chubarian, V.Z. Goldberg, F.Q. Guo, D. Lee, D.M. Moltz, J. Powell, B.B. Skorodumov, G. Tabacaru, X.D. Tang, R.E. Tribble, B.A. Brown, A. Volya, J. Cerny, Phys. Rev. C 74 (2006) 024306.
[383] D.W. Lee, K. Peräjärvi, J. Powell, J.P. O'Neil, D.M. Moltz, V.Z. Goldberg, J. Cerny, Phys. Rev. C 76 (2007) 024314.
[384] G. Tabacaru, A. Azhari, J. Brinkley, V. Burjan, F. Carstoiu, C. Fu, C.A. Gagliardi, V. Kroha, A.M. Mukhamedzhanov, X. Tang, L. Trache, R.E. Tribble, S. Zhou, Phys. Rev. C 73 (2006) 025808.
[385] G.V. Rogachev, J.J. Kolata, F.D. Becchetti, P.A. DeYoung, M. Hencheck, K. Helland, J.D. Hinnefeld, B. Hughey, P.L. Jolivette, L.M. Kiessel, H.-Y. Lee, M.Y. Lee, T.W. OD́onnell, G.F. Peaslee, D. Peterson, D.A. Roberts, P. Santi, S.A. Shaheen, Phys. Rev. C 64 (2001) 061601.
[386] G.V. Rogachev, J.J. Kolata, A.S. Volya, F.D. Becchetti, Y. Chen, P.A. DeYoung, J. Lupton, Phys. Rev. C 75 (2007) 014603.
[387] B. Harss, C.L. Jiang, K.E. Rehm, J.P. Schiffer, J. Caggiano, P. Collon, J.P. Greene, D. Henderson, A. Heinz, R.V.F. Janssens, J. Nolen, R.C. Pardo, T. Pennington, R.H. Siemssen, A.A. Sonzogni, J. Uusitalo, I. Wiedenhöver, M. Paul, T.F. Wang, F. Borasi, R.E. Segel, J.C. Blackmon, M. Smith, A. Chen, P. Parker, Phys. Rev. C 65 (2002) 035803.
[388] F. de Oliveira Santos, P. Himpe, M. Lewitowicz, I. Stefan, N. Smirnova, N.L. Achouri, J.C. Angelique, C. Angulo, L. Axelsson, D. Baiborodin, F. Becker, M. Bellegui, E. Berthoumieux, B. Blank, C. Borcea, A. Cassimi, J.M. Daugas, G. de France, F. Dembinski, C.E. Demonchy, Z. Dlouhy, P. Dolegieviez, C. Donzaud, G. Georgiev, L. Giot, S. Grevy, D.G. Mueller, V. Lapoux, E. Lienard, M.J.L. Jimenez, K. Markenroth, I. Matea, W. Mittig, F. Negoita, G. Neyens, N. Orr, F. Pougheon, P.R. Chomaz, M.G.S. Laurent, F. Sarazin, H. Savajols, M. Sawicka, O. Sorlin, M. Stanoiu, C. Stodel, G. Thiamova, D. Verney, Eur. Phys. J. A 24 (2004) 237.
[389] J.C. Dalouzy, L. Achouri, M. Aliotta, C. Angulo, H. Benhabiles, C. Borcea, R. Borcea, P. Bourgault, A. Buta, A. Coc, A. Damman, T. Davinson, F. de Grancey, F. de Oliveira Santos, N. de Séréville, J. Kiener, M.G. Pellegriti, F. Negoita, A.M. Sánchez-Benítez, O. Sorlin, M. Stanoiu, I. Stefan, P.J. Woods, Phys. Rev. Lett. 102 (2009) 162503.
[390] B. Harss, J.P. Greene, D. Henderson, R.V.F. Janssens, C.L. Jiang, J. Nolen, R.C. Pardo, K.E. Rehm, J.P. Schiffer, R.H. Siemssen, A.A. Sonzogni, J. Uusitalo, I. Wiedenhöver, M. Paul, T.F. Wang, F. Borasi, R.E. Segel, J.C. Blackmon, M.S. Smith, A. Chen, P. Parker, Phys. Rev. Lett. 82 (1999) 3964.
[391] J.C. Blackmon, D.W. Bardayan, W. Bradfield-Smith, A.E. Champagne, A.A. Chen, T. Davinson, K.I. Hahn, R.L. Kozub, Z. Ma, P.D. Parker, G. Rajbaidya, R.C. Runkle, C.M. Rowland, A.C. Shotter, M.S. Smith, K.B. Swartz, D.W. Visser, P.J. Woods, Nuclear Phys. A 688 (2001) 142.
[392] T. Rauscher, R. Bieber, H. Oberhummer, K.-L. Kratz, J. Dobaczewski, P. Möller, M.M. Sharma, Phys. Rev. C 57 (1998) 2031.
[393] G. Kraus, P. Egenhof, H. Emling, E. Grosse, W. Henning, R. Holzmann, H. Körner, J. Kratz, R. Kulessa, C. Schiessl, J. Schiffer, W. Wagner, W. Walus, H. Wollersheim, Z. Phys. A 340 (1991) 339.
[394] K.L. Jones, R.L. Kozub, C. Baktash, D.W. Bardayan, J.C. Blackmon, W.N. Catford, J.A. Cizewski, R.P. Fitzgerald, M.S. Johnson, R.J. Livesay, Z. Ma, C.D. Nesaraja, D. Shapira, M.S. Smith, J.S. Thomas, D.W. Visser, Phys. Rev. C 70 (2004) 067602.
[395] J.S. Thomas, D.W. Bardayan, J.C. Blackmon, J.A. Cizewski, U. Greife, C.J. Gross, M.S. Johnson, K.L. Jones, R.L. Kozub, J.F. Liang, R.J. Livesay, Z. Ma, B.H. Moazen, C.D. Nesaraja, D. Shapira, M.S. Smith, Phys. Rev. C 71 (2005) 021302.
[396] J.S. Thomas, G. Arbanas, D.W. Bardayan, J.C. Blackmon, J.A. Cizewski, D.J. Dean, R.P. Fitzgerald, U. Greife, C.J. Gross, M.S. Johnson, K.L. Jones, R.L. Kozub, J.F. Liang, R.J. Livesay, Z. Ma, B.H. Moazen, C.D. Nesaraja, D. Shapira, M.S. Smith, D.W. Visser, Phys. Rev. C 76 (2007) 044302.
[397] A.M. Mukhamedzhanov, F.M. Nunes, P. Mohr, Phys. Rev. C 77 (2008) 051601.
[398] N. de Séréville, A. Coc, C. Angulo, M. Assunçao, D. Beaumel, B. Bouzid, S. Cherubini, M. Couder, P. Demaret, F. de Oliveira Santos, P. Figuera, S. Fortier, M. Gaelens, F. Hammache, J. Kiener, A. Lefebvre, D. Labar, P. Leleux, M. Loiselet, A. Ninane, S. Ouichaoui, G. Ryckewaert, N. Smirnova, V. Tatischeff, J.-P. Thibaud, Phys. Rev. C 67 (2003) 052801.
[399] R.L. Kozub, D.W. Bardayan, J.C. Batchelder, J.C. Blackmon, C.R. Brune, A.E. Champagne, J.A. Cizewski, T. Davinson, U. Greife, C.J. Gross, C.C. Jewett, R.J. Livesay, Z. Ma, B.H. Moazen, C.D. Nesaraja, L. Sahin, J.P. Scott, D. Shapira, M.S. Smith, J.S. Thomas, P.J. Woods, Phys. Rev. C 71 (2005) 032801.
[400] R.L. Kozub, D.W. Bardayan, J.C. Batchelder, J.C. Blackmon, C.R. Brune, A.E. Champagne, J.A. Cizewski, U. Greife, C.J. Gross, C.C. Jewett, R.J. Livesay, Z. Ma, B.H. Moazen, C.D. Nesaraja, L. Sahin, J.P. Scott, D. Shapira, M.S. Smith, J.S. Thomas, Phys. Rev. C 73 (2006) 044307.
[401] P.N. Peplowski, L.T. Baby, I. Wiedenhöver, S.E. Dekat, E. Diffenderfer, D.L. Gay, O. Grubor-Urosevic, P. Höflich, R.A. Kaye, N. Keeley, A. Rojas, A. Volya, Phys. Rev. C 79 (2009) 032801.
[402] A. Azhari, V. Burjan, F. Carstoiu, C.A. Gagliardi, V. Kroha, A.M. Mukhamedzhanov, F.M. Nunes, X. Tang, L. Trache, R.E. Tribble, Phys. Rev. C 63 (2001) 055803.
[403] X. Tang, A. Azhari, C.A. Gagliardi, A.M. Mukhamedzhanov, F. Pirlepesov, L. Trache, R.E. Tribble, V. Burjan, V. Kroha, F. Carstoiu, Phys. Rev. C 67 (2003) 015804.
[404] A.M. Mukhamedzhanov, H.L. Clark, C.A. Gagliardi, Y.-W. Lui, L. Trache, R.E. Tribble, H.M. Xu, X.G. Zhou, V. Burjan, J. Cejpek, V. Kroha, F. Carstoiu, Phys. Rev. C 56 (1997) 1302.
[405] A. Azhari, V. Burjan, F. Carstoiu, H. Dejbakhsh, C.A. Gagliardi, V. Kroha, A.M. Mukhamedzhanov, L. Trache, R.E. Tribble, Phys. Rev. Lett. 82 (1999) 3960.
[406] L. Trache, A. Azhari, F. Carstoiu, H.L. Clark, C.A. Gagliardi, Y.-W. Lui, A.M. Mukhamedzhanov, X. Tang, N. Timofeyuk, R.E. Tribble, Phys. Rev. C 67 (2003) 062801.
[407] C.A. Gagliardi, R.E. Tribble, A. Azhari, H.L. Clark, Y.-W. Lui, A.M. Mukhamedzhanov, A. Sattarov, L. Trache, V. Burjan, J. Cejpek, V. Kroha, Š. Piskoř, J. Vincour, Phys. Rev. C 59 (1999) 1149.
[408] A.M. Mukhamedzhanov, P. Bém, B.A. Brown, V. Burjan, C.A. Gagliardi, V. Kroha, J. Novák, F.M. Nunes, Š. Piskoř, F. Pirlepesov, E. Šimečková, R.E. Tribble, J. Vincour, Phys. Rev. C 67 (2003) 065804.
[409] A.M. Mukhamedzhanov, P. Bém, V. Burjan, C.A. Gagliardi, B.F. Irgaziev, V. Kroha, J. Novák, Š. Piskoř, E. Šimečková, R.E. Tribble, F. Veselý, J. Vincour, Phys. Rev. C 73 (2006) 035806.

[410] J.C. Blackmon, D.W. Bardayan, C.R. Brune, A.E. Champagne, R. Crespo, T. Davinson, J.C. Fernandes, C.A. Gagliardi, U. Greife, C.J. Gross, P.A. Hausladen, C. Iliadis, C.C. Jewett, R.L. Kozub, T.A. Lewis, F. Liang, B.H. Moazen, A.M. Mukhamedzhanov, C.D. Nesaraja, F.M. Nunes, P.D. Parker, D.C. Radford, L. Sahin, J.P. Scott, D. Shapira, M.S. Smith, J.S. Thomas, L. Trache, R.E. Tribble, P.J. Woods, C.H. Yu, Nuclear Phys. A 718 (2003) 587.
[411] E.D. Johnson, G.V. Rogachev, A.M. Mukhamedzhanov, L.T. Baby, S. Brown, W.T. Cluff, A.M. Crisp, E. Diffenderfer, V.Z. Goldberg, B.W. Green, T. Hinners, C.R. Hoffman, K.W. Kemper, O. Momotyuk, P. Peplowski, A. Pipidis, R. Reynolds, B.T. Roeder, Phys. Rev. Lett. 97 (2006) 192701.
[412] L. Trache, F. Carstoiu, C.A. Gagliardi, R.E. Tribble, Phys. Rev. Lett. 87 (2001) 271102.
[413] L. Trache, F. Carstoiu, C.A. Gagliardi, R.E. Tribble, Phys. Rev. C 69 (2004) 032802.
[414] W.F. Mueller, J.A. Church, T. Glasmacher, D. Gutknecht, G. Hackman, P.G. Hansen, Z. Hu, K.L. Miller, P. Quirin, Nucl. Instrum. Methods A 466 (2001) 492.
[415] D. Galaviz, A.M. Amthor, D. Bazin, B.A. Brown, A. Cole, T. Elliot, A. Estrade, Z. Fulop, A. Gade, T. Glasmacher, R. Kessler, G. Lorusso, M. Matos, F. Montes, W. Muller, J. Pereira, H. Schatz, B. Sherrill, F. Schertz, Y. Shimbara, E. Smith, A. Tamii, M. Wallace, R.G.T. Zegers, J. Phys. G 35 (2008) 014030.
[416] A. Gade, T. Glasmacher, Prog. Part. Nuclear Phys. 60 (2008) 161.
[417] A. Jungclaus, L. Cáceres, M. Górska, M. Pfützner, S. Pietri, E. Werner-Malento, H. Grawe, K. Langanke, G. Martínez-Pinedo, F. Nowacki, A. Poves, J.J. Cuenca-García, D. Rudolph, Z. Podolyak, P.H. Regan, P. Detistov, S. Lalkovski, V. Modamio, J. Walker, P. Bednarczyk, P. Doornenbal, H. Geissel, J. Gerl, J. Grebosz, I. Kojouharov, N. Kurz, W. Prokopowicz, H. Schaffner, H.J. Wollersheim, K. Andgren, J. Benlliure, G. Benzoni, A.M. Bruce, E. Casarejos, B. Cederwall, F.C.L. Crespi, B. Hadinia, M. Hellström, R. Hoischen, G. Ilie, J. Jolie, A. Khaplanov, M. Kmiecik, R. Kumar, A. Maj, S. Mandal, F. Montes, S. Myalski, G.S. Simpson, S.J. Steer, S. Tashenov, O. Wieland, Phys. Rev. Lett. 99 (2007) 132501.
[418] J. Eberth, H. Thomas, P. Brentano, R. Lieder, H. Jäger, H. Kämmerfing, M. Berst, D. Gutknecht, R. Henck, Nucl. Instrum. Methods A 369 (1996) 135.
[419] T. Kautzsch, W. Walters, M. Hannawald, K.-L. Kratz, V. Mishin, V. Fedoseyev, W. Böhmer, Y. Jading, P. Van Duppen, B. Pfeiffer, A. Wöhr, P. Möller, I. Klöckl, V. Sebastian, U. Köster, M. Koizumi, J. Lettry, H. Ravn, Eur. Phys. J. A 9 (2000) 201.
[420] I. Dillmann, K.-L. Kratz, A. Wöhr, O. Arndt, B.A. Brown, P. Hoff, M. Hjorth-Jensen, U. Köster, A.N. Ostrowski, B. Pfeiffer, D. Seweryniak, J. Shergur, W.B. Walters, Phys. Rev. Lett. 91 (2003) 162503.
[421] S.J. Steer, Z. Podolyák, S. Pietri, M. Górska, P.H. Regan, D. Rudolph, E. Werner-Malento, A.B. Garnsworthy, R. Hoischen, J. Gerl, H.J. Wollersheim, K.H. Maier, H. Grawe, F. Becker, P. Bednarczyk, L. Cáceres, P. Doornenbal, H. Geissel, J. Grebosz, A. Kelic, I. Kojouharov, N. Kurz, F. Montes, W. Prokopowicz, T. Saito, H. Schaffner, S. Tashenov, A. Heinz, M. Pfützner, T. Kurtukian-Nieto, G. Benzoni, A. Jungclaus, D.L. Balabanski, C. Brandau, B.A. Brown, A.M. Bruce, W.N. Catford, I.J. Cullen, Z. Dombrádi, M.E. Estevez, W. Gelletly, G. Ilie, J. Jolie, G.A. Jones, M. Kmiecik, F.G. Kondev, R. Krücken, S. Lalkovski, Z. Liu, A. Maj, S. Myalski, S. Schwertel, T. Shizuma, P.M. Walker, O. Wieland, Phys. Rev. C 78 (2008) 061302.
[422] W.R. Hix, O.E.B. Messer, A. Mezzacappa, M. Liebendörfer, J. Sampaio, K. Langanke, D.J. Dean, G. Martínez-Pinedo, Phys. Rev. Lett. 91 (2003) 201102.
[423] K. Ikeda, S. Fujii, J.I. Fujita, Phys. Lett. 3 (1963) 271.
[424] K.P. Jackson, A. Celler, W.P. Alford, K. Raywood, R. Abegg, R.E. Azuma, C.K. Campbell, S. El-Kateb, D. Frekers, P.W. Green, O. Häusser, R.L. Helmer, R.S. Henderson, K.H. Hicks, R. Jeppesen, P. Lewis, C.A. Miller, A. Moalem, M.A. Moinester, R.B. Schubank, G.G. Shute, B.M. Spicer, M.C. Vetterli, A.I. Yavin, S. Yen, Phys. Lett. B 201 (1988) 25.
[425] D. Frekers, Nuclear Phys. A 731 (2004) 76.
[426] M. Fujiwara, H. Akimune, A.M. van den Berg, M. Cribier, I. Daito, H. Ejiri, H. Fujimura, Y. Fujita, C.D. Goodman, K. Hara, M.N. Harakeh, F. Ihara, T. Ishikawa, J. Jänecke, T. Kawabata, R.S. Raghavan, K. Schwarz, M. Tanaka, T. Yamanaka, M. Yosoi, R.G.T. Zegers, Phys. Rev. Lett. 85 (2000) 4442.
[427] Y. Fujita, Y. Shimbara, I. Hamamoto, T. Adachi, G.P.A. Berg, H. Fujimura, H. Fujita, J. Görres, K. Hara, K. Hatanaka, J. Kamiya, T. Kawabata, Y. Kitamura, Y. Shimizu, M. Uchida, H.P. Yoshida, M. Yoshifuku, M. Yosoi, Phys. Rev. C 66 (2002) 044313.
[428] R.G.T. Zegers, E.F. Brown, H. Akimune, S.M. Austin, A.M. van den Berg, B.A. Brown, D.A. Chamulak, Y. Fujita, M. Fujiwara, S. Galès, M.N. Harakeh, H. Hashimoto, R. Hayami, G.W. Hitt, M. Itoh, T. Kawabata, K. Kawase, M. Kinoshita, K. Nakanishi, S. Nakayama, S. Okumura, Y. Shimbara, M. Uchida, H. Ueno, T. Yamagata, M. Yosoi, Phys. Rev. C 77 (2008) 024307.
[429] R.G.T. Zegers, R. Meharchand, T. Adachi, S.M. Austin, B.A. Brown, Y. Fujita, M. Fujiwara, C.J. Guess, H. Hashimoto, K. Hatanaka, M.E. Howard, H. Matsubara, K. Nakanishi, T. Ohta, H. Okamura, Y. Sakemi, Y. Shimbara, Y. Shimizu, C. Scholl, A. Signoracci, Y. Tameshige, A. Tamii, M. Yosoi, Phys. Rev. C 78 (2008) 014314.
[430] A. Galonsky, J.P. Didelez, A. Djaloeis, W. Oelert, Phys. Lett. B 74 (1978) 176.
[431] R.G.T. Zegers, H. Akimune, S.M. Austin, D. Bazin, A.M. den Berg, G.P.A. Berg, B.A. Brown, J. Brown, A.L. Cole, I. Daito, Y. Fujita, M. Fujiwara, S. Galès, M.N. Harakeh, H. Hashimoto, R. Hayami, G.W. Hitt, M.E. Howard, M. Itoh, J. Jänecke, T. Kawabata, K. Kawase, M. Kinoshita, T. Nakamura, K. Nakanishi, S. Nakayama, S. Okumura, W.A. Richter, D.A. Roberts, B.M. Sherrill, Y. Shimbara, M. Steiner, M. Uchida, H. Ueno, T. Yamagata, M. Yosoi, Phys. Rev. C 74 (2006) 024309.
[432] M.E. Howard, R.G.T. Zegers, S.M. Austin, D. Bazin, B.A. Brown, A.L. Cole, B. Davids, M. Famiano, Y. Fujita, A. Gade, D. Galaviz, G.W. Hitt, M. Matos, S.D. Reitzner, C. Samanta, L.J. Schradin, Y. Shimbara, E.E. Smith, C. Simenel, Phys. Rev. C 78.
[433] G.W. Hitt, R.G.T. Zegers, S.M. Austin, D. Bazin, A. Gade, D. Galaviz, C.J. Guess, M. Horoi, M.E. Howard, W.D.M. Rae, Y. Shimbara, E.E. Smith, C. Tur, Phys. Rev. C 80 (2009) 014313.
[434] C.D. Goodman, C.A. Goulding, M.B. Greenfield, J. Rapaport, D.E. Bainum, C.C. Foster, W.G. Love, F. Petrovich, Phys. Rev. Lett. 44 (1980) 1755.
[435] F. Osterfeld, Rev. Modern Phys. 64 (1992) 491.
[436] W. Alford, B. Spicer, Adv. Nuclear Phys. 24 (1998) 1.
[437] T. Aumann, Prog. Part. Nuclear Phys. 59 (2007) 3.
[438] C.K. Gelbke, Prog. Part. Nuclear Phys. 62 (2009) 307.
[439] http://ns.ph.liv.ac.uk/~mc/EXL/ns-instrum-exl.html.
[440] http://www.gsi.de/forschung/kp/kr/R3B_e.html.
[441] http://groups.nscl.msu.edu/charge_exchange/public/experiments/libe_inv.htm.
[442] http://groups.nscl.msu.edu/charge_exchange/public/experiments/pn_inverse.htm.
[443] P.F. Mantica, J. Phys. G 31 (2005) S1617.
[444] T. Mehren, B. Pfeiffer, S. Schoedder, K.-L. Kratz, M. Huhta, P. Dendooven, A. Honkanen, G. Lhersonneau, M. Oinonen, J.-M. Parmonen, H. Penttilä, A. Popov, V. Rubchenya, J. Äystö, Phys. Rev. Lett. 77 (1996) 458.
[445] J.C. Wang, P. Dendooven, M. Hannawald, A. Honkanen, M. Huhta, A. Jokinen, K.L. Kratz, G. Lhersonneau, M. Oinonen, H. Penttil, K. Perjrvi, B. Pfeiffer, J. yst, Phys. Lett. B 454 (1999) 1.
[446] M. Hannawald, K.-L. Kratz, B. Pfeiffer, W.B. Walters, V.N. Fedoseyev, V.I. Mishin, W.F. Mueller, H. Schatz, J. VanRoosbroeck, U. Köster, V. Sebastian, H.L. Ravn, Phys. Rev. C 62 (2000) 054301.
[447] V.E. Iacob, Y. Zhai, T. Al-Abdullah, C. Fu, J.C. Hardy, N. Nica, H.I. Park, G. Tabacaru, L. Trache, R.E. Tribble, Phys. Rev. C 74 (2006) 045810.
[448] J.I. Prisciandaro, A.C. Morton, P.F. Mantica, Nucl. Instrum. Methods A 505 (2003) 140.
[449] G. Lorusso, J. Pereira, P. Hosmer, L. Kern, K. Kratz, F. Montes, P. Reeder, P. Santi, H. Schatz, F. Schertz, A. Wöhr, PoS(NIC-IX) 243. http://pos.sissa.it//archive/conferences/028/243/NIC-IX_243.pdf.
[450] R. Kumar, F. Molina, S. Pietri, E. Casarejos, A. Algora, J. Benlliure, P. Doornenbal, J. Gerl, M. Gorska, I. Kojouharov, Z. Podolyk, W. Prokopowicz, P. Regan, B. Rubio, H. Schaffner, S. Tashenov, H.-J. Wollersheim, Nucl. Instrum. Methods A 598 (2009) 754.
[451] P.T. Hosmer, H. Schatz, A. Aprahamian, O. Arndt, R.R.C. Clement, A. Estrade, K.-L. Kratz, S.N. Liddick, P.F. Mantica, W.F. Mueller, F. Montes, A.C. Morton, M. Ouellette, E. Pellegrini, B. Pfeiffer, P. Reeder, P. Santi, M. Steiner, A. Stolz, B.E. Tomlin, W.B. Walters, A. Wöhr, Phys. Rev. Lett. 94 (2005) 112501.
[452] F. Montes, A. Estrade, P.T. Hosmer, S.N. Liddick, P.F. Mantica, A.C. Morton, W.F. Mueller, M. Ouellette, E. Pellegrini, P. Santi, H. Schatz, A. Stolz, B.E. Tomlin, O. Arndt, K.-L. Kratz, B. Pfeiffer, P. Reeder, W.B. Walters, A. Aprahamian, A. Wöhr, Phys. Rev. C 73 (2006) 035801.

[453] J. Pereira, S. Hennrich, A. Aprahamian, O. Arndt, A. Becerril, T. Elliot, A. Estrade, D. Galaviz, R. Kessler, K.-L. Kratz, G. Lorusso, P.F. Mantica, M. Matos, P. Möller, F. Montes, B. Pfeiffer, H. Schatz, F. Schertz, L. Schnorrenberger, E. Smith, A. Stolz, M. Quinn, W.B. Walters, A. Wöhr, Phys. Rev. C 79 (2009) 035806.
[454] D. Bazin, F. Montes, A. Becerril, G. Lorusso, A. Amthor, T. Baumann, H. Crawford, A. Estrade, A. Gade, T. Ginter, C.J. Guess, M. Hausmann, G.W. Hitt, P. Mantica, M. Matos, R. Meharchand, K. Minamisono, G. Perdikakis, J. Pereira, J. Pinter, M. Portillo, H. Schatz, K. Smith, J. Stoker, A. Stolz, R.G.T. Zegers, Phys. Rev. Lett. 101 (2008) 252501.
[455] J.B. Stoker, P.F. Mantica, D. Bazin, A. Becerril, J.S. Berryman, H.L. Crawford, A. Estrade, C.J. Guess, G.W. Hitt, G. Lorusso, M. Matos, K. Minamisono, F. Montes, J. Pereira, G. Perdikakis, H. Schatz, K. Smith, R.G.T. Zegers, Phys. Rev. C 79 (2009) 015803.
[456] B. Rubio, W. Gelletly, Lect. Notes Phys. 764 (2009) 99.
[457] H. Schatz, K. Blaum, Europhys. News 37 (2006) 16.
[458] G. Bollen, S. Becker, H.J. Kluge, M. König, R.B. Moore, T. Otto, H. Raimbault-Hartmann, G. Savard, L. Schweikhard, H. Stolzenberg, Nucl. Instrum. Methods A 368 (1996) 675.
[459] K. Blaum, G. Audi, D. Beck, G. Bollen, P. Delahaye, S. George, C. Guénaut, F. Herfurth, A. Herlert, A. Kellerbauer, H.-J. Kluge, D. Lunney, M. Mukherjee, S. Schwarz, L. Schweikhard, C. Yazidjian, Nuclear Phys. A 752 (2005) 317.
[460] J. Clark, R.C. Barber, C. Boudreau, F. Buchinger, J.E. Crawford, S. Gulick, J.C. Hardy, A. Heinz, J.K.P. Lee, R.B. Moore, G. Savard, D. Seweryniak, K.S. Sharma, G. Sprouse, J. Vaz, J.C. Wang, Z. Zhou, Nucl. Instrum. Methods B 204 (2003) 487.
[461] G. Savard, J. Wang, K. Sharma, H. Sharma, J. Clark, C. Boudreau, F. Buchinger, J. Crawford, J. Greene, S. Gulick, A. Hecht, J. Lee, A. Levand, N. Scielzo, W. Trimble, J. Vaz, B. Zabransky, Int. J. Mass Spectrom. 251 (2006) 252.
[462] J. Dilling, D. Ackermann, J. Bernard, F.P. Hessberger, S. Hofmann, W. Hornung, H.J. Kluge, E. Lamour, M. Maier, R. Mann, G. Marx, R.B. Moore, G. Münzenberg, W. Quint, D. Rodriguez, M. Schädel, J. Schönfelder, G. Sikler, C. Toader, L. Vermeeren, C. Weber, G. Bollen, O. Engels, D. Habs, P. Thirolf, H. Backe, A. Dretzke, W. Lauth, W. Ludolphs, M. Sewtz, Hyperfine Interact. 127 (2000) 491.
[463] M. Block, D. Ackermann, D. Beck, K. Blaum, M. Breitenfeldt, A. Chauduri, A. Doemer, S. Eliseev, D. Habs, S. Heinz, F. Herfurth, F.P. Heßberger, S. Hofmann, H. Geissel, H.-J. Kluge, V. Kolhinen, G. Marx, J.B. Neumayr, M. Mukherjee, M. Petrick, W. Plass, W. Quint, S. Rahaman, C. Rauth, D. Rodrguez, C. Scheidenberger, L. Schweikhard, M. Suhonen, P.G. Thirolf, Z. Wang, C. Weber, The SHIPTRAP collaboration, Eur. Phys. J. A 25 (2005) s1.49.
[464] M. Block, D. Ackermann, K. Blaum, A. Chaudhuri, Z. di, S. Eliseev, R. Ferrer, D. Habs, F. Herfurth, F.P. Heßberger, S. Hofmann, H.-J. Kluge, G. Maero, A. Martín, G. Marx, M. Mazzocco, M. Mukherjee, J.B. Neumayr, W.R. Plaß, W. Quint, S. Rahaman, C. Rauth, D. Rodríguez, C. Scheidenberger, L. Schweikhard, P.G. Thirolf, G. Vorobjev, C. Weber, Hyperfine Interact. 173 (2006) 133.
[465] V.S. Kolhinen, S. Kopecky, T. Eronen, U. Hager, J. Hakala, J. Huikari, A. Jokinen, A. Nieminen, S. Rinta-Antila, J. Szerypo, J. Äystö, Nucl. Instrum. Methods A 528 (2004) 776.
[466] A. Jokinen, T. Eronen, U. Hager, I. Moore, H. Penttilä, S. Rinta-Antila, J. Äystö, Int. J. Mass Spectrom. 251 (2006) 204.
[467] S. Schwarz, G. Bollen, D. Lawton, P. Lofy, D.J. Morrissey, J. Ottarson, R. Ringle, P. Schury, T. Sun, V. Varentsov, L. Weissman, Nucl. Instrum. Methods B 204 (2003) 507.
[468] G. Bollen, S. Schwarz, D. Davies, P. Lofy, D. Morrissey, R. Ringle, P. Schury, T. Sun, L. Weissman, Nucl. Instrum. Methods A 532 (2004) 203.
[469] R. Ringle, P. Schury, T. Sun, G. Bollen, D. Davies, J. Huikari, E. Kwan, D. Morrissey, A. Prinke, J. Savory, S. Schwarz, C. Sumithrarachchi, International J. Mass Spectrom. 251 (2006) 300.
[470] J. Dilling, R. Baartman, P. Bricault, M. Brodeur, L. Blomeley, F. Buchinger, J. Crawford, J.C. Lopez-Urrutia, P. Delheij, M. Froese, G. Gwinner, Z. Ke, J. Lee, R. Moore, V. Ryjkov, G. Sikler, M. Smith, J. Ullrich, J. Vaz, Int. J. Mass Spectrom. 251 (2006) 198.
[471] B. Franzke, H. Geissel, G. Münzenberg, Mass Spectrometry Rev. 27 (2008) 428.
[472] T. Radon, T. Kerscher, B. Schlitt, K. Beckert, T. Beha, F. Bosch, H. Eickhoff, B. Franzke, Y. Fujita, H. Geissel, M. Hausmann, H. Irnich, H.C. Jung, O. Klepper, H.-J. Kluge, C. Kozhuharov, G. Kraus, K.E.G. Löbner, G. Münzenberg, Y. Novikov, F. Nickel, F. Nolden, Z. Patyk, H. Reich, C. Scheidenberger, W. Schwab, M. Steck, Phys. Rev. Lett. 78 (1997) 4701.
[473] M. Hausmann, F. Attallah, K. Beckert, F. Bosch, A. Dolinskiy, H. Eickhoff, M. Falch, B. Franczak, B. Franzke, H. Geissel, T. Kerscher, O. Klepper, H.J. Kluge, C. Kozhuharov, K.E.G. Löbner, G. Münzenberg, F. Nolden, Y.N. Novikov, T. Radon, H. Schatz, C. Scheidenberger, J. Stadlmann, M. Steck, T. Winkler, H. Wollnik, Nucl. Instrum. Methods A 446 (2000) 569.
[474] A. Coc, R.L. Gac, M.D.S. Simon, C. Thibault, F. Touchard, Nucl. Instrum. Methods A 271 (1988) 512.
[475] D. Lunney, N. Vieira, G. Audi, C. Gaulard, M. de SaintSimon, C. Thibault, Int. J. Mass Spectrom. 251 (2006) 286.
[476] D.K. Barillari, J.V. Vaz, R.C. Barber, K.S. Sharma, Phys. Rev. C 67 (2003) 064316.
[477] L. Bianchi, B. Fernandez, J. Gastebois, A. Gillibert, W. Mittig, J. Barrette, Nucl. Instrum. Methods A 276 (1989) 509.
[478] M. Matos, A. Estrade, M. Amthor, A. Aprahamian, D. Bazin, A. Becerril, T. Elliot, D. Galaviz, A. Gade, S. Gupta, G. Lorusso, F. Montes, J. Pereira, M. Portillo, A.M. Rogers, H. Schatz, D. Shapira, E. Smith, A. Stolz, M. Wallace, J. Phys. G 35 (2008) 014045.
[479] G. Auger, W. Mittig, A. Lépine-Szily, L. Fifield, M. Bajard, E. Baron, D. Bibet, P. Bricault, J. Casandjian, M. Chabert, M. Chartier, J. Ferme, L. Gaudard, A. Gillibert, M. Lewitowicz, M. Moscatello, N. Orr, E. Plagnol, C. Ricault, A. Villari, Y.Y. Feng, Nucl. Instrum. Methods A 350 (1994) 235.
[480] W. Mittig, A. Lépine-Szily, N.A. Orr, Ann. Rev. Nucl. Part. Sci. 47 (1997) 27.
[481] D. Lunney, J.M. Pearson, C. Thibault, Rev. Modern Phys. 75 (2003) 1021.
[482] Y.E. Penionzhkevich, Hyperfine Interact. 132 (2001) 263.
[483] A.H. Wapstra, G. Audi, C. Thibault, Nuclear Phys. A 729 (2003) 129.
[484] G. Audi, A.H. Wapstra, C. Thibault, Nuclear Phys. A 729 (2003) 337.
[485] J.W. Truran, J.J. Cowan, C.A. Pilachowski, C. Sneden, Publ. Astron. Soc. Pac. 114 (2002) 1293.
[486] S. Wanajo, S. Goriely, M. Samyn, N. Itoh, Astrophys. J. 606 (2004) 1057.
[487] S. Baruah, G. Audi, K. Blaum, M. Dworschak, S. George, C. Guénaut, U. Hager, F. Herfurth, A. Herlert, A. Kellerbauer, H.-J. Kluge, D. Lunney, H. Schatz, L. Schweikhard, C. Yazidjian, Phys. Rev. Lett. 101 (2008) 262501.
[488] M. Dworschak, G. Audi, K. Blaum, P. Delahaye, S. George, U. Hager, F. Herfurth, A. Herlert, A. Kellerbauer, H.-J. Kluge, D. Lunney, L. Schweikhard, C. Yazidjian, Phys. Rev. Lett. 100 (2008) 072501.
[489] G. Martinez-Pinedo, D. Mocelj, N. Zinner, A. Kelic, K. Langanke, I. Panov, B. Pfeiffer, T. Rauscher, K.-H. Schmidt, F.-K. Thielemann, Prog. Part. Nuclear Phys. 59 (2007) 199.
[490] B.A. Brown, R.R.C. Clement, H. Schatz, A. Volya, W.A. Richter, Phys. Rev. C 65 (2002) 045802.
[491] H. Schatz, Int. J. Mass Spectrom. 251 (2006) 293.
[492] J.A. Clark, G. Savard, K.S. Sharma, J. Vaz, J.C. Wang, Z. Zhou, A. Heinz, B. Blank, F. Buchinger, J.E. Crawford, S. Gulick, J.K.P. Lee, A.F. Levand, D. Seweryniak, G.D. Sprouse, W. Trimble, Phys. Rev. Lett. 92 (2004) 192501.
[493] P. Schury, C. Bachelet, M. Block, G. Bollen, D.A. Davies, M. Facina, C.M.F. III, C. Guénaut, J. Huikari, E. Kwan, A. Kwiatkowski, D.J. Morrissey, R. Ringle, G.K. Pang, A. Prinke, J. Savory, H. Schatz, S. Schwarz, C.S. Sumithrarachchi, T. Sun, Phys. Rev. C 75 (2007) 055801.
[494] J. Savory, P. Schury, C. Bachelet, M. Block, G. Bollen, M. Facina, C.M. Folden III, C. Guénaut, E. Kwan, A.A. Kwiatkowski, D.J. Morrissey, G.K. Pang, A. Prinke, R. Ringle, H. Schatz, S. Schwarz, C.S. Sumithrarachchi, Phys. Rev. Lett. 102 (2009) 132501.
[495] D. Rodríguez, V.S. Kolhinen, G. Audi, J. Äystö, D. Beck, K. Blaum, G. Bollen, F. Herfurth, A. Jokinen, A. Kellerbauer, H.J. Kluge, M. Oinonen, H. Schatz, E. Sauvan, S. Schwarz, Phys. Rev. Lett. 93 (2004) 161104.
[496] H. Schatz, A. Aprahamian, V. Barnard, L. Bildsten, A. Cumming, M. Ouellette, T. Rauscher, F.-K. Thielemann, M. Wiescher, Phys. Rev. Lett. 86 (2001) 3471.
[497] V.-V. Elomaa, G.K. Vorobjev, A. Kankainen, L. Batist, S. Eliseev, T. Eronen, J. Hakala, A. Jokinen, I.D. Moore, Y.N. Novikov, H. Penttilä, A. Popov, S. Rahaman, J. Rissanen, A. Saastamoinen, H. Schatz, D.M. Seliverstov, C. Weber, J. Äystö, Phys. Rev. Lett. 102 (2009) 252501.

[498] C. Mazzocchi, R. Grzywacz, S.N. Liddick, K.P. Rykaczewski, H. Schatz, J.C. Batchelder, C.R. Bingham, C.J. Gross, J.H. Hamilton, J.K. Hwang, S. Ilyushkin, A. Korgul, W. Królas, K. Li, R.D. Page, D. Simpson, J.A. Winger, Phys. Rev. Lett. 98 (2007) 212501.
[499] C. Fröhlich, G. Martínez-Pinedo, M. Liebendörfer, F.-K. Thielemann, E. Bravo, W.R. Hix, K. Langanke, N.T. Zinner, Phys. Rev. Lett. 96 (2006) 142502.
[500] R. Buras, M. Rampp, H.-T. Janka, K. Kifonidis, Astron. Astrophys. 447 (2006) 1049.
[501] C. Weber, V.-V. Elomaa, R. Ferrer, C. Fröhlich, D. Ackermann, J. Äystö, G. Audi, L. Batist, K. Blaum, M. Block, A. Chaudhuri, M. Dworschak, S. Eliseev, T. Eronen, U. Hager, J. Hakala, F. Herfurth, F.P.H. berger, S. Hofmann, A. Jokinen, A. Kankainen, H.-J. Kluge, K. Langanke, A. Martín, G. Martínez-Pinedo, M. Mazzocco, I.D. Moore, J.B. Neumayr, Y.N. Novikov, H. Penttilä, W.R. Plaß, A.V. Popov, S. Rahaman, T. Rauscher, C. Rauth, J. Rissanen, D. Rodríguez, A. Saastamoinen, C. Scheidenberger, L. Schweikhard, D.M. Seliverstov, T. Sonoda, F.-K. Thielemann, P.G. Thirolf, G.K. Vorobjev, Phys. Rev. C 78 (2008) 054310.
[502] J. Stadlmann, M. Hausmann, F. Attallah, K. Beckert, P. Beller, F. Bosch, H. Eickhoff, M. Falch, B. Franczak, B. Franzke, H. Geissel, T. Kerscher, O. Klepper, H.J. Kluge, C. Kozhuharov, Y.A. Litvinov, K.E.G. Löbner, M. Matos, G. Münzenberg, N. Nankov, F. Nolden, Y.N. Novikov, T. Ohtsubo, T. Radon, H. Schatz, C. Scheidenberger, M. Steck, H. Weick, H. Wollnik, Phys. Lett. B 586 (2004) 27.
[503] T. Eronen, V.-V. Elomaa, U. Hager, J. Hakala, A. Jokinen, A. Kankainen, T. Kessler, I.D. Moore, S. Rahaman, J. Rissanen, C. Weber, J. Äystö, Phys. Rev. C 79 (2009) 032802.
[504] Universal nuclear energy density functional (UNEDF), SciDAC/DOE theory collaboration, http://unedf.org.